WELDING Journal

December 2006

- Digital Stud Welding
- Welding Developments for NASCAR®
- Gas Purging of Weld Roots

PUBLISHED BY THE AMERICAN WELDING SOCIETY TO ADVANCE THE SCIENCE, TECHNOLOGY AND APPLICATION OF WELDING AND ALLIED PROCESSES, INCLUDING JOINING, BRAZING, SOLDERING, CUTTING, AND THERMAL SPRAYING

Select-Arc Electrodes Wear Well.

Select-Arc has introduced a comprehensive line of hardsurfacing electrodes specially developed to tackle formidable welding applications. SelectWear™ hardsurfacing wires are formulated to improve your welding productivity, enhance performance and reduce machinery downtime by increasing component life. In addition, these Select-Arc electrodes can provide heightened resistance to other conditions including impact, adhesion, corrosion, erosion and elevated temperatures.

Of course, all Select-Arc hardsurfacing products deliver the same exceptional electrode quality that our customers have come to rely on over the past decade.

For more information on the hardsurfacing electrodes designed with tough applications in mind, call Select-Arc at **1-800-341-5215** or visit our website: **www.select-arc.com.**

SELECT ARC INC.®

Circle No. 31 on Reader Info-Card

THESE GUYS DRIVE TO WIN.

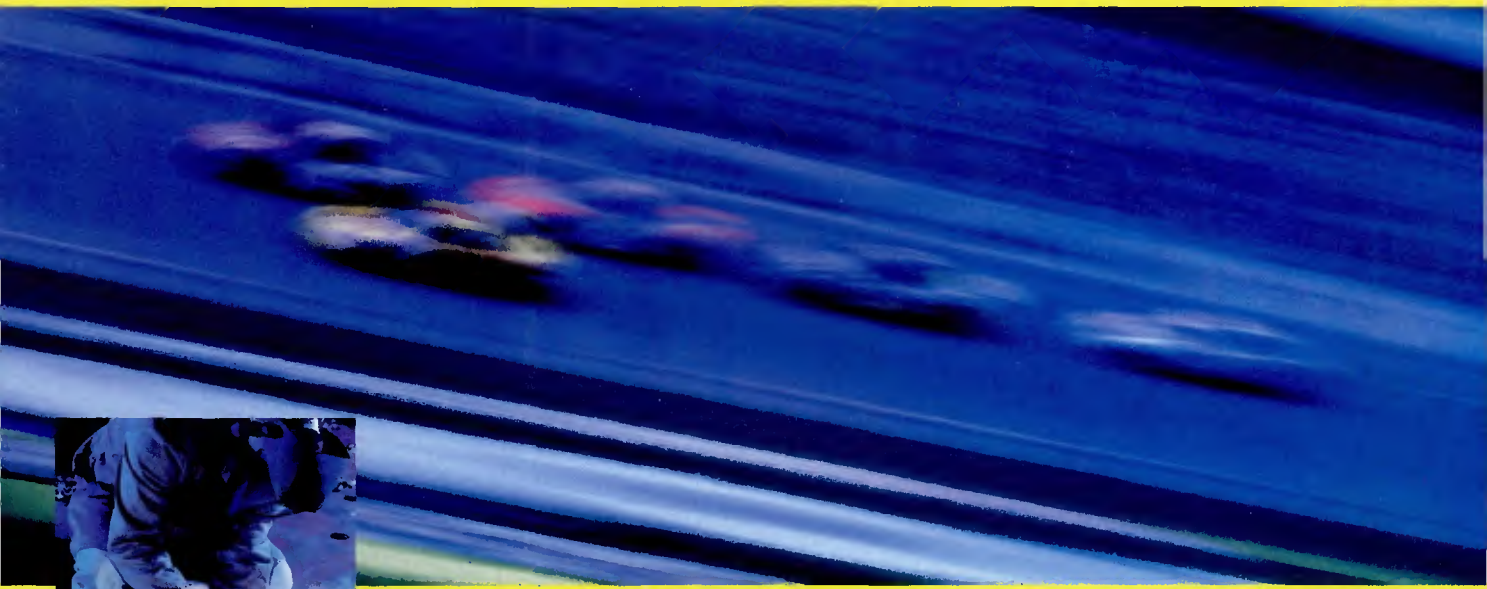

WHICH IS WHAT DRIVES THEM TO ESAB FOR THEIR WELDING AND CUTTING NEEDS.

1.800.ESAB.123 **www.esabna.com**

Racing around the track at well over 100 mph, today's drivers literally put their lives on the line to get to the checkered flag first. They need to trust their cars and their crews.

No wonder so many nationally ranked crews trust ESAB for their welding and cutting equipment. Because when so much is at stake, you go with the leader as a partner. And ESAB is the worldwide leader in cutting and welding, with over a century's experience – on the job, in the field, wherever quality matters most.

So whether you're risking it all on the track, or risking your productivity on the shop floor, ask for ESAB by name.

ESAB® *Your Partner in Welding & Cutting Since 1904*

Circle No. 19 on Reader Info-Card

WELDING | CUTTING | FILLER METALS

WEMCO's biggest networking opportunity is a few months away...

Don't miss it!

Join us at the 11th Annual Welding Equipment Manufacturers Committee (WEMCO) Meeting taking place on January 11-13, 2007, at the breathtaking La Quinta Resort and Club, located in Palm Springs, California. Top leaders in the welding product industry will be at this event, sharing informative and valuable insight on ways to launch the industry and its associated technologies forward into the 21st century. So pack your bags and join us in Palm Springs. Be a catalyst in the future of welding!

Our dynamic array of speakers are top executives in the welding industry, including:

- *Dr. Jeff Dietrich, Institute for Trends Research:* Economic Forecasting.
- *John Stropki, Lincoln Electric:* Improving the Productivity of the American Workforce.
- *Mike Molinini, Airgas:* Welding Distribution Channels
- *Phil Pratt, SilverHawk Associates:* Solution Management to Deliver Value.

In addition, AWS Past Presidents Ernest Levert and Lee Kvidahl will participate in our Industry Leader Panel Discussion.

We invite you to be a part of this spectacular WEMCO event, and to experience the beauty and opulence of the La Quinta Resort in Palm Springs, California. You will not want to miss this!

You do not need to be a WEMCO member to attend.

11th Annual WEMCO Meeting
January 11 – 13, 2007
La Quinta Resort and Club
Palm Springs, California

Meeting Fee:	$720
Spouse Fee:	$225
Spouse Tour:	$80

WEMCO has established a special group rate at $230 per night.

Don't delay! Reserve your accommodations today by visiting WEMCO online at *www.aws.org/wemco/annual/11th_2007.html*

You may also register by:

Telephone:	(800) 443-9353, ext. 444
Fax:	(305) 442-7451
E-mail:	wemco@aws.org

See you in Palm Springs! We'll be waiting for you!

A STANDING COMMITTEE OF
American Welding Society

WEMCO
WELDING EQUIPMENT MANUFACTURERS COMMITTEE

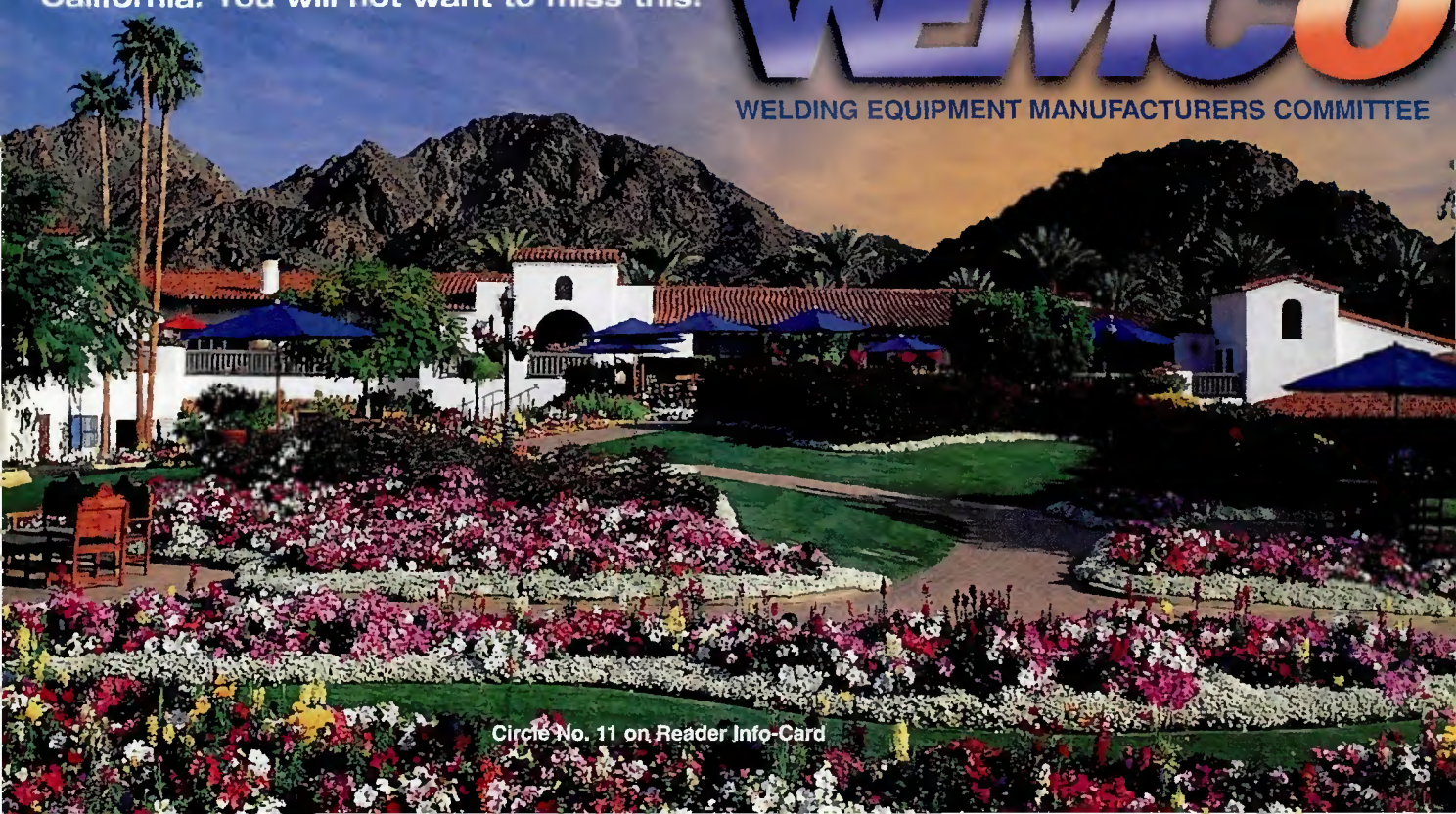

Circle No. 11 on Reader Info-Card

CONTENTS

December 2006 • Volume 85 • Number 12 AWS Web site http://www.aws.org

Features

Welding Research Supplement

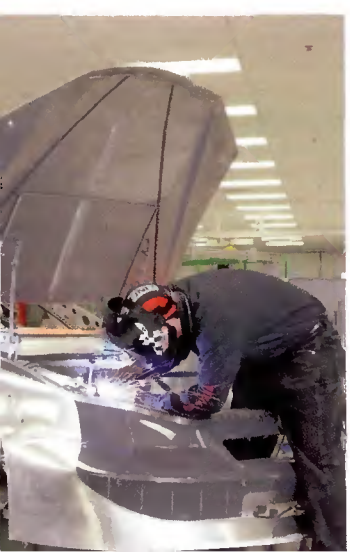

Cover photo: Chrome-moly is now being used in some chassis extension components at Joe Gibbs Racing. (Photo courtesy of The Lincoln Electric Co., Cleveland, Ohio.)

Departments

Welding Journal (ISSN 0043-2296) is published monthly by the American Welding Society for $120.00 per year in the United States and possessions, $160 per year in foreign countries; $7.50 per single issue for AWS members and $10.00 per single issue for nonmembers. American Welding Society is located at 550 NW LeJeune Rd., Miami, FL 33126-5671; telephone (305) 443-9353. Periodicals postage paid in Miami, Fla., and additional mailing offices. **POSTMASTER:** Send address changes to Welding Journal, 550 NW LeJeune Rd., Miami, FL 33126-5671.

BY HUGH K. WEBSTER
AWS WASHINGTON GOVERNMENT AFFAIRS OFFICE

Workplace Injuries, Illnesses Rates Remain Steady

Nonfatal workplace injuries and illnesses occurred at a rate of 4.6 cases per 100 equivalent full-time workers among private industry employers in 2005, according to the U.S. Bureau of Labor Statistics. This is a slight decline from the rate of 4.8 cases per 100 equivalent full-time workers reported for 2004. The rate resulted from a total of 4.2 million nonfatal injuries and illnesses in private industry workplaces during 2005, relatively unchanged compared to 2004.

Small establishments (those employing 1 to 10 workers) reported the lowest rate for injuries and illnesses combined (2.0 cases per 100 full-time workers), while midsize establishments (those employing 50 to 249 workers) reported the highest rate (5.8 cases per 100 full-time workers). The rate for large establishments (those employing 1000 or more workers) declined significantly in 2005 to 5.2 cases per 100 full-time workers, down from 5.4 in 2004.

Three manufacturing industries reported 100,000 or more cases in 2005 — transportation equipment manufacturing with 146,800 cases; fabricated metal product manufacturing with 121,800 cases; and food manufacturing with 114,200 cases. These accounted for nearly 43% of all cases reported in manufacturing, but only one-third of manufacturing employment in 2005. The injury and illness rate for each of these industries was significantly higher than that for the manufacturing sector as a whole.

OSHA Amends Hexavalent Chromium Standard

The U.S. Occupational Safety and Health Administration (OSHA) has adopted a minor amendment to the compliance date provision of its hexavalent chromium standard for general industry. The amendment is part of a settlement agreement with several organizations that had filed a legal challenge to the standard.

The amendment creates an optional, alternative compliance timetable for metal- and surface-finishing operations at eligible facilities. Facilities that become parties to the agreement must implement engineering controls for electroplating operations on an expedited schedule (by Dec. 31, 2008), but will have relief from certain respirator requirements in the interim. The amendment has no impact on the compliance requirement for facilities that are not eligible to or do not become parties to the agreement.

While this development is viewed as a positive outcome of a legal challenge to the standard, several other court challenges remain, including one brought by the National Association of Manufacturers. In fact, OSHA historically has had great difficulty in setting or updating "permissible exposure limits" for chemicals in the workplace. Exposure limits for some 400 chemicals were set when OSHA was created in 1971. Only about 20 have been reviewed and revised since, largely due to the legal and regulatory complexities.

Business Web Site Newly Updated

The federally sponsored Web site *www.business.gov* has been revamped to provide business owners with a one-stop resource that searches the federal government agencies that regulate or serve businesses for compliance information or resources. The Web site makes it easier to find information on taxes, immigration laws, workplace safety, environmental requirements, and other regulations that can present challenges for small and midsized businesses.

The site is managed by the U.S. Small Business Administration in a partnership with 21 other federal agencies. Originally launched in 2004, the Web site initially provided information on starting, growing, and managing a small business. The new compliance focus is designed to better meet the needs of the business community.

Tort Reform Measure Appears to Be Working

The Class Action Fairness Act was passed by Congress in 2005 in order to make it easier for multijurisdictional class action lawsuits to be tried in federal courts rather than state courts. This measure had been supported by the business community based on concerns about the fairness of state court proceedings for corporate defendants, especially in negligence and personal injury suits against corporations and entire industries. A new study by the Federal Judicial Center, an arm of the federal courts, concludes that the legislation has been effective with a significant number of class actions being successfully moved from state to federal court.

Hexavalent Chromium Guidance Issued

The Occupational Safety and Health Administration has issued safety and health compliance guidance for small businesses related to the new hexavalent chromium requirements for general industry, construction, and shipyards. The guide generally describes the steps that employers are required to take to comply with the rules. Permissible exposure limits, exposure determination, regulated areas, methods of compliance, respiratory protection, protective work clothing and equipment, hygiene areas and practices, housekeeping, and medical surveillance are the major topics included in the guide.

Next Nuclear Plant Generation Activity

The U.S. Department of Energy (DOE) has announced that it will make awards valued at about $8 million to three companies to perform engineering studies and develop a preconceptual design to guide research on the Next Generation Nuclear Plant (NGNP). Contracts will be issued to Westinghouse Electric Co., AREVA NP, and General Atomics. The NGNP research and development program is part of DOE's Generation IV nuclear energy systems initiative aimed at developing next generation reactor technologies and is authorized by Congress in the Energy Policy Act of 2005.

Pipeline Safety Legislation Passed

The House Energy and Commerce Committee has passed unanimously the Pipeline Safety Improvement Act of 2006. This bill, in addition to reauthorizing federal pipeline safety programs, would increase federal authority to enforce damage prevention rules and encourage states to adopt effective damage prevention programs. The bill also would increase funding to state pipeline safety programs, and require the Department of Transportation to review corrosion control regulations, study critical infrastructure, and regulate low-stress pipelines in the same way that higher-stress pipelines are regulated.

Contact the AWS Washington Government Affairs Office at 1747 Pennsylvania Ave. NW, Washington, DC 20006; e-mail hwebster@wc-b.com; *FAX (202) 835-0243.*

SEE YOUR PROCESSED IMAGE ON-SITE IN LESS THAN A MINUTE. KODAK INDUSTREX Digital Systems for Non-Destructive Testing offer portable solutions that let you see if you've got what you need before you leave—saving you time, money, and effort. Plus, our legendary global service and support means you're covered anywhere the job takes you. Visit www.kodak.com/go/ndtproducts to see the full line of INDUSTREX Digital Systems. For a personal demonstration, call 877.909.4280, or e-mail us at ndtproducts@kodak.com.

Circle No. 26 on Reader Info-Card

FILM PRODUCTS | DIGITAL PRODUCTS | FILM DIGITIZERS | GLOBAL SERVICE AND SUPPORT

Kodak

Edison Welding Institute Joins American Council of the International Institute of Welding

The American Welding Society (AWS) and Edison Welding Institute (EWI) recently announced EWI has joined the American Council of the International Institute of Welding (IIW), a committee that includes AWS and the Welding Research Council that represents the United States welding industry. The addition of the company to the American Council enhances North America's involvement and role in the IIW and strengthens its representation of the welding industry internationally.

The official signing of EWI's induction took place at the 2006 FABTECH International & AWS Welding Show at the Georgia World Congress Center in Atlanta.

The IIW is made up of nearly fifty member countries and provides a global forum for the exchange of information related to welding technologies and applications. The objectives of the American Council are to serve the United States welding industry and related joining technologies, with a focus on the advancement of welding research and technology, standards, codes, and procedures. In addition, the Council is responsible for the promotion and development of international welding standards that reflect the interests of the United States.

Deformation Resistance Welding Receives Certification by the American Society of Mechanical Engineers

Delphi Corp.'s deformation resistance welding (DRW) technology is now nationally recognized by the American Society of Mechanical Engineers (ASME) as a manufacturing process standard for heat exchanger tube-to-tubesheet welding.

"We hope this recognition will allow us to accelerate bringing the DRW technology to commercial welding applications," said Timothy Forbes, Delphi Corp. director for technology commercialization and licensing.

What makes DRW unique is its formation of a near-instantaneous, full-strength, leak-tight weld by heating metal surfaces only to the point of softening, followed by rapid, engineered compression of the joint.

Louisville First in Southeast for Manufacturing Jobs

According to the 2007 *Kentucky Manufacturers Register*, a manufacturers' directory published annually by Manufacturers' News, Inc. (MNI), Evanston, Ill., Louisville ranks as the Southeast's top manufacturing city. MNI reports the city accounts for 65,071 manufacturing jobs, ranking it first in the nine-state region in industrial employment.

Louisville ranks above Atlanta by 5000 jobs, with the second-ranked city accounting for 60,803 workers. Third-ranked Charlotte is home to 49,957 jobs while Miami and Jacksonville rank fourth and fifth, respectively, with 49,603 and 44,780 jobs.

The *Register's* newest data also show that statewide, Kentucky is home to 6163 manufacturing companies employing 328,393 workers, and it accounts for 8.4% of the Southeast's manufacturing employment. The *Register's* survey profiles large and small Kentucky manufacturers, including startup companies with just a few employees.

Airgas Acquires Union Industrial Gas Group

Airgas, Inc., Radnor, Pa., recently acquired most of the assets and operations of Dallas, Tex.-based Union Industrial Gas Group (UIG), including 14 branches in Louisiana, New Mexico, and Texas. The operations that were acquired, effective November 1, had annual sales of $38 million.

Airgas is integrating most of the operations into two of its regional companies. Airgas Southwest has assumed operations of four locations near Houston, San Antonio, and El Paso, Tex., doing business as Gulf Oxygen, Union Industrial Gas, and Valley Gas, as well as five locations in Albuquerque, Farmington, Las Cruces, Alamogordo, and Santa Fe, N.Mex., doing business as Valley Gas. Airgas Gulf States has assumed operation of four locations in New Orleans, Baton Rouge, and Houma, La., doing business as Doussan.

The company has also offered employment to more than 100 employees of UIG affected by the acquisition.

WELDING journal

Publisher *Andrew Cullison*

Editorial
Editor/Editorial Director *Andrew Cullison*
Senior Editor *Mary Ruth Johnsen*
Associate Editor *Howard M. Woodward*
Assistant Editor *Kristin Campbell*
Peer Review Coordinator *Erin Adams*

Publisher Emeritus *Jeff Weber*

Graphics and Production
Managing Editor *Zaida Chavez*
Senior Production Coordinator *Brenda Flores*

Advertising
National Sales Director *Rob Saltzstein*
Advertising Sales Representative *Lea Garrigan Badwy*
Advertising Production *Frank Wilson*

Subscriptions
acct@aws.org

American Welding Society
550 NW LeJeune Rd., Miami, FL 33126
(305) 443-9353 or (800) 443-9353

TREGASKISS + INNOVATION = LOWER TOTAL COST OF OWNERSHIP.

For 40 years, leading manufacturers in the transportation and heavy equipment industries have trusted and relied on TOUGH GUN® MIG Welding Torches from Tregaskiss.

At Tregaskiss, our commitment to excellence and innovation has led to industry first features like our lifetime warranty on handles and switches, our patented TOUGH LOCK® Contact Tip System and our double life MIG torch system.

What does lower total cost of ownership mean to you?

- Lower maintenance costs
- Reduced downtime
- Common consumable platform
- Increased production

TOUGH GUN MIG Torches from Tregaskiss lower your **TOTAL COST OF OWNERSHIP** without compromising quality.

Contact Tregaskiss today at **1-800-787-6966** or visit us online at **www.tregaskiss.com**.

TOUGH GUN® Tregaskiss

Tregaskiss WELDING PRODUCTS

THE FREEDOM TO INNOVATE

BEST MANAGED COMPANIES

Circle No. 32 on Reader Info-Card

Looking Back; Looking Forward

Due to the change in the AWS fiscal year, necessitated by the shift from a spring AWS Annual Meeting to a fall AWS Annual Meeting, I had the privilege of serving as AWS president for 19 months. In June 2005, that seemed like a very long time. Not so today: January 1, Jerry Uttrachi becomes AWS president.

One of the things I hoped to accomplish was to improve relations between AWS and its counterparts in other countries. To that end, Kate, my bride of 43 years, and I will have visited 14 countries during my term. I met with counterparts in those countries, and we held discussions regarding matters of mutual interest including certification programs, publication of welding information, the image of welding, and the shortage of welders. We soon learned that issues faced in other parts of the world are not so different from those in the USA. This work was not done by neglecting the domestic scene, however, as I also visited 26 domestic Sections, accompanied by Kate in most cases. I don't think I could have survived all of this activity without her.

During the past few years, AWS has reversed a rather serious downward trend in its financial position and is now enjoying significant surpluses. A lot of the credit for this goes to Executive Director Ray Shook and his staff at headquarters. At the same time, the AWS Welding Show has undergone a huge change, merging with the FABTECH International Show and shifting from spring to autumn. This has reversed downward trends in Welding Show exhibit space and attendance. The downturn in AWS memberships that took place following the 9/11 disaster (which was less severe for AWS than for other societies in the United States) has also been reversed. It seems likely that AWS will soon exceed its historic high of about 50,000 members.

All of the above seems to portend a rosy future for AWS and the welding industry. However, there is a looming crisis for the industry in the USA, and that is the shortage of welders. We have all, by now, learned of the U.S. Department of Labor's prediction of a shortage of 200,000 welders by the year 2010. The shortage is already significant and growing rapidly as the aging workforce of welders enters retirement. Without welders, we have no welding industry, resulting in severe crippling of the U.S. manufacturing industry and of the development of infrastructure. The USA is not alone in this crisis — much of the industrialized world shares this problem. It is possible to export manufacturing jobs to developing countries, although AWS certainly does not advocate that. But it is not possible to export infrastructure development to developing countries. Without an adequate workforce of welders, the USA will not erect high rise buildings, will not build power plants to meet increasing energy demand, will not build the bridges and rail systems for high-speed transportation. The list goes on and on.

Accordingly, I applaud the October 2006 decision of the Hobart Brothers/Miller Electric organization to contribute $1 million to the AWS Foundation, earmarked for workforce development. This is an important move toward addressing the welder shortage, but a great deal more funding for this effort is needed. And, funding alone will not eliminate the shortage of welders. We need to recruit young people to enter the training programs. We need to reverse the decline in the number of institutions training welders. We need to see to it that these training institutions are equipped with modern welding equipment, so that the welders who emerge from these training programs are ready to use the up-to-date equipment they'll find on the job. We need to improve the quality of the welding environment, both in training institutions and in the workplace, so that young people will see fit to learn the trade and to make a career of it.

If we allow the shortage of welders to cripple the welding industry and with it the economies of the developed countries, all of the gains of the recent years will disappear. We must not allow this to happen.

Damian J. Kotecki
AWS President

New Class of Jets Will Fly High With Help of NASA Research

The Eclipse 500 will soon be the first very light jet certified by the Federal Aviation Administration and delivered ready for flight. One NASA-supported technology that has helped make this jet a reality is friction stir welding. (Photo courtesy of Eclipse Aviation Corp.)

The Eclipse 500, built by Eclipse Aviation Corp., Albuquerque, N.Mex., is soon to be the first very light jet certified by the Federal Aviation Administration (FAA) and delivered ready for flight. Very light jets are designed to be fast, safe, and reliable four-to-six passenger planes capable of using very small airports. They also feature technologies that reduce the cost and could revolutionize the ease of flying at jet speeds.

"The Eclipse 500 and other very light jets have the potential to change the way people fly with the help of innovations that NASA and its partners worked on for more than a decade," said Bruce J. Holmes, former head of two NASA/industry alliances that worked to improve small plane technology at NASA's Langley Research Center in Hampton, Va.

One NASA-supported technology that has helped make the Eclipse 500 a reality is friction stir welding. This allows a faster, more automated assembly process of the jet's aluminum structure.

"Testing at NASA Langley verified the effectiveness and safety of our friction stir welding manufacturing technique. That testing helped us gain FAA approval for friction stir welding a year ahead of schedule," said Vern Raburn, Eclipse chief executive officer. "Friction stir welding enables a drastic reduction in aircraft assembly time and eliminates the need for thousands of rivets resulting in reduced assembly costs, better quality joining, and stronger, lighter joints."

"Eclipse is using a solid-state weld that doesn't melt the materials," said Scott Forth, a senior engineer in the Mechanics of Structures and Materials Branch at NASA Langley at the time of the testing. "A tool is inserted into the parts that need to be bonded, and it plastically mixes the materials together."

NASA is testing to see how effective the welds are for aircraft flight loads. "We had to come up with all new procedures because the welds have never been tested like we're testing them," said Forth. "Our testing has shown the bond created is incredibly effective...better than I anticipated."

CenterPoint Energy Gas Transmission Receives Certificate to Build Pipeline

CenterPoint Energy Gas Transmission Co., Houston, Tex., has received a certificate from the Federal Energy Regulatory Commission to build and operate a natural gas pipeline from Carthage, Tex., to the company's Perryville Hub in northeast Louisiana.

This pipeline will provide market access for growing production from east Texas and north Louisiana through interconnects with interstate and intrastate pipelines serving the East Coast, Midwest, and Southeast U.S. markets. It is expected to be in service in the first quarter of 2007.

Additionally, the $425 million, fully subscribed 172-mile, 42-in. pipeline will be built in two phases and have the capacity to transport approximately 1.2 billion ft^3 per day. Phase one will consist of nearly 1 billion ft^3 per day, and the remaining capacity in phase two will go into service in the summer of 2007.

Union Ratifies ESAB Contract

Members of UAW Local 1968, the labor union representing most of ESAB Welding and Cutting Product's Hanover, Pa., employees, recently voted to ratify a new contract. The contract, hammered out by union and ESAB negotiators, ends the union strike that began March 27.

Bob Kahlbaugh, president of Local 1968, said the union is assessing how many members will return to the plant.

The three-year contract will include a new 24-hour, seven-day-a-week work schedule at the plant. It now operates five days a week. The new schedule alleviates one of the union's main concerns during the original negotiations — mandatory overtime. Also, the revised schedule will increase the number of employees at the plant from about 255 to about 340, meaning many of the replacement workers will retain their jobs.

The contract includes substantial wage increases, modifications to the healthcare plan that includes employee contributions, and a new 401k plan with a company match.

U.S. Navy Awards General Dynamics $35 Million Contract

The U.S. Navy has awarded General Dynamics Electric Boat a one-year $34.8-million contract with four one-year options to staff and operate the New England Maintenance Manpower Initiative at the Naval Submarine Base in Groton, Conn.

The overall contract, with all options exercised and funded,

has a potential value of $202 million and a completion date of Sept. 30, 2011. This award is a follow-on to a five-year, $130.5-million contract that ran from October 2001 through September 2006.

Under the terms of the contract, the company will provide a wide spectrum of intermediate and depot-level overhaul, repair, and modernization services in support of operational nuclear-powered submarines, floating dry-docks, support and service craft, and other platforms and equipment at the submarine base.

Carpenters Union Opens $15 Million Training Center in California

The Southwest Regional Council of Carpenters recently opened a $15-million, 72,211-sq-ft training center in Ontario, Calif. Its mission is to teach union apprentice carpenters and journeymen the latest construction techniques and safety measures in order to increase their job productivity and work quality.

The center is a facility for the Carpenters Union. Its 39,885-sq-ft open floor accommodates instruction in steel stud framing, drywall installation, concrete forms, scaffold erection, and bridge construction.

Separate classrooms for welder training have been set up as well as classrooms dedicated to blueprint reading, construction safety, first aid/CPR, mathematics, and language skills.

Thermadyne Industries Partners withDaimlerChrysler

Thermadyne Industries, Inc., St. Louis, Mo., has become the single source provider of welding equipment and welder training at the United Auto Workers National Training Center for DaimlerChrysler, outside of Detroit, in Warren, Mich.

A welder at the United Auto Workers National Training Center at the DaimlerChrysler headquarters in Warren, Mich., is shown using Thermadyne arc welding equipment. Thermadyne Industries, Inc., has become the single source provider of welding equipment and welder training at the center.

The training facility features 12 welding stations and two cutting stations. Additionally, it contains equipment from four of Thermadyne's product lines.

Approximately 650 individuals annually are trained at the facility, where they receive everything from safety presentations to welder certification.

Industry Notes

• Praxair Distribution, Inc., a subsidiary of Praxair, Inc., Dan-

bury, Conn., has acquired Hobart Industrial Gases of Fort Wayne, Ind. The company has supplied a wide array of packaged gases, welding equipment, supplies, and services to Indiana and Ohio since 1956.

- Alcan Rolled Products - Ravenswood, a wholly owned subsidiary of Alcan, Inc., has signed an agreement with Bombardier Aerospace to supply the aircraft manufacturer with advanced lightweight aluminum products. The supply agreement will support the company's major aerospace programs.
- The Murrysville, Pa., manufacturing plant of MSA has recently been designated a national VPP (Voluntary Protection Program) Star Site by the Occupational Safety and Health Administration (OSHA). The plant was recognized for many achievements, including the following: a 62% reduction in OSHA reportable (injury/illness Total Case Incident) rates since 2001, and an 89% improvement in employee safety perception survey scores since 2000. The majority of the work performed at the plant involves many processing technologies, including sonic welding, that are central to the production of its safety equipment.
- Noble International, Ltd., Warren, Mich., has acquired the stock of Pullman Industries, Inc., a manufacturer of tubular and shaped structures using roll forming and other processes, primarily for the automotive industry. The company, headquartered in Troy, Mich., operates four manufacturing facilities in the United States and two in Mexico. The purchase price was approximately $120 million.
- Northwest Pipe Co., Portland, Ore., has been named as pipe supplier to Bar Constructors of Lancaster, Tex., to supply approximately 43,000 ft of 84-in.-diameter steel pipe, valued at approximately $15 million. The pipe is for the East Fork Raw Water Supply Pipeline, a project of the North Texas Municipal Water District. Also, it is expected to be manufactured in the company's Saginaw, Tex., and Parkersburg, W.Va., divisions with delivery scheduled to begin in the second quarter of 2007.
- CNH Case New Holland said its plant in Burlington, Iowa, has been recognized by the Burlington area Chamber of Commerce as the top manufacturer of 2006. The 950,000-sq-ft plant, the roots of which go back to 1937, employs 446 workers who produce construction equipment.
- DXP Enterprises, Inc., has acquired Gulf Coast Torch & Regulator, Inc., a full-service distributor of welding supplies. It has operated in Houston, Tex., since 1978. DXP paid approximately $5.5 million, net of acquired cash, for the company.
- Nucor Corp., Charlotte, N.C., has selected Brigham City, Utah, as the location for a new facility to produce metal building systems and components. In May, the company announced plans to construct, in the western United States, its fourth metal building systems plant. The facility is expected to cost approximately $27 million and employ more than 200 people. Operations are expected to begin by the first quarter of 2008.
- Felco Industries, a manufacturer of roller wheel and vibratory compaction buckets as well as bedding and backfill conveyor systems based in Missoula, Mont., has recently been awarded a grant from the Montana Department of Commerce Trade Show Assistance Program. With help from the grant assistance, the company was able to attend the American Public Works Association, Best Show in Public Works trade show in Kansas City, Mo., in September.
- Empire Industries Ltd., Toronto, Ont., Canada, has signed a letter of intent to acquire 100% of Sorge's Pro Welding Ltd., a private company based in Fort McMurray, Alb., Canada. The company also signed a letter of intent to purchase a 49% interest in Sorge's Welding Ltd., an Aboriginal majority owned, private company, also based in Fort McMurray. The companies currently generate $8 million of revenue.

AWS FELLOWSHIPS

To: Professors Engaged in Joining Research

Subject: **Request for Proposals for AWS Fellowships for the 2007-08 Academic Year**

The American Welding Society (AWS) seeks to foster university research in joining and to recognize outstanding faculty and student talent. We are again requesting your proposals for consideration by AWS.

It is expected that the winning researchers will take advantage of the opportunity to work with industry committees interested in the research topics and report work in progress.

Please note, there are important changes in the schedule which you must follow in order to enable the awards to be made in a timely fashion. Proposals must be received at American Welding Society by **February 16, 2007**. New AWS Fellowships will be announced at the AWS Annual Meeting, November 11–14, 2007

THE AWARDS

The Fellowships or Grants are to be in amounts of up to $25,000 per year. A maximum of six students are funded for a period of up to three years of research at any one time. However, progress reports and requests for renewal must be submitted for the second and third years. Renewal by AWS will be contingent on demonstration of reasonable progress in the research or in graduate studies.

The AWS Fellowship is awarded to the student for graduate research toward a Masters or Ph.D Degree under a sponsoring professor at a North American University. The qualifications of the Graduate Student are key elements to be considered in the award. The academic credentials, plans and research history (if any) of the student should be provided. **The student must prepare the proposal for the AWS Fellowship**. However, the proposal must be under the auspices of a professor and accompanied by one or more letters of recommendation from the sponsoring professor or others acquainted with the student's technical capabilities. Topics for the AWS Fellowship may span the full range of the joining industry. Should the student selected by AWS be unable to accept the Fellowship or continue with the research at any time during the period of the award, the award will be forfeited and no (further) funding provided by AWS. The bulk of AWS funding should be for student support. AWS reserves the right not to make awards in the event that its Committee finds all candidates unsatisfactory.

DETAILS

The Proposal should include:

1. Executive Summary
2. Annualized Breakdown of Funding Required and Purpose of Funds (Student Salary, Tuition, etc.)
3. Matching Funding or Other Support for Intended Research
4. Duration of Project
5. Statement of Problem and Objectives
6. Current Status of Relevant Research
7. Technical Plan of Action
8. Qualifications of Researchers
9. Pertinent Literature References and Related Publications
10. Special Equipment Required and Availability
11. Statement of Critical Issues Which Will Influence Success or Failure of Research

In addition, the proposal must include:

1. Student's Academic History, Resume and Transcript
2. Recommendation(s) Indicating Qualifications for Research
3. Brief Section or Commentary on Importance of Research to the Welding Community and to AWS, Including Technical Merit, National Need, Long Term Benefits, etc.
4. Statement Regarding Probability of Success

The technical portion of the Proposal should be about ten typewritten pages; maximum pages for the Proposal should be thirty typewritten pages. Proposal should be sent electronically by **February 16, 2007**

Gricelda Manalich (*gricelda@aws.org*)
Executive Assistant, Board Services/IIW
American Welding Society
550 N.W. LeJeune Rd., Miami, FL 33126

Yours sincerely,

Ray W. Shook
Executive Director
American Welding Society

BY TONY ANDERSON

Q: I have been informed that the 6xxx series aluminum-based alloys are very crack sensitive. If this is a correct statement, then why is it that people weld it every day without a cracking problem?

A: First I need to explain my understanding of the term very crack sensitive.

There are some aluminum alloys — the 6xxx series happens to be one of them — that are particularly susceptible to cracking under certain circumstances. This problem is associated with solidification crack sensitivity, which in turn is directly associated with the actual chemistry in the weld pool during solidification.

In order to appreciate this problem, we need to understand that additions of various alloying elements within aluminum can seriously affect the material's crack sensitivity. The specific alloying elements can be identified, along with the amount and range at which these elements increase solidification crack sensitivity. This information can be obtained from solidification crack sensitivity curves (Fig. 1) and used during welding procedure development in order to prevent undesirable chemistry mixtures in the weld.

In the case of the 6xxx series base alloys, it is the amount of magnesium silicide (Mg_2Si) present in the aluminum that controls its susceptibility to cracking.

You are quite correct; the 6xxx series aluminum alloys, when welded correctly, are welded every day without cracking problems. However, it is not uncommon to experience cracking problems with these alloys if they are incorrectly welded. The two most common reasons for experiencing solidification cracking in the 6xxx series alloys are welding them with the gas tungsten arc welding (GTAW) process without adequate filler metal addition, and using joint designs unsuitable for providing adequate dilution when welding with 5xxx series filler metals.

Welding the 6xxx series base alloys using the GTAW process without adequate filler metal addition. This group of alloys contains approximately 1.0% magnesium silicide (Mg_2Si), which falls close to the peak of the solidification crack sensitivity curve (Fig. 1 at Al-Mg_2Si curve). When we GTA weld the 6xxx series alloys, it is often possible to produce a weld, particularly on thin-section corner joints, by melting both edges of the base metal together without adding filler material. This technique should not be used as it will invariably result in solidification cracking.

When welding these alloys, the cracking tendency of the base metal is lowered

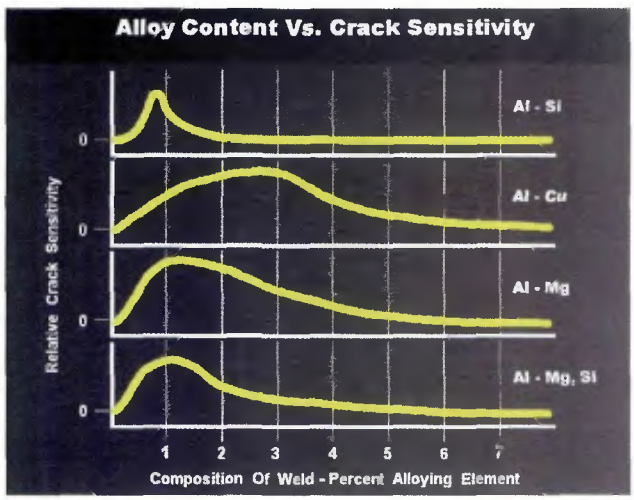

Fig. 1 — The crack sensitivity curves for Al-Si, Al-Cu, Al-Mg, and Al-MgSi.

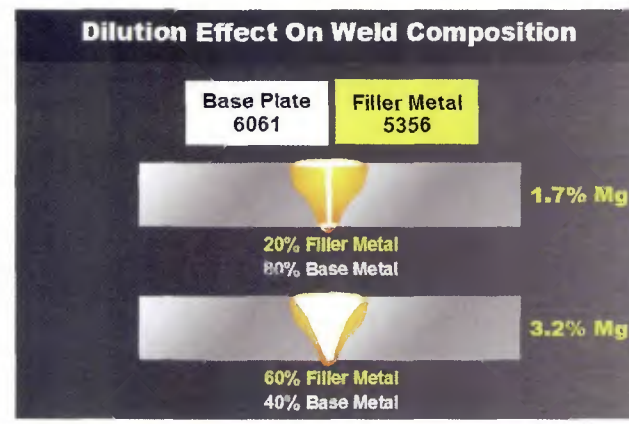

Fig. 2 — Here we see the approximate amount of magnesium that we would expect to be present in two welds of the same base alloy, using the same filler metal, but with two different joint configurations.

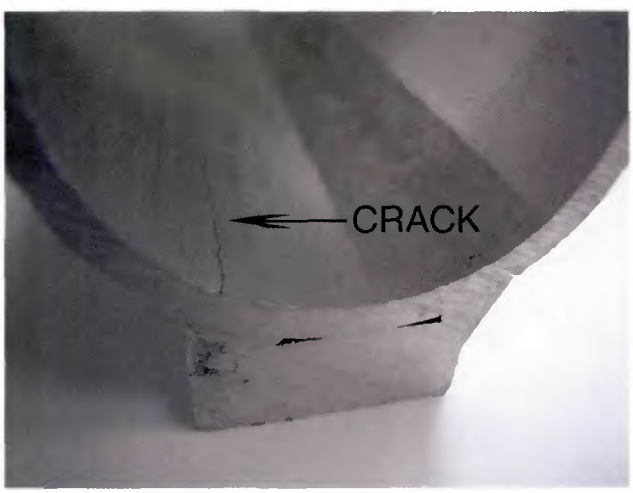

Fig. 3 — A longitudinal crack can be seen in the inside of this pipe on the opposite side of the fillet weld.

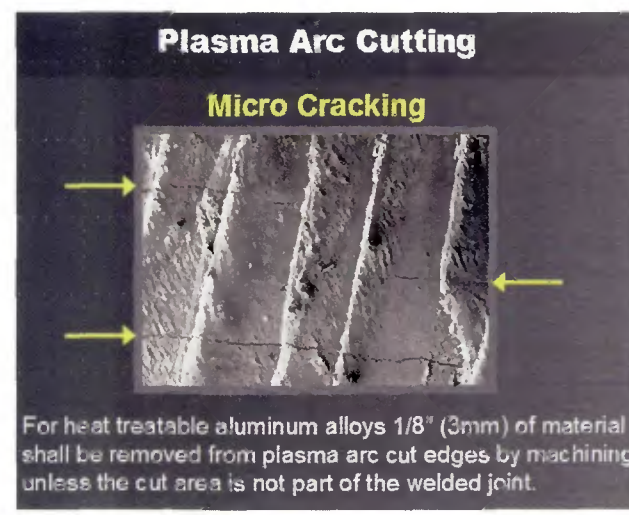

Fig. 4 — Microcracking can develop on the edge of a 6xxx series plate during plasma cutting.

to acceptable levels by the dilution of the weld pool with a filler metal that is of a completely different chemistry than that of the base alloy. This is achieved through the use of excess magnesium (when using the 5xxx series Al-Mg filler metals) or excess silicon (when using the 4xxx series Al-Si filler metals). In the majority of arc welding applications with this base metal, we must add filler material if we want to have consistently crack-free welds.

When welding groove welds in the 6xxx series base alloys with 5xxx series filler metals, we need to ensure that we use joint designs suitable for providing adequate dilution. If we consider the alloying effect of magnesium (Mg) in aluminum, we see that weld crack sensitivity is shown to increase sharply with an increased Mg content up to about 1.5% and then decrease with further Mg additions (Fig. 1 at Al-Mg curve). When welding the 6xxx series base alloy with the 5xxx series filler metals, we need to consider the effect of joint design on base alloy and filler metal dilution. Square groove welds in this alloy can be particularly susceptible to cracking because very little filler metal is mixed with the base metal during welding.

If we examine Fig. 2, "Dilution Effect on Weld Composition," we can see the difference in the amount of Mg in each of the joint designs. The square groove showing dilution of 20% of the 5% Mg found in the 5356 filler metal plus 80% of the 1% Mg found in the 6061 base alloy provides a total Mg content of around 1.7% in the weld. In comparison, the single bevel groove weld configuration has 60% of the 5% Mg in the filler metal and 40% of the 1% Mg found in the base alloy, and provides a much higher Mg content of around 3.2% in the weld.

If we look again at Fig. 1, we can see from the Al-Mg curve that there is a considerable difference in crack sensitivity between a weld with 1.7% Mg and one with 3.2% Mg. The 1.7% Mg is marginally past peak crack sensitivity, and the 3.2% is well beyond that point.

Other potential problems with solidification cracking when welding and cutting the 6xxx series alloys. There are two other areas associated with solidification cracking of the 6xxx series alloys of which we should be aware.

If we apply excessive amounts of heat together with deep weld penetration to a relatively thin material, we can create a situation where partial melting can actually occur that is away from the weld pool. As noted earlier, this "chemistry" is almost certain to crack upon solidification because of the lack of adequate filler metal. Figure 3 shows a 6061-T6 tube with a longitudinal crack in the base metal that is on the opposite side from the weld.

The susceptibility of the 6xxx series alloys to solidification cracking is recognized by AWS D1.2, *Structural Welding Code — Aluminum* (section 4.11.3), which requires that ⅛ in. (3 mm) of material shall be removed from plasma arc cut edges by machining when the cut edge is to be incorporated into the immediate weld area. The heat of the plasma cutting melts this area, and cracking develops upon solidification. Figure 4 shows the edge of a plasma cut 6xxx series plate with solidification cracking.◆

TONY ANDERSON is corporate technical training manager for ESAB North America and coordinates specialized training in aluminum welding technology for AlcoTec Wire Corporation. He is a Senior Member of TWI and a Registered Chartered Engineer. He is chairman of the Aluminum Association Technical Advisory Committee for Welding and holds numerous positions including chairman, vice chairman, and member of various AWS technical committees. Questions may be sent to Mr. Anderson c/o Welding Journal, 550 NW LeJeune Rd., Miami, FL 33126, or via e-mail at tanderson@esab.com.

Mobile Filtration Unit Cleans Up Fumes

The mobile Farr Cart™ fume and dust collector provides powerful filtration in welding workshops and industrial settings. The unit will extract moderate concentrations of smoke and light dust generated by intermittent processes. With its sturdy injection-molded plastic construction, large rubber wheels, and slim design, the unit offers high mobility and ease of use, even where space constraints are tight. In addition, environmental benefits include a low noise level and low power consumption. It comes ready to use with no installation required, and the long-life pleated filter can be easily changed in minutes. The handle comes with a 10-ft flexible fume-extraction arm and built-in halogen spotlight in the hood. Accessories include a HEPA safety filter and spark protection device.

Farr Air Pollution Control 100
3505 S. Airport Rd., Jonesboro, AR 72401

Temperature Indicator Gives Accurate Results

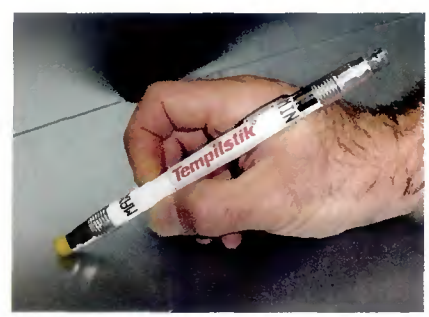

The min-max Tempilstik permits welders and inspectors to obtain accurate and repeatable results in interpass temperature testing. Users will know when the lower-rated mark melts that the workpiece has reached temperature; if the higher-rated mark also melts, the piece is too hot and has to cool. The welder will be able to measure both temperatures by simply flipping the holder. A plastic custom kit of five min/max holders contains sticks with ratings from 100° to 2000°F (40° to 1000°C). Replacement indicator sticks with SKU identification are easily inserted in the durable holders.

Tempil 101
2901 Hamilton Blvd., South Plainfield, NJ 07080

Respiratory System Contains Particle Filter Service Life Indicator

A particle filter service life indicator has been added to the 3M™ Adflo™ respiratory protection system. It is designed to enable users to easily determine when to replace the unit's particle filter. If the user misses a filter change, the Adflo turbo unit has a safety alarm that warns the user when the airflow becomes insufficient. And, if the user keeps working despite the alarm, the unit turns off automatically as an extra safety measure. The indicator is the only change made to the Adflo System. Airflow settings and warnings for low flow are the same as in the previous unit. Also, the company notes the indicator applies only to the particle filter.

3M 102
3M Center, St. Paul, MN 55144-1000

Wires Offer Impact Values at Low Temperatures

As part of its Tri-Mark® brand of filler metals, the company has added high-strength filler metal options to its Metalloy® family of gas-shielded metal cored wires — Metalloy 90, Metalloy 100, and Metalloy 110. Formulated for use with an argon/CO_2 shielding gas mixture, the wires offer Charpy V-notch impact values at temperatures as low as –60°F. Each type of wire is suitable for single or multipass applications and is available in 0.045- and 1/16-in.

— continued on page 19

2007-2008
AWS CONGRESSIONAL FELLOW PROGRAM

I. PREFACE

A. Technology is affecting society to an ever-increasing extent;

B. Public policy issues affecting a broad constituency are increasingly based on technological factors;

C. Informed decisions regarding public policy issues require the input of the engineering profession, among others;

D. The engineering professional constitutes one of the nation's most valuable resources, and

E. This resource should be applied in the public interest to matters having a technological content.

II. POLICY

A. AWS declares that it is the continuing policy of the American Welding Society to
   1. be sensitive to the public's interests;
   2. provide government at all levels with advice on science, engineering and technology matters and
      policies affecting the public interest; and
   3. maintain a climate of understanding and credibility that will foster continuing dialogue with the government.

B. As one measure for furthering its policy, The Board of Directors establishes a Congressional Fellow Program to assist legislators and officials of the Congress in public policy deliberations. Each year, AWS will select a member, in a manner herein described, to serve as Congressional Fellow to assist legislators and other federal officials.

C. AWS prefers that AWS and the Fellow's employer share the compensation and the expenses of the Fellow so that all parties have a financial interest in the program. However, a Fellow may serve with full employer support, provided that she or he is selected in accordance with this policy and she or he adheres to all AWS policies and guidelines of the program. AWS's share shall not exceed the amount annually budgeted. A Fellow may also participate with no employer support but recognizing the limited stipend.

D. Although the Congressional Fellow is sponsored by AWS, the Fellow's primary objective is to provide assistance to Congress.

   In addition, AWS will help in furnishing whatever technical assistance a Congressional Fellow will request of the Society.

E. It is desirable that the Congressional Fellow be familiar with AWS operations and organizational structure in order to obtain assistance promptly and efficiently.

F. Congressional Fellows must comply with the AWS policy on Conflict of Interest and any appropriate rules of ethics of the host federal office.

III. PROCEDURE

A. Solicitation of applicants and Selection of Congressional Fellows

1. AWS will solicit applicants through appropriate means, including letters to companies, announcements in the *Welding Journal*, and appeals to the AWS leadership to identify candidates.

2. The AWS Government Affairs Liaison Committee shall
   a. Review applications;
   b. Interview highly marked applicants;
   c. Identify the best qualified among these for possible selection as a Congressional Fellow;
   d. Forward list of recommendations for the AWS Congressional Fellows for final selection and approval.

3. Individuals chosen to be Congressional Fellow(s) will be assisted by the AWS Washington Government Affairs Office in his or her placement with the staff of a Representative, Senator or a congressional committee.

4. The selection of the Congressional Fellow will be announced by the President of AWS.

B. Requirements

The requirements for the Congressional Fellow Program are as follows:

1. A Congressional Fellow's term shall be twelve months, beginning in September.

2. The Government Affairs Liaison Committee shall select the Fellow(s) using objective selection criteria, including a candidate's application, to determine a candidate's ability to communicate both orally and in written form, and such other attributes as the committee deems necessary for a candidate who will represent the welding profession.

3. Sex, creed, race, ethnic background and political affiliation are expressly excluded as selection criteria for Congressional Fellows.

4. Candidates shall hold at least the AWS grade of Member prior to submitting an application for Congressional Fellow.

5. Candidates shall be citizens of the United States of America.

Deadline for Receiving Applications is March 16, 2007.

For an application form, contact:
Richard Depue
Director, Education and Government Advocacy
American Welding Society
1-800-443-9353, Ext. 237
e-mail: *rdepue@aws.org*

American Welding Society
550 N.W. LeJeune Rd.,
Miami, Florida 33126

— continued from page 16

diameters. In addition, they offer good bead appearance with minimal spatter and wetting action, along with the ability to bridge part gaps without melt-through.

Hobart Brothers Co. **103**
101 Trade Square East, Troy, OH 45373

Environmental Control Booth Helps Contain Dust

The company has designed an industrial control booth to help contain dust in the industrial workplace. The system incorporates a three-stage media-style filtration system, powered by an electrical

motor and Class 1 or 2 blower package. Three standard sizes are available — 6, 10, and 20 ft widths. The booth housing is modular in design with acoustical sound control. The air filtration module also has forklift slips and an airflow range from 4500 to 15,000 ft^3/min. The outer cabinet shell is manufactured using a recycled polyethylene plastic. The booth systems do not require use of compressed air and have a low energy consumption rate.

Industrial Maid LLC **104**
351 S. 12th Rd., Cortland, NE 68331

Pressure Washers Available in Many Models

There are 16 PHWS industrial pressure washer models with cleaning power that ranges from 2.5 to 4.8 gal/min and

from 1000 to 3000 lb/in.^{2} of pressure. They all use diesel or heating oil to heat the water, and the models operate off a variety of electrical configurations. The washers also feature the company's industrial, high-pressure pump. Features include the following: the company's cold-rolled Schedule 80 Duracoil with a five-year warranty; spring-loaded, insulated trigger gun with variable pressure wand for remote operation of the spray, plus remote application of the soap; detergent-injection system; and 50 ft of wire-braid Tuff-Skin hose rated for up to 5800 lb/in.^{2}

Landa Water Cleaning Systems **106**
4275 NW Pacific Rim Blvd., Camas, WA 98607

Motorized Curtain Useful for Robotic Welding Areas

The Gortite® NT automated weld curtain features a custom engineered

frame with programmable acceleration, deceleration, and partial opening and closing. The motorized curtain moves up to 2 m per second. The NT drive unit requires no limit switches and has a maintenance-free gearless direct drive. The curtain is useful for robotic welding areas and other automated equipment cells. Software is included for programming the drive.

A & A Mfg. Co., Inc. **105**
2300 S. Calhoun Rd., New Berlin, WI 53151

Winches Maximize Lift Control, Safety

These winch hoists feature self-locking worm gear reduction for positive load

holding and a brake circuit for instant stopping. The B-series motor brake completes a triple brake redundancy system that enhances overall braking power and provides optimum load control for lifting and spotting. Four different models offer 1- to 3-ton lifting and include a one-year warranty on parts and workmanship. The motor is also available separately, and it can be easily installed on the company's existing single-phase winch hoists.

My-te Products, Inc. **107**
9880 E. 30th St., Indianapolis, IN 46229

Clear PVC Reinforced Hose has Smooth Interior

Flexaust® Flexadux® ADC is a medium-weight PVC hose that is reinforced with a spring steel wire helix and features a smooth inner surface to minimize friction loss and enhance air flow

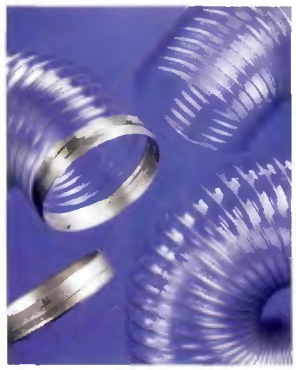

characteristics. Suitable for a variety of positive-pressure and light-vacuum applications, it has a wide pitch with a 9:1 compression ratio for tight bending and easy storage. The hose is offered in sizes from 4 to 18 in. I.D. and standard 25-ft lengths. Additionally, it operates over a 20° to 160°F range and resists chemicals, weathering, and moisture.

The Flexaust Co., Inc. **108**
1510 Armstrong Rd., PO Box 4275, Warsaw, IN 46581-4275

Burnisher Features Electronic Speed Stabilization

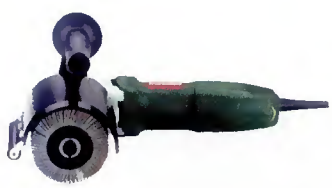

The Model SE 12-115 burnisher features the company's Vario Tacho Constamatic electronic speed stabilization. The burnisher features a durable motor with a winding protection grid that deflects dust and debris. Also, auto-stop carbon brushes protect the motor from damaging arcing. Spiral bevel gears allow for an efficient transfer of power from the motor to the spindle. Safety features include double insulation that protects users against electric shock, and a spindle lock that allows for easy and safe removal and tightening of the accessories. The tool is rated at 10 A, an input rating of 1200 W, and a no-load speed of 900–2810 rpm. It is 13.5 in. long and weighs 6.25 lb.

Metabo Corp. **109**
1231 Wilson Dr., West Chester, PA 19380

Abrasive Belt Tool Deburrs, Polishes

The company has introduced a lightweight, compact version of the Dynafile II abrasive belt machine. This 0.4-hp, 25,000-rpm air tool can grind, deburr, blend, finish, and polish. The compact, low-profile housing allows for easy access in tight spots. The grinding head pivots 360 deg for additional flexibility. Also, the tool features a 7-deg offset handle for added hand comfort and control. It accepts contact arms for 18-in.-long belts in widths from ⅛–¾ in. wide. A pop-off belt guard for quick abrasive belt change is included.

Dynabrade, Inc. **110**
8989 Sheridan Dr., Clarence, NY 14031-1490

GTAW Torch Offers Precision Performance

The patented WP-50 air-cooled torch is rated at 60% duty cycle up to 50 A. The

— *continued on page 69*

AWS Foundation Celebrates a Banner Year

Record-breaking scholarships and donations make 2006 the Foundation's best year ever

When the brand-new Foundation Capital Campaign — "Welding for the Strength of America" — surpassed $1 million in donations, founding donor Ron Pierce said, "Today, our dream has been realized."

Welding for the Strength of America
The Campaign for the American Welding Society

In 2006, the AWS Foundation, along with Section support, surpassed $360,000 in scholarship and fellowship funding, serving over 290 students – the most ever. The Foundation also launched its first capital campaign, with the theme "Welding for the Strength of America."

As of November, the campaign had raised $1.1 million, from the following donors.

$100,000 Donation by Joyce and Ron Pierce

When the capital campaign surpassed $1 million, Ron Pierce, chairman of the AWS Foundation and AWS past president said, "When my wife and I pledged $100,000 to launch this capital campaign just a few months ago, our vision was that others would step up to initiate efforts to have a powerful impact on the future. Today, our dream has been realized." At the time of the gift, Sam Gentry, executive director of the Foundation said, "Ron and Joyce Pierce have always been major givers and supporters of the scholarship efforts of the Foundation. With this additional pledge and financial support of the capital campaign it further illustrates their leadership and vision."

$1,000,000 Donation by Miller Electric Mfg. Co. and Hobart Brothers to Create the American Welding Society Welder WorkForce Development Program

The million dollar gift by Miller Electric and Hobart Brothers is the largest gift ever received by the Foundation. It establishes a fund that the "founding donors" are encouraging others to participate in and to assist in addressing specific business needs for welder workforce development. Bruce Albrecht, AWS board member and Foundation Trustee said, "It is the expectation of Miller and Hobart Brothers for this gift to serve as a catalyst for other welding-related companies to support the cause."

Miller Electric President Mike Weller said, "Miller was the first corporate sponsor of the AWS Foundation when it was formed in 1989 to provide scholarships to welding students, and we continue to fund two AWS welding engineering scholarships, as well as the World Skills Competition Scholarship. We are proud to make yet another commitment to the future of welding in North America."

Sundaram Nagarajan, Hobart Brothers group vice president, said, "Our industry must support the efforts that AWS has undertaken. We are extremely proud to be the founding sponsor of this program, but it must be an effort of the entire welding industry to address the critical shortage of welders."

Sam Gentry, executive director of the Foundation said, "We hope this unprecedented donation will encourage other industry partners to join Miller and Hobart Brothers to help us build a stronger welding workforce for America."

The Mission of the AWS Foundation:

To meet the needs for education and research in the field of welding and related joining technologies.

We greatly appreciate the hundreds of individuals and companies who support the industry's future by contributing to the Foundation's educational programs, which provide scholarships and fellowships to students pursuing a career within welding or related materials joining sciences.

Services and Programs Offered by the AWS Foundation

National Scholarship Program
Howard E. and Wilma J. Adkins Memorial Scholarship
Airgas–Jerry Baker Scholarship
Airgas–Terry Jarvis Memorial Scholarship
Arsham Amirikian Engineering Scholarship
Jack R. Barckhoff Welding Management Scholarships
Edward J. Brady Memorial Scholarship
William A. and Ann M. Brothers Scholarship
Donald F. Hastings Scholarship
Donald and Shirley Hastings Scholarship
William B. Howell Memorial Scholarship
Hypertherm–International HyTech Leadership Scholarship
ITW Welding Companies Scholarships
John C. Lincoln Memorial Scholarship
Matsuo Bridge Company, Ltd. of Japan Scholarship
Miller Electric World Skills Competition Scholarship
Robert L. Peaslee–Detroit Brazing and Soldering Division Scholarship
Praxair International Scholarship
Resistance Welder Manufacturers Association Scholarship
Jerry Robinson – Inweld Corporation Scholarship
James A. Turner, Jr. Memorial Scholarship

Section Named Scholarship
Amos and Marilyn Winsand–Detroit Section Named Scholarship
Ronald C. and Joyce Pierce–Mobile Section Named Scholarship

Scholarship Programs in Development
Shirley Bollinger–District 3 Named Scholarship
Donald and Jean Cleveland–Willamette Valley Scholarship
Gold Collar Scholarship
Robert L. O'Brien Memorial Scholarship
Ted B. Jefferson Scholarship
Thermadyne Industries Scholarship

AWS International Scholarship

Graduate Research Fellowships
Glenn J. Gibson Fellowship
Miller Electric Fellowship
AWS Fellowships (3)

History of Welding CD
This CD provides a story of welding history, stressing the importance of welding and the critical shortage of skilled manpower.

Educational Tools
Engineering Your Future
Welding So Hot It's Cool Video/CD
Hot Careers in Welding Video

Miller Electric Mfg. Co. – Sponsor of the World Skills Competition Scholarship
The Miller Electric Manufacturing Company established this $40,000 scholarship in 1995 to recognize and provide financial assistance to contestants representing the United States in the World Skills Competition. To qualify, an applicant must be a SkillsUSA state gold medalist, then advance through the SkillsUSA Championships to compete in the Weld Off at the AWS Welding Show, and then win the biennial U.S. Open Weld Trials at the SkillUSA Championship the following year. Past recipients competing in the World Skills Competition are:

2005	Joel Stanley II
2003	Miles Tilley
2001	Dien Tran
1999	Ray Connolly
1997	Glen Kay III
1995	Branden Muehlbrandt
1993	Nick Peterson*
1991	Robert Pope*

*1991 and 1993 recipients received alternate scholarship funds, which were prior to the start of the Miller Electric Mfg. Co. Scholarship.

We Would Like to Thank the Following Major Donors Who Have Supported the Foundation:

Individuals
Wilma J. Adkins
Osama Al-Erhayem
Richard Amirikian
Richard L. Arn
Roman F. Arnoldy
Jack R. Barckhoff
Hil J. Bax
D. Fred Bovie
William A. and Ann M. Brothers
Alan Christopherson
Joseph M. and Debbie A. Cilli
Donald E. and Jean Cleveland
Jack and Jo Dammann
Mr. and Mrs. J. F. Dammann
Louis DeFreitas
Frank G. DeLaurier
William T. DeLong
Estate of Esther Baginsky
Richard D. French
Glenn J. Gibson
Joyce E. Harrison
Donald F. and Shirley Hastings
Robb F. Howell
Jeffrey R. Hufsey
Joseph R. Johnson
Deborah H. Kurd
J. J. McLaughlin
L. William and Judy Myers
Robert and Annette O'Brien
Robert L. Peaslee
Joyce and Ronald C. Pierce
Jerome L. Robinson
Robert and Mitzie Roediger
Sandy and Ray W. Shook
Myron and Ginny Stepath
Charley A. Stoody
R. D. Thomas, Jr.
James A. Turner, Jr.
Gerald and Christine Uttrachi
Nelson Wall
Amos O. and Marilyn Winsand
Nannette Zapata

Corporations
Airgas
Air Liquide America Corporation
Air Products and Chemicals, Inc.
American Welding Society
Caterpillar, Inc.
Chemalloy Company, Inc.
C-K Worldwide
Cor-Met, Inc.
ESAB Welding & Cutting Products
Edison Welding Institute
Eutetic Castolin
The Fibre-Metal Products Company
Gases and Welding Distributors Association
Gibson Tube, Inc.
Malcolm T. Gilliland, Inc.
Gullco International, Inc.
Harris Calorific, Inc.
High Purity Gas
Hobart Brothers Company
Corex
McKay Welding Products
Tri-Mark
Hypertherm, Inc.
Illinois Tool Works Companies
Independent Can Company
Inweld Corporation
The Irene & George A. Davis Foundation
J. W. Harris Company, Inc.
Kirk Foundation
Kobelco Welding of America, Inc.
The Lincoln Electric Company
The Lincoln Electric Foundation
MK Products, Inc.
Matsuo Bridge Co. Ltd.
Miller Electric Mfg. Co.
Mountain Enterprises, Inc.
National Electric Mfg. Association
National Welders Supply Company
Navy Joining Center
NORCO, Inc.
ORS NASCO, Inc.
OXO Welding Equipment Company
Pferd, Inc.
Praxair Distribution, Inc.
Roberts Oxygen Company, Inc.
RWMA
Saf-T-Cart
Select-Arc, Inc.
SESCO
Shawnee Steel & Welding, Inc.
Shell Chemical LP – WTC
Thermadyne Holdings Corporation
Trinity Industries, Inc.
Uvex Safety, Inc.
Webster, Chamberlain & Bean
Welding Engineering Supply Co., Inc.
Weldstar Company
Wolverine Bronze Company

Foundation, Inc.
Building Welding's Future through Education

Welding NASCAR's New Materials

BY **DENNIS KLINGMAN**

The move to improve safety has also helped drive the use of newer materials and new welding technologies

NASCAR® purists prefer that the sport remain focused on the skills of the drivers and less on the advancement of technology. In an effort to maintain a level playing field, many contend that emerging technologies be left to racing circuits that feature the cars.

Ironically, the move to further improve NASCAR's safety has ushered in a host of new technologies, many of which unintentionally also boost performance. Where to draw the line, however, is a debate likely to continue for years.

With that, NASCAR strictly regulates which materials can be used for each specific component. Balancing safety and performance, technology unavoidably advances, following closely in the footsteps of Formula One™ racing and the aerospace industry.

However, while the issue remains in dispute, race team fabricators nonetheless work to stay ahead of approaching technologies. On the forefront of the latest debate are materials such as Inconel® 625 and chrome-moly 4130. Both are finding their way onto more and more racing "stock cars" every day, as the sport's ruling body acknowledges the need and grants permission.

Over the past few years, the trend in materials has moved some NASCAR components from carbon steel to stainless steel. Today, that trend is shifting again from stainless steel to Inconel, and many race shop welders are trying their hand at titanium in anticipation that that, too, will be allowed on selected car components. Currently, titanium is limited to a handful of engine parts that are rarely welded, but race shop welders anticipate a widening use that could be only a few years away.

New Materials

Inconel, a trademarked name for a family of high-strength nickel-based alloys, exhibits exceptional anticorrosion and heat-resistant properties. The nickel-based alloys are, in many ways, a vast improvement over stainless steel.

Inconel has been used in a variety of high-tech applications, such as military vehicle exhaust ducts, submarine propulsion motors, underwater cables, heat exchangers, and gas turbine shroud rings.

Inconel also has been used in Formula One and Champ Car exhaust systems for years. But, more recently, several Nextel Cup® racing teams have incorporated Inconel 625 for ultralight and highly durable exhaust systems and headers.

Race teams today continually push the limits of ground clearance restrictions in an effort to lower their cars' center of

DENNIS KLINGMAN (dennis_klingman@lincolnelectric.com) *is manager of Technical Training, The Lincoln Electric Co., Cleveland, Ohio. He teaches an annual class on advanced motorsport welding to some of the top teams in NASCAR, including Joe Gibbs Racing, Chip Ganassi Racing, and Penske South Racing.*

A ropey overly convex appearance on high-alloy materials often signals too little heat input and the potential for weld failure.

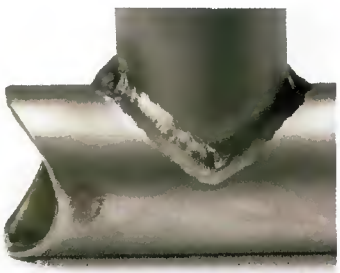

Here, the appearance is improved over cold welds but an overly convex bead profile means too much weld metal may be present.

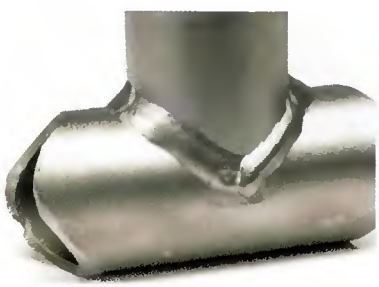

Note the flat bead face and smooth bead appearance with good wetting and wash-in at the weld edges.

gravity to enhance acrodynamics and handling. In doing so, they often abuse the car's undercarriage exhaust systems, which can scrape along the track during hard turns and throw a plume of sparks behind the car.

Because of this, teams are sometimes forced to repair or even replace exhaust systems. Using Inconel can actually extend the life of exhausts and limit needed repairs.

As an added benefit, Inconel's higher strength and often thinner wall thickness has actually yielded increased horsepower for some Nextel Cup cars. Inconel, used in exhaust tubing, has also proven to resist vibration and withstand thermal

Top Ten Facts about Gas Tungsten Arc Welding Chrome-Moly 4130

Yes, you can gas tungsten arc (GTA) weld 4130 tubing up to 0.120-in. wall thickness easily with the techniques and procedures described below. These procedures apply to typical sporting applications such as experimental airplanes, race car frames, roll cages, go-carts, bicycles, and motorcycle frames. The suitability of these techniques and procedures must be evaluated for your specific application.

Q: Can I weld 4130 using the GTAW process?

A: Yes, 4130 chrome-moly has been GTA welded in the aerospace and aircraft industries for years. As with all welding, proper procedures and techniques must be followed.

Q: Do I need to preheat?

A: Thin-wall tubing less than 0.120-in. does not typically require the normal 300–400°F preheat to obtain acceptable results. However, tubing should be around 70°F or above before welding.

Q: What filler material should I use?

A: Although there are several good filler materials, ER80S-D2 is one you should consider. This material is capable of producing welds that approximate the strength of 4130. ER70S-2 is an acceptable alternative to ER80S-D2, as is ER70S-6, although weld strength will be slightly lower.

Q: When I use ER70S-2 filler material, do I sacrifice strength for elongation?

A: Yes. The filler material, when diluted with the base material, will typically undermatch the 4130. However, with the proper joint design, such as cluster or gusset, the cross-sectional area and linear inches of weld can compensate for the reduced weld deposit strength.

Q: Why is 4130 filler metal not recommended?

A: 4130 filler typically is used for applications where the weld will be heat treated. Due to its higher hardness and reduced elongation, it is not recommended for sporting applications such as experimental airplanes, race car frames, and roll cages.

Q: Can I weld 4130 using any other filler materials?

A: Some fabricators prefer austenitic stainless steel filler metals to weld 4130 tubing. This is acceptable provided 310 or 312 stainless steel filler metals are used. Other stainless steel filler metals can cause cracking. Stainless steel filler material is typically more expensive.

Q: Do I need to heat treat (stress relieve) 4130 after welding?

A: Thin wall tubing normally does not require stress relief. For parts thicker than 0.120 in., stress relieving is recommended. 1100°F is the optimum temperature for tubing applications. An oxyacetylene torch with neutral flame can be used. It should be oscillated to avoid hot spots.

Q: Do I need to preclean 4130 material?

A: Remove surface scale and oils with mild abrasives and acetone. Wipe to remove all oils and lubricants. All burrs should be removed with a hand scraper or deburring tool. Better welding results with clean materials.

Q: Do I need to backpurge 4130 material?

A: Backpurging is not normally necessary, although some fabricators do. It will not hurt the weld and may improve the root pass of some welds.

Q: Should I quench the metal after I finish welding?

A: Absolutely not. Rapid quenching of the metal will create problems such as cracking and lamellar tearing. Always allow the weld to slow cool.

Fabricators at Chip Ganassi Racing use GTAW to repair and customize Nextel Cup exhaust components.

cycle heating and cooling better than other materials.

Chrome-moly is an abbreviation for chromium-molybdenum steel. It comprises a range of low-alloy steels that have been used for things such as bicycle frames and race car roll cages.

Chrome-moly has the advantage of high tensile strength. It is easily welded, and is considerably stronger and more durable than standard 1020 steel tubing.

Chrome-moly has found its way onto some NASCAR suspension systems and chassis extensions, where heavier, lower tensile strength carbon steel was previously used. Its use in racing is growing each year.

Titanium is a strong, lustrous, and corrosion-resistant metal. It is most commonly alloyed with vanadium and aluminum. NASCAR currently allows titanium only for a limited number of engine parts, but race teams anticipate a wider use is not far off.

Titanium is noted for its high strength-to-weight ratio. It is a light, strong metal with low density, which when pure is quite ductile and relatively easy to work.

Titanium 6Al4V grade has a tensile strength equal to that of high-strength low-alloy steels, but weighs 33% less. When compared to 6061-T6 aluminum alloy, titanium exhibits a higher strength-to-weight ratio, making it ideal for a number of race car components.

A welder uses an inverter-based gas tungsten arc welding machine on exhaust headers at Penske South Racing.

Welding Steel and Chrome-Moly Steel

The massive steel cage-like chassis structures of NASCAR cars are made of carbon steel and generally are welded using gas metal arc welding (GMAW). However, many of the cars' fabricated components are meticulously gas tungsten arc (GTA) welded.

Weight-to-strength ratios are a primary concern in race car welding. So the goal for both GMA and GTA welding is to create a strong, deeply penetrating weld. Top team fabricators pride themselves on being able to produce a proper slightly convex bead profile. Overly convex bead profiles are generally unacceptable and are considered to add unnecessary weight.

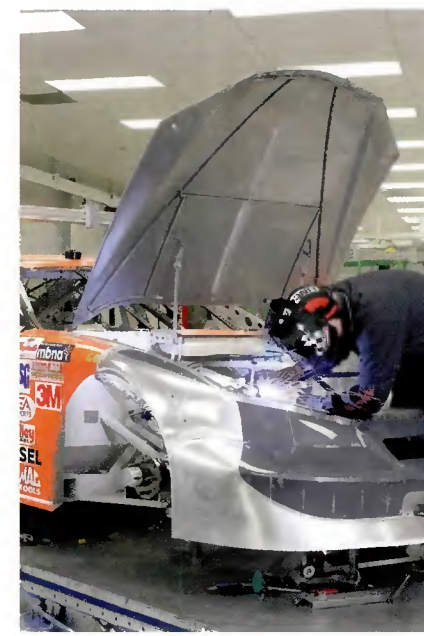

Chrome-moly is now being used in some chassis extension components at Joe Gibbs Racing.

Welding chrome-moly is very similar to welding carbon steel. Team fabricators have come to learn that the techniques, practices, and rules of thumb common in industrial welding on thicker chrome-moly material often do not apply to the thinner gauge welding typically performed on racing components.

Textbook guidelines often assume that the material is thicker than 0.120 in., and they recommend preheating chrome-moly from 300° to 400°F as well as postweld heat treatment. However, since racing components are typically fabricated from thinner material, preheating and postweld heat treatment is not typically necessary.

Some top race welders purge their tubing applications when welding on chrome-moly, in order to preserve or enhance the material's mechanical properties.

Inconel 625 is a more difficult material to weld than chrome-moly or standard steel. First, the Inconel pool does not reach the same level of fluidity as when welding on carbon steel. The pool is more difficult to manipulate. It is less forgiving of poor fitup, and it can be more difficult to maneuver across gaps.

Thus, certain precautions are recommended. Proper shielding on the front and back sides of the welds in any nickel-based alloy is very important to avoid porosity and reduced ductility. An Inconel tube must be purged of its inside air and replaced with argon before welding.

Tight fitup is essential. Gaps require more welding manipulation and present an increased chance for error. Because of this, team fabricators often lay an increased number of tack welds to improve fitup. Careful, thorough cleaning of the material avoids contamination, porosity, and subsequent cracking. Nextel Cup welders use 100% argon shielding and ERNiCrMo-3 filler metal (AWS specification A5.14) for Inconel 625.

Today, NASCAR teams either purchase prefabricated Inconel headers or build them themselves. Regardless of the arrangement, all teams that use Inconel headers are required to weld them in some way, whether to simply install them or to repair or modify them.

A set of Inconel headers can cost $5000 to $7000, so it is important that any welding work is done correctly the first time. However, the thinness of the material — generally about 0.035 in. or less — allows welders just one pass, and that weld must be carefully performed. There are no subsequent passes that can compensate for inferior workmanship on the first pass. Everything must be perfect. Poor welds would require cutting the section out and rewelding one or more welds to fit in a replacement section to complete the fabrication or repair.

Titanium and most titanium alloys can be welded using GMAW or GTAW. However, with the racing focus on code-quality welding on thin materials, GTAW is almost exclusively preferred. Operators will find that a titanium pool has good fluidity compared to Inconel 625.

Welding titanium requires thorough surface cleaning and the correct use of shielding gas surrounding the entire weld as molten titanium reacts readily with oxygen, nitrogen, and hydrogen. Exposure to these elements or surface contaminants can adversely affect the weld and lead to cracking. Heat-affected areas must be shielded until temperatures cool below 600°F. Shielding a titanium pool with 100% argon is preferred, but some helium or argon/helium mixtures are also effective. Auxiliary purging systems and very large gas cups are often used.

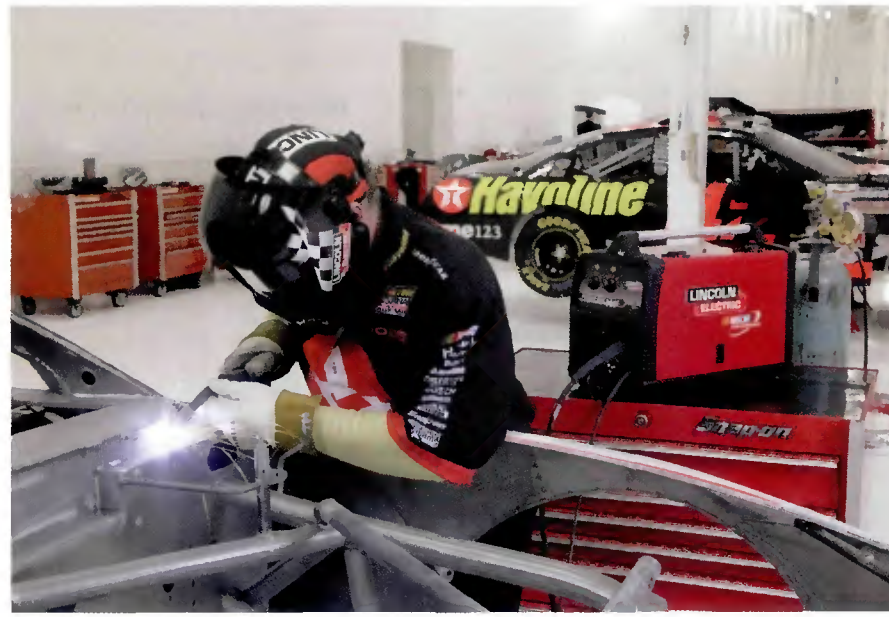

Chip Ganassi Racing fabricators evaluating new gas metal arc welding machines.

Note that titanium cannot be welded to most other metals because brittle metallic compounds will form that often lead to cracking.

Welding Technology

Many NASCAR rules are designed to help race teams maintain relatively low operating costs while simultaneously maximizing driver safety. The average NASCAR car today costs roughly $185,000, which is about the same price for the transmission on a Formula One car.

With a NASCAR focus on controlling costs and maintaining a competitive environment for the team while continually increasing driver safety, the teams increasingly seek and benefit from advancements in technology.

Introducing new materials such as titanium and Inconel was often considered impractical in the past because welding such materials was difficult and required very skilled craftspeople, additional time,

Elite NASCAR fabricators practice hands-on skills with instruction from specialized welding instructors at the Lincoln Electric Advanced Motorsports Seminar.

and more money.

Today, however, welding these new materials has become considerably more commonplace with recent advancements in welding equipment, furthering NASCAR's likelihood to allow them on race cars.

Inverter-Based Welding Power Sources

In particular, inverter-based welding power source technology has become prevalent, allowing operators to set software-driven welding parameters to a specific material and application. For example, welding waveform programs can be developed to control heat input, penetration, and other arc characteristics on Inconel or titanium on a specific thickness, with a particular shielding gas or a specific joint design.

The advantages of chrome-moly steel include high tensile strength, good weldability, and durability.

Inverter-based welding power sources operate at frequencies above 20 kHz, as compared to traditional power sources, which operate at a line frequency of 50 or 60 Hz. Some inverter-based system advantages include smaller, therefore lighter, components such as chokes and transformers, a higher electrical efficiency, and a faster response to the welding arc.

Inverter power sources were first introduced to the industry in the early 1980s. The initial attraction was their small size and portability. Today, inverters are designed for many different arc welding processes, including shielded metal arc, gas tungsten arc, flux cored arc, and submerged arc welding.

Inverters today provide optimum arc characteristics for very specific applications, such as welding thin Inconel — important for race welders. Many inverter models are software programmable to allow operators to manipulate the welding output characteristics. Inverters from The Lincoln Electric Co. are programmed with Waveform Control Technology™, an embedded software program that allows the ability to customize the waveform output. Operators can choose from a predefined set of programs and manipulate the parameters of that program to best fit a given application.

Winning Welds

NASCAR team fabricators frequently review new welding technology. Many relentlessly seek new ways to improve the quality of their work and deliver innovations in welding practices or techniques uniquely adapted to high-performance race car fabrication.

For the vast majority of NASCAR welders, safety is the No. 1 concern, knowing that their welds must hold up to 200 mph turns, high G-forces, and punishing collisions. Team fabricators work hard to build these machines by hand with the highest quality, because they know their driver's life is on the line every time they climb in to practice or race.

In NASCAR, the weld shops are as competitive as the drivers and the pit crews who run the races each Sunday. They, too, weld to win, and as safety drives the technological advancement of NASCAR, it is certain that performance will follow close behind. ♦

Impact of Digital Technology on Stud Welding

Stud welding advances from the analog world to the digital

Historians estimate that humans have been experimenting with and perfecting welding techniques for more than 5000 years. In the ancient world, the mastery of welding and other forms of metalworking was equated with success in the marketplace, even political power.

While its importance in the marketplace did not change much over the centuries, the welding process did. In the 1940s, a welder with a covered electrode, like many welders before him, stuck his electrode into a weld pool, but this time the welder had the idea of putting threads onto the electrode — and stud welding was born.

During the 1940s, the immediate application of stud welding was for the Navy to help install wood decking onto naval vessels. During WWII, this helped to vastly speed up production of ships for the U.S. Navy. The method was crude with the operators controlling the arc timing with their thumbs, but it was vastly superior to welding the deck retention fasteners by hand.

Since this initial application of stud welding, it has continued to evolve.

The Stud Welding Process

In the stud welding process, a metal stud is joined to a metal workpiece by heating both parts with an arc. Unlike other fastening processes, stud welding attaches the fastener to the workpiece without marring or requiring access to the other side. The benefits to this type of welding include the following:

- A strong weld that will not break, loosen, or weaken
- Faster, easier assembly with greater productivity
- Single-sided fastening
- Increased cosmetic appeal without marring the other side
- Fewer manufacturing steps saves time and money
- Greater design freedom.

Going Digital

During the 1990s, a major stud welding company, based in northwestern Chicago, designed and developed the first digital welding equipment, significantly changing the industry.

With the introduction of digital stud welding equipment into the marketplace, the industry has seen increases in productivity and reliability. Why is this? First of all, digital stud welding equipment uses microprocessors and/or digital signal processing to monitor and control the weld profile in narrow time increments (miliseconds). In traditional analog power controllers, electrical component tolerance is such that typical systems need wider control limits to make the system economical. Much of the equipment delivers power to ±20% of the desired output.

With digital back-end control, analog functions have been converted into software; therefore, component tolerance is not a significant factor, and power is typically controlled to ±2% or better. This makes the welding process more consistent, repeatable, and predictable over time. Additionally, it is more economical to outfit digital controls with advanced features such as weld setup memory, weld counters, automatic profile adjustments, and multiple weld outputs.

The Drawn Arc Stud Welding Process

All of the above technological advances serve the unique needs of drawn arc stud welding. Drawn arc stud welding provides welding success under a broad range of conditions. Producing one-sided, full cross-sectional welds, the process

Information provided by Image Industries, Inc. (www.imageindustries.com), *Huntley, Ill.*

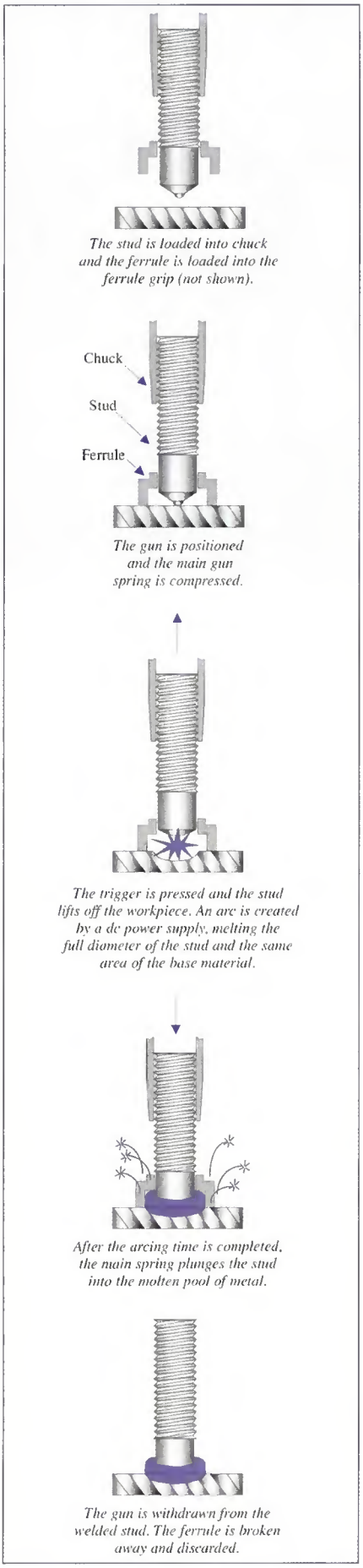

The stud is loaded into chuck and the ferrule is loaded into the ferrule grip (not shown).

The gun is positioned and the main gun spring is compressed.

The trigger is pressed and the stud lifts off the workpiece. An arc is created by a dc power supply, melting the full diameter of the stud and the same area of the base material.

After the arcing time is completed, the main spring plunges the stud into the molten pool of metal.

The gun is withdrawn from the welded stud. The ferrule is broken away and discarded.

Fig. 1 — Main steps in drawn arc stud welding.

forms a weld that is stronger than the surrounding metal. Drawn arc welds offer structural integrity, productivity, and leak and corrosion resistance. They will not break, loosen, or weaken over time.

Drawn arc stud welding can produce welds in as little as 0.06 seconds for base metals of 0.048 in. (1.2 mm) or thicker. The process has good penetration, and it welds almost any size or configuration of metal stud to a workpiece.

The drawn arc process utilizes a DC power supply to create the arc, a stud welding tool, and metal fasteners. There are three common processes within drawn arc stud welding: flux and ferrule, short cycle arc, and gas arc.

Flux and Ferrule

In drawn arc stud welding, the stud is loaded into the stud gun chuck, and a ferrule (ceramic shield that encases the molten metal) is placed over the end. The gun is placed against the work position, and the trigger is pressed. The DC power supply sends a signal that energizes the weld tool's internal lift mechanism, lifting the stud and drawing a pilot arc. As the stud and base metal are joined, the metal begins to solidify and the weld is created. The gun is lifted and the ferrule is easily discarded.

Flux, embedded in the stud, cleanses the atmosphere during the weld. During arcing, the flux is vaporized and combines with the contaminating elements in the air to keep the weld zone clean at all times. A graphic representation of the drawn arc process is shown in Fig. 1.

Additional assembly steps in the process such as punching, drilling, tapping, and riveting are eliminated, making drawn arc stud welding even more efficient.

Short Cycle Arc Stud Welding

Short cycle arc stud welding uses no flux load or ferrule and offers the shortest welding times of all the drawn arc stud welding methods. While it's suitable for high-volume, lower-strength applications, it can produce porous welds and should be selected when speed and cost are a priority over strength.

Gas Arc Stud Welding

The gas arc method uses inert shielding gas with no flux or ferrule, making it easier to automate, but it provides less fillet control and less depth of penetration in comparison with the flux and ferrule process. In gas arc welding, a spark shield delivers the gas. The stud is loaded, and the gun is positioned for welding. When the user pulls the trigger, shielding gas (preflow) floods the welding zone. The stud is lifted, and the arc is generated. While the stud remains lifted, the arc melts the stud and base metal. Once the arc time is complete, the stud is plunged into the molten pool. The gas continues to flow until the molten metal cools. The gun can then be removed. Since no ferrule is used, this process lends itself well to automation and robotics.

Drawn Arc Stud Welding Applications

Today, the drawn arc stud welding process has found extensive use in a wide variety of applications across an array of industries including the following:

- Automotive — heat shields, power steering, insulation, exhaust systems, lighting systems, hydraulic/brake/fluid lines, electrical wire routing, and trim

- Construction — bridges, buildings, conduit, and piping

- Farm equipment — fenders, brackets, cabs, spreaders, shrouding, thresher teeth, and wiring and hose management

- Highway equipment — cover plates, nonskid devices, wiring, and hose management

- Metal products — barbecue equipment, enclosures, heating/plumbing apparatus, insulation enclosures, HVAC units, and water storage systems

- Industrial — inspection cover plate attachments, enclosures, flow indicators, material handling equipment, and controls

- Power generation and distribution — power transformer tanks and transducers

- Shipbuilding — insulation, wire management, and hatch covers

- Electrical/electronic — electrical enclosures and hydraulic lines.

As valuable as digital innovations are to techniques like drawn arc stud welding, they've proven essential to processes that demand a high level of precision, such as capacitor discharge (CD) stud welding.

The Impact of Digital CD Stud Welding

Applying digital technology to CD welding has yielded several benefits. First, the voltage control is more precise. In other words, the

charge/discharge hysteresis window is smaller with digital controls. This means that the actual weld voltage is more accurate and repeatable.

Digital electronics control the charge profile more precisely via exacting phase control. This means that a larger capacity welding machine can be used with lower amperage building line supplies without tripping any circuit breakers.

Furthermore, in some applications, microprocessor control has allowed the heavy bulky transformer to be eliminated to achieve CD welding power supplies that weigh as little as 10.5 lb with ¼-in. fastener capability.

Most importantly, digital controls have enabled advanced operator safety. In analog systems with a shorted weld SCR, capacitor voltage can be present within the weld tool at any time, endangering the operator. The microprocessor in digital power supplies is able to actively monitor component health and deactivate the power supply completely in the event of critical component failures.

Capacitor Discharge Process Advances

As with drawn arc stud welding, technological advances in the capacitor discharge equipment have basically reinvented the process for lightweight applications. Capacitor discharge, or CD stud welding, is a popular option when appearance is a critical product feature. Using very short weld times, it permits the welding of small-diameter studs to thin, lightweight materials with very little distortion, discoloration, or burning. The weld cycle can be completed in 0.004 to 0.01 s on material as thin as 0.020 in. (0.5 mm). The fast weld times of CD help to minimize heat buildup. Additionally, it allows the welding of dissimilar metals because the weld penetration is so slight that it avoids metallurgical conflicts. Metals typically used in this process include mild steel, stainless steel, and aluminum, as well as brass, tungsten, and copper.

A CD welding system, using a capacitor storage system, delivers a rapid electrical discharge, stud welding tools, and fasteners. Ferrules and flux are not needed.

Two techniques used in the CD method are contact and gap. Both use a specially designed stud with a projection, or ignition tip, on its weld end. The stud tip provides accurate welding time control with repeatable precision.

The quality, productivity, and cost advantages of CD stud welding include

• Attractive appearance with minimal burn. Often important in cosmetic applications, CD stud welding offers appealing one-sided welds with no reverse side dimples.

• Strength in lightweight applications. This method creates a strong, high-quality bond on very lightweight materials that would normally be compromised when using other fastening processes.

• Minimal backside marking. CD stud welding allows backsides to be prepainted without damage to the paint.

Contact CD Stud Welding

During the contact method, the stud is loaded into the gun and positioned in contact with the workpiece. Energy is then discharged instantaneously from capacitors through the stud's projection. Since the size of the ignition tip cannot handle the current density of the capacitor's stored energy, it vaporizes, creating a gap that allows an arc to be formed. As the arc begins to melt the stud and workpiece, the two pieces are forced together, and a weld is produced in milliseconds as the metal cools.

Gap CD Stud Welding

The gap CD stud welding process offers very short weld times with higher current densities when compared with contact CD stud welding. With such quick welding capability, this technique is particularly well suited to cosmetic applications, since it produces very minimal backside marking.

While the contact CD process rests the stud on the workpiece, the stud for the gap process is positioned above it. When the stud is released, it accelerates toward the base metal. When the stud contacts the workpiece, the ignition tip is vaporized and the pieces are melted, then brought together to form the weld. Because the stud starts in motion, the weld times are even faster than those created in the contact process — approximately 0.004 s with peaks of 12,000–15,000 A.

Gap CD stud welding is ideal when welding aluminum or nonferrous alloys, which have an excellent ability to conduct heat. With slower techniques, the base material can draw heat away too fast for a weld to occur, but gap CD welding's fast weld times overcome this phenomenon. The stages of both gap and contact CD stud welding can be found in Fig. 2.

Capacitor Discharge Stud Welding Applications

Capacitor discharge stud welding creates high-integrity welds on the thinnest gauge of materials. Because it provides fast welds on lightweight

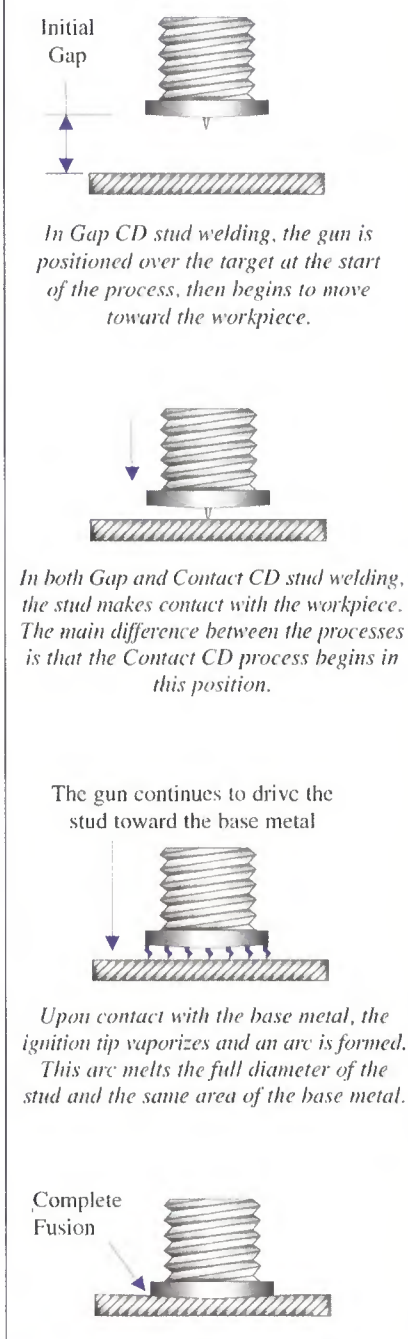

In Gap CD stud welding, the gun is positioned over the target at the start of the process, then begins to move toward the workpiece.

In both Gap and Contact CD stud welding, the stud makes contact with the workpiece. The main difference between the processes is that the Contact CD process begins in this position.

Upon contact with the base metal, the ignition tip vaporizes and an arc is formed. This arc melts the full diameter of the stud and the same area of the base metal.

As the pieces are forced together by spring pressure, weight, gravity, or air pressure, the stud forms a complete bond with the base material.

Fig. 2 — Various steps in gap and contact capacitor discharge stud welding.

Technological advances in the capacitor discharge equipment have basically reinvented the process for lightweight applications.

materials with minimal distortions, popular applications of the CD method include:

- Jewelry — earrings, pins
- Hardware — brackets, cleats, and tool handles
- Cookware — utensils, pots and pans, and handles
- Electrical housewares — electric frying pans, cookers, oven assemblies, and microwave guides
- Electrical/electronic — components, terminals, pumps, motors, communication equipment, and electronic systems
- Doors — commercial doors, escutcheon plates, and insulation.

The Future of Digital Stud Welding

Stud welding is a science and, like all sciences, continues to evolve. We can expect numerous improvements to refine the digital stud welding process. Welding tools will keep getting smaller, lighter, and more adaptable. The precision of welding equipment and the ease of sensor read-outs will increase with each new technological advancement. As a result, the process itself will become faster, easier, and more affordable, putting digital stud welding in the hands of more people and opening still more practical applications for stud welding.◆

WHEN TIME IS OF THE ESSENCE

HOW FAST DO YOU WANT TO WELD A STUD?

How about 0.004 seconds

Eliminate drilling, tapping, punching, riveting, gluing, and screwing.

Stud Welding: Fast • Strong • Durable

Drawn Arc Systems
for Studs up thru 1" diameter

Capacitor Discharge Systems
for Studs up thru 3/8" diameter

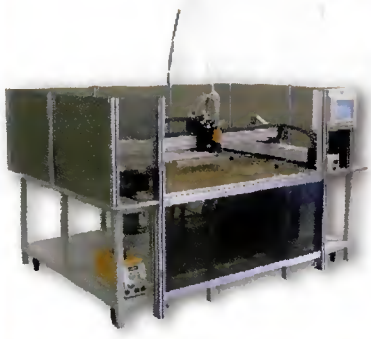

CNC Systems
Automated Machines for
High Volume Applications

Circle No. 25 on Reader Info-Card

KEYSTONE

FASTENING TECHNOLOGIES, INC.

Stud Welding Technology

Systems • Studs • Application Engineering

409 PARKWAY VIEW DRIVE • PITTSBURGH, PA 15205
1-800-659-5972 • 1-412-787-5970 • FAX: 1-412-788-6627
Web: www.keystonefastening.com • E-mail: info@keystonefastening.com

As one of the premier race teams in NASCAR, Dale Earnhardt, Inc., serves as the benchmark for success, from racing strategy right down to the quality welding equipment used in the shop and at the track.

Taking Welding to the Track

NASCAR® teams are turning to lightweight, portable gas metal arc welding machines to cut weight on their transporters

BY ANDY WEYENBERG

*ANDY WEYENBERG is motorsports manager, Miller Electric Mfg. Co. (*www.millerwelds.com*), Appleton, Wis.*

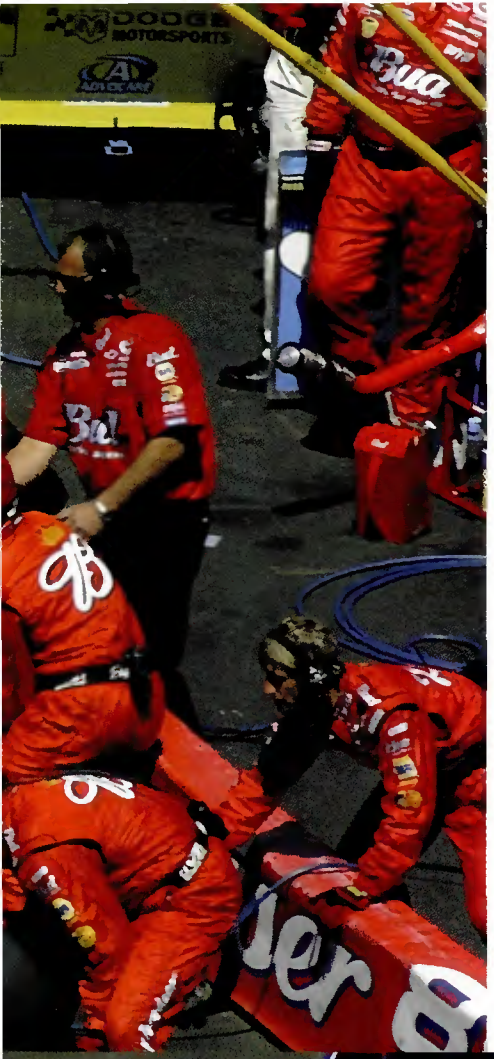

Nextel Cup teams are continually looking for ways to cut the weight on their transporters and to save space in the shop. On average, it takes two days for a NASCAR® team to pack for a race. It's no small task for Hendricks Motorsports transport driver Kirk George to juggle tools and parts in a never-ending battle to reduce the weight on his transporter. "We have to restock and reload everything each week," George said. "Sometimes equipment and parts need to be sent by an external company because we are overweight and can't fit everything in." Every transporter has a legal weight limit of 80,000 lb while traveling on the interstate system, so NASCAR fabricators and transport drivers value lighter tools, such as portable gas metal arc welding (GMAW) machines that offer quality performance.

Once they get to the race, Hendrick fabricators encounter a variety of damage that needs to be repaired as quickly as possible. In one instance, Jimmie Johnson (#48) experienced a crash during a Talladega race that tore the nose off his car. Back in the pits, four crewmembers removed the mangled tubing and welded a whole new assembly back on within five minutes, allowing Johnson to continue on with the race.

The front-end, the most commonly damaged portion of the car, requires fabricators to weld a wide range of material thicknesses when they encounter a crash like that one. For example, the fender brace tube measures between 0.040 and 0.060 in., while frame horns measure as thick as 0.120. The fabrication crew needs to be able to repair damaged components as quickly as possible, with the crew's time measured in number of "laps down," or the number of laps that have passed since the car has entered the pit area, and portable GMAW machines help with that job — Fig. 1.

Driving the Welds at Dale Earnhardt, Inc.

Likewise, fabricators at Dale Earnhardt, Inc. (DEI), use portable GMAW machines to weld the body panels, a process known as "skinning." To skin a car, DEI fabricators produce thousands of tack welds spaced approximately 1 to 2 in. apart on the body panels. Fabricators must produce a complete penetration tack weld with only one pull of the GMA gun trigger, without melting through or warping the workpiece.

To connect the 24-gauge body panels to the 0.120-in. structural tubing, DEI fab-

Jeff Gordon in car number 24 and Jimmie Johnson in car 48 played a key role in bringing home several championships for the Hendrick Motorsports Team. Rick Hendrick is just the second team owner in NASCAR's modern era to earn more than 100 Cup Series victories.

Fig. 1 — For quick repairs, Hendrick fabricators use a "crash cart" to quickly deploy a welding machine to the scene of a crash.

ricators run a hotter arc with a slower wire feed speed to ensure complete penetration without melting through the sheet metal. DEI fabricators also weld on heavier mild steel components such as motor mounts that measure ¼ in. thick. The welds on the motor mounts of the vehicle must fully penetrate the base metal to achieve structural integrity — Fig. 2. A "cold weld" (a weld with little or no penetration) poses a major safety issue for the driver because the weld would simply not be strong enough to remain intact during a crash.

Performance Welding Racks at Roush

At Roush Racing, whose drivers include Matt Kenseth (#17) and Mark Martin (#6), portable GMAW machines play an important role in the chassis and body shop. Roush owns dozens of teams, and often has up to 80 racecars in just one of their many shops. With the large number of pieces of equipment, fabricators, mechanics, parts, and racecars in one area, space savings and reduced clutter is a major priority for Al Allen, body fabrication manager, Roush Racing. Those are the reasons he uses portable GMAW machines such as the Millermatic® Passport™. It is an all-in-one machine that weighs 45 lb, including the internal gas bottle.

Roush fabricates its racecars in special "body hanging bays," where lasers center the body panels and the chassis to ensure perfect symmetry. Allen devised a unique

Fig. 2 — Fabricators at Dale Earnhardt, Inc., use portable gas metal arc welding machines to weld structural tubing in the shop and make repairs when needed at the track.

way of saving floor space by directly mounting the small welding machines onto the overhead corners in each bay, so that 12 machines can run off of one large shielding gas bottle — Fig. 3. This allows multiple fabricators to work on one car simultaneously without having to worry about the machines or cables taking up valuable floor space.

Roush fabricators weld mild steel as thin as 24-gauge to ⅛ in. thick. To prevent the body panels from warping, fabricators produce thousands of tack welds with identical penetration and bead sizes — Fig. 4. "We can create a shorter, flatter tack weld by slightly increasing the voltage setting," explained Allen.

New Equipment, New Successes

NASCAR is truly a team sport — everyone plays an integral role in successes and failures. Today's professional racing industry represents the latest in cutting edge technology, which means every tool, every computer, and every bolt-on component has been tested, proven, and leveraged for one sole purpose: to get the car across the finish line first and hold it together for the victory lap. Checkered flags aside, the tools of the trade have evolved, advancing this "cutting edge toolbox" to new heights. However, with all these new tools, space savings and portability are increasingly valuable to NASCAR fabrication teams. ♦

Fig. 3 — To save space in their shop, Roush fabricators mounted portable GMAW machines directly onto their "body hanging bay."

Fig. 4 — Roush fabricators can produce thousands of identical tack welds on a single racecar.

Gas Purging Optimizes Root Welds

Purging gas contaminants from the weld area results in quality pipe welds

BY M. FLETCHER

In circumstances where welds have to be designed to withstand stress in service, special consideration needs to be given to their metallurgy and profiles.

The mechanical properties of welds, particularly their fatigue properties, can be influenced significantly by their shape and composition. In particular, at the weld root, a positive reinforcement combined with smooth transition from weld to base metal are prerequisites to achieve optimum mechanical strength.

Good Practice

Joints of high quality between cylindrical sections such as tubes and pipes can only be made by ensuring that atmospheric gases are eliminated, and positive, smooth weld reinforcement is provided.

The presence of oxygen, and to a lesser extent nitrogen, around the molten weld can lead to wide-ranging defects. Discoloration is unsightly and in some instances might reflect metallurgical imbalance, especially with some stainless steels. Gross oxidation inevitably results in reduction in mechanical properties and can cause catastrophic loss of corrosion resistance. Nitrogen contamination can result in brittleness. Gases in the weld may give rise to cracking during or after cooling.

It is clear that a reduction in weld section at the root, as evidenced by a concave geometry, will reduce the joint strength. Perhaps not so evident, but in many applications of crucial importance is the presence of notches or cracks, which tend to appear at the weld/base metal interface. These can propagate in service and cause failure.

Basic Principles

Weld root quality when making tubular joints can be ensured by applying appropriate safeguards based on removal of air from the fusion zone by the provision of inert gas. This is achieved by gas purging, and the general principles are shown in Fig. 1.

Purging Gases

The most commonly used purging gas in Europe is commercial quality argon; in the U.S., helium is in more general use, being less expensive. For specialized applications, purging techniques using argon-hydrogen and helium-argon mixtures and nitrogen have been developed.

The materials being joined and the welding process used are two main factors in the selection of the optimum gas or gas mixture. Purge gas flow rate and pressure also need to be established, and once selected, they should be included in the formal welding procedure.

Variation in purge gas quality may arise during welding, and it may be desirable to apply continuous gas monitoring, especially to control oxygen and moisture content. For this purpose, dedicated oxygen analyzers and dewpoint meters are available commercially.

Purging Procedure

The first requirement is to provide gas entry and exit points. Gas is fed through one end seal with an exit hole at the other end to prevent an undesirable buildup of pressure. Argon has a greater density than air, and the gas inlet should be at a lower elevation than the bleed end so that air is expelled effectively from the pipe bore.

Total Purging

On small pipes and tubes, where the internal volume is small, the cost of continuous total purging may not be significant. Under these circumstances wooden or plastic discs simply taped to the tube ends will be adequate. Plastic caps employed, for example, to protect pipe ends and threads during transit are commonly used. It is most important that potential leak paths are eliminated and that any branch pipes are vented to ensure complete removal of air.

When total purging is impractical, perhaps because the pipe volume is large or because access is difficult, alternative containment techniques are available.

Water Soluble Papers and Pastes

A low-cost and effective solution to providing gas coverage is to make discs from water-soluble paper and tape them inside the pipes to be joined. They should not be placed in position until after any preweld heat treatment and be far enough apart, typically 500 mm, to avoid thermal damage during welding. Purge gas is introduced into the area between the soluble dams by means of a hypodermic tube through the weld joint line.

On small-diameter pipes, an effective dam can be produced simply by crumpling the paper and pushing it into the pipe bore. Soluble pastes are also available and can be convenient for small diameters.

On completion of the welding operation, the paper or paste can be removed by passing water into the pipe and allowing time for it to dissolve the barrier medium.

Thermally Disposable Barriers

Water-soluble products are not always acceptable, and an alternative method is to use cardboard discs. These are simply

M. FLETCHER is with Delta Consultants, Carmarthen, UK. Information available from Huntingdon Fusion (www.huntingdonfusion.com), *Carmarthen, UK.*

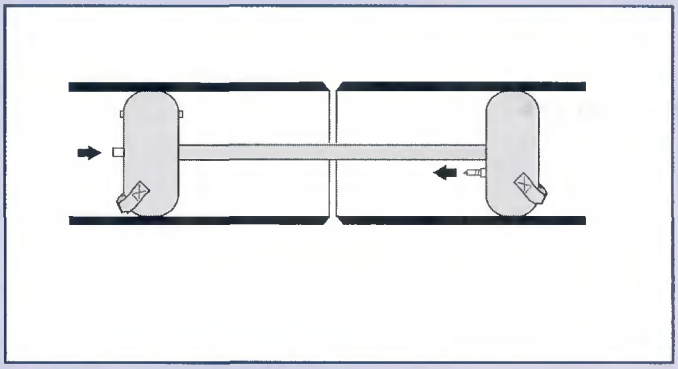

Fig. 1 — Schematic of a setup for purging.

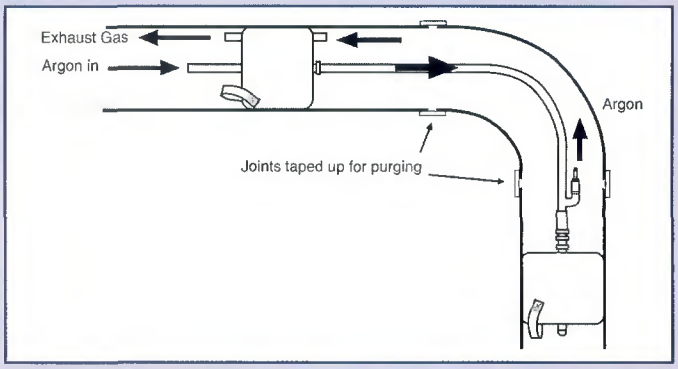

Fig. 2 — Purging a 90-deg bend.

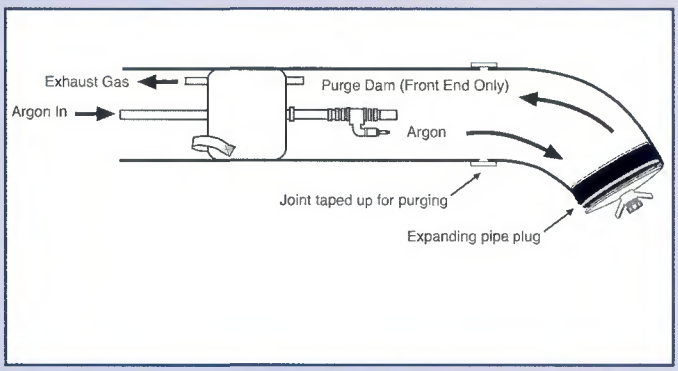

Fig. 3 — Purging a short elbow.

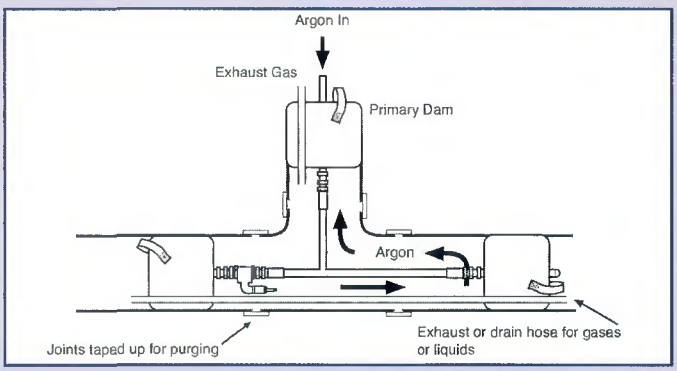

Fig. 4 — Purging a Tee piece.

cut to fit the internal diameter of the pipe and, if necessary, taped in position to provide a gas seal. The distance between discs should be typically 500 mm to avoid thermal damage during welding.

The thermally disposable disc solution is convenient if welding is to be followed by a postweld heat treatment cycle since the card is removed effectively by incineration. Otherwise, general heating by torch is a sound method of removal.

The water-soluble and thermally disposable barriers are expedient solutions where access to the tube or pipe bore is impractical after welding. If access can be gained, several alternative purge gas damming techniques, which include collapsible discs, rubber gasket discs, and inflatable bladders, can be considered.

These dams are normally placed in the pipe at the time of joint assembly, the recovery cord or rod projecting down the access route. A spacing of 150 to 200 mm will usually prevent thermal damage during welding, but it should be noted that greater spacing is prudent if preweld heat treatment is to be applied.

Table 1 — Purge Times for Various Pipe Diameters and Flow Rates

Purge Times for Gas Tungsten Arc Welding of Steel Pipe

Pipe Diameter		Flow Rate		Purge Time	Vent Diameter	
in.	mm	ft^3/h	L/min	min	in.	mm
3	75	20	10	3	1/16	1.5
4	100	20	10	3	1/16	1.5
5	125	20	10	5	1/8	3
6	150	20	10	6	1/8	3
8	200	25	12	8	1/8	3
10	250	25	12	13	1/8	3
12	300	30	15	13	1/8	3
14	350	30	17	16	—	—
20	500	35	17	25	—	—

Note: Purge time and flow rates were those required to reduce the oxygen to 1% or less, based on enclosure of 12 in. (300 mm) in length. When enclosure exceeds 12 in. length, increase flow time proportionally. Upon completion of purging cycle, reduce flow rate to maintain slight positive pressure during welding.

Collapsible Disc Barriers

Discs can be made from any rigid sheet material; plywood is a good medium if in-house manufacture is planned. The discs are split across the diameter and hinged and a sealing pad of synthetic foam bonded to the periphery. Cords attached to the discs are used to collapse the dam after welding and to remove the discs from the pipe.

Rubber Gasket Dam

A rubber disc can be sandwiched between a pair of wooden or metal discs and some adjustment to diameter can be effected by applying axial pressure. This gasket technique is not collapsible, and after welding the discs must be pulled out past the weld root, an operation which may cause difficulties.

Inflatable Bladder Dam

An efficient purge gas containment method is to use inflatable dams such as the Argweld system. This has been developed specifically to provide a reusable solution to gas purging. It is easy to use and

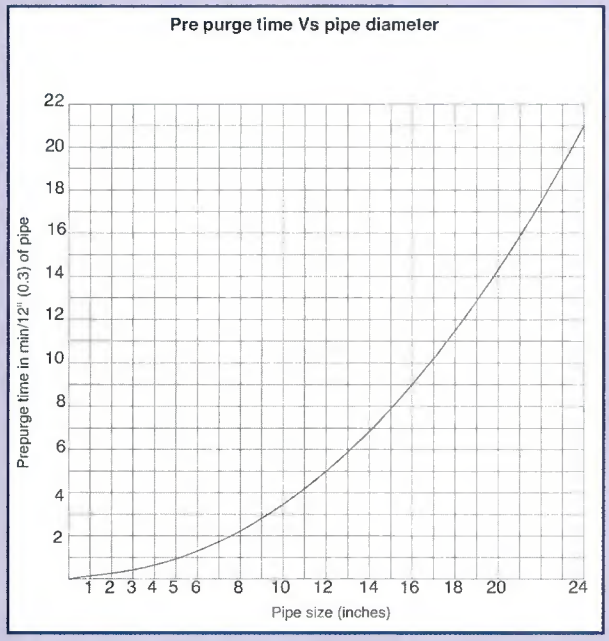

Fig. 5 — Prepurge time vs. pipe diameter. Time is for a 12-in. pipe at a flow rate of 50 ft³/h (23.5 L/min). To calculate the prepurge time for any length of pipe, multiply the value obtained from the chart by the length of pipe. For example, find the time for prepurging 200 ft (60 m) of 5-in. (127-mm) pipe. From the chart, it takes 1 min to purge 12 in. of a 5-in. pipe. Hence, it takes 200 min (3 h 20 min) to purge 200 ft of 5-in. pipe.

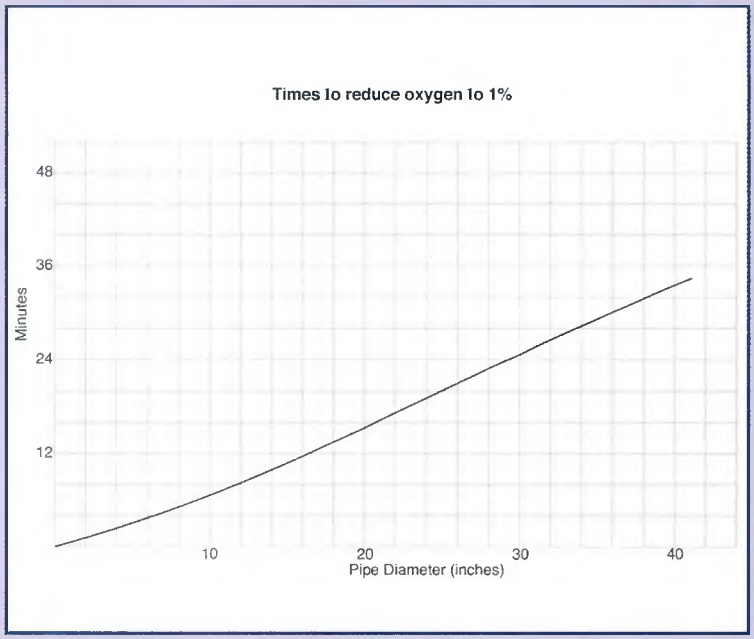

Fig. 6 — Time to reduce oxygen content to below 1%.

economical when several similar joints need to be produced.

The bladder, which has sufficient length to ensure sound sealing, is manufactured from rubber with a protective canvas cover. One is placed on each side of the joint and inflated using either compressed air or the purge gas itself. The latter is much preferred since it overcomes any problems that might arise from leakage of the bladder. Figures 2–4 illustrate the bladder concept. Variations on the basic equipment are commercially available.

Purge inlet and outlet pipes can be incorporated in the bladder to allow the full circumference to seal against the pipe wall.

High-temperature covers can be provided to afford protection during weld preheat cycles, and single bladders can be used for closed end joints. Inflation and purging gas pressures can be separately controlled.

Longer or shorter spinal connecting tubes are available, and provision can be made for continuous alteration in gas flow rate up to 20 L/min.

The Prepurge Process

A prepurge is used to displace air present in the pipework system or dam volume. Numerous factors control the prepurge time such as pipe diameter, purge volume, and maximum permitted oxygen level. A common misconception is that increasing the purge flow rate will reduce the purge time. This is a fallacy. An increase in flow rate increases turbulence and results in unwanted mixing of purge gas and air and can actually extend the purge time.

As a general rule, the prepurge flow rate and time should allow for about five volume changes in the pipe system or dam volume, but a typical gas flow rate will be in the region of 20 L/min. Figure 5 is an illustration of the relationship between prepurge time and pipe diameter based on a pipe purge length of 300 mm. For different purge lengths, it is reasonable to use a prorata calculation. Table 1 presents examples of purge times for different pipe diameters and flow rates.

Weld joints that require a root opening or have poor fitup, both of which characteristics provide an unwanted leak path for the purge gas, can be sealed by taping.

Oxygen and moisture levels in the purge gas should be checked using appropriate equipment with checking taking place at the outlet point. Where dam inserts are being used, the outlet point needs to be extended with a flexible pipe to a convenient access position. If this is impractical, a system that has the purge inlet and outlet in the same dam unit should be used.

Figure 6 gives times to reduce the dam volume oxygen content to below 1% using inflatable bladders. While 1% residual oxygen is a suitable working level for materials such as stainless steels, the level needs to be as low as 20 ppm when welding the more sensitive alloys based on titanium and other reactive metals.

The Weld Purge Process

Once the quality of the gas in the dammed volume has reached the required level, gas flow can be reduced to about 5 L/min for the welding operation. On a more practical level, it should just be possible to feel the gas flow from the exit point. Excessive flow can cause the internal pressure in the pipe to rise and create concavity in the weld root geometry and in more extreme cases can cause complete ejection of the molten weld pool.

To restrict leakage on joints not fully sealed, a higher flow rate will be necessary to avoid contamination. Toward the end of the weld run, however, as the joint becomes permanently sealed, the gas flow rate will need to be reduced to avoid overpressurization. ◆

EWI Provides Modeling and Testing for Forming AHSS and Steels

The advanced vehicle concepts for both military and commercial applications require new steels with increased strengths that can enable lighter-weight designs.

The primary thrust for using this type of steel has been driven by the demands for improved passenger safety, vehicle performance, and fuel economy. It has led to an increase in the use of the advanced high-strength steels (AHSS) in the automotive industry.

The AHSS are proving to be much more difficult to form than traditional mild steels. Driven by customer interest, Edison Welding Institute (EWI), Columbus, Ohio, is developing approaches to aid customers with the welding and forming of these AHSS.

One of the key challenges with sheet metal forming is controlling the material's springback. Springback refers to the part shape change due to its elastic recovery after forming. The magnitude of springback depends on the stress-strain distribution across the sheet thickness. Due to their inherent properties, AHSS are much more prone to springback than mild steels.

Prior to cutting forming dies, engineers utilize computer-aided engineering (CAE) models to determine how the metal will perform during the forming process — Fig. 1. Based on these computer models, prototype dies are developed. Due to material variability and an inability to accurately incorporate material properties into the CAE models, several iterations of prototype tools may be necessary as engineers attempt to predict the springback. These challenges can cost manufacturers months of delays and hundreds of thousands of dollars.

As AHSS become more complex, an in-depth knowledge about their properties and the effects of the forming process are becoming more important. Edison Welding Institute has made significant advances in addressing some of the industry's AHSS-forming challenges. Its research has shown that variations in the through-thickness property can lead to errors of 20% in the predicted models. The Institute has developed a numerical prediction methodology to consider these variations in incoming steels. Through physical verification tests, results have shown EWI's predictive models accuracy in predicting springback, and that there is a way to minimize variations by focusing on the uniformity of through-thickness properties. Along similar lines, EWI has developed innovative nondestructive evaluation methodologies to evaluate the subtle property variations in these AHSS.

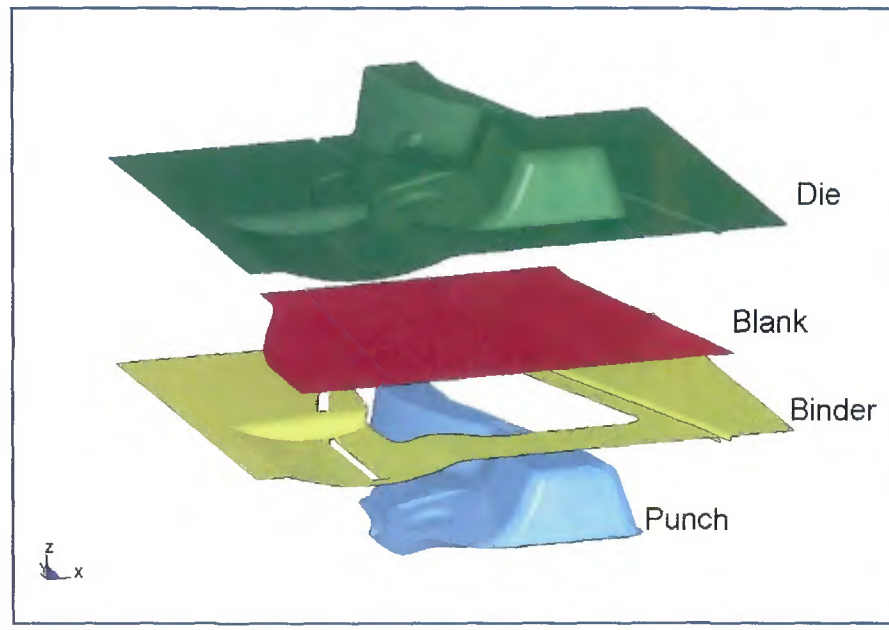

Fig. 1 — Computer-generated stamping model for forming advanced high-strength steels.

The Institute can provide an integrated engineering consultancy to deal with material formability and its effects on weld ability through a modeling and testing simulation capability. This EWI capability was developed through interfaces with commercial software *LS-DYNA* and *Abacus*. Through these tools, EWI customers can accelerate the deployment of AHSS and reduce the expensive experimentation involved in both forming and welding.

For more information on EWI's modeling and testing of AHSS and steels, contact **Jon Jennings** at (614) 688-6144, *jon_jennings@ewi.org;* or **Suresh Babul** at (614) 688-5206, *suresh_babu@ewi.org.*

NJC Operated by EWI

The Navy Joining Center
1250 Arthur E. Adams Dr.
Columbus, OH 43221
Phone: (614) 688-5010
FAX: (614) 688-5001
e-mail: *NJC@ewi.org*
www: *http://www.ewi.org*
Contact: Larry Brown

Register to Attend

The Friction Stir Welding Technology for Defense Applications Workshop

The third in a series of Friction Stir Welding Workshops will be held Feb. 21, 22, 2007, at Edison Welding Institute in Columbus, Ohio.

This workshop is sponsored by the Navy ManTech Program and Office of Naval Research. It is organized by the Navy Joining Center and Navy Metalworking Center.

This event will provide industry and Department of Defense representatives with the latest advancements in the development and implementation of friction stir welding technology for defense applications.

Due to ITAR restrictions, workshop attendees must be U.S. citizens with an approved DD2345.

For complete information and online registration, visit the News and Events link at *www.nmc.etc.com,* or contact **Connie Kotula** at (614) 688-5156, *connie_kotula@ewi.org.*

COMING EVENTS

NOTE: A DIAMOND (♦) DENOTES AN AWS-SPONSORED EVENT.

ShipTech 2007. Jan. 30, 31. Beau Rivage Resort, Biloxi, Miss. Cosponsored by ManTech, ONR Mfg. Technology Program, Nat'l Shipbuilding Research Program. Visit Web site for admission requirements. Contact *www.nmc.ctc.com.*

The Power of Paint and Coatings. Feb. 11–14. Dallas Convention Center, Dallas, Tex. Contact: The Society for Protective Coatings, *www.sspc.org.*

Friction Stir Welding and Processing IV Symposium, and TMS Fall Meeting. Feb. 21–March 1. Orlando, Fla. Sponsored by The Minerals, Metals & Materials Society. Contact *www.tms.org.*

Tube and Pipe Journal (TPJ) Symposium. March 14–16. Disney's Contempory Resort, Lake Buena Vista, Fla. Sponsored by The Tube & Pipe Assn., Int'l, and *The Tube & Pipe Journal®.* Visit *www.tpatube.org.*

ILSC® 2007, Int'l Laser Safety Conference. March 19–22, Airport Marriott, San Francisco, Calif. Contact *www.laserinstitute.org/conferences/ilsc.*

MetalForm. March 25–28, Donald E. Stephens Convention Center, Rosemont, Ill. Sponsored by Precision Metalforming Assn. Visit *www.metalform.com.*

World Trade Fair for Industrial Technology. April 16–20, Hannover Fairgrounds, Hannover, Germany. Organized by Deutsche Messe AG. Visit *www.messe.de.*

ALUMEX 2007, 4th Int'l Aluminum Exhibition. April 22–24, Dubai Int'l Convention Centre, Dubai, UAE. Contact: *www.alumexdubai.com.*

14th Int'l Conf. on the Joining of Materials (JOM-14), and 5th Int'l Conf. on Education in Welding. April 29–May 2, at LO-Skolen, Helsingör, Denmark. For more information, contact: *jom_aws@post10.tele.dk.*

Int'l Welding and Joining Conf. — Korea 2007. May 10–12, COEX Convention Center, Seoul, Korea. Contacts: *iwjc@iwjc2007.org* or visit *www.iwjc2007.org.*

XXXVIII Int'l Steelmaking Seminar. May 20–23, Belo Horizonte, Minas Gerais, Brazil. Sponsored by ABM (Associação Brasileira de Metalurgia c Materials). Papers will have simultaneous translations in English and Portugese. Visit: *www.abmbrasil.com.br/seminarios.*

♦**8th Int'l Conf. on Brazing, High-Temperature Brazing, and Diffusion Bonding (LÖT 2007).** June 19–21, Aachen, Germany. Cosponsors include American Welding Society and ASM Int'l. Contact the German Welding Society (DVS), *tagungen@dvs-hg.de; www.dvs-ev/loet2007.*

EMO Hannover — World of Machine Tools and Metalworking. Sept. 17–22, Hannover Fairgrounds, Hannover, Germany. Visit: *www.hf-usa.com/emo.*

24th Annual ASM Heat Treating Society Conference and Exposition. Sept. 17–19, Cobo Hall, Detroit, Mich. Visit *www.asminternational.org/heattreat/.*

Southeast Asia Wire and Tube Trade Fairs. Oct. 16–18, Bangkok, Thailand. Contact Messe Düsseldorf North America, *info@mdna.com; www.mdna.com.*

Educational Opportunities

Design of Experiments for the Shop Floor. Feb. 15, 16. Courses held in downtown Chicago, contact Atema at (312) 861-3000, or visit *www.atemainc.com.*

Boiler and Pressure Vessel Inspectors Training Courses and Seminars. Columbus, Ohio. Contact Richard McGuire, (614) 888-8320, *rmcguire@nationalboard.org, www.nationalboard.org.*

CWI/CWE Course and Exam. This 10-day program prepares students for the AWS CWI/CWE exam. For schedule and entry requirements, contact Hobart Institute of Welding Technology (800) 332-9448, *www.welding.org.*

CWI Preparation. Courses on ultrasonic, eddy current, radiography, dye penetrant, magnetic particle, and visual at Levels 1–3. Meet SNT-TC-1A and NAS-410 requirements. On-site training available. T.E.S.T. NDT, Inc., 193 Viking Ave., Brea, CA 92821; (714) 255-1500; *ndtguru@aol.com*; *www.testndt.com.*

CWI Preparatory and Visual Weld Inspection Courses. Classes presented in Pascagoula, Miss., Houston, Tex., and Houma and Sulphur, La. Course lengths range from 40 to 80 hours. Contact Real Educational Services, Inc., (800) 489-2890; *info@realeducational.com*.

Environmental Health and Safety-Related Web Seminars. These 30-minute-long Web seminars on various topics are online, real-time events conducted by industry experts. Most seminars are free. Contact: *www.augustmack.com/Web%20Seminars.htm.*

EPRI NDE Training Seminars. EPRI offers NDE technical skills training in visual examination, ultrasonic examination, ASME Section XI, and UT operator training. Contact Sherryl Stogner, (704) 547-6174, e-mail: *sstogner@epri.com*.

Fabricators and Manufacturers Assn., and Tube and Pipe Assn. Courses. Contact (815) 399-8775; *www.fmametalfab.org; info@fmametalfab.org*.

Hellier NDT Courses. For schedule of courses, contact Hellier, 277 W. Main St., Ste. 2, Niantic, CT 06357. (860) 739-8950, FAX: (860) 739-6732.

Machining and Grinding Courses. Contact TechSolve at *www.TechSolve.org*.

Machine Safeguarding Seminars. Contact Rockford Systems, Inc., PO Box 5525, Rockford, IL 61125, (800) 922-7533; FAX: (815) 874-6144; *www.rockfordsystems.com*.

NACE Int'l Training and Certification Courses. Contact Nat'l Assoc. of Corrosion Engineers, (281) 228-6223, FAX: (281) 228-6329, *www.nace.org*.

AWS Certification Schedule

Certification Seminars, Code Clinics and Examinations

Application deadlines are six weeks before the scheduled seminar or exam. Late applications will be assessed a $250 Fast Track fee.

Certified Welding Inspector (CWI)

Location	Seminar Date	Exam Date
Fresno, CA	Jan. 7-12	Jan. 13
New Orleans, LA	Jan. 7-12	Jan. 13
Knoxville, TN	EXAM ONLY	Jan. 20
Corpus Christi, TX	Exam Only	Jan. 27
Pittsburgh, PA	Jan. 21-26	Jan. 27
Seattle, WA	Jan. 21-26	Jan. 27
Miami, FL	Jan. 21-26	Jan. 27
Denver, CO	Jan. 28-Feb. 2	Feb. 3
Indianapolis, IN	Jan. 28-Feb. 2	Feb. 3
Milwaukee, WI	Feb. 4-Feb. 9	Feb. 10
Atlanta, GA	Feb. 4-Feb. 9	Feb. 10
Miami, FL	EXAM ONLY	Feb. 15
Dallas, TX	Feb. 11-16	Feb. 17
San Diego, CA	Feb. 11-16	Feb. 17
Norfolk, VA	Feb. 25-Mar. 2	Mar. 3
Anchorage, AK	Feb. 25-Mar. 2	Mar. 3
Boston, MA	Mar. 4-9	Mar. 10
Portland, OR	Mar. 4-9	Mar. 10
Mobile, AL	EXAM ONLY	Mar. 17
Perrysburg, OH	EXAM ONLY	Mar. 17
Rochester, NY	EXAM ONLY	Mar. 17
Houston, TX	Mar. 18-23	Mar. 24
Miami, FL	Mar. 18-23	Mar. 24
Phoenix, AZ	Mar. 25-30	Mar. 31
Chicago, IL	Mar. 25-30	Mar. 31
York, PA	EXAM ONLY	Mar. 31
Corpus Christi, TX	EXAM ONLY	Apr. 7
Miami, FL	EXAM ONLY	Apr. 19
Baton Rouge, LA	Apr. 15-20	Apr. 21
Portland, ME	Apr. 15-20	Apr. 21
Columbus, OH*	Apr. 16-20	Apr. 21
Las Vegas, NV	Apr. 22-27	Apr. 28
Nashville, TN	Apr. 22-27	Apr. 28
St. Louis, MO	EXAM ONLY	Apr. 28
Jacksonville, FL	Apr. 29-May 4	May 5
Baltimore, MD	Apr. 29-May 4	May 5
Waco, TX	EXAM ONLY	May 5
Detroit, MI	May 6-11	May 12
Miami, FL	May 6-11	May 12
Corpus Christi, TX	EXAM ONLY	May 19
Long Beach, CA	EXAM ONLY	May 26
Albuquerque, NM	May 20-25	May 26
San Francisco, CA	May 20-25	May 26
Oklahoma City, OK	May 20-25	May 26
Birmingham, AL	Jun. 3-8	Jun. 9
Hartford, CT	Jun. 3-8	Jun. 9
Miami, FL	Exam Only	Jun. 14
Fargo, ND	Jun. 10-15	Jun. 16
Kansas City, MO	Jun. 10-15	Jun. 16
Anchorage, AK	Jun. 24-29	Jun. 30
Phoenix, AZ	Jun. 24-29	Jun. 30
Orlando, FL	Jul. 8-13	Jul. 14
Spokane, WA	Jul. 8-13	Jul. 14
Miami, FL	Exam Only	Jul. 19
Bakersfield, CA	Jul. 15-20	Jul. 21
Louisville, KY	Jul. 15-20	Jul. 21

* Mail seminar registration and fees for Columbus seminars only to National Board of Boiler & Pressure Vessel Inspectors, 1055 Crupper Ave., Columbus, OH 43229-1183. Phone (614) 888-8320. Exam application and fees should be mailed to AWS.

9-Year Recertification for CWI and SCWI

Location	Seminar Dates	Exam Date
New Orleans, LA	Jan. 22-27	NO EXAM**
Denver, CO	Feb. 12-17	NO EXAM**
Dallas, TX	Mar. 19-24	NO EXAM**
Sacramento, CA	Apr. 23-28	NO EXAM**
Pittsburgh, PA	Jun. 11-16	NO EXAM**
San Diego, CA	Aug. 13-18	NO EXAM**

**For current CWIs needing to meet education requirements without taking the exam. If needed, recertification exam can be taken at any site listed under Certified Welding Inspector.

Certified Welding Supervisor (CWS)

Location	Seminar Dates	Exam Date
Atlanta, GA	Jan. 15-19	Jan. 20
Houston, TX	Jan. 22-26	Jan. 27
Baton Rouge, LA	Feb. 12-16	Feb. 17
Chicago, IL	Mar. 19-23	Mar. 24
Nashville, TN	Apr. 16-20	Apr. 21
Atlanta, GA	Apr. 23-27	Apr. 28
Columbus, OH	May 7-11	May 12
Minneapolis, MN	Jun. 11-15	Jun. 16
Philadelphia, PA	Jul. 16-20	Jul. 21

Certified Radiographic Interpreter (RI)

Location	Seminar Dates	Exam Date
Long Beach, CA	Jan. 29-Feb. 2	Feb. 3
Indianapolis, IN	Feb. 26-Mar. 2	Mar. 3
Houston, TX	Mar. 26-30	Mar. 31
Philadelphia, PA	Apr. 30-May 4	May 5
Nashville, TN	Jun. 4-8	Jun. 9
Manchester, NH	Jul. 23-27	Jul. 28

Radiographic Interpreter certification can be a stand-alone credential or can exempt you from your next 9-Year Recertification.

Certified Welding Educator (CWE)

Seminar and exam are given at all sites listed under Certified Welding Inspector. Seminar attendees will not attend the Code Clinic portion of the seminar (usually first two days).

Senior Certified Welding Inspector (SCWI)

Exam can be taken at any site listed under Certified Welding Inspector. No preparatory seminar is offered.

Certified Welding Fabricator

This program is designed to certify companies to specific requirements in the ANSI standard AWS B5.17, *Specification for the Qualification of Welding Fabricators*. There is no seminar or exam for this program. Call ext. 448 for more information.

Code Clinics & Individual Prep Courses

D1.1, API-1104, Welding Inspection Technology, and Visual Inspection workshops are offered at all sites where the CWI seminar is offered. D1.1 and API-1104 Code Clinics are held on Sundays and Mondays and are prep courses for CWI Exam-Part C. Welding Inspection Technology is held Wednesdays and Thursdays and is a general knowledge course and a prep course for CWI Exam-Part A. The Visual Inspection workshop is usually held on Fridays and is a prep course for CWI Exam-Part B.

On-site Training and Examination

On-site training is available for larger groups or for programs that are customized to meet specific needs of a company. Call ext. 219 for more information.

For information on any of our seminars and certification programs, visit our website at **www.aws.org** or contact AWS at (800/305) 443-9353, Ext. 273 for Certification and Ext. 223 for Seminars.

Please **apply early** to save Fast Track fees. **This schedule is subject to change without notice.** Please verify the dates with the Certification Dept. and confirm your course status before making final travel plans.

American Welding Society

Founded in 1919 to advance the science, technology and application of welding and allied joining and cutting processes, including brazing, soldering and thermal spraying.

STUD WELDING ALUMINUM

It is important to prepare the surface areas to which the stud will be welded prior to welding. The surface should be clean and free of foreign matter including paint, moisture, heavy oxide film, oil and grease, indelible markings, and anodic coatings.

The cleaning can be accomplished by milling, stainless steel wire brushing, or chemical methods, although solvents with chlorinated hydrocarbons should be avoided. Welding should take place within eight hours of cleaning.

Arc stud welding and drawn arc capacitor discharge stud welding generally use a shielding gas of 99.95% pure argon. Helium may be used with large studs to take advantage of the higher arc energy generated with this gas. The gas should be directed to the weld area and permitted to flow only while the gun is held against the work in the welding position. Use the gas flow rates recommended by the stud manufacturer. Shielding gas is not required with contact or gap capacitor discharge welding.

Arc stud welding of aluminum should be performed with direct current electrode positive (DCEP). Capacitor discharge welding should follow the electrical hook-up recommended by the manufacturer. The arc stud welding gun should be equipped with a dampening device to control the plunge rate of the stud at the completion of the weld time. Studs can be welded on flat, vertical, or overhead surfaces.

Welding Techniques for Aluminum

Recommended welding current, weld time, and shielding gas are presented in the table. The welding current should not be switched off until the stud plunges into the work. After inserting the stud into the gun, the ferrule should be placed over the stud base and seated against the ferrule holder. The leg(s) should be adjusted so that the stud extends the required plunge distance as stated by the equipment manufacturer.

The stud gun should be held perpendicular to the work surface with the ferrule and shielding gas adaptor foot firmly seated against the work. The trigger on the stud gun should not be moved during the welding cycle. After the cycle has been completed, the gun should be held in position momentarily to allow the molten metal to solidify and then withdrawn. The ferrule should be removed from the stud and the weld visually inspected (see figure).

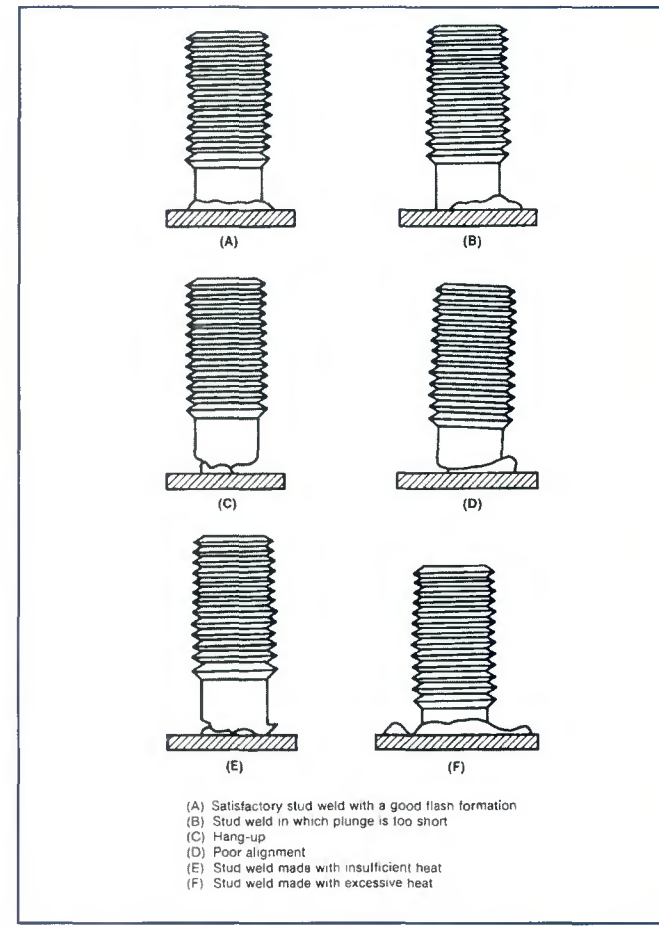

Evaluating arc stud welds. A — Satisfactory stud weld with a good flash formation; B — stud weld with plunge too short; C — hang up; D — poor alignment; E — stud weld made with insufficient heat; F — stud weld made with excessive heat.

Typical Welding Conditions for Arc Stud Welding of Aluminum Alloys[a]

Stud Base Diameter				Shielding Gas Flow[c]		
in.	mm	Weld Time, cycles (60 Hz)	Welding Current[b], amps	ft³/h	L/min	Plunge, in.[d]
¼	6.4	15	250	15	7.1	1/16
5/16	7.9	20	370	1	57.1	3/32
⅜	9.5	25	540	20	9.4	3/32
7/16	11.1	30	570	20	9.4	⅛
½	12.7	43	640	20	9.4	1/16

Notes:
a. Settings should be adjusted to suit job conditions.
b. The values shown are actual welding currents, not dial settings.
c. Shielding gas — 99.95% argon.
d. Lift — 1/32 in.

Excerpted from AWS C5.4, *Recommended Practices for Stud Welding.*

SOCIETY NEWS

BY HOWARD M. WOODWARD

D1 Committee Meets in Vancouver

Shown at the AWS D1 Structural Welding Committee meeting in Vancouver, B.C., Canada, on September 15 are, from left, sitting: Heather Gilmer, Hardy Campbell, Peter Marshall, Nick Altebrando, and Dean Phillips. From left to right, standing are Paul Sullivan, Keith Landwehr, Doug Luciani, Todd Niemann, Dave McQuaid, Krishna Verma, First Vice Chair Duane Miller, Rob Lawrence, Tom Schlafly (obscured), Lacy Collins, David Dunn, Karl Fogleman, Gene Bickford, Ron Dennis, Joe Kiefer, Bruce Butler, Don Scott, Nate Lindell, Viji Kuruvilla, Michael Mayes, Jack Kenney, Buck Roberds (obscured), Chairman Don Rager, Jim Merrill, Second Vice Chair Allen Sindel, Gary Martin, Ray Stieve, Stephen Luckowski, Pat Newhouse, John Lawmon, Bob Montes, Darcy Yantz, Bob Shaw, and Peter Kinney.

New Orleans Section Hosts 2nd Annual Weld Competition

Travis Moore, New Orleans Section chair, instructed the students on the rules, then launched the 2nd Annual Student Welding Competition at the New Orleans Pipe Trades facility.

Held October 7, the defining project was to make a ⅜-in. fillet weld in the 3F position within a 15-minute time limit. The coupons were judged by the Section's CWIs **Paul Hebert, Chris Gatango, Anthony DeMarco, John Pajak,** and **Michael Kirwin.** The winners were **Chris Fernandez, Keith Roberston, Noil Vaughn, Sean St. Amant, Trey Warren,** and **Allen Weise.** Their Student Advisor is **Anthony DeMarco.** Five welding instructors also participated, performing a 4F project. The instructors included **Butch White** (LTC-River Parishes), **Tommy Garcia** (LTC-West Jefferson), **Aldo Duron** (Ironworkers Local 58), **Curtis Mezzic** (Local 60), and **Carey Addison** (Northrop Grumman Ship Systems). Additional New Orleans Section information appears on page 54.

Student winners in the New Orleans Section welding competition held October 7 are (front row, from left) Chris Fernandez (Local 60), and Noil Vaughn, Keith Roberston, and Trey Warren (LTC River Parishes); (back row, from left) Sean St. Amant and Allen Weise (Local 60), and Student Advisor Anthony DeMarco.

Tech Topics

Technical Committee Meeting

All AWS technical committee meetings are open to the public. To attend a meeting, call (800/305) 443-9353, at the extension listed.

Dec. 5, 6, Safety & Health Committee. Miami, Fla. Contact: S. Hedrick, ext. 305.

Standards for Public Review

A5.2/A5.2M:200X, *Specification for Carbon and Low-Alloy Steel Rods for Oxyfuel Gas Welding.* Revised — $25. 11/20/06.

D8.1M:200X, *Specification for Automotive Weld Quality — Resistance Spot Welding of Steel.* New — $32. 12/18/06.

AWS was approved as an accredited standards-preparing organization by the American National Standards Institute (ANSI) in 1979. AWS rules, as approved by ANSI, require that all standards be open to public review for comment during the approval process. The listed standards are submitted for public review. Order draft copies from **Rosalinda O'Neill,** (800/305) 443-9353, ext. 451; *roneill@aws.org.*

ISO Draft for Public Review

ISO/DIS 14175, *Welding Consumables — Shielding Gases for Fusion Welding and Allied Processes.*

Copies of this standard are available for review and comment through your national sandards body, which in the United States is ANSI, 25 W. 43rd St., 4th Floor, New York, NY 10036; (212) 642-4900. Comments regarding ISO documents should be sent to your national standards body. In the United States, if you wish to participate in the development of international standards for welding, contact **Andrew Davis, technical director,** at *adavis@aws.org,* (800/305) 443-9353, ext. 466.

Standards Approved by ANSI

G2.4/G2.4M:2007, *Guide for the Fusion Welding of Titanium and Titanium Alloys.* New. 9/20/06.

A4.4M:2001 (R2006), *Standard Procedures for Determination of Moisture Content of Welding Fluxes and Welding Electrode Flux Coverings.* Reaffirmed 9/29/06.♦

Member-Get-A-Member Campaign

Listed are the members participating in the 2006–2007 Campaign for the period June 1, 2006, through May 31, 2007. See page 51 for rules and the prize list. Call the Membership Dept. (800/305) 443-9353, ext. 480, for information about your status as a member proposer.

Winner's Circle

AWS Members who have sponsored 20 or more new members, per year, since 6/1/1999. The superscript denotes the number of times Winners Circle status has been earned if more than once.

J. Compton, San Fernando Valley[6]
E. H. Ezell, Mobile[4]
J. Merzthal, Peru[2]
G. Taylor, Pascagoula[2]
B. A. Mikeska, Houston
R. L. Peaslee, Detroit
W. Shreve, Fox Valley
M. Karagoulis, Detroit
S. McGill, NE Tennessee
T. Weaver, Johnstown/Altoona
G. Woomer, Johnstown/Altoona
R. Wray, Nebraska
M. Haggard, Inland Empire

President's Guild

Sponsored 20 or more new members.
L. Taylor, Pascagoula — 20

President's Roundtable

Sponsored 9–19 new members.
J. Compton, San Fernando Valley — 18
M. Palko, Detroit — 16
R. Myers, L.A./Inland Empire — 10
R. Ellenbecker, Fox Valley — 9

President's Club

Sponsored 3–8 new members.
W. Shreve, Fox Valley — 8
R. Wilsdorf, Tulsa — 7
J. Bruskotter, New Orleans — 5
B. Converse, Detroit — 4
T. Ferri, Boston — 4
G. Taylor, Pascagoula — 4
P. Zammit, Spokane — 4
S. Chuk, International — 3
J. Goldsberry Jr., SE Nebraska — 3
G. Lau, Cumberland Valley — 3
J. Leen, Chicago — 3

President's Honor Roll

Sponsored 1 or 2 new members.
G. Cottrell, South Florida — 2
E. Ezell, Mobile — 2
R. Gollihue, Tri-State — 2
H. Jackson, L.A/Inland Empire — 2
M. Lamarre, Palm Beach — 2
D. Lawrence, Peoria — 2
D. Malkiewicz, Niagara Frontier — 2
M. Rieb, Inland Empire — 2
R. Wright, San Antonio — 2

Student Member Sponsors

Sponsored 3+ new members.
C. Daily, Puget Sound — 64
A. Demarco, New Orleans — 45
G. Euliano, Northwestern Penn. — 43
H. Jackson, L.A/Inland Empire — 41
S. Burdge, Stark Central — 34
B. Suckow, Northern Plains — 22
B. Lavallee, Northern New York — 18
W. Harris, Pascagoula — 16
S. Robeson, Cumberland Valley — 14
J. Ciaramitaro, N. Central Florida — 11
G. Koza Jr., Houston — 10
L. Davis, New Orleans — 8
A. Mattox, Lexington — 8
G. Putnam, Green & White Mts. — 8
D. Newman, Ozark — 7
C. Schiner, Wyoming — 7
W. Younkins, Mid-Ohio Valley — 7
G. Saari, Inland Empire — 6
J. Angelo, El Paso — 5
A. Badeaux, Washington D.C. — 5
D. Combs, Santa Clara Valley — 5
J. Carney, Western Michigan — 4
A. Dropik, Northern Plains — 4
D. Kowalski, Pittsburgh — 4
C. Schiner, Wyoming — 4
C. Yaeger, Northeastern Carolina — 4
J. Boyer, Lancaster — 3
C. Bridwell, Ozark — 3
R. Hutchison, Long Beach/Or. Cty. — 3
R. Richwine, Indiana — 3
R. Vann, South Carolina — 3♦

SECTION NEWS

DISTRICT 1

Director: Russ Norris
Phone: (603) 433-0855

BOSTON

OCTOBER 16

Activity: The Section members toured Innov-X Systems, Inc., in Woburn, Mass. **Monet MacGillivray,** regional sales manager, and **Kris Krueger,** sales engineer, demonstrated the company's XRF analyzers programmed to automatically identify as many as 1000 metallic alloys using UNS, ASME, MIL specs, common names, etc., without using radioactive isotopes. **Russ Norris,** District 1 director, presented the District Meritorious Certificate Award to outgoing chair **Gary Hylan.** Also honored was **Tom Ferri** who received the Deputy District Director's pin and the Boston Section Chairman's pin.

Gary Hylan (left) and Tom Ferri (center) received awards from Russ Norris, District 1 director, at the Boston Section program.

Shown at the Boston Section program are (from left) Monet MacGillivray, Tom Ferri, and Kris Krueger.

DISTRICT 2

Director: Kenneth R. Stockton
Phone: (732) 787-0805

NEW JERSEY

SEPTEMBER 19

Spcaker: **Seann T. Bradley,** sales engineer
Affiliation: The Lincoln Electric Co.
Topic: How AWS classifications determine filler metal selection for the SMA, FCA, and GMA welding processes
Activity: The program was held at L'Affaire Restaurant in Mountainside, N.J.

OCTOBER 17

Speakers: **A. Ozekcin,** senior engineer
Affiliation: ExxonMobil Research and Engineering Co., Annandale, N.J.; and **Richard A. Haber,** director, Ceramic and Composite Material Center, Rutgers University
Topic: Friction stir welding
Activity: This New Jersey Section program included members from the local chapter of ASM International. The meeting was held at L'Affaire Restaurant in Mountainside, N.J.

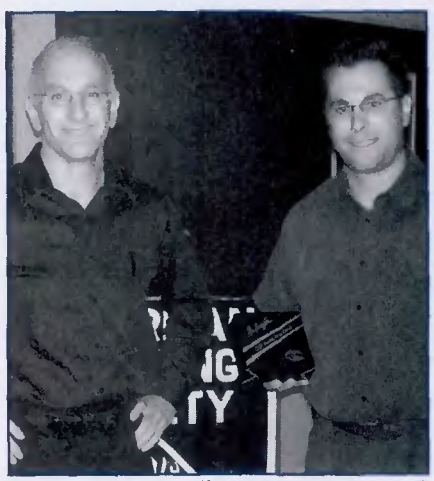

Speaker Seann Bradley (right) is shown with Vince Murray, chairman of the New Jersey Section.

Speaker A. Ozekcin (right) is shown with Steven DeFillipps Jr., New Jersey Section technical program chair, at the October meeting.

Shown at the Philadelphia Section program are (from left) Chair James Korchowsky, Vice Chair Gary Atherton, and Awards Chair Jim Rynex.

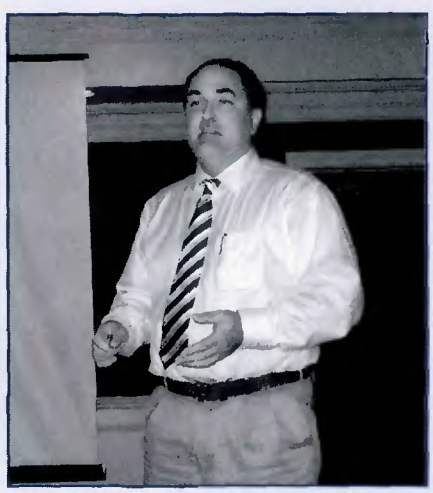

Richard Haber discussed friction stir welding at the joint meeting of the New Jersey Section and ASM International.

PHILADELPHIA

OCTOBER 11

Activity: Vice Chair **Gary Atherton** received the District Meritorious Service Award from Awards Chair **Jim Rynex** and

Cumberland Valley Section members and families enjoy their picnic in Hagerstown, Md.

Janis (left) and Pat Herschkowitz conducted a tour of PRL Industries for members of the Reading and Lancaster Sections.

Shown at the York Central Pennsylvania Section program are (from left) Ravi Menon, Chair Margaret Malehorn, and Jim Henry.

Bill Rhodes (far left), secretary, is shown with the first-place team members in the Southwest Virginia Section golf tournament (from left) Greg McQuaid, Brent Craddock, Jack Green, and Randy Adams.

James Korchowsky. The Section held a roundtable discussion led by **John DiSantis** and Chair **Jim Korchowsky.**

DISTRICT 3

Director: Alan J. Badeaux Sr.
Phone: (301) 753-1759

CUMBERLAND VALLEY

SEPTEMBER 17

Activity: The Section held its first annual picnic in Hagerstown, Md.

READING/LANCASTER

OCTOBER 12

Activity: The Reading and Lancaster Sections convened for a joint outing to tour PRL Industries in Cornwall, Pa., to study its radiographic and other nondestructive testing operations. The guides for the tour were owners **Janis Herschkowitz,** president, and her sister **Pat.** The facility is engaged with military and nuclear work under contract to the U.S. government.

YORK CENTRAL PA.

OCTOBER 5

Speakers: **Ravi Menon,** VP technology; and **Jim Henry,** technical sales manager
Affiliation: Stoody Co.
Topics: History of Stoody Company, and specialty flux cored wires for joining and surfacing
Activity: The program was held at Meadow Hill Family Restaurant in York, Pa.

DISTRICT 4

Director: Ted Alberts
Phone: (540) 674-3600, ext. 4314

SOUTHWEST VIRGINIA

SEPTEMBER 29

Activity: The Section hosted its annual golf outing at Countryside Golf Club in Roanoke, Va. Special achievement awards went to **Brent Craddock** (longest drive) and **Robbie Templeton** and **Roger Snider** for closest to the pin. The fist-place team included **Greg McQuaid, Brent Craddock, Jack Green,** and **Randy Adams.**

DISTRICT 5

Director: Leonard P. Connor
Phone: (954) 981-3977

FLORIDA WEST COAST

OCTOBER 11

Speaker: **David Rice**
Affiliation: ESAB Welding and Cutting

Recruit Members and Win **All-New Prizes** in the **2006-2007 AWS** Member-Get-A-Member Campaign*

Limited Edition

MISSION: Looking for a few good Members.

AWS is looking for individuals to become part of an exclusive group of AWS Members who get involved and win. Give back to your profession, strengthen AWS and **win great limited-edition prizes** by participating in the 2006-2007 Member-Get-A-Member Campaign. By recruiting new members to AWS, you're adding to the resources necessary to expand your benefits as an AWS Member. Year round, you'll have the opportunity to recruit new members and be eligible to win special contests and prizes. Referrals are our most successful member recruitment tool. Our Members know first-hand how useful AWS Membership is, and with your help, AWS will continue to be the leading organization in the materials joining industry.

To recruit new Members, use the application on the reverse, or visit www.aws.org/mgm

PRIZE CATEGORIES

President's Honor Roll:
Recruit 1-2 new Individual Members and receive an AWS dog tag key chain.

President's Club:
Recruit 3-8 new Individual Members and receive an American Welder™ camouflage hat and an AWS dog tag key chain.

President's Roundtable:
Recruit 9-19 new Individual Members and receive an American Welder™ camouflage t-shirt, hat and an AWS dog tag key chain.

President's Guild:
Recruit 20 or more new Individual Members and receive a Timex camouflage watch, an American Welder™ camouflage hat, a one-year free AWS Membership, the "Shelton Ritter Member Proposer Award" Certificate and membership in the Winner's Circle.

Winner's Circle:
All members who recruit 20 or more new Individual Members will receive annual recognition in the *Welding Journal* and will be honored at FABTECH International and the AWS Welding Show.

SPECIAL PRIZES

Participants will also be eligible to win prizes in specialized categories. Prizes will be awarded at the close of the campaign (June 2007).

Sponsor of the Year:
The individual who sponsors the greatest number of new Individual Members during the campaign will receive a plaque, a trip to the 2007 FABTECH International & AWS Welding Show, and recognition at the AWS Awards Luncheon at the Show.

Student Sponsor Prize:
AWS Members who sponsor two or more Student Members will receive an AWS dog tag key chain.

The AWS Member who sponsors the most Student Members will receive a free, one-year AWS Membership, an American Welder™ camouflage t-shirt, hat and an AWS dog tag key chain.

International Sponsor Prize:
Any member residing outside the United States, Canada and Mexico who sponsors the most new Individual Members will receive a complimentary AWS Membership renewal.

LUCK OF THE DRAW

For every new member you sponsor, your name is entered into a quarterly drawing. The more new members you sponsor, the greater your chances of winning. Prizes will be awarded in November 2006, as well as in February and June 2007.

Prizes Include:
- Complimentary AWS Membership renewal
- American Welder™ camouflage t-shirt
- American Welder™ camouflage hat

SUPER SECTION CHALLENGE

The AWS Section in each District that achieves the highest net percentage increase in new Individual Members before the June 2007 deadline will receive special recognition in the *Welding Journal*.

The AWS Sections with the highest numerical increase and greatest net percentage increase in new Individual Members will each receive the Neitzel Membership Award.

American Welding Society
550 N.W. LeJeune Rd. • Miami, FL 33126
Visit our website http://www.aws.org

**The 2006-2007 MGM Campaign runs from June 1, 2006 to May 31, 2007. Prizes are awarded at the close of the campaign.*

SPECIAL OFFER FOR NEW AWS INDIVIDUAL MEMBERS – TWO YEARS FOR $135 (a $25 savings)

★ *PLUS... Get a popular welding publication for only $25 ($192 value)*

AWS MEMBERSHIP APPLICATION

4 Easy Ways to Join or Renew:

Mail this form, along with your payment, to AWS
Call the Membership Department at (800) 443-9353, ext. 480
Fax this completed form to (305) 443-5647
Join or renew on our website <www.aws.org/membership>

❑ Mr. ❑ Ms. ❑ Mrs. ❑ Dr. Please print • Duplicate this page as needed

Last Name _____

First Name _____ M.I. _____

Title _____ Birthdate _____

Were you ever an AWS Member? ❑ YES ❑ NO If "YES," give year____and Member # _____

Primary Phone ( )_____ Secondary Phone ( ) _____

FAX ( )_____ E-Mail _____

Did you learn of the Society through an AWS Member? ❑ Yes ❑ No

If "yes," Member's name:_____ Member's # (if known): _____

From time to time, AWS sends out informational emails about programs we offer, new Member benefits, savings opportunities and changes to our website. If you would prefer not to receive these emails, please check here ❑

ADDRESS

NOTE: This address will be used for all Society mail.

Company (if applicable) _____

Address _____

Address Con't. _____

City_____State/Province_____Zip/Postal Code _____Country _____

PROFILE DATA

NOTE: This data will be used to develop programs and services to serve you better.

❶ Who pays your dues?: ❑ Company ❑ Self-paid ❷ Sex: ❑ Male ❑ Female

❸ Education level: ❑ High school diploma ❑ Associate's ❑ Bachelor's ❑ Master's ❑ Doctoral

PAYMENT INFORMATION (Required)

ONE-YEAR AWS INDIVIDUAL MEMBERSHIP $80

TWO-YEAR AWS INDIVIDUAL MEMBERSHIP† ..... ~~$160~~ $135

SAVE $25 (New Members Only)

New Member? ___Yes ___No

If yes, add one-time initiation fee of $12 .....$_____

Domestic Members add $25 for book selection ($192 value), and save up to 87%††..... $_____ (Optional)

International Members add $75 for book selection (note: $50 is for international shipping) ††..$_____ (Optional)

(Note: Book Selection applies to new Individual Members only – Book selections on upper-right corner)

TOTAL PAYMENT.....$_____

AWS STUDENT MEMBERSHIP†††

❑ Domestic (Canada & Mexico incl.).....$15

❑ International $50

TOTAL PAYMENT.....$_____

NOTE: Dues include $18.70 for *Welding Journal* subscription and $4.00 for the AWS Foundation.

$4.00 of membership dues goes to support the AWS Foundation.

Payment can be made (in U.S. dollars) by check or money order (international or foreign), payable to the American Welding Society, or by charge card.

❑ Check ❑ Money Order ❑ Bill Me

❑ American Express ❑ Diners Club ❑ Carte Blanche ❑ MasterCard ❑ Visa ❑ Discover ❑ Other

Your Account Number _____ Expiration Date (mm/yy) _____

Signature of Applicant: _____ Application Date: _____

Office Use Only Check #_____ Account # _____

Source Code **WJ** Date _____ Amount _____

American Welding Society
P.O. Box 440367
Miami, FL 33144-0367
Telephone (800) 443-9353
FAX (305) 443-5647
Visit our website: www.aws.org

Member Services Revised 5/4/06

†Two-year Individual Membership Special Offer: applies only to new AWS Individual Members. ††Discount Publication Offer: applies only to new AWS Individual Members. Select one of the four listed publications for an additional $25; International Members add $75 ($25 for book selection and $50 for international shipping); Multi-Year Discount: First year is $80, each additional year is $75. No limit on years (not available to Student Members). †††Student Member: Any individual who attends a recognized college, university, technical, vocational school or high school is eligible. Domestic Members are those students residing in North America (incl. Canada & Mexico). This membership includes the *Welding Journal* magazine. Student Memberships do not include a discounted publication. Airmail Postage Option: International Members may receive their magazines via Airmail by adding $99 to the annual dues amount.

BOOK/CD-ROM SELECTION
(Pay Only $25... up to a $192 value)

NOTE: Only *New* Individual Members are eligible for this selection. Be sure to add $25 to your total payment.
ONLY ONE SELECTION PLEASE.

❑ ***Jefferson's Welding Encyclopedia (CD-ROM only)***

❑ ***Design and Planning Manual for Cost-Effective Welding***

❑ ***Welding Metallurgy***

❑ ***Welding Handbook (9th Ed., Vol. 2)***

❑ New Member ❑ Renewal

A free local Section Membership is included with all AWS Memberships

Section Affiliation Preference (if known):

Type of Business (Check ONE only)

A ❑ Contract construction
B ❑ Chemicals & allied products
C ❑ Petroleum & coal industries
D ❑ Primary metal industries
E ❑ Fabricated metal products
F ❑ Machinery except elect. (incl. gas welding)
G ❑ Electrical equip., supplies, electrodes
H ❑ Transportation equip. — air, aerospace
I ❑ Transportation equip. — automotive
J ❑ Transportation equip. — boats, ships
K ❑ Transportation equip. — railroad
L ❑ Utilities
M ❑ Welding distributors & retail trade
N ❑ Misc. repair services (incl. welding shops)
O ❑ Educational Services (univ., libraries, schools)
P ❑ Engineering & architectural services (incl. assns.)
Q ❑ Misc. business services (incl. commercial labs)
R ❑ Government (federal, state, local)
S ❑ Other

Job Classification (Check ONE only)

01 ❑ President, owner, partner, officer
02 ❑ Manager, director, superintendent (or assistant)
03 ❑ Sales
04 ❑ Purchasing
05 ❑ Engineer — welding
20 ❑ Engineer — design
21 ❑ Engineer — manufacturing
06 ❑ Engineer — other
10 ❑ Architect designer
12 ❑ Metallurgist
13 ❑ Research & development
22 ❑ Quality control
07 ❑ Inspector, tester
08 ❑ Supervisor, foreman
14 ❑ Technician
09 ❑ Welder, welding or cutting operator
11 ❑ Consultant
15 ❑ Educator
17 ❑ Librarian
16 ❑ Student
18 ❑ Customer Service
19 ❑ Other

Technical Interests (Check all that apply)

A ❑ Ferrous metals
B ❑ Aluminum
C ❑ Nonferrous metals except aluminum
D ❑ Advanced materials/Intermetallics
E ❑ Ceramics
F ❑ High energy beam processes
G ❑ Arc welding
H ❑ Brazing and soldering
I ❑ Resistance welding
J ❑ Thermal spray
K ❑ Cutting
L ❑ NDT
M ❑ Safety and health
N ❑ Bending and shearing
O ❑ Roll forming
P ❑ Stamping and punching
Q ❑ Aerospace
R ❑ Automotive
S ❑ Machinery
T ❑ Marine
U ❑ Piping and tubing
V ❑ Pressure vessels and tanks
W ❑ Sheet metal
X ❑ Structures
Y ❑ Other
Z ❑ Automation
1 ❑ Robotics
2 ❑ Computerization of Welding

Products
Topic: Plasma arc cutting and gouging processes
Activity: **Bill Machnovitz,** Florida West Coast Section treasurer, conducted a raffle to support the Section's scholarship fund. The program was held at Frontier Steak House in Tampa, Fla.

SOUTH CAROLINA

SEPTEMBER 21
Speakers: 1) **Bob Rhyne,** Ron Wallace & Associates; and 2) **Timothy Reading,** The Harris Products Group
Topics: 1) Abrasive finishing products, and 2) Using a gas guard regulator to control costly gas surges
Activity: Chairman **Gale Mole** presented certificates of appreciation for outstanding support to the Section's activities to Treasurer **Odell Haselden,** Vice Chair **Beneditto Magrone,** and **Richard Temple.**

SOUTH FLORIDA

SEPTEMBER 21
Activity: The Section members enjoyed a behind-the-scenes tour of the Thunder Cycle Design facility in Ft. Lauderdale, Fla. **Eddie Trotta,** a two-time Discovery Channel Biker Build-Off winner, and Easy Rider Builder of the Year, conducted the tour of the custom motorcycle design and fabrication shop.

DISTRICT 6

Director: Neal A. Chapman
Phone: (315) 349-6960

NORTHERN NEW YORK

OCTOBER 3
Activity: The Section members met at the Snow Dock at the foot of Madison Ave., in Albany, N.Y., to tour the USS *Slater*, one of the destroyer escorts built to battle submarines during WW II. **Doug Tanner,** a volunteer tour guide, conducted the program. The dinner for the 24 members was served below deck in the ward room.

DISTRICT 7

Director: Don Howard
Phone: (814) 269-2895

DAYTON

SEPTEMBER 22
Activity: The Section held its annual golf outing at Sugar Isle Golf Course. The event was named in honor of **Les Vesey** who died earlier this year. Mr. Vesey, a past chairman, was the organizer of the Section's golf outings. The money raised from the event was donated to fund a scholarship in his name.

Florida West Coast Section members and guests are shown at their October meeting.

Speaker David Rice (right) is shown with Lee Clemmens, Florida West Coast Section chair.

Shown at the South Carolina Section program are Chairman Gale Mole (left) and Odell Haselden.

Shown at the South Carolina Section program are (from left) Bob Rhyne, Chairman Gale Mole, Timothy Reading, and Richard Temple.

Shown aboard the USS Slater *during the Northern New York Section's tour are (from left) Nort Chapin, guide Doug Tanner, and Dave Parker.*

The Dynamic Industries staff members attended the New Orleans program.

Chairman Travis Moore (left) is shown with speaker Joe Tortomase at the New Orleans Section program in September.

Shown are the participants in the New Orleans Section Student Welding Competition held Oct. 7.

Shown are the junior Columbiana CCCTC Student Chapter members.

Shown are the senior Columbiana CCCTC Student Chapter members.

DISTRICT 8

Director: Wallace E. Honey
Phone: (256) 332-3366

HOLSTON VALLEY

OCTOBER 4

Activity: Chairman **Jerry Sullivan** held an executive committee meeting to plan the year's activities. The incoming slate of officers includes **Jerry Sullivan,** chairman; **Walt Rose** and **Tracy Trevitte,** vice chairs; **Roger Painter,** secretary; **Glen Wade,** treasurer; **Bob Thomas,** publicity chair; **Charlie Bloomer,** education committee chair; **Mark Callahan,** technical representative; and **Dale Hicks,** certification committee chair.

DISTRICT 9

Director: John Bruskotter
Phone: (504) 394-0812

NEW ORLEANS

SEPTEMBER 19

Speaker: **Joe Tortomase,** vice president of operations
Affiliation: Dynamic Industries
Topic: Careers in welding
Activity: The 78 attendees included employees of Dynamic Industries staff, and student welders from local vo-tech schools and Louisiana pipe trade schools. District 9 Director **John Bruskotter** presented the various Section and District awards. The meeting was held at the Dynamic Industries facilities in Harvey, La.

OCTOBER 7

Activity: The New Orleans Section hosted its 2nd Annual Student Welding Competition with 78 participants from Louisiana technical colleges in East Jefferson Parish, West Jefferson Parish, and St. John Parish, as well as apprentices from Plumbers & Steamfitters Local-60, and Local 58 Ironworkers in Metairie, La. Headed by Chairman **Travis Moore,** the competition used a welding procedure specification (WPS) prepared by the welding engineers and CWIs from the Section's executive committee. The students competed for $2600 in Section-sponsored scholarships. The competition sponsors included Louisiana Lift and Equipment, Audubon Engineering, Northrop Grumman Ship Systems, Marse Welding Supplies, DeMarco Welding Services, and **D. J. Berger** of New Orleans Pipe Trades for providing his facility for the event. See color photo on page 47.

DISTRICT 10

Director: Richard A. Harris
Phone: (440) 338-5921

CLEVELAND

SEPTEMBER 12

Activity: The Section hosted a Steak and Cars program featuring speakers **Berry Lobeck** of Lobeck's Hot Rod Parts, and **Greg Stelma** of Mongoose Motorsports. Lobeck builds hot rods to SCCA specs. Stelma builds 1963 Corvette GS and other kit cars. In attendance were about 60 welding engineers, managers, welders, and students. On display were several hand-crafted hot rods and replica Corvette cars and components valued up to $400,000. The evening was topped off with a steak dinner.

Columbiana CCCTC Student Chapter

NO DATE GIVEN

Activity: The Chapter held its election of officers for its senior (Sr.) and junior (Jr.) members. Elected were **Jen Baker,** chairman; **Justin Rohrbaugh,** vice chair; **Josh Voigt,** secretary; **Stan Roberts** (Sr.) and **Nick Reckner** (Jr.), publicity chairs; **Brian Talbot** (Sr.) and **Travis Coleman** (Jr.), treasurers; **Mike Riley** (Sr.) and **Ted Ingledue** (Jr.), membership chairs; and **Marcus Turner** (Sr.) and **Andrew Gibbs** (Jr.), SkillsUSA representatives.

DISTRICT 11

Director: Eftihios Siradakis
Phone: (989) 894-4101

CENTRAL MICHIGAN

SEPTEMBER 19

Speaker: **Dan Pendell,** cryogenics engineer

Affiliation: Nat'l Superconductivity Cyclotron Lab at Michigan State University

Topic: Welding for the next generation of nuclear accelerators

Activity: On hand were **Bill Eggleston,** chair; and **Jeff Grossman** and **Roy Bailiff,** vice chairs. The program was held in East Lansing, Mich.

DETROIT

OCTOBER 12

Speakers: **Mark Siehling,** VP engineering; and **Don DeCorte,** VP sales and marketing

Affiliation: RoMan Mfg. Co.

Topic: The history and future prospects of MFDC inverter power supplies

Activity: The program was held at the Ukrainian Cultural Center in Warren, Mich.

WESTERN MICHIGAN

SEPTEMBER 18

Speaker: **Birgit Klohs,** president

Affiliation: The Right Place, Inc.

Topic: The status of manufacturing in western Michigan

Activity: **Richard Freiberg** was named to represent the Section at the FABTECH Int'l & AWS Welding Show in Atlanta. The meeting was held at the RoMan manufacturing facility in Grand Rapids, Mich.

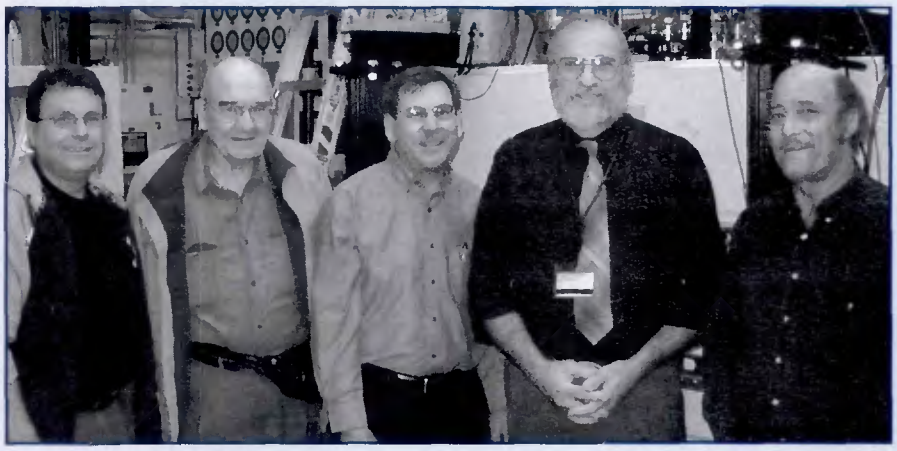

Shown at the Central Michigan Section program are (from left) Roy Bailiff, Bill Mumford, Chairman Bill Eggleston, speaker Dan Pendell, and Jeff Grossman.

Carl Hildebrand (left), Jim Goode (center), and Bill Mumford together total more than 150 years of AWS memberships. All three are past Detroit Section chairs, and Mumford is a past District 11 director.

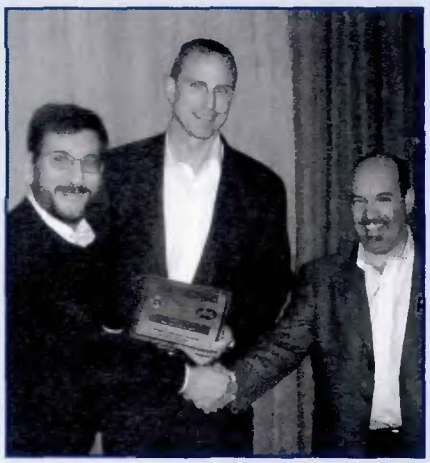

Mark Siehling (center) and Don DeCorte (right) receive a speaker plaque from Mike Karagoulis, Detroit Section technical program chair.

Ron Leibovitz (right) accepts a speaker gift from Kevin Fleming, Western Michigan Section chair, at the October meeting.

Speaker Birgit Klohs is shown with Kevin Fleming, Western Michigan Section chairman, at the September program.

OCTOBER 16

Speaker: **Ron Leibovitz,** vice president

Affiliation: Unitrol, Northbrook, Ill.

Topic: Soft Touch — Keeping spot welding machine operators safe

Activity: The program was held at O'Malley's Grill & Pub in Auburn Hills, Mich.

Shown are some of the participants in the welding workshop held at Miller Electric for instructors in District 12.

Fox Valley members get ready to demonstrate their shooting skills in September.

Dan Jones presented a two-day workshop for welding instructors in District 12.

Scott Kennedy proudly displays his top-prize-winning score card (49 hits out of 50 shots) at the Fox Valley clay shoot outing.

Speaker Brian Farkas (left) chats with Jeff McLeod, chairman of the Lakeshore Section.

DISTRICT 12

Director: Sean P. Moran
Phone: (920) 954-3828

District Event

OCTOBER 13, 14

Activity: Members from five District 12 Sections participated in a two-day Welding 101 Workshop taught by **Dan Jones,** Wisconsin Technical Educational Assn., Portage High School, and hosted by the Miller Electric Mfg. Co. Training Facility. Representatives from the Milwaukee, Fox Valley, Madison-Beloit, Racine-Kenosha, and Lakeshore Sections attended. Jones, who also serves as Wisconsin SkillsUSA coordinator, presented the class for 23 welding instructors.

FOX VALLEY

SEPTEMBER 16

Activity: The Section members participated in its Autumn Sporting Clay Event at J&H Game Farm in Shiocton, Wis. The hands-down winner was **Scott Kennedy** with 49 hits out of 50 shots.

LAKESHORE

SEPTEMBER 14

Activity: The Section members visited Marinette Marine Corp. for a tour of the construction areas and shops associated with the manufacture of the Lockheed Martin Littoral Combat Ship (LCS), which was launched on Sept. 23. **Bruce Halverson,** director of quality, presented an informative talk about the specially welded, semiplaning steel monohull design that affords the 377-ft-long vessel a draft of less than 13 ft.

OCTOBER 12

Speaker: **Brian Farkas,** technical manager
Affiliation: AlcoTec Wire Corp.
Topic: Cracking issues in aluminum from metallurgical and welding aspects
Activity: This Lakeshore Section program was held at Lighthouse Inn on the Lake, in Two Rivers, Wis.

MILWAUKEE

SEPTEMBER 21

Speaker: **David A. Maloney,** CWI, and Section publicity chairman
Affiliation: Team Industrial Services
Topic: The science behind nondestructive testing methods
Activity: Following the talk, Maloney held a lively question and answer session using the Stump the Expert format. About 45 members participated in the event.

UPPER PENINSULA

SEPTEMBER 14

Activity: The Section joined with members of the Lakeshore Section to tour Marinette Marine Corp. The guides included **Bruce Halverson,** QA manager; **Dan Roland,** quality engineer; **Jeff Bond,** training coordinator; and **Jeff Hoffman,** foreman. The highlight of the tour was viewing the activities to complete the first Littoral Combat Ship (LCS) *Freedom*, which was later launched on Sept. 23.

DISTRICT 13

Director: Jesse L. Hunter
Phone: (309) 359-3063

Mike Fitzpatrick (right) receives a speaker plaque from Gary Dugger, Indiana Section chairman, at the September program.

The frosting on this cake says it all.

Dan Roland, Upper Peninsula Section secretary, took this perfectly timed photograph of the launching of the LCS Freedom *on September 23. The U.P. Section toured the Marinette Marine facility where it was built on Sept. 14.*

Shown at the Milwaukee Section program are (from left) Joe Lefko, Don Cywinski, speaker David Maloney, and Craig Wentzel, Section chairman.

CHICAGO

OCTOBER 11

Speaker: **Mike Murphy,** sales manager
Affiliation: Miller Fall Protection, a Bacou-Dalloz Safety Co.
Topic: Personal fall protection
Activity: The program was held at Moraine Valley Community College in Palos Hills, Ill. Murphy's seminar included demonstrations of a variety of personal fall-protection equipment.

DISTRICT 14

Director: Tully C. Parker
Phone: (618) 667-7744

INDIANA

SEPTEMBER 18

Activity: The Section toured the U.S. Inspections Facility in Indianapolis, Ind. **Mike Fitzpatrick,** manager, presented a talk then conducted the tour. Section Chairman **Gary Dugger** announced that the Indiana Section had been selected to receive the prestigious AWS National Image of Welding Award. The announcement was topped off with a sheet cake decorated to celebrate the achievement. The award presentation took place at the FABTECH Int'l & AWS Welding Show in Atlanta.

LEXINGTON

AUGUST 23

Activity: Chairman **Frank McKinley,** of Hazard Technical College, and **Greg Cambell,** sales representative, Scott Gross Welding Co., presented the Woodrow Scott Memorial Scholarship Award to **Coy Hall.** Hall's mother, **Linda Whisman,** was present. The presentation was held at Hazard Technical College.

SEPTEMBER 28

Speaker: **Dave Griffith,** regional alloy specialist
Affiliation: The Lincoln Electric Co.
Topic: Welding nickel and stainless alloys
Speaker: **Jim Kerley,** president
Affiliation: Kentucky Community and Technical College
Topic: Why you need to become a pro-

Shown at the Chicago Section program are speaker Mike Murphy (left) and Chairman Martin Vondra.

Dave Griffith explained techniques for welding stainless steels to the college students at the Lexington Section program in September.

Shown at the Lexington Section scholarship-presentation program in August are (from left) Linda Whisman, Chair Frank McKinley, Coy Hall, and Greg Cambell.

Monty Rogers (left) accepts certificates of appreciation for serving as chairman of the Nebraska Section from current Chair Rich Hanny.

Nebraska Section members study thermite welding procedures used at Union Pacific Rail Yard. Shown (clockwise, from front) are Aaron Hernandez, Bob Moos, Tommy Hanchette, Chad Wirth, Chairman Rick Hanny, and Mike Frasier.

Shown at the Kansas City Charity Golf Tournament are (from left) Clay Shoemaker, Don Price, Chair Dennis Wright, Jim Keller, and Matt Calvert.

Adam Oberdorfer (left) and Jake Rabbass received scholarships at the Nebraska Section program in October.

fessional welder
Activity: This Lexington Section program, held at Kentucky Community and Technical College in Lexington, Ky., was attended by 95 people, including many college students.

DISTRICT 15

Director: Mace V. Harris
Phone: (952) 925-1222

DISTRICT 16

Director: Charles F. Burg
Phone: (515) 233-1333

KANSAS CITY

SEPTEMBER 13
Activity: The Section hosted its Charity Golf Tournament at Shoal Creek Golf Course in Kansas City, Mo., headed by Chairman **Dennis Wright.** The award winners included **King Doolen, Kip Smythia, Ron Frasier, Shane Eddleman, Scott Forbes, Jim Lanning, Will Lanning, Don Price, Matt Calvert, Jim Keller, Clay Shoemaker, Jeff Hilfiker, Dave Block, Marc Guernon, Dennis Castiglia, Troy Wyatt,** and **Jim Keller.**

SEPTEMBER 19
Activity: The Kansas City Section members toured the SPX Cooling Towers fa-

cility to study operations in its fabrication department, weld shop, and assembly areas. **Howard Rinne** conducted the program.

NEBRASKA

SEPTEMBER 21

Activity: The Section members met at Union Pacific Rail Yard in Missouri Valley, Iowa, for a demonstration of thermite welding. **Mike Boos,** manager of track programs, and **Aaron Hernandez,** senior instructor of track welding, demonstrated the procedures used to remove track sections and repair damaged and cracked rails.

OCTOBER 3

Activity: The Nebraska Section presented its scholarship awards at Metropolitan Community College, Omaha, Neb. **Adam Oberdorfer** earned the District 16 $1000 scholarship to continue his welding studies. The $1250 Rex Stacy Memorial Scholarship was awarded to **Jake Rabbass.** Both students study at the college.

OCTOBER 19

Speaker: **Rich DePue,** director, education and government advocacy
Affiliation: American Welding Society
Topic: Where can welding take you?
Activity: Students from Hastings College traveled 150 miles to attend this program. The meeting was held at Holiday Inn in Omaha, Neb. **Dan Fogelman** of Linweld has recently taken the post of treasurer.

Hastings College students attended the Nebraska Section program in October.

Rich DePue (right) accepts a speaker appreciation plaque from Mike Frazer, Nebraska Section vice chair, at the October program.

Speaker Rodger Johnson (left) is shown with Howie Sifford, North Texas Section chair.

DISTRICT 17

Director: Oren P. Reich
Phone: (254) 867-2203

NORTH TEXAS

OCTOBER 16

Speaker: **Rodger Johnson**
Affiliation: Red-D-Arc, Houston, Tex.
Topic: Automation and fabrication fixturing and rental arrangements
Activity: The meeting was held at Spring Creek Barbeque in Dallas, Tex.

OZARK

OCTOBER 19

Speaker: **Dick Cady,** territory manager
Affiliation: Kirk Welding Supply, Kansas City
Topic: Shielding gases for use with gas metal arc welding of stainless steels
Activity: Cady demonstrated the short circuit and spray transfer techniques using Trimix, a specially formulated argon-based gas. **Alan Schumann** from 3M Safety presented a short talk on hexavalent chromium emissions during welding of stainless steels. The meeting was held at Ozarks Technical Community College in Springfield, Mo.

Dan Lawson (left) and Jay Rufner man the Tulsa Section's display booth at the Tulsa State Fair.

In October, Tulsa Section member Tim Cruse was recognized by the Tulsa Technology Center for his career achievements.

TULSA

SEPTEMBER 28–OCTOBER 8

Activity: The Section manned a booth for ten days at the Tulsa State Fair in Tulsa, Okla., to stimulate local interest in the welding profession. Included were representatives from several welding distributors, area welding schools, private industry, welding engineers, supervisors, retired welding experts, and laboratories engaged in weld testing.

SEPTEMBER 26

Speakers: **Robert Strattan,** prof. emeritus electrical engineering; and **Andrew Harmon,** engineering graduate student
Topic: Tulsa University's latest hybrid gas-

The District 19 conference attendees included representatives from the Alaska, British Columbia, Inland Empire, Northern Alberta, Olympic, Portland, Puget Sound, and Spokane Sections.

Shown at the Tulsa Section program in September are (from left) Chair Jerry Knapp, speakers Robert Strattan and Andrew Harmon, and Joshua Buck.

Speaker Vincent Summa (left) is shown with Glynn Savage, Sabine Section chairman at the September program.

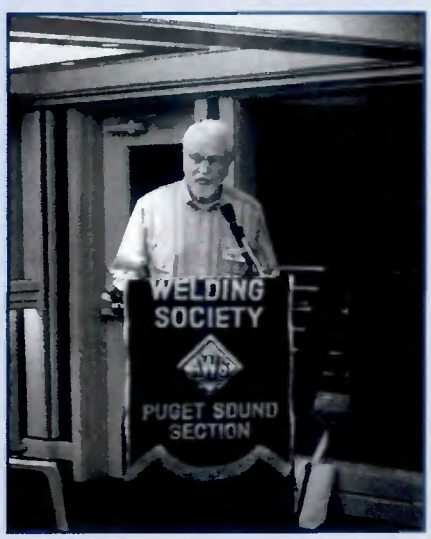

Shipbuilding historian James Cole shared his stories with the Puget Sound Section members.

electric vehicle project, sponsored by General Motors and the U.S. DOE
Activity: The program was held in Tulsa Okla.

OCTOBER 1
Activity: The Tulsa Section honored **Tim Cruse,** a member of its executive committee, for his story published in the fall issue of the Tulsa Technology Center newsletter, *Advisor Success.* Cruse, who studied at Tulsa Tech during the 80s, credits the center for equipping him with the trades skills that have provided him with a prosperous career. Currently, he works for Tulsa's Linde BOC Process Plant as general foreman at the structural and vessels shop, and serves as a member of the Tulsa Tech Advisory Committee.

DISTRICT 18

Director: John L. Mendoza
Phone: (210) 353-3679

SABINE

SEPTEMBER 19
Speaker: **Vincent Summa,** president
Affiliation: Techcorr, Houston, Tex.
Topic: Guided wave ultrasonics
Activity: The incoming officers and directors were introduced. **Carey Wesley** was recognized on his retirement for his 40 years of service to the welding program at Lamar Institute of Technology.

DISTRICT 19

Director: Phil Zammit
Phone: (509) 468-2310, ext. 120

District 19 Conference

MAY 26, 27
Activity: Representatives from all of the

District 19 Sections met for their annual business meeting. Sections represented included Alaska, British Columbia, Inland Empire, Northern Alberta, Olympic, Portland, Puget Sound, and Spokane.

PUGET SOUND

OCTOBER 5

Speaker: **James Cole**

Affiliation: Elliot Bay Design Group

Topic: A history of shipbuilding in the Pacific Northwest from 1788 to the present

Activity: The program was held at Rock Salt Steak House in Seattle, Wash., for 53 attendees.

OCTOBER 6

Activity: The Puget Sound Section hosted a technical seminar at Renton Technical College in Renton, Wash. Six speakers discussed a varienty of topics on welding process for joining titanium and stainless steels. The speakers included AWS President **Damian Kotecki,** Lincoln Electric Co.; **Steve Lamb,** consultant, Inco Alloys; **Roger Bushey,** research engineer, ESAB; **Jim Richardson,** a titanium fabrication consultant; **Blaine Maki,** manager, Metaltest; and **J. M. Dwight,** welding engineer, Chehalis. On hand were 29 students from Nooksack Valley High School, and 30 students from Renton Technical College. **Stephen Pollard,** welding engineer, answered technical questions presented to him by the attendees.

Shown at the Puget Sound program Oct. 6 are (from left) Stephanie Carlberg, Robby Alex, Marshall Judy, Jon Kooistra, Rhonda Juergens, and John Graep.

The first-place team members in the Spokane Section's golf outing are (from left) Greg Walmsley, Don Nelson, Jerry Nelson, and Brandon Rackham.

SPOKANE

SEPTEMBER 19

Activity: The Section participated in a students' night program at Spokane Skills Center. Speakers included **Karl Susz,** Lincoln Electric, **Ben Finnoe,** plant manager at Brooklyn Iron Works, and **Brad Johnson** of Career Path Services of Spokane. Each spoke on various aspects of the shortage of welders, industry needs locally and nationwide, welder requirements, the various career paths welders can follow after entering the industry, and wages currently paid in the various levels of employment. The tour of the facility was conducted by **Andrew Syder,** director, and a welding instructor. Certificates of appreciation were presented to outgoing Section Chair **Rick Henson** of Oxarc, and outgoing District 19 Director **Phil Zammit** of Brooklyn Iron Works.

SEPTEMBER 30

Activity: The Spokane Section held its annual golf outing at Deer Park Golf Club in Spokane, Wash. The first-place team included **Greg Walmsley, Don Nelson, Jerry Nelson,** and **Brandon Rackham.**

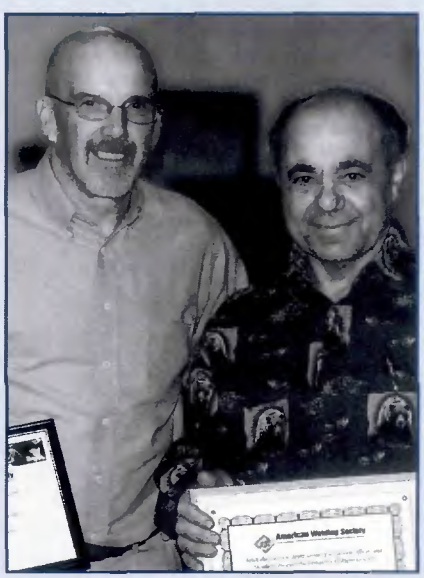

Outgoing Spokane Section Chair Rick Henson (left) and Phil Zammit, outgoing District 19 director, display their certificates of appreciation for their many years of service to the Society.

Rich Irving (left) is presented a plaque for his outstanding service to the Spokane Section by Phil Zammit, District 19 director.

Albuquerque Section winners included (from left) Mike Thomas, Richard MacFarland III, Ron Hackney, Ken Caraveo, Manuel Aragon, and Dave Drake.

Kelly Bingham (left) receives the Dalton E. Hamilton Memorial Section CWI of the Year Award from Albuquerque Vice Chair Tom Lienert.

Steve Siderius discussed weld nondestructive inspection techniques at the Spokane Section meeting in October.

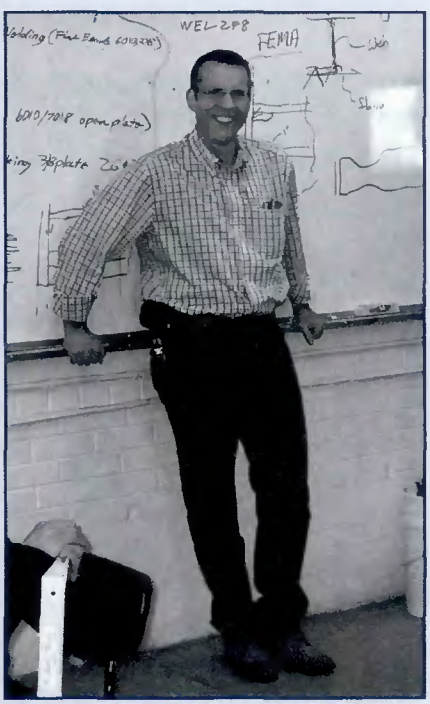

Bill Komlos, District 20 director, discussed the AWS and the D1.8 welder qualification test at the Colorado Section program.

Dean Mitchell, welding instructor at the Emily Griffith Opportunity School in Denver, is shown at the Colorado Section program in September.

OCTOBER 18
Speaker: **Steve Siderius,** operations manager
Affiliation: Mountain Inspection Services
Topic: Welding NDE techniques
Activity: Spokane Section Chair **Art Sabiston** introduced the incoming officers. District 19 Director **Phil Zammit** presented a plaque for outstanding long-term service to the Section to **Rich Irving** of Brooklyn Iron Works. The meeting was held at Cathay Inn in Spokane, Wash.

DISTRICT 20

Director: William A. Komlos
Phone: (801) 560-2353

ALBUQUERQUE

SEPTEMBER 28
Speakers: **Tom Lienert,** vice chairman; and **Kelly Bingham,** CWI and treasurer
Affiliation: Los Alamos Nat'l Laboratory
Topics: Introduction to metallurgy for welding personnel, and welding code requirements and how to meet them
Activity: The speakers directed their talks to the welding students attending Central New Mexico Community College, where the program was held. The Section Appreciation Award was presented to Program Chair **Mike Thomas** and **Dave Drake. Richard MacFarland III** received the Student Chapter Member Award; **Ron Hackney** received the Section Meritorious Award; **Manuel Aragon** and **Jeremy Weidner** received the State SKILLS Award; and **Kelly Bingham** received the Dalton E. Hamilton Memorial Section CWI of the Year Award. **Ken Caraveo** was the recipient of a District 20 scholarship.

COLORADO

SEPTEMBER 8
Speaker: **William Komlos,** District 20 director
Affiliation: ArcTech LLC
Topic: D1.8 welder qualifications
Activity: The program was held at the Emily Griffith Opportunity School in Denver, Colo., where Komlos addressed the students and staff in the welding program. The school's fully accredited AWS SENSE program offers certifications up to the Master Welder level, headed by instructor **Dean Mitchell,** an AWS CWE.

UTAH

SEPTEMBER 20
Activity: The Section board held a meeting at the Airport Hilton in Salt Lake City. The new board members are **Greg Bugni,** chairman; **Michelle Nicholson,** vice chair; **Woody Cook,** treasurer; and **John Miller,** secretary. **William Komlos,** District 20 director, attended the meeting.

Speaker Regis Geisler (left) accepts a speaker gift from Lorne Grimes, Sacramento Section vice chair.

DISTRICT 21

Director: Jack D. Compton
Phone: (661) 362-3218

DISTRICT 22

Director: Kent S. Baucher
Phone: (559) 276-9311

SACRAMENTO

SEPTEMBER 20

Speaker: **Regis Geisler,** CWI, sales engineer
Affiliation: The Lincoln Electric Co., El Dorado Hills, Calif.
Topic: FEMA 353, welding guidelines for seismic structural retrofit, and the migration to using AWS D1.8

OCTOBER 18

Speaker: **Simon L. Engel**
Affiliation: HDE Technologies
Topic: The future of laser beam welding
Activity: **Bob Milliron,** a founding member of the Sacramento Valley Section, was presented his Life Membership Award for 35 years of service to the Society. **Mark Bell,** a Director-at-large and a past District 22 director, spoke on behalf of Milliron's participation in the Society. Section Secretary **Don Robinson** received the District Meritorious Award, Treasurer **Mark Feuerbach** received the District Educator Award, Past Chair **Kerry Shatell** received the Section Meritorious Award, and Chairman **Mike Rabo** received the Section Educator Award. The program was held at Ohana Gardens Restaurant in Rancho Cordova, Calif.

SAN FRANCISCO

OCTOBER 4

Speaker: **Bill Kiikvee,** product manager
Affiliation: Advanced Pressure Technology, Napa, Calif.
Topic: Welding valves and regulators for high-purity applications
Activity: The program was held at Spenger's Restaurant in Berkeley, Calif.

Shown at the Utah Section program are incoming officers (from left) Treasurer Woody Cook, Secretary John Miller, Vice Chair Michelle Nicholson, and Chairman Greg Bugni.

The Sacramento Section members posed for a group shot at their October meeting.

Bob Milliron (left) accepts his Life Member Award from Mike Rabo, Sacramento Section chairman, in October.

Mark Bell detailed many of Bob Milliron's contributions to the Society at the Sacramento Section program in October.

SANTA CLARA VALLEY

OCTOBER 9

Speaker: **Steve Mellinger**
Affiliation: Terminal Manufacturing
Subject: Challenges in today's welding industries
Activity: The meeting was held at Harry's Hofbrau in San Jose, Calif.

Speaker Bill Kiikvee (center) is shown with Richard Hashimoto (left), San Francisco Section chairman, and Vice Chairman Tom Smeltzer.

New AWS Supporters

Supporting Companies

Engineered Lifting Technologies, Inc.
100 W. Drullard Ave.
Lancaster, NY 14086

Gestamp Alabama, Inc.
7000 Jefferson Metropolitan Pkwy.
McCalla, AL 35111

ICM, Inc.
310 N. First St.
Colwich, KS 67030

Integrity Aero Service LLC
14900 Bristol Pk. Blvd., Ste. C
Edmond, OK 73013

Lax Fabricating LLC
215 Twilight St.
La Crescent, MN 55947

Melton Machine & Control Co.
6350 Bluff Rd.
Washington, MO 63090

Nibrock, Inc.
7105 Arden Rd., PO Box 99
Chanchula, AL 36521

Quincy Joist Co.
520 S. Virginia St.
Quincy, FL 32551

Affiliate Companies

BW Custom Welding
256 Cherry Point Rd. N.
Okatie, SC 29909

CFC & Associates, Inc.
5989 Haines Rd.
St. Petersburg, FL 33714

Delval Equipment Corp.
295 Meadowlands Blvd.
Washington, PA 15301

GCL, Inc.
2559 Brandt School Rd., Ste. 200
Wexford, PA 15090

Hybriweld, LLC
PO Box 422
Berwick, LA 70342

Industrial Mfg. Services
1282 Camp Creek Rd.
Lancaster, SC 29720

Iron Specialist, Inc.
1102 Sharp Cir.
North Las Vegas, NV 89030

Kowloon-Canton Railway Corp.
9 Lok King St. Fo Tan Sha Tin
N T Hong Kong, China

Lachlan, Inc.
8801 Torchwood Dr.
Trinity, FL 34655

MAC Fabrication
PO Box 219
4300 N. Sherman Rd.
Winnebago, WI 54985

MTR Corp., Ltd.
LRC 8/7 MTR Tower 1
Teffod Plaza Kowloon Bay
Kowloon, Hong Kong

Educational Institutions

Botetourt Technical Education Center
253 Poor Farm Rd., PO Box 97
Fin Castle, VA 24090-0097

Coleman Independent School District
201 W. 15th St.
Coleman, TX 76834

General Distributing Co.
1327 S. 29th St. W.
Billings, MT 59102

Kermit High School
601 S. Poplar, Kermit, TX 79745

Laser Advantage LLC
5 Pines St. Extension
Nashua, NH 03060

Sabin Schellenberg Center
14211 SE Johnson Rd.
Milwaukie, OR 97267

Southeastern Technical College
3001 E. First St.
Vidalia, GA 30474

Southwest Applied Technology College
510 W. 800 S.
Cedar City, UT 84720

Systems Contracting Corp.
214 N. Washington, Ste. 700
El Dorado, AR 71730

Texarkana Area Vocational Center
1500 Jefferson Ave.
Texarkana, AR 71854

University of Idaho
875 Perimeter Dr.
Moscow, ID 83844-2281

Warren County Area
Technology Center
365 Technology Way
Bowling Green, KY 42101 ♦

Membership Counts

Member Grades	As of 11/1/06
Sustaining	447
Supporting	271
Educational	400
Affiliate	361
Welding distributor	46
Total corporate members	**1,525**
Individual members	44,752
Student + transitional members	5,007
Total members	**49,759**

Nominations Sought for Robotic Arc Welding Award

December 31 is the deadline for submitting your nominations for candidates to receive the 2007 Robotic and Automatic Arc Welding Award.

The nomination packet should include a summary statement of the candidate's accomplishments, interests, educational background, professional experience, publications, honors, and awards.

Send the nomination packet to Wendy Sue Reeve, awards coordinator, 550 NW LeJeune Rd., Miami, FL 33126. Contacts: (800/305) 443-9353, ext. 293, or e-mail *wreeve@aws.org*.

The award was created to recognize individuals for their significant achievements in the area of robotic arc welding.

This work can include the introduction of new technologies, establishment of the proper infrastructure (training, service, etc.) to enable success, and any other activity having significantly improved the state of a company and/or industry.

The Robotic and Automatic Arc Welding Award is funded by private contributions. It is presented annually at the AWS Awards/AWS Foundation Recognition Ceremony and Luncheon, held in conjunction with the FABTECH International & AWS Welding Show. ♦

Guide to AWS Services

550 NW LeJeune Rd., Miami, FL 33126
www.aws.org; phone (800/305) 443-9353; FAX (305) 443-7559
(Phone extensions are shown in parentheses.)

AWS PRESIDENT

Damian J. Kotecki
Damian_Kotecki@lincolnelectric.com
The Lincoln Electric Co.
22801 St. Clair Ave.
Cleveland, OH 44117-1199

ADMINISTRATION

Executive Director
Ray W. Shook.. *rshook@aws.org* .....(210)

CFO/Deputy Executive Director
Frank R. Tarafa.. *tarafa@aws.org* .....(252)

Associate Executive Director
Cassie R. Burrell.. *cburrell@aws.org* ....(253)

Associate Executive Director
Jeff Weber.. *jweber@aws.org* .....(246)

Executive Assistant for Board Services
Gricelda Manalich.. *gricelda@aws.org* ..(294)

Administrative Services

Managing Director
Jim Lankford.. *jiml@aws.org* .....(214)

IT Network Director
Armando Campana..*acampana@aws.org* .(296)

Director
Hidail Nunez..*hidail@aws.org*.....(287)

COMPENSATION and BENEFITS

Director
Luisa Hernandez.. *luisa@aws.org* .....(266)

INT'L INSTITUTE of WELDING

Senior Coordinator
Sissibeth Lopez . . *sissi@aws.org* .....(319)
Provides liaison services with other national and international professional societies and standards organizations.

GOVERNMENT LIAISON SERVICES

Hugh K. Webster..... *hwebster@wc-b.com*
Webster, Chamberlain & Bean
Washington, D.C.
(202) 466-2976; FAX (202) 835-0243
Identifies funding sources for welding education, research, and development. Monitors legislative and regulatory issues of importance to the industry.

Brazing and Soldering Manufacturers' Committee

Jeff Weber.. *jweber@aws.org* .....(246)

RWMA — Resistance Welding Manufacturing Alliance

Manager
Susan Hopkins.. *susan@aws.org* .....(295)

WEMCO — Welding Equipment Manufacturers Committee

Manager
Natalie Tapley.. *tapley@aws.org* .....(444)

CONVENTION and EXPOSITIONS

Associate Executive Director
Jeff Weber.. *jweber@aws.org* .....(246)

Corporate Director, Exhibition Sales
Joe Krall.. *krall@aws.org* .....(297)

Organizes the annual AWS Welding Show and Convention, regulates space assignments, registration items, and other Expo activities.

PUBLICATION SERVICES

Department Information .....(275)

Managing Director
Andrew Cullison.. *cullison@aws.org* ....(249)

Welding Journal

Publisher/Editor
Andrew Cullison.. *cullison@aws.org* ....(249)

National Sales Director
Rob Saltzstein.. *salty@aws.org* .....(243)

Society and Section News Editor
Howard Woodward..*woodward@aws.org* (244)

Welding Handbook

Welding Handbook Editor
Annette O'Brien.. *aobrien@aws.org* ....(303)

Publishes the Society's monthly magazine, *Welding Journal*, which provides information on the state of the welding industry, its technology, and Society activities. Publishes *Inspection Trends*, the *Welding Handbook*, and books on general welding subjects.

MARKETING COMMUNICATIONS

Director
Ross Hancock.. *rhancock@aws.org* ....(226)

Assistant Director
Adrienne Zalkind.. *azalkind@aws.org* . .(416)

MEMBER SERVICES

Department Information .....(480)

Associate Executive Director
Cassie R. Burrell.. *cburrell@aws.org* ....(253)

Director
Rhenda A. Mayo... *rhenda@aws.org* ....(260)
Serves as a liaison between Section members and AWS headquarters. Informs members about AWS benefits and activities.

EDUCATION SERVICES

Director, Education Services Administration and Convention Operations
John Ospina.. *jospina@aws.org* .....(462)

Director, Education and Government Advocacy
Richard J. DePue.. *rdepue@aws.org* ....(237)

Director, Education Product Development
Christopher Pollock.. *cpollock@aws.org* (219)

Tracks effectiveness of programs and develops new products and services. Coordinates in-plant seminars and workshops. Administers the S.E.N.S.E. program. Assists Government Liaison Committee with advocacy efforts. Works with Education Committees to disseminate information on careers, national education and training trends, and schools that offer welding training, certificates, or degrees.
Also responsible for conferences, exhibitions, and seminars on topics ranging from the basics to the leading edge of technology. Organizes CWI, SCWI, and 9-year renewal certification-driven seminars.

AWS AWARDS, FELLOWS, COUNSELORS

Senior Manager
Wendy S. Reeve.. *wreeve@aws.org* .....(293)
Coordinates AWS awards and AWS Fellow and Counselor nominees.

CERTIFICATION OPERATIONS

Department Information .....(273)

Managing Director
Peter Howe.. *phowe@aws.org* .....(309)

Director, Operations
Terry Perez.. *tperez@aws.org* .....(470)

Director, Int'l Business Accreditation and Welder Certification
Walter Herrera.. *walter@aws.org* .....(475)
Provides information on personnel certification and accreditation services.

TECHNICAL SERVICES

Department Information .....(340)

Managing Director
Andrew R. Davis.. *adavis@aws.org* .....(466)
Int'l Standards Activities, American Council of the International Institute of Welding (IIW)

Director, National Standards Activities
John L. Gayler.. *gayler@aws.org* .....(472)
Structural Welding, Machinery and Equipment Welding, Robotic and Automatic Welding, Computerization of Welding Information

Manager, Safety and Health
Stephen P. Hedrick.. *steveh@aws.org* . .(305)
Metric Practice, Personnel and Facilities Qualification, Safety and Health, Joining of Plastics and Composites

Technical Publications

AWS publishes about 200 documents widely used in the welding industry.

Senior Manager
Rosalinda O'Neill.. *roneill@aws.org* ....(451)

Technical Editor
Cynthia Jenney .. *cynthiaj@aws.org* ....(304)
Brazing Handbook, Soldering Handbook, Technical Editing

Staff Engineers/Committee Secretaries
Annette Alonso.. *aalonso@aws.org* ....(299)
Welding in Sanitary Applications, Automotive Welding, Resistance Welding, High-Energy Beam Welding, Aircraft and Aerospace, Oxyfuel Gas Welding and Cutting

Stephen Borrero.. *sborrero@aws.org* ....(334)
Welding Iron Castings, Joining of Metals and Alloys, Brazing and Soldering, Brazing Filler Metals and Fluxes

Rakesh Gupta.. *gupta@aws.org* .....(301)
Filler Metals and Allied Materials, Int'l Filler Metals, Instrumentation for Welding, UNS Numbers Assignment

Brian McGrath . *bmcgrath@aws.org* ....(311)
Methods of Inspection, Mechanical Testing of Welds, Thermal Spray, Arc Welding and Cutting, Welding in Marine Construction, Piping and Tubing, Titanium and Zirconium Filler Metals, Filler Metals for Naval Vessels

Selvis Morales.....*smorales@aws.org* . .(313)
Welding Qualification, Friction Welding, Railroad Welding, Definitions and Symbols

Note: *Official interpretations of AWS standards may be obtained only by sending a request in writing to the Managing Director, Technical Services. Oral opinions on AWS standards may be rendered. However, such opinions represent only the personal opinions of the particular individuals giving them. These individuals do not speak on behalf of AWS, nor do these oral opinions constitute official or unofficial opinions or interpretations of AWS. In addition, oral opinions are informal and should not be used as a substitute for an official interpretation.*

Nominees for National Office

Only Sustaining Members, Members, Honorary Members, Life Members, or Retired Members who have been members for a period of at least three years shall be eligible for election as a director or national officer.

It is the duty of the National Nominating Committee to nominate candidates for national office. The committee shall hold an open meeting, preferably at the Annual Meeting, at which members may appear to present and discuss the eligibility of all candidates.

To be considered a candidate for the positions of president, vice president, treasurer, or director-at-large, the following qualifications and conditions apply:

President: To be eligible to hold the office of president, an individual must have served as a vice president for at least one year.

Vice President: To be eligible to hold the office of vice president, an individual must have served at least one year as a director, other than executive director and secretary.

Treasurer: To be eligible to hold the office of treasurer, an individual must be a member of the Society, other than a Student Member, must be frequently available to the national office, and should be of executive status in business or industry with experience in financial affairs.

Director-at-Large: To be eligible for election as a director-at-large, an individual shall previously have held office as chairman of a Section; as chairman or vice chairman of a standing, technical, or special committee of the Society; or as District director.

Interested parties should write a letter stating which office they seek, including a statement of qualifications, their willingness and ability to serve if nominated and elected, and 20 copies of their biographical sketch.

This material should be sent to James E. Greer, Chairman, National Nominating Committee, American Welding Society, 550 NW LeJeune Rd., Miami, FL 33126.

The next meeting of the National Nominating Committee is scheduled for November 2007. The term of office for candidates nominated at this meeting will commence January 1, 2009. ♦

Honorary Meritorious Awards

The Honorary-Meritorious Awards Committee makes recommendations for the nominees presented for Honorary Membership, National Meritorious Certificate, William Irrgang Memorial, and the George E. Willis Awards. These awards are presented during the FABTECH International & AWS Welding Show held each fall. The deadline for submissions is December 31 prior to the year of awards presentations. Send candidate materials to Wendy Sue Reeve, Secretary, Honorary-Meritorious Awards Committee, 550 NW LeJeune Rd., Miami, FL 33126. Descriptions of the awards follow.

National Meritorious Certificate Award: This award is given in recognition of the candidate's counsel, loyalty, and devotion to the affairs of the Society, assistance in promoting cordial relations with industry and other organizations, and for the contribution of time and effort on behalf of the Society.

William Irrgang Memorial Award: This award is administered by the American Welding Society and sponsored by The Lincoln Electric Co. to honor the late William Irrgang. It is awarded each year to the individual who has done the most over the past five-years to enhance the American Welding Society's goal of advancing the science and technology of welding.

George E. Willis Award: This award is administered by the American Welding Society and sponsored by The Lincoln Electric Co. to honor George E. Willis. It is awarded each year to an individual for promoting the advancement of welding internationally by fostering cooperative participation in areas such as technology transfer, standards rationalization, and promotion of industrial goodwill.

International Meritorious Certificate Award: This award is given in recognition of the recipient's significant contributions to the worldwide welding industry. This award reflects "Service to the International Welding Community" in the broadest terms. The awardee is not required to be a member of the American Welding Society. Multiple awards can be given per year as the situation dictates. The award consists of a certificate to be presented at the awards luncheon or at another time as appropriate in conjunction with the AWS president's travel itinerary, and, if appropriate, a one-year membership in the American Welding Society.

Honorary Membership Award: An Honorary Member shall be a person of acknowledged eminence in the welding profession, or who is accredited with exceptional accomplishments in the development of the welding art, upon whom the American Welding Society sees fit to confer an honorary distinction. An Honorary Member shall have full rights of membership. ♦

Hang out with your fellow members online.

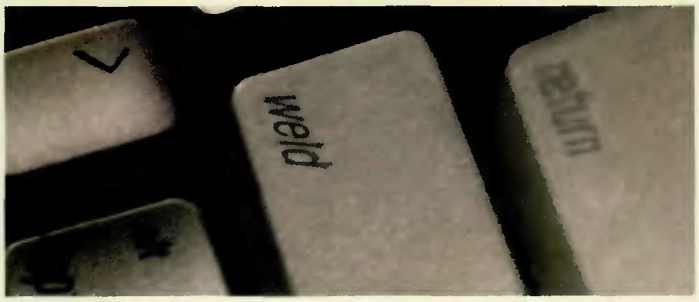

The AWS website includes an online forum with dozens of welding topics and over 20,000 interesting posts. Browse through used equipment for sale, pose questions to the welding community, and share your own "tricks of the trade."

Just surf to http://www.aws.org/cgi-bin/mwf/forum_show.pl

See you on the Weld-Wide Web!

American Welding Society

Founded in 1919 to advance the science, technology and application of welding and allied processes including joining, brazing, soldering, cutting and thermal spraying.

Circle No. 12 on Reader Info-Card

Corrosion Control Topic of New Text

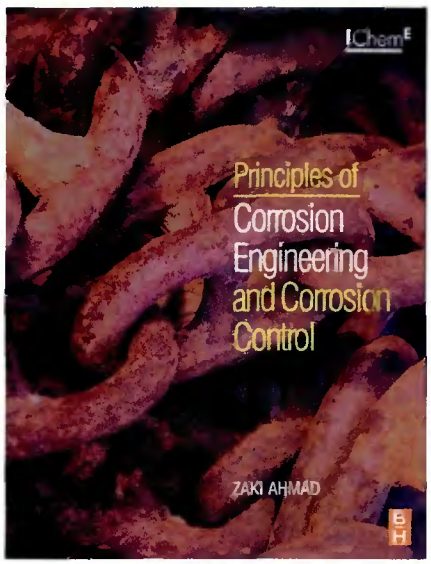

Principles of Corrosion Engineering and Corrosion Control is written for mechanical, civil, and petrochemical engineers as well as students and practicing corrosion engineers. Its well-illustrated 672 pages provide worked examples and definitions, covers basic corrosion principles as well as more advanced information for postgraduate students and professionals. Included are the basic principles of electrochemistry and chemical thermodynamics as background information. Each form of corrosion is covered by definition, description, mechanism, examples, and preventative methods. Case histories of failures are cited for each form. The end-of-chapter questions are keyed to an online solutions manual. The author, Zaki Ahmad, is from King Fahd University of Petroleum & Minerals, Saudi Arabia. The $69.95 paperback volume may be ordered from *www.books.elsevier.com/engineering.*

Clamping Products Pictured in Catalog

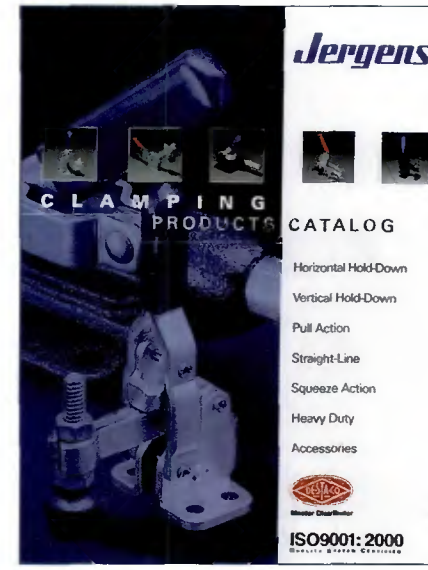

A 72-page catalog illustrates and describes the company's line of horizontal and vertical hold-down, pull-action, straight-line, squeeze-action, and heavy-duty toggle clamp products. Included is a large selection of De-Sta-Co clamping products. The product data include photographs, dimensions, specifications, schematic drawings, ordering, and installation information. Presented is a convenient conversion chart that cross-references part numbers for clamping products from other manufacturers: Carr Lane, De-Sta-Co, and Good Hand.

Jergens, Inc. **114**
Jergens Way, 15700 S. Waterloo Rd., Cleveland, OH 44110-3898

UltraCore™ Wire Products Detailed in Literature

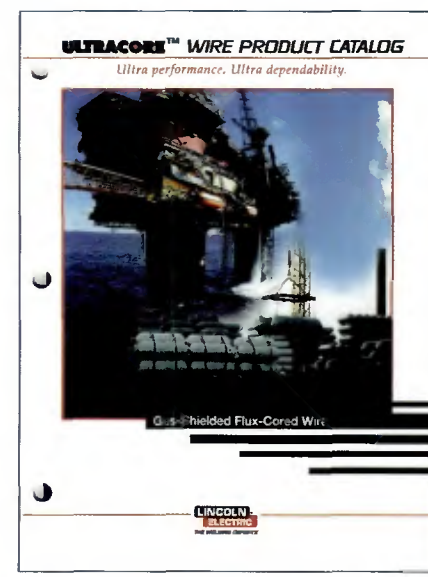

A 22-page, full-color catalog details the UltraCore™ gas shielded flux cored wire

product line specified for a wide range of stuructural and general fabrication applications. Included is a detailed selection guide to match shielding gases, AWS class, diffusible hydrogen levels, and arc performance with the corresponding wire. Wires are detailed for mechanical properties, deposit composition, and typical operating procedure. A question and answer section clarifies the flux cored wire classifications and their applications.

The Lincoln Electric Co. **115**
22801 St. Clair Ave., Cleveland, OH 44117-1199

CD Handbook Details High-Temperature Products

The 68-page handbook, *The Ultimate Guide to High-Temp Adhesives and Specialty Materials for Use to 3000°F,* available on a CD, contains detailed product descriptions, illustrations, users' reports, instructions, and convenient conversion tables for fast-setting epoxies, stainless steel putties, fast-setting ceramic adhesives, ultrafine alumina adhesives, and other products for high-temperature applications. Designed for use in laboratories, research facilities, and industrial plants, the CD offers desktop access to principal components, performance, thermal and electrical conductivity, resistance to heat and corrosives, melting points, tensile and bond strengths, elongation, density, ductility, hardness, specific heats, and other engineering design factors.

Cotronics Corp. **116**
3379 Shore Pkwy., Brooklyn, NY 11235

NEW PRODUCTS

— continued from page 21

tool's miniature torch head is ⅝ in. long and ⅜ in. in diameter. Available with 70- and/or 180-deg head configurations, it is also maneuverable. The entire torch is 8½ in. long and ¾ in. in diameter at its widest point. Compatible tungsten sizes include 0.020, 0.040, and 1/16 in. diameters. This torch can be ordered with either a 12.5- or 25-ft

power cable, and is available with a built-in gas control valve for use with power sources that do not feature solenoid valves.

Weldcraft **111**
2741 N. Roemer Rd., Appleton, WI 54911

Cutting Wheel Features Rib Design

The ZIP™ cutting wheels are manufactured with a process that imparts a high-low rib design into each wheel for faster cutting, less friction, straighter cuts, cooler cutting, and longer life. They are designed to give straighter cuts with better operator

control on mild steel, stainless steel, aluminum, titanium, and other materials. Also, the rib design cuts so smooth and cool, there is virtually no heat discoloration when cutting thin stainless sheet.

J. Walter, Inc. **112**
141 Locust St., Hartford, CT 06114-1504

Check Tube Design Includes Poppet Housing

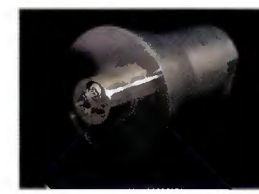

The company's check tube design for its ultrahigh-pressure waterjet intensifier pumps feature a low-pressure poppet and high-pressure poppet that open and close, allowing low-pressure water to flow into the high-pressure cylinder and ultrahigh-pressure water to leave the high-pressure cylinder. The check tube design includes an improved low-pressure poppet, poppet housing, and simplified check tube design. Also, the design allows the low-pressure poppet assembly to be secured by a single hollow screw and does not require an adhesive.

Jet Edge, Inc. **113**
12070 43rd St. NE, St. Michael, MN 55376-8427

Hobart Names VP

Grant Harvey

Hobart Brothers, Troy, Ohio, has named **Grant Harvey** as vice president and general manager for its North American Tubular Wire Div. With more than 20 years of experience in the field, Harvey most recently served as vice president of sales and marketing for the company's Global Tubular Wire Div.

Airgas Names Two Executives

Airgas, Radnor, Pa., has appointed **Robert M. McLaughlin** as senior vice president and CFO, and **John C. van Roden Jr.** to a director. McLaughlin previously served the company as controller since 2001. Van Roden, executive vice president of P. H. Glatfelter Co., will complete the term of Director **Robert L. Yohe,** who has retired.

Canadian Welding Bureau Fills Key Post

Douglas R. Luciani

The Canadian Welding Bureau (CWB), Mississauga, Ont., Canada, has appointed **Douglas R. Luciani** president and CEO of CWB Group — Industry Services. Previously, Luciani served the Canadian Welding Bureau as its general manager.

National Standard Names Weld Sales Manager

Jim Harbaugh has been promoted to national weld sales manager at National Standard, Niles, Mich. With the company for 41 years, Harbaugh most recently served as director of sales and marketing and district sales weld manager.

Hypertherm Hires Sales Manager

Brent Malik

Hypertherm, Inc., Hanover, N.H., has appointed **Brent Malik** as district sales manager for Michigan and northern Ohio. He succeeds **Alan Hughes** who has retired. Previously, Malik worked for D-M-E where he was the sales representative for Choice Mold Components.

Cyl-Tec Expands Regional Sales Team

Cyl-Tec, Inc., Aurora, Ill., a supplier of cylinders, cylinder services, and accessories for the compressed gas industry, has

appointed **Rich Braatz, Alan Bustamante,** and **Stan Urban** as regional sales managers. Braatz will manage the Midwest business, Bustamante will service the Northeast region, and Urban will head the Southeast region.

Shiloh Industries Makes Executive Appointments

Shiloh Industries, Valley City, Ohio, a supplier of engineered welded blanks, stampings, and modular assemblies for the automotive industries, has named **Jim Walker** as vice president, sales and business development; **Tony Parente** as vice president, manufacturing operations; and **Jim Keys** as senior vice president and chief technology officer for Shiloh Industries. Walker previously worked at Takata Holdings, Inc.; Parente, with the company for 27 years, most recently was group general manager; and Keys previously served the company as senior vice president of advanced technology/sales and marketing.

Member Milestone

Edward A. Metzbower

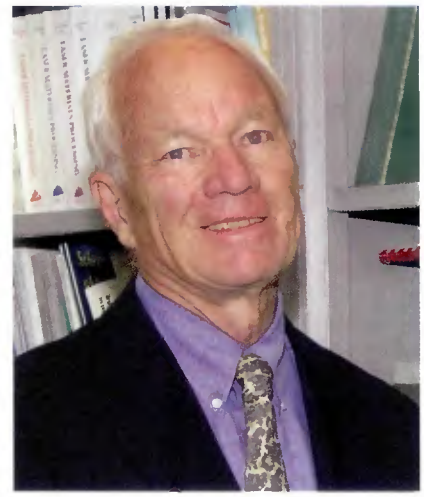

Edward A. Metzbower

Edward A. Metzbower, a Fellow of the American Welding Society and a member of the Washington, D.C., Section, has been selected to receive the 2006 Schawlow Award from the Laser Institute of America (LIA). The award is given to recognize individuals who have made distinguished contributions to applications of lasers in science, industry, or education. It is the LIA's highest achievement award, named for Prof. Arthur Schawlow who received a Nobel Prize for physics in 1981 for his contributions to the development of laser spectroscopy.

Dr. Metzbower is a metallurgist in the Navy Research Laboratory's Materials Science and Technology Division. He is presently involved in a program involving modeling of the laser beam welding process that includes the resultant microstructures and properties of the process. His other research interests are the utilization of neural networks for the prediction of properties of high-strength, low-alloy (HSLA) plates and welds as well as the influence of a subsequent weld bead on deposited weld beads in gas metal arc welding.

He is a Fellow of The Welding Institute (England), the Laser Institute of America, and ASM International.

Obituaries

Akira Matsunawa

Akira Matsunawa, 68, a Fellow of the American Welding Society, died September 20. He received his undergraduate and doctor's degree in welding engineering from Osaka University, Japan. Upon graduation in 1968, he served as an assistant professor at the university. In 1978, he became a lecturer at the Joining and Welding Research Institute of Osaka University, an associate professor in 1980, and a professor in 1986. He was named professor emeritus of the university in 2002.

Akira Matsunawa

Prof. Matsunawa established an outstanding reputation in the field of welding arc physics and laser technologies. His research papers spanned a wide range of topics. He studied anode and cathode discharge mechanisms of a high-current arc, underwater arc welding, arc characteristics in high pressure, and the interaction between a supersonic jet and burning iron in oxygen gas cutting.

Since 1980, his research focused on laser materials processing, resulting in numerous technical papers. His topics included laser-matter interaction, heat and mass transfer in laser and arc welding, modeling of melting and solidification behavior during laser spot welding, keyhole dynamics, and evaluation of laser weldability of aluminum alloys. Prof. Matsunawa's work was of practical value to the laser and welding industries by offering remedies for the prevention of welding defects through detailed elucidation and scientific interpretation of complicated arc and laser welding phenomena.

His work earned him numerous prestigious awards, including the Light Metal Welding Paper Award (1998) from the Japan Light Metal Welding and Construction Assn., The Japan Welding Society Paper Award (2001), Comfort A. Adams Lecture Award (2002) from the American Welding Society, Arthur L. Schawlow Award from the Laser Institute of America (LIA) (2002), among others.

Prof. Matsunawa was an active member of the International Institute of Welding (IIW) Commission IV, Power Beam Processes; V1, Welding Terms; SG212, Welding Physics; and the Select Committee of Underwater. He chaired the IIW Commission IV since 2002.

In 1994, Prof. Matsunawa was named a Fellow of LIA, and inducted as an AWS Fellow in 1998.

Ronald W. Leonzal

Ronald W. Leonzal, 73, an AWS Life Member, died October 5 at his home in Duluth, Minn. He was a charter member of the AWS Arrowhead Section where he served as chairman 1990–1992, and served two terms as District 15 director (1993–1999).

Ronald W. Leonzal

Mr. Leonzal worked his way up from a city desk position at Wallner Welding Supply in 1959, to manager in 1968, vice president in 1971, and elected president in 1985. In 1988, he accepted the position of salesman for the F. H. Bathke Co. for the Duluth and Iron Range areas, and later was appointed manager for the Duluth and Iron Range divisions. In 1992, the F. H. Bathke Co., and Genex merged to form Genex Minnesota, Ltd. Mr. Leonzal was a member of St. Joseph's Church in Duluth Heights, and the Knights of Columbus. He is survived by two sons, two daughters, eight grandchildren, two great grandchildren, friend Blanche Rapp, and many nieces and nephews.

Part 1 — WELDING JOURNAL SUBJECT INDEX

AUTHORS FOR FEATURE ARTICLES

Part 2 – RESEARCH SUPPLEMENT SUBJECT INDEX

AUTHORS FOR RESEARCH SUPPLEMENTS

CAREER OPPORTUNITIES

Welders Needed

Colorado Railcar Mfg, LLC, the premiere manufacturer of luxury railcars, has openings for full-time welders at our Fort Lupton, Colorado facility for both 1st and 2nd shift.

Applicants must be able to pass FCAW " 6G tube V-Groove welding test.

Apply in person at:

1011 14th Street
Fort Lupton, CO 80621
or call Garry at 303-857-1066.
You may apply online at
www.coloradorailcar.com

QUALITY ASSURANCE MANAGER

1OCFR50 Appendix B (Nuclear) and ASME U/NBIC R for ASME Section VIII (Pressure Vessel) - ASME Section III. MO in near future.

Ecker-Erhardt Company, Chicago serving all industry for Maintenance Machining & Engineering. Small but highly regarded. This is a hands-on position. Engineering and machine shop experience is a plus.

Submit resume and statement of personal goals to: 2347 W. 18th Street, Chicago, IL 60608

Sales Rep/Account Executive

Leading manufacturer of tube, pipe and profile bending machinery seeks full-time representatives for Texas, Salt Lake City and Seattle areas. Successful candidates must be hands on, highly motivated with strong work ethic. Strong communication, computer skills and clean driving record are required. Must be willing to travel frequently to effectively cover large geographic area. Previous experience in machinery sales a plus but not required. Compensation includes base salary with sales commission; expense reimbursement; vehicle provided; health insurance; and 401 K. US residents only.

Send resumé to
CML USA Inc Ercolina
Attn: GM 8506 North Fairmount
Davenport IA 52806
stunis@ercolina-usa.com

WANTED
Independent Sales Reps

To demonstrate welding alloys to end users.

– Consumables market
– Repeat Customers
– Complements Industrial Rep's present line(s) of products.

Very unique opportunity.

Contact Bob Turner
(800) 642-9885

Welding Engineer

ALSTOM Power Services currently has an opening for a Welding Engineer (US Virginia 420101329): Responsible for the welding and metallurgical design, development, testing, analysis, and production support of steam / gas turbine and generator rotating and stationary component repairs and refurbishment for Alstom and other OEM equipment. Thorough understanding of engineering theories, concepts, principles and techniques. Work is subject to general overview to ensure quality. Qualifications: BS or MS in Welding Engineering from a 4 year accredited college or university with seven to ten years experience in turbine generator rotating and stationary equipment welding, material testing, metallurgical analysis, heat treatment, NDE, and material evaluation / recommendation.

To apply visit our website at
www.careers.alstom.com or
Monster.com EOE

Welding Trainer
National Academy of Railroad Sciences

Johnson County Community College in Overland Park, Kansas is looking for a Welding Trainer. This position requires a Bachelor's degree or a minimum of two years related work experience. For a complete description of the position and application requirements please visit our website, www.jccc.edu, or call (913) 469-3877.

Welding Equipment Repair Technician

F&M Mafco, Inc., the Powerful Solutions People, is a leader in the equipment rental and construction supply distribution industry is seeking a qualified Welding Equipment Repair Technician.
This position is responsible for the troubleshooting, repair and service of various types of welding equipment to include rectifiers, inverters, diesel and gas powered machines, wire feeders and plasma cutters. Qualified candidates will have 3+ years experience in the repair of welding equipment to include: Miller and Lincoln. Must be a team player, have good communications skills, high energy, with the ability to interact with people at all levels. Selected candidates must have own repair tools; bench equipment supplied. We offer a drug and smoke-free work environment with a competitive compensation and benefit package. If you are interested in joining our team, applications will be accepted from 7-5/M-F at 9149 Dry Fork Road, Harrison, OH 45030 or fax credentials to (513) 202-8820 or e-mail hogues@fmmafco.com EOE M/F/V/H

Product Development Engineer

Requirements: BS in metallurgy, welding engineering, or equivalent. Good knowledge of welding processes for high-nickel alloys. Good computer skills, spreadsheet and databases. Will supervise development and testing of products, deliver in-house and outside technical presentations, and resolve customer product concerns. E.O.E.

Submit résumé to Jeannie Martin:
jmartin@smwpc.com;
FAX (828) 464-8993.
Special Metals Welding Products Co.,
Newton, NC.

EQUIPMENT FOR SALE OR RENT

CINCINNATI, OHIO **800-288-9414**
WELD PLUS www.weldplus.com
WELD PLUS, INC. Fax: 513-467-3585 email: melissa@weldplus.com

JUST IN!!
PMC Fab 12' Flat Sheet Planisher/Grinder - Polisher
8 - Posi-Tech Model "G" Simple Air Manipulators

OVER 50 "BRAND NEW" POSITIONERS IN STOCK!!!
"BRAND NEW 2006" IN OUR STOCK!!!
PANDJIRIS POSITIONERS!!! JETLINE SEAMERS!!
MBC POSITIONERS!!! WEBB TURNING ROLLS!!!
RANSOME MANIPULATORS!!!
Well Over 150 Positioners Total, Up to 60 Tons!! Head/Tailstocks, Turntables up to 100 Tons. Manipulators up to 14' x 14'. Travel cars, Longitudinal Seamers from 6 in. to 26 ft. Turning Rolls up to 400 Tons. Circular Weld Systems, Welding Lathes, Motoman and Panasonic Welding Robots.

"WE KNOW WELDING"
TALK TO US!! ... COME VISIT US!!
800-288-9414
Pete, Paul, Dennis, Jared or Melissa

Welding Positioners & Turning Rolls
New and Used

Large selection in stock for immediate delivery.

www.allfabcorp.com

Call, Fax or Email for a free catalog.

All-Fab Corp.
Email: sales@allfabcorp.com
Web: www.allfabcorp.com
Phone: 269-673-6572
Fax: 269-673-1644

RED-D-ARC
Quality-Checked™ Used Equipment
www.red-d-arc.com
An Excellent Selection of Used Welding and Positioning Equipment for Sale
1-800-245-3660
Service Centers Across North America

VERSA-TIG™
MULTIPLE TIG TORCH SELECTORS
www.versa-tig.com

Portable System
Stops Distortion
up to 90% Better
"A natural for welders"

www.Bonal.com
(800) 638-2529

Turning Rolls
Positioners
& Manipulators
New and Used

Joe Fuller LLC
@ www.joefuller.com
or email joe@joefuller.com

Phone: 979-277-8343
Fax: 281-290-6184

We Buy & Sell Surplus
Welding Rod & Wire
All types, sizes & Quantities

Liberty Alloys INC.

Call us first!

800-523-2791
PA: 610-825-1250
FAX: 610-825-1553

ATTENTION!!
RETOOLING? CHANGING PRODUCTS?
CLOSING SHOP? GOIN' FISHING?
We pay good prices for used welding machinery!
We are looking for any used welding machinery like: Turning Rolls, Positioners, Manipulators, Seamers, etc.
Send Photos to:
melissa@weldplus.com **WELD PLUS**
or call 800.288.9414

We buy and sell
WELDING RODS & WIRE
**ALL TYPES ** ALL SIZES **
ALL QUANTITIES

Excess Welding Alloys, Inc.
A division of Weld Wire Company Inc.
800-523-1266 FAX 610-265-7806
www.weldwire.net

Place Your Classified Ad Here!

Contact Frank Wilson, Advertising Production Manager

(800) 443-9353, ext. 465
fwilson@aws.org

AWS JobFind
Post Jobs. @ Find Jobs.
www.aws.org/jobfind
Job categories for welders, engineers, inspectors, and more than 17 other materials joining industry classifications!

CERTIFICATION & TRAINING

REAL Educational Services, Inc.

Call About Courses for 9-Year Renewal

CWI PREPARATORY
Guarantee - Pass or Repeat FREE!

2-WEEK COURSE (10 DAYS)
MORE HANDS-ON/PRACTICAL APPLICATIONS
Pascagoula, MS, Dec. 4–15 Jan. 17–26
Atlanta, GA, Jan. 31–Feb. 9
Houston, TX Feb. 14–23

SAT–FRI COURSE (7 DAYS)
EXTRA INSTRUCTION TO GET A HEAD START
Pascagoula, MS, Dec. 9–15 Jan. 20–26
Atlanta, GA, Feb. 3–9
Houston, TX Feb. 17–23

MON–FRI COURSE (5 DAYS)
GET READY - FAST PACED COURSE
Pascagoula, MS, Dec. 11–15 Jan. 22–26
Atlanta, GA, Feb. 5–9
Houston, TX Feb. 19–23
(Test follows on Saturday at same facility)

SENIOR CWI PREPARATORY
Pascagoula, MS, Dec. 11–15 Jan. 22–26
Atlanta, GA, Feb. 5–9
Houston, TX Feb. 19–23

FOR DETAILS CALL OR E-MAIL:
1-800-489-2890
info@realeducational.com

The AWS Certification Committee

Is seeking the donation of sets of Shop and Erection drawings of highrise buildings greater than ten stories with Moment Connections including Ordinary Moment Resistant Frame (OMRF) and Special Moment Resistant Frame (SMRF) for use in AWS training and certification activities. Drawings should be in CAD format for reproduction purposes. Written permission for unrestricted reproduction, alteration, and reuse as training and testing material is requested from the owner and others holding intellectual rights.

For further information, contact:

Joseph P. Kane
(631) 265-3422 (office)
(516) 658-7571 (cell)
joseph.kane11@verizon.net

Place Your Classified Ad Here!

Contact Frank Wilson, Advertising Production Manager

(800) 443-9353, ext. 465
fwilson@aws.org

Industrial Welding Instruction On-Site and Worldwide

40 years experience
Excellent credentials

Ferrous and nonferrous metals (pipe and plate), GTA, SMA, GMA, underwater welding and burning, and C-4 explosives.

PH: (419) 367-1344
FX: (419) 474-6027

SERVICES

MITROWSKI RENTS

1000 Ton Aronson Tank Turning Rolls

www.mitrowskiwelding.com
sales@mitrowskiwelding.com
800-218-9620
713-943-8032

South Bay Inspection

Visual and Non Destructive Testing Services

Radiography	AWS Certified Weld Inspection
Ultrasonics	API 510 Pressure Inspection
Liquid Penetrant	API 653 Tank Inspection
Magnetic Particle	API 570 Piping Inspection
NDT Training	Level III Services

Turnaround Inspection Staffing
Field and Laboratory Testing

SOUTH BAY INSPECTION
1325 W Gaylord St.
Long Beach, CA 90813
Phone: (562) 983-5505 **Fax:** (562) 983-5237

VISIT US ON THE WEB
www.southbayinspection.com

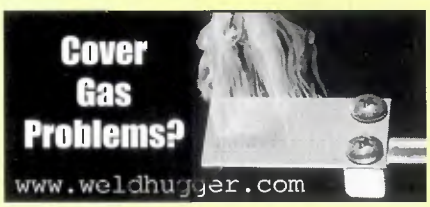

LITERATAURE

Speciality Welds

A Diver-Welder's Companion

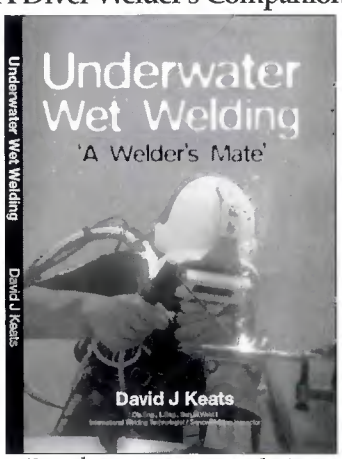

Purchase on our website at www.specialwelds.com

ADVERTISER INDEX

IFC = Inside Front Cover

IBC = Inside Back Cover

OBC = Outside Back Cover

RI = Reader Information Card

WELDING CONSULTANTS

Do You Have Some News to Tell Us?

If you have a news item that might interest the readers of the *Welding Journal*, send it to the following address:

Welding Journal Dept.
Attn: Mary Ruth Johnsen
550 NW LeJeune Rd.
Miami, FL 33126.

Items can also be sent via FAX to (305) 443-7404 or by e-mail to *mjohnsen@aws.org*.

WELDING RESEARCH

SUPPLEMENT TO THE *WELDING JOURNAL*, DECEMBER 2006
Sponsored by the American Welding Society and the Welding Research Council

Simulation of Weld Pool Dynamics in the Stationary Pulsed Gas Metal Arc Welding Process and Final Weld Shape

A computer simulation accurately predicts weld pool fluid flow convection and final weld shape

BY M. H. CHO, Y. C. LIM, AND D. F. FARSON

ABSTRACT. The pulsed gas metal arc welding (GMAW-P) process was modeled numerically using a code based on the volume of fluid (VOF) technique, chosen primarily for its ability to accurately calculate the shape and motion of free fluid surfaces, which is needed for subsequent study of welding phenomena such as bead hump formation, incomplete fusion in narrow groove welds, and weld toe geometry. According to the mathematical models with parameters obtained from analysis of high-speed video images and data acquisition (DAQ) system, GMAW-P was simulated and then validated by comparison of measured and predicted weld deposit geometry, transient radius, and temperature history. Based on the weld simulation parameters, a parametric study of weld simulation was performed to demonstrate and understand the effectiveness of individual simulation parameters on heat and fluid flow in the molten weld pool and the final configuration of stationary welds. Constricted current density drastically increased the weld penetration and decreased the weld radius, primarily by reducing the convexity of the weld deposit and promoting heat transfer to the bottom of the weld pool. Conversely, decreased arc force and increased arc pressure radius both decreased the weld penetration for the same reason. Based on the understanding of weld pool spreading, GMAW-P was simulated with an additional heat source to demonstrate the utility of the simulation in predicting final weld shape in complex welding situations.

M. H. CHO(ch.130@osu.edu) *is postdoctoral researcher, Y. C. Lim (lim.746@osu.edu) is graduate research associate, and D. F. Farson* (farson.4@osu.edu)*is associate professor, Department of Industrial, Welding and Systems Engineering, The Ohio State University, Columbus, Ohio.*

Introduction

During arc welding processes such as gas metal arc welding (GMAW) and gas tungsten arc welding (GTAW), fluid flow and heat flow are key factors that determine the final weld shape. Therefore, many previous efforts have been made to predict these two aspects of arc welding by numerical simulation. While currently available welding heat flow and distortion simulations are quite comprehensive and accurate enough for many practical purposes, phase change and fluid flow phenomena occurring in arc welding are complex and have still not been realistically simulated. In particular, numerical model-based prediction of the dynamic changes in the shape of the liquid weld pool surface would be useful in many applications if they were possible. Examples include weld toe shape (Ref. 1) and weld bead hump formation (Ref. 2).

In GMAW, heat input to the weld pool is composed of a direct arc heat input and the enthalpy of molten droplets transferring from the welding wire. In numerical weld pool simulations, the current density is also needed to predict the distribution of Lorentz force in the weld pool fluid. These parameters are difficult to measure for GMAW because of difficulties posed by filler metal transfer, but measurements have been made for GTAW. To quantify direct heat and also the electrical current distributions on the weld pool surface, Lu and Kou (Ref. 3) measured power and current density distributions using a split copper block. Based on the analysis by the Abel inversion method, the shape of power and current distribution were found out to be Gaussian density functions, so the arc shape could be described by the total magnitudes (i.e., total heat input and current) and Gaussian distribution parameters.

The shape of the weld pool and bead shape are also strongly affected by the flow of plasma in the welding arc. The forces exerted by the arc plasma jet on the weld pool are the arc stagnation pressure and drag force. Arc pressure acts on the weld pool surface in the normal direction, depressing the molten deposit. Arc pressure density distribution on the weld pool surface has also been investigated for GTAW (Ref. 4), and was characterized as a Gaussian density distribution function. Adonyi et al. (Ref. 5) studied its effect on the weld pool dynamics and found that the arc pressure mainly caused the depression of the weld pool surface. Drag force is a shear stress on the liquid metal surface produced by plasma gas flow. Tanaka et al. (Ref. 6) investigated the driving forces for weld pool convection during gas tungsten arc welding, and the drag force and the Marangoni force (discussed below) were

KEYWORDS

3-D Numerical Simulation
Fluid Flow
Heat Flow
Pulsed GMAW
Volume of Fluid
Weld Shape
Weld Simulation

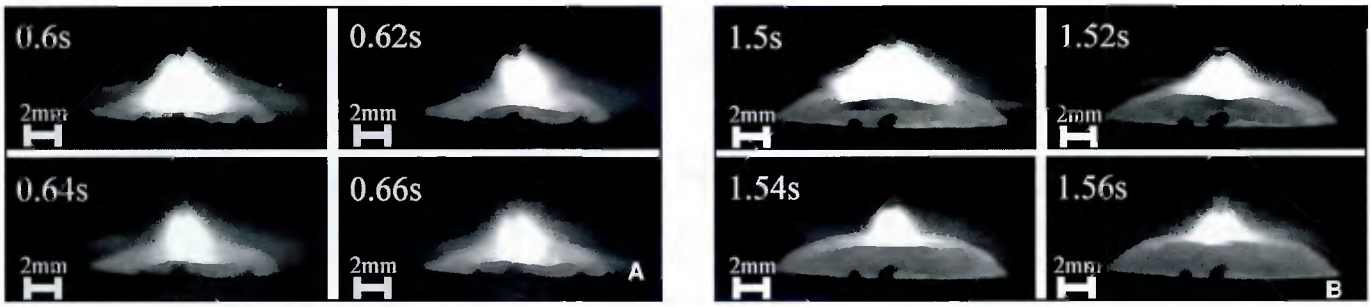

Fig. 1 — High-speed video sequences showing different metal transfer of molten droplets at later times.

Fig. 2 — Images of electrode tip used to measure the tip taper angles.

found to be dominant. Convection caused by surface tension gradients has major effects (Ref. 3) on weld pool shape. The mechanism was studied by Heiple and Roper (Refs. 7, 8). They proposed that the final weld shape can be significantly altered by variations of the surface active elements (e.g., sulfur) that changes the direction of surface tension gradient induced flow (Marangoni flow) in GTA welding conditions.

Based on understanding the well-known forces and heat input in the weld pool, many researchers simulated arc welding processes and studied weld pool convection, the formation of the weld pool and molten droplets, droplet transfer, and solidified weld bead shape. The idea of solving for the shape of the free surface of a fluid volume as a static energy minimization problem (Ref. 9) has been applied to calculate weld bead shape by a number of authors (Refs. 10–14). Zhang et al. (Refs. 15–17) studied the three-dimensional numerical simulation of the complex geometry such as fillet welds based on the surface energy minimization for the surface deformation tracking. Also, Kumar and DebRoy (Ref. 18) developed optimization algorithm to minimize the error between the experimental results and the simulation results by the determination of unknown variables from a limited volume of experimental data.

Since the molten weld metal is not stationary and is also cooling and solidifying as it accumulates and spreads to form a weld bead, a more accurate analysis of bead shape takes simultaneous fluid and heat flow into account in addition to the forces included in the static balance. Trapaga and Szekely (Ref. 19) used the VOF numerical technique to simulate the isothermal spreading of impacting droplets on surfaces. Zheng (Ref. 20) modeled the spreading of an impacting droplet using the level set method, another interface tracking scheme with similarities to VOF. Wang and Tsai (Ref. 21) investigated the dynamics of periodic filler droplets impinging onto weld pool and phase change, using VOF technique that can handle a transient deformed weld pool surface and the continuum model (Ref. 22), respectively.

More recently, the VOF technique has been used to simulate melting and detachment of metal droplets from welding wire in GMAW (Refs. 23–28), and Fan and Kovacevic (Ref. 29) developed the unified two-dimensional axisymmetric model to study droplet formation and detachment, droplet transfer in arc plasma, impingement of droplets on the weld pool, and solidification in gas metal arc welding.

In summary, GMAW simulations using the VOF technique in the previous research papers were limited to a two-dimensional axisymmetric model, which is not useful in most welding applications. Also, arc pressure and drag force on the weld pool surface induced by plasma gas flow were neglected, which is very significant when the welding current is high enough to generate the spray metal transfer mode.

In this article, a three-dimensional numerical simulation of a high peak current GMAW-P using the VOF method is developed based on mathematical models, especially including arc pressure and plasma drag force, obtained from the previous research papers. In order to arrive at a GMAW-P simulation that can be executed in a relatively short time and is also accurate enough for engineering use, the arc effects were represented as boundary and body inputs. Thus, simulation parameters to characterize the molten filler metal droplets and arc dimensions were measured from experiments. Also, the real-time weld pool radius measurements, thermal history measurements at selected positions, and cross sections of final weld

Table 1 — Thermophysical Material Properties of A36 Used in the Simulation

Density	7800 kg/m^3	Thermal expansion coefficient	14.4 x 10^{-6} m/m K
Dynamic viscosity	6 x10^{-3} kg/m s	Liquidus temp.	1798 K
Thermal conductivity (s)	Temp. dependant	Solidus temp.	1768 K
Thermal conductivity (l)	26W/m K	Vaporized temp.	2900 K
Specific heat (s)	686 J/kg K	Heat transfer coefficient	100 W/m^2 K
Specific heat (l)	866 J/kg K	Emissivity	0.5
Latent heat of fusion	2.77 x 10^{5}J/kg	Material permeability	1.26 x 10^{-6} H/m
Latent heat of vaporization	7.34 x 10^6 J/kg	Drag coefficient constant	1

Table 2 — Pulsed GMAW Current Waveform and Welding Parameters

Peak current	384 A	Instantaneous avg. power	8842 W
Background current	87.4 A	Wire feed speed (WFS)	148 mm/s
Peak voltage	35.5 V	Welding wire type	ER70S-6
Background voltage	24.4 V	Wire diameter	1.125 mm
Pulse time	2.2 ms	CTWD	19.05 mm
Pulse frequency	250 Hz	Shielding gas/flow rate	Ar,10CO_2/40 ft^3/h

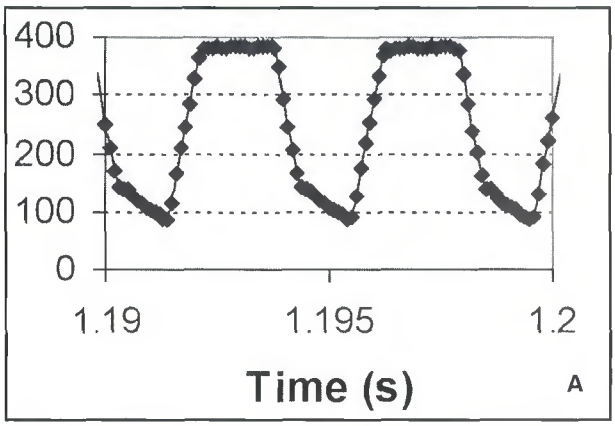

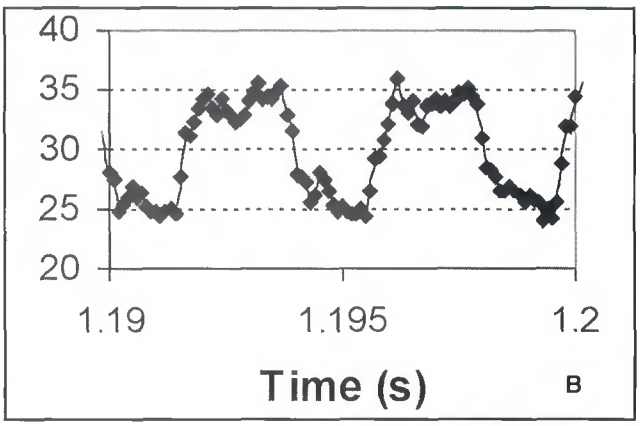

Fig. 3 — GMAW-P. A — Current waveform; B — voltage waveform.

profiles and fusion boundaries were used for simulation validation. The effects of selected individual simulation parameters on GMA weld pool flow and final weld shape were also investigated.

Finally, predictions of the transient and final weld shape for a dual heat source process influence are shown to illustrate the usefulness of the simulation for welding process development, which cannot be simulated using a two-dimensional axisymmetric model.

Experimental Procedure

Stationary welds were made for 1.8 s using the pulsed gas metal arc welding process (using a Thermal Arc 500P power supply). Materials selected for the experiment were 6.35-mm-thick ASTM A-36 steel, containing 50 ppm sulfur, with sandblasted surface preparation for the workpiece and 1.143 mm diameter of ER70S-6 welding wire. Contact-tip-to-work distance (CTWD) was 19.1 mm. Thermophysical material properties of A-36 steel are shown in Table 1.

During the welds, measurements were made with a high-speed CCD camera and a data acquisition system (DAQ). Images of the arc and molten metal pool were captured by the high-speed CCD camera with a 950 nm ±10 nm band pass filter mounted between high-speed camera lenses used to filter out unwanted arc light in order to capture the clear images of metal transfer and weld deposit growth. According to video images of metal transfer (Fig. 1), one drop per pulse metal transfer was observed after 1.2 s of weld time. Before that time, the molten metal transfer was somewhat random but the transfer rate was approximately one drop every two pulses. It is supposed that this difference in transfer corresponds to differences in the temperature distribution in the welding wire extension. The arc length measured from the arc images was approximately 4 mm.

As shown in Fig. 2, the electrode tip was relatively blunt at the beginning of the weld, but became sharper when the metal transfer stabilized. The tip angle was measured to be approximately 90 deg before 1.2 s and 60 deg after 1.2 s. The transient weld deposit profile and radius were measured from images taken at 500 frames per second.

The velocity of molten droplets was too high to analyze at the 500 frames per second rate, so the recording rate was increased to 4500 frames per second to analyze their size and speed.

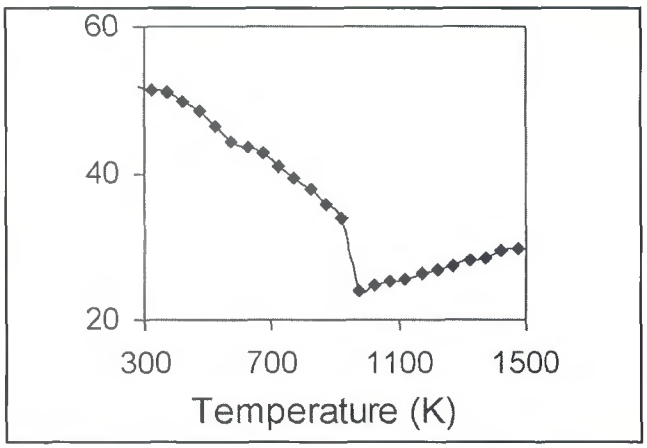

Fig. 4 — Temperature vs. thermal conductivity used in the simulations.

Welding current and voltage waveforms were acquired at a sampling rate of 10 kHz. Examples of the waveforms are shown in Fig. 3. Peak values and background values of current and voltage, pulse frequency, and pulse duration were obtained from the waveforms and used to calculate the instantaneous average power, peak power, and background power for the heat input in the weld system during the process. The waveform parameters and welding parameters are displayed in Table 2.

Mathematical Modeling and Numerical Simulation

The GMAW-P weld pool and bead deposit were mathematically modeled using 3-D Cartesian coordinate system, and the governing equations were solved numerically to simulate the arc welding process using Flow3D commercial code. The liquid metal was considered to be an incompressible Newtonian fluid, and flow was laminar. The density change of molten metal was only considered for the buoyancy term in the momentum equation using a Boussinesq approximation. The flow at the solid/liquid phase interface was modeled using a porous media drag concept (Ref. 39). Arc heat input (defined as the direct heat input to the workpiece) and arc pressure on the molten pool surface were modeled as Gaussian density distributions. The total heat input applied to the workpiece, calculated by multiplying the instantaneous average arc power by a process efficiency, was the sum of direct heat input and the latent heat of droplets.

The weld pool simulation was based on the numerical solution of mass, momentum, and energy conservation relationships

$$B = -\frac{1}{\rho}\left(\frac{2\rho}{2t}\right) \tag{1}$$

$$\frac{\partial \mathrm{v}}{\partial t} + \mathrm{v}\cdot\nabla\mathrm{v} = -\frac{1}{\rho}\nabla P + \nu\nabla^2\mathrm{v} + f + \frac{\dot{m}_s}{\rho}\cdot\mathrm{v} - K\mathrm{v} \tag{2}$$

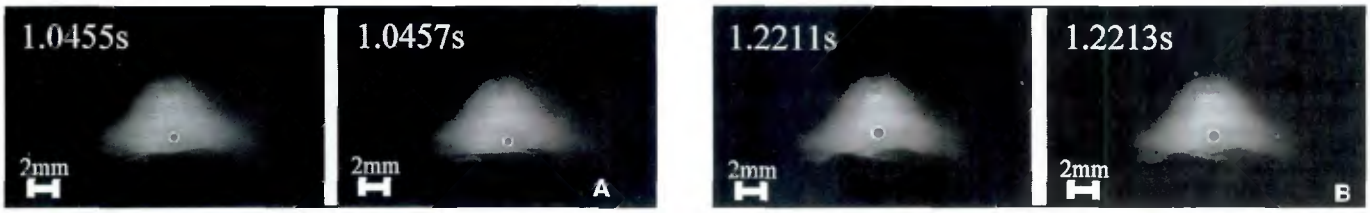

Fig. 5 — Drop velocity measurement. A — For one drop per every two pulses (125 Hz); B — one drop per pulse (250 Hz).

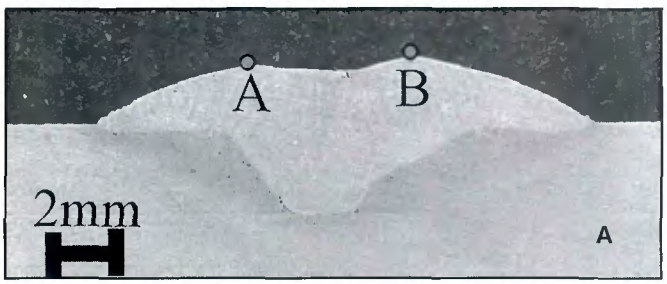

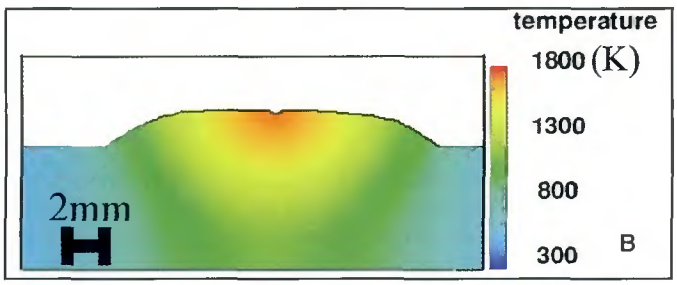

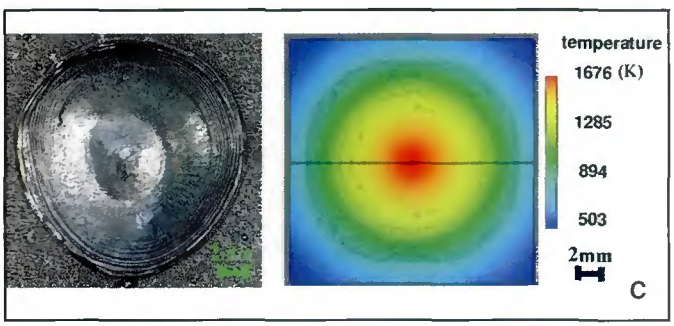

Fig. 6 — A — Cross sections of actual weld; B — simulated weld after the solidification of weld; C — top views of the weld for the experiment and the simulation.

$$\rho\left(\frac{\partial U}{\partial t}+\mathrm{v}\bullet\nabla U\right)=\nabla\bullet(k\nabla T)+\dot{U}_s \qquad (3)$$

where v is molten metal velocity, $\dot{m}_s$ is a mass source term, P is hydrodynamic pressure, v is kinematic viscosity, f is body accelerations due to body force (e.g., gravity acceleration), ρ is a fluid density, K is the drag coefficient for a porous media model, U is internal energy per unit mass, k is thermal conductivity (temperature-dependent values), T is a local temperature and, $\dot{U}_s$ is an energy source term due to a mass source term.

To model solid-liquid phase changes, the mathematical model of enthalpy-temperature relationship is

$$h=\begin{cases}\rho_s C_s T & (T\le T_s)\\ h(T_s)+h_{sl}\dfrac{T-T_s}{T_l-T_s} & (T_s<T\le T_l)\\ h(T_l)+\rho_l C_l(T-T_l) & (T_l<T)\end{cases} \qquad (4)$$

where h is enthalpy, ρ_s and ρ_l are solid and liquid density, respectively, C_s and C_l are specific heat at constant volume of the solid and liquid phases, T_s and T_l are solidus and liquidus temperatures of the metal alloy, and h_{sl} is the latent heat of fusion for phase change between liquid and solid.

The simulation technique used in this work is based on an additional advection relationship that expresses the conservation of volume fraction in the fluid flow at the free surface and fluid interfaces (for a two-fluid model). It is derived from the conservative form of the mass conservation law using density and fluid volume fraction relationships

$$\frac{\partial\rho}{\partial t}+\nabla\bullet(\mathrm{v}\rho)=\dot{m}_s \qquad (5)$$

$$\rho=\rho_o F \qquad (6)$$

$$\dot{m}_s=\rho_o\dot{F}_s \qquad (7)$$

where ρ is the zone density at the current cell, ρ_o is the density of material, F is a volume fraction of a fluid, and $\dot{F}_s$ represents the change of the volume fraction of fluid associated with the mass source m_s in the continuity equation. Substituting Equations 6 and 7 into 5 results in the volume of fluid (VOF) Equation 8, which can be used to effectively track the location of free fluid surfaces in the simulation domain.

$$\frac{\partial F}{\partial t}+\nabla\bullet(\mathrm{v}F)=\dot{F}_s \qquad (8)$$

Based on Equation 8, free surface cells are defined as those that have void (zero volume fraction) neighbor cells. A numerical technique for tracking the shape and volume of the free surface of fluid and a volume advection algorithm presented by Hirt and Nichols (Ref. 30) is not reiterated here.

Since a single fluid is used in the model, the solid and liquid phases are distinguished based on the enthalpy-temperature relationship (Equation 4). The fluid temperature of each cell is determined from its enthalpy, which is computed based on conduction and convection of material. If the temperature is between liquidus and solidus temperatures, the cell becomes a part of a mushy zone. The amount of solid phase is calculated in terms of the temperature ratio and is used for the determination of the effective viscosity and the drag coefficient in the mushy zone.

To model flow in the mushy zone, it is divided into three subregions distinguished by the critical solid fraction and the coherent solid fraction. Fluid in each subregion is assigned a different drag coefficient and a local viscosity. The first region consists of cells with solid fraction below the coherent solid fraction. The local viscosity is varied due to the amount of solid fraction according to

$$\mu=\mu_0\left(1-\frac{F_s}{F_{cr}}\right)^{-1.55} \qquad (9)$$

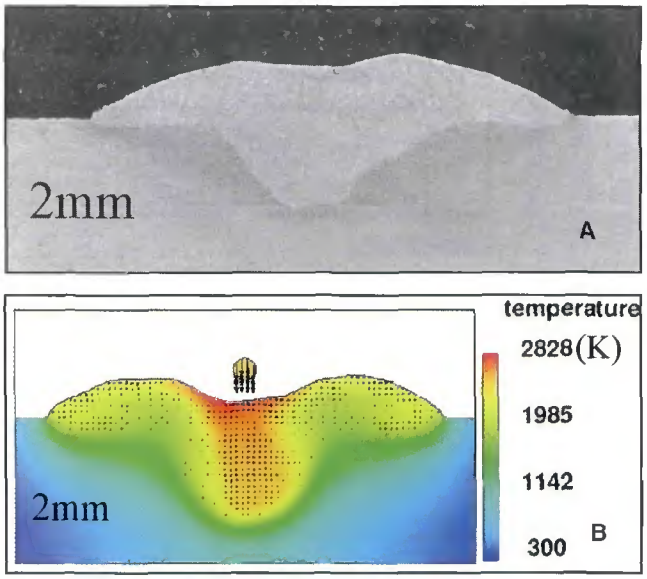

Fig. 7 — A — Cross sections of actual weld; B — simulated weld at the arc termination time. Simulated penetration is deeper than actual weld.

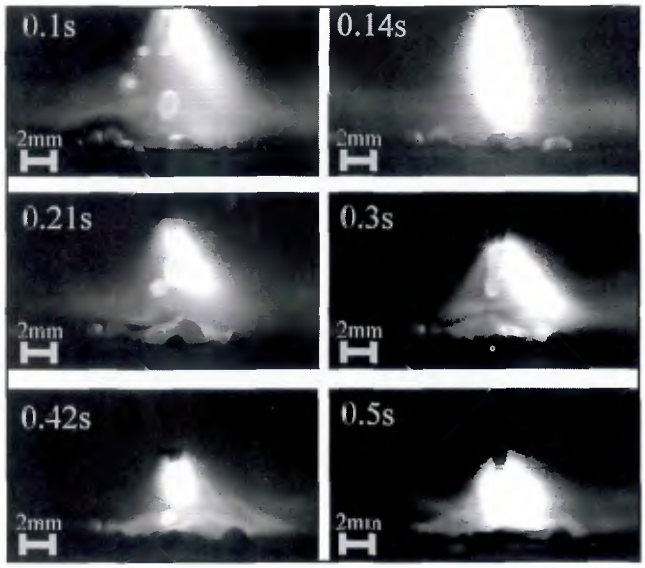

Fig. 8 — High-speed video sequences showing erratic initial metal transfer of molten droplets.

Table 3 — The Summary of Weld Geometry from the Experimental Results and the Simulation

Deposit Characteristics	Measured	Simulated	Difference
Height	2.3/1.9 mm	1.88 mm	0.42/0.02 mm
Average radius	8.25 mm	8.5 mm	0.25 mm
Center penetration	3.2 mm	4.6 mm	1.4 mm
Edge penetration	0.5 mm	0.6 mm	0.1 mm
Left-side toe angle	30.4 deg	31.8 deg	1.4 deg
Right-side toe angle	32.6 deg	33.2 deg	0.6 deg

where μ_0 is dynamic viscosity, F_s is the local solid fraction in the given cell, and F_{cr} is the critical solid fraction.

The second region of the mushy zone consists of cells where the solid fraction is above the coherent solid fraction but less than the critical solid fraction. In this region, the microstructure is acting as a porous media so the Carman-Koseny equation (Ref. 31) that is derived from Darcy model (Refs. 32, 33) is used to compute the drag coefficient

$$K = C_o \bullet \frac{F_s^2}{(1-F_s)^3 + \varepsilon} \quad (10)$$

where K is the drag coefficient, C_o is the drag coefficient constant (equal to 1 for steel), and ε is the positive zero (for computation purposes). In this region, Equation 9 is still needed to calculate the local viscosity of fluid to compute the precise fluid resistance in the computational cell.

In the region above the critical solid fraction, the microstructure is assumed to be fully developed into a complete rigid structure, and there is assumed to be infinite resistance to fluid flow. Thus, fluid flow is stopped due to an effectively infinite drag coefficient computed by Equation 10.

Boundary Conditions

The axisymmetric free surface heat input from the arc was modeled as a fixed Gaussian density function (Ref. 34).

$$q(r) = \frac{Q}{2\pi\sigma_a^2} \exp\left(\frac{-r^2}{2\sigma_a^2}\right) \quad (11)$$

where Q is the actual heat input directly from the arc to the substrate and σ_a is the Gaussian heat distribution parameter. The Gaussian heat distribution parameter is the main factor to adjust the heat input distribution on the free surface of the weld pool. Additionally, convection and radiation are applied on the free surface. Therefore, the heat input on the free surface is expressed as

$$q(r) = \frac{Q}{2\pi\sigma_a^2} \exp\left(\frac{-r^2}{2\sigma_a^2}\right) - h_c(T - T_0) - \sigma\varepsilon\left(T^4 - T_0^4\right) \quad (12)$$

where h_c is heat transfer coefficient, T is temperature. T_0 is ambient temperature, σ is the Stefan-Boltzmann constant (5.67×10^{-8} W/m^2• K^4), and ε is the emissivity. The wall boundary condition was applied to solid free surface cells

$$-k\frac{\partial T}{\partial n} = -h_c(T - T_0) \quad (13)$$

To model Marangoni flow, the shear stress balance as boundary condition on the free surface is described as

$$\mu\frac{\partial v_t}{\partial n} = -\frac{\partial \gamma}{\partial T}\frac{\partial T}{\partial r} \quad (14)$$

where μ is the dynamic viscosity, v_t is the tangential velocity vector, n is the normal to the free surface, $\partial\gamma/\partial T$ is the surface tension gradient, and r is the tangential direction on the free surface. An additional plasma drag shear stress is described below. Also, the normal pressure balance as boundary condition on the free surface is expressed as

$$-p + 2\mu\frac{\partial v_n}{\partial n} = -p_{arc} + \gamma\left(\frac{1}{R_1} + \frac{1}{R_2}\right) \quad (15)$$

where p is the liquid pressure at the free surface in the normal direction, v_n is the normal velocity vector, p_{arc} is the arc pressure (described below), γ is the surface

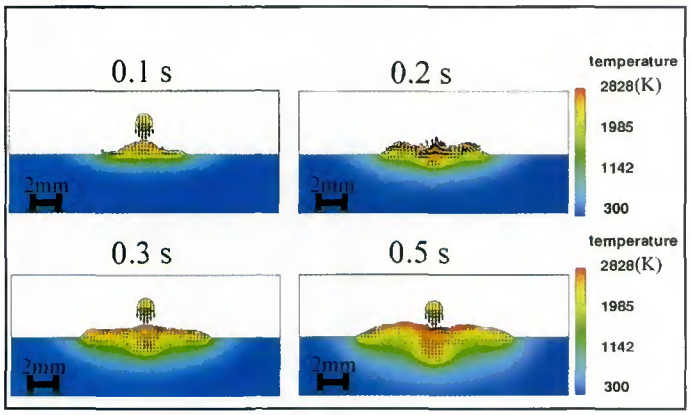

Fig. 9 — Cross-section views of the simulated weld at early weld times showing the progress of the fluid flow development and the weld penetration.

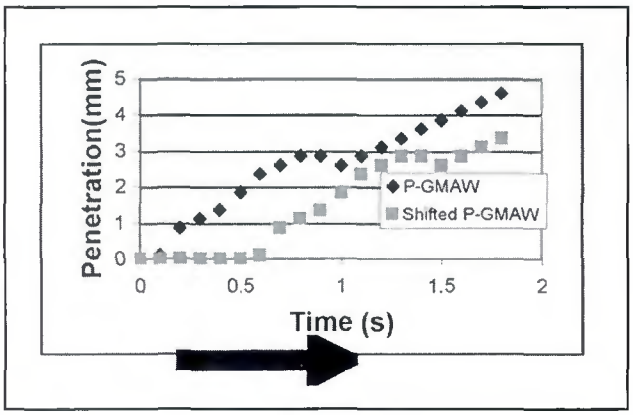

Fig. 10 — Simulated weld penetration vs. time showing a shift of about 0.5 s matched experimental measurements.

tension, and R_1 and R_2 are the principal radii of surface curvature. For this study, surface tension is obtained from the formula developed by Sahoo et al. (Ref. 35). The equation of surface tension as a function of temperature with sulfur active element in a binary Fe-S system is expressed by

$$\gamma(T)=\gamma_m^o - A\bullet(T-T_m) - R\bullet T\bullet\Gamma_s\bullet\ln\left(1+k_1\bullet a_i\bullet e^{-\Delta H^o/RT}\right) \quad (16)$$

where γ^o_m is the surface tension of pure metal at the melting point, 1.943, A is the negative of surface tension gradient for pure metal, 4.3E-4, T_m is the melting point of the material, 1798 K, R is gas constant, Γ_s is the surface excess at saturation, 1.3E-8, k_1 is the entropy factor, 0.00318, a_i is weight percent of sulfur, 0.005%, and ΔH_o is the heat of absorption, –1.66E+8. According to Equation 16, the negative surface tension gradient at temperatures above 2000 K is large so a strong outward Marangoni force spreads the molten metal.

Pressure gradients generated by Lorentz force in the arc plasma causes downward (along the negative z-coordinate) flow of the ionized gas. A stagnation pressure that is consistent with the redirection of this downward flow is approximated as Gaussian density distribution whose magnitude and radius are based on analysis of experimental results (Ref. 4)

$$p_{arc}(r)=\frac{P}{2\pi\sigma_p^2}\exp\left(\frac{-r^2}{2\sigma_p^2}\right) \quad (17)$$

where σ_p is Gaussian pressure distribution parameter and P is total force (N).

When the plasma jet flow impinges on the weld pool surface, the plasma drag force is induced on the weld pool surface. This plasma drag force creates outward fluid flow of liquid metal at the surface and also changes with weld pool configuration. In this work, an analytical solution (Ref. 36) of the wall shear stress produced by the normal impingement of a plasma jet on a flat surface was used to determine and apply the drag force as the boundary condition on the free surface cell. For the axisymmetric case, the theoretical equation in terms of Reynolds number, a ratio of jet height, and nozzle diameter, is expressed as

$$\frac{\tau}{\rho_p u_o^2}\mathrm{Re}_o^{1/2}\left(\frac{H}{D}\right)^2 = g_2\left(\frac{r}{H}\right) \quad (18)$$

where τ is shear stress (N/m^2), ρ_p is plasma density (Kg/m^3), u_o is the initial plasma velocity (m/s), Re_o is Reynolds number, H is a nozzle height (m), D is the nozzle diameter (m), r is the radius (m) from the center, and g_2 is the universal function plotted in reference paper (Ref. 36). The initial plasma jet velocity is calculated based on the maximum plasma stagnation pressure at the weld pool center using Bernoulli's equation in order to obtain Reynolds number. The jet height and the jet nozzle diameter are assumed to be the arc length and the electrode size. The computed drag force is applied into the free surface cells as a body force in the momentum Equation 2.

A key feature of the simulation is the representation of melting of the GMA welding wire and the transfer of resulting droplets to the weld pool. Welding wire melting was modeled as a periodic stream of spherical droplets with velocity vectors in the negative z direction. Conservation of mass was applied to calculate the initial droplet radius from welding wire diameter and welding parameters (wire feed speed and drop frequency). The initial velocity of spherical droplets was directly measured from sequential arc images. Many researchers add the plasma drag force to the transferring droplets, computed as a function of droplet radius, drag coefficient for a sphere, and the plasma gas velocity in momentum equation, acting on the liquid droplet between the electrode tip and the base metal. In this model, the velocity of liquid droplet right before impinging on the weld pool was measured and used as the initial velocity of liquid droplet, and also the height of liquid droplet is fixed with respect to the free surface of the weld pool to maintain the same condition when measuring the velocity of liquid droplet. Due to the small traveling distance of the liquid droplet, the model assumes that the plasma drag force exerting on the liquid droplet can be ignored.

Body Forces in the Weld Pool

The body force term in momentum Equation 2 was comprised of the sum of two terms $\mathbf{f} = \mathbf{f}_b + \mathbf{f}_L$ where $\mathbf{f}_b$ is buoyancy force and $\mathbf{f}_L$ is Lorentz force. For the buoyancy force term, Boussinesq approximation concept was applied to account for the effect of a small density change in the gravity term

$$\mathrm{f}_b = -\beta\bullet(T-T_0)g \quad (19)$$

where $B=-\frac{1}{p}(\frac{2p}{2t})_p$ is the thermal expansion coefficient.

Lorentz force was obtained from an analytical solution (Refs. 37, 38) based on the current flow and associated magnetic field in the substrate material. The electric field is assumed to be quasi-steady state, the electrical conductivity is assumed to be constant and the material domain is a semi-infinite plate. Then, the electric potential field ϕ in the weldment is given by Laplace's equation

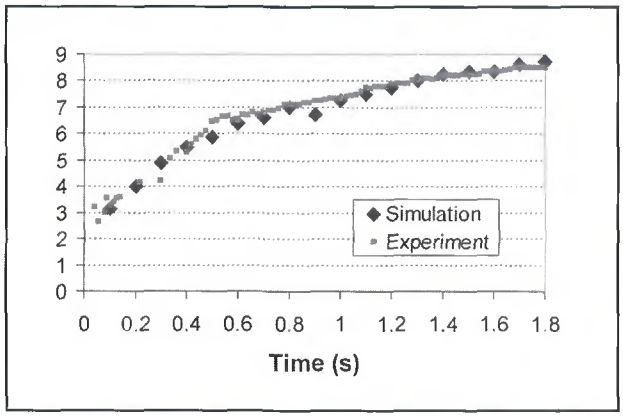

Fig. 11— Measured radius and simulated radius of weld deposits showing good correspondence.

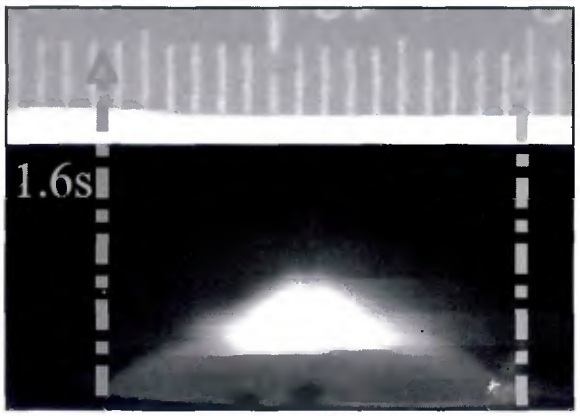

Fig. 12 — The sample of captured images showing the measurement of weld pool radius at 1.6 s weld time.

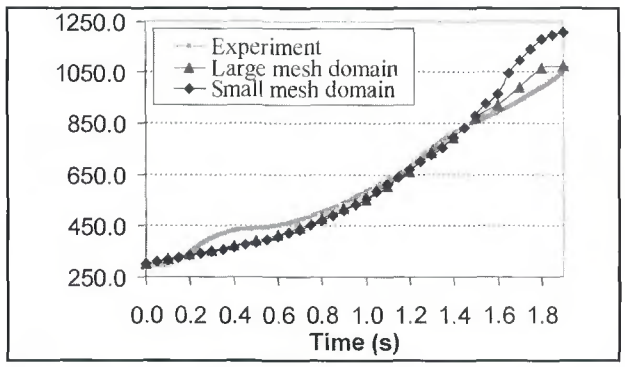

Fig. 13 — Temperature history measured at a location 0.4 mm away from the final weld edge and the predicted temperature for two different mesh domain sizes.

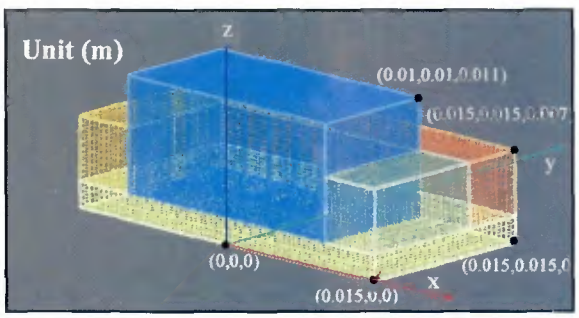

Fig. 14 — Coordinates of large mesh used for half symmetry simulation of stationary spot welds.

$$\nabla^2\phi = \frac{1}{r}\frac{\partial}{\partial r}\left(r\frac{\partial\phi}{\partial r}\right) + \frac{\partial^2\phi}{\partial z^2} = 0 \qquad (20)$$

The axisymmetric solution of Equation 20 is obtained using a Hankel transformation with boundary conditions

$$J_z(r,0) = -\sigma_e\frac{\partial\phi}{\partial z} = \frac{I}{2\pi\sigma_c^2}\exp\left(\frac{-r^2}{2\sigma_c^2}\right)$$

$$\frac{\partial\phi}{\partial z}(r,c) = 0 \qquad \frac{\partial\phi}{\partial r}(0,z) = 0 \qquad \frac{\partial\phi}{\partial r}(\infty,z) = 0 \qquad (21)$$

where σ_e is the electrical conductivity of the weld metal, σ_c is the Gaussian current parameter (m), I is a current (A), and c is the thickness of the workpiece. Note that the current distribution on the top of the free surface of the material is also described as Gaussian distribution function. This Gaussian distribution is varied as a function of the welding current and the Gaussian current parameter.

The two-dimensional axisymmetric Lorentz force must be converted to three-dimensional Cartesian coordinates for substitution into the momentum equation. The r and z Lorentz force components were calculated for the individual cells in 3-D Cartesian coordinate system based on the analytical solution. The r direction component was then split into x and y components.

Numerical Simulation

To perform the numerical simulation of the welding process, two regions, void and fluid, were generated in the computational domain with the fluid representing the material with the phase change capability. Due to weld pool surface deformation during the welding process, free surface modeling is applied to track the deformed free surface. In the fluid region either solid or liquid, governing Equations 1–4 and 8 with the required boundary conditions are numerically solved through the following steps (Ref. 39):

First, the new velocities at the current time level are approximated using the explicit method based on variables for the previous time level.

Second, the pressure correction formula (Poisson equation) was solved by the successive overrelaxation (SOR), method to satisfy the continuity equation and then the energy equation is solved by the implicit method.

Finally, the configuration of the free surface is updated using the VOF equation. These steps are repeated at every time step until the desired simulation time is reached.

There are four free surface boundary conditions to implement the effects of the electric arc on the weld pool — arc heat input, arc pressure, drag force, and drop generation. To numerically apply Gaussian heat flux on the free surface, the free surface cells were tracked, and at every time step an appropriate increment is added to their stored energy. The source term ($\dot{U}_s$) in energy Equation 3 is used to add the calculated thermal energy into the free surface cells. Also, the Gaussian arc stagnation pressure is numerically implemented in the momentum Equation 2 as a boundary condition at free surface. The corresponding pressure acts on the surface-normal direction on fluid in cells on the weld pool surface. Similarly, plasma drag force calculated from the theoretical equation as a function of the maximum pressure and the distance from the arc center is applied on the momentum Equa-

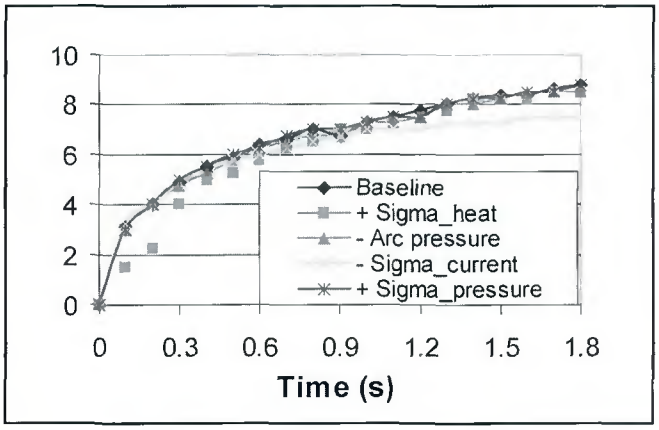

Fig. 15 — Comparison of the transient radius showing that increased heat input distribution radius slowed initial spreading and decreased current distribution radius slowed spreading at later times.

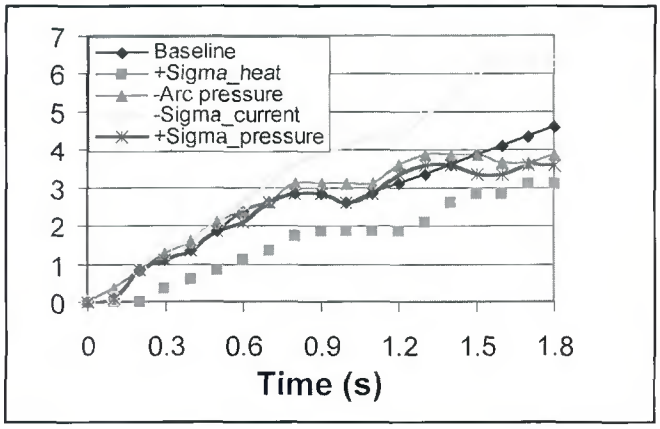

Fig. 16 — Comparison of transient weld penetration showing that increased heat and pressure input distribution and reduced arc pressure all decreased the final weld penetration while decreased current distribution radius caused deeper weld penetration.

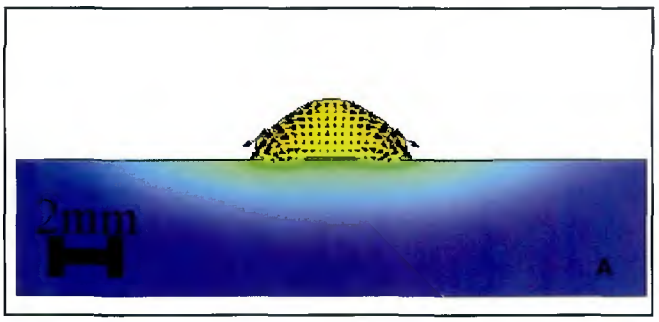

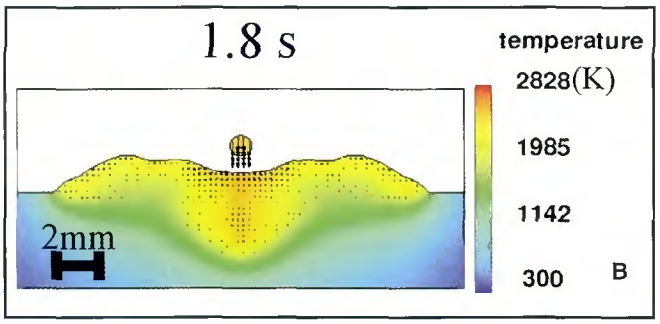

Fig. 17 — A — Cross section at the initial weld time showing arrest of molten metal spreading; B — at the later weld time showing the temperature distribution in the weld pool for the large Gaussian heat distribution parameter case.

tion 2 for the free surface cells.

Terms were added to all governing equations to model the generation of molten droplets in the void region. To add the mass of droplet, source terms in governing Equations 1 and 5 are modified to create the droplet, and then the momentum equation is used to set the initial velocity of the molten metal droplet and their height with respect to the free surface of a weld pool. In the energy Equation 3, the initial temperature of droplets (Refs. 40, 41) is used to calculate the amount of enthalpy that deposits into cells that correspond to droplet locations.

Simulation Parameters

The simulation parameters for Gaussian heat input, arc pressure, drag force, drop generation, and other physical parameters needed to conduct GMAW-P stationary weld simulations were based on current and voltage waveforms, video images of weld pool and metal transfer, and values from literature. Details of the parameters and measurements are summarized below.

Temperature-dependent thermal conductivity for the solid phase, shown in Fig. 4, was used to accurately evaluate the thermal diffusion. For the generalized solidification model (Ref. 42), the coherent solid fraction (0.48) and the critical solid fraction (0.64) were estimated based on application of established theory to the iron-iron carbide binary phase diagram. In order to apply the generalized theory, it is necessary to have a eutectic phase transformation, so the phase diagram in the peritectic reaction region was approximated by a larger triangle, producing a region similar to a eutectic phase transformation. The coherent and critical temperature lines were proportionally drawn onto the modified binary iron-iron carbide binary phase diagram. Two intersection points with vertical lines passing through the liquidus and solidus temperatures were found to calculate the coherent solid fraction and the critical solid fraction using tie line and lever rules.

Gaussian Heat Input

Gaussian heat input was defined by the arc power and Gaussian heat distribution parameter as discussed previously. For the pulsed GMAW process, the instantaneous power calculated as the product of simultaneous current and voltage samples varies during the weld, so the instantaneous average power, 8842 W was calculated as the average of these values. This is larger than the actual energy deposited into the weld, so the actual power is adjusted by multiplying by the arc efficiency value measured by liquid nitrogen calorimetry (Ref. 43) as 0.74, which is typical of GMAW arc efficiencies measured by this technique. This actual power is still an average power, so the peak power and

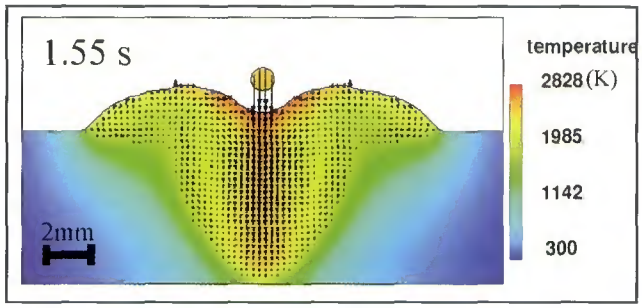

Fig. 18 — Cross-sectional view at 1.55 s for larger Lorentz force case showing complete penetration of the base material, finger-like penetration shape, and weak outward circulation at the weld pool edge.

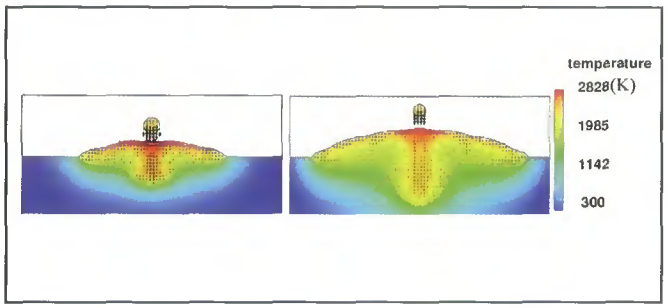

Fig. 19 — Cross-sectional views for decreased total force case at 0.5 and 1.7. Final weld penetration was decreased.

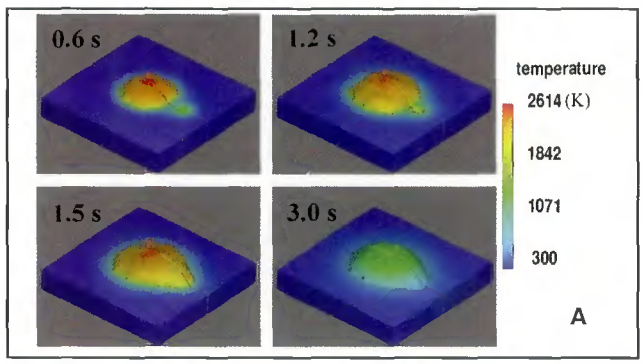

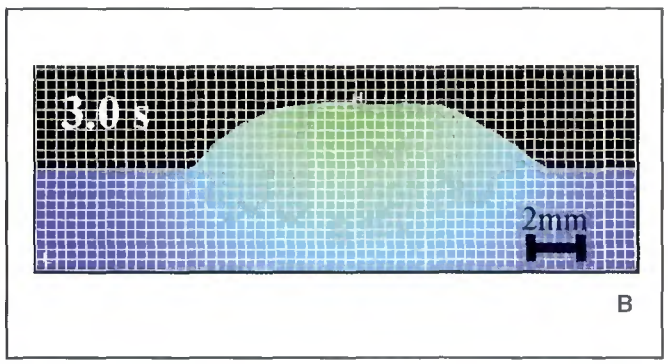

Fig. 20 — A — 3-D sequential images; B — cross section of two-heat sources simulation result. The additional heat is applied at the right edge of weld pool with 1-mm-radius laser beam.

the background power measured from current and voltage waveforms are used to represent the pulsing behavior of actual heat input during the weld, and then the actual power was further split to the arc power and the power consumed for molten drop generation.

To determine the heat input density distribution on the weld pool surface, the Gaussian heat distribution parameter for a direct heat input was estimated based on the empirical equation obtained from the literature (Ref. 34). This equation is a function of current for a 4-mm arc length case expressed as

$$\sigma_a = 0.533I^{0.2941} \qquad (22)$$

where σ_a is Gaussian heat distribution parameter (mm) and I is current (amps). Current measurements from the DAQ system were used to compute this value.

Arc Pressure, Drag Force, and Lorentz Force

From Equation 17, total arc force and Gaussian pressure distribution parameter are required to calculate the arc pressure on the weld pool. For the arc pressure computation, the current waveforms and the electrode tip angles were measured in order to estimate the arc pressure from literature formulas. According to the previous research papers (Refs. 4, 16), the empirical equations for the total force and Gaussian pressure distribution parameter as a function of current and electrode tip angle were expressed as

$$P = \begin{cases} -0.04017 + 0.0002553 \cdot I(N) & \text{(60-deg tip angle)} \\ -0.04307 + 0.0001981 \cdot I(N) & \text{(90-deg tip angle)} \end{cases} \qquad (23)$$

$$\sigma_p = \begin{cases} 1.4875 + 0.00123 \cdot I(mm) & \text{(60-deg tip angle)} \\ 1.4043 + 0.00174 \cdot I(mm) & \text{(90-deg tip angle)} \end{cases} \qquad (24)$$

where P is the total force (N), I is current (amps), and σ_p is Gaussian pressure distribution parameter (mm). The time-dependent current waveforms and electrode tip angles discussed previously were used in Equations 23 and 24 to compute these values.

The analytical solution (Ref. 36) for drag force calculation obtained from the literature requires Reynolds number and a ratio of jet height and nozzle diameter. The jet nozzle height was taken as 4 mm based on high-speed video arc length measurements and the jet diameter was set at 1 mm, approximately equal to the electrode diameter. Reynolds number contains the plasma jet velocity term that is computed using Bernoulli's equation based on the maximum arc pressure at the weld pool center computed from the arc pressure calculation at zero radius. Other terms involved in Reynolds number are the material properties of the plasma jet found from the literature (Ref. 44). The density and dynamic viscosity of argon plasma are 0.046 kg/m^3 and 0.00005 kg/m·s at 10,000 K plasma temperature.

The theoretical equation of Lorentz force in the weld pool derived based on the fixed boundary conditions except the free surface boundary condition. The current density distribution on the free surface is varying with time, so the input parameters to determine Lorentz force are pulse current and relative Gaussian current density parameters obtained from the previous research paper (Ref. 34). The empirical equation for Gaussian current density distribution parameter is expressed as

$$\sigma_c = 0.5342I^{0.2684} \qquad (25)$$

where σ_c is Gaussian current density distribution parameter (mm) and I is current (amps).

Drop Generation

For simulated drop generation, velocity, height, frequency, temperature, and drop radius were needed. Most of the parameters were obtained from analysis of video images, and drop temperature was set from literature values. In the simulation, molten drops were generated as spherical shape droplets.

There are two metal transfer behaviors seen in the video images in Fig. 1. For metal transfer at early weld times (before 1.2 s), the drop frequency was one drop per every two pulses, or a drop generation rate of 125 Hz, and drop velocity was 0.9 m/s at a distance 1.2 mm away from the weld pool surface. These values were measured from the metal transfer sequences observed in the high-speed video images shown in Fig. 5A. At weld times of 1.2 s and greater, metal transfer was more stable, and transfer rate was one drop per pulse, or a drop frequency of 250 Hz. Drop velocity was increased to 1.35 m/s, measured from the video images of metal transfer presented in Fig. 5B. The drop temperature for both transfer behaviors was set to be 2400 K from previous research reports (Ref. 40).

Results and Discussion

With simulation parameters determined from direct measurements and the literature, the simulation of pulsed GMA welding was conducted, and simulation results were validated with experimental results as detailed below.

Comparison of Final Weld Geometry

A very common way to validate weld simulations is to compare the dimensions of weld cross-sections measured from experiments with those predicted by the simulation. In Fig. 6, the actual weld cross-sectional images and the simulated cross-sectional weld views are displayed in order to compare reinforcement, radius, toe angles, and penetration. The quantitative comparison of the simulation and the experimental results is given in Table 3. Weld reinforcement measurements of the actual weld shown in Fig. 6A vary from 1.9 to 2.3 mm depending on the measuring locations (A and B). The average height, 2.1 mm, is comparable to the simulated weld height of 1.9 mm. There are two penetrations observed at the center and the edge of the weld shown in Fig. 6A. The inward circulation developed by drop momentum, arc pressure, and Lorentz force generates the center weld penetration, but the outward circulation induced by Marangoni force and plasma drag force produces the penetration at the weld edge. To compare weld penetrations, the simulation result at the weld termination time (1.8 s) when the maximum penetration occurs during the weld was used to measure the weld penetrations and the two clear circulations observed in Fig. 7.

In summary, differences in weld radius, the height of weld reinforcement, weld toe angles, and penetration at the edge are 10%, but the simulated weld penetration at the center is significantly deeper than the experimental measurement. This discrepancy is attributed to the high efficiency of drop momentum and heat transfer mainly due to fluid convection in the simulation. According to Fig. 8, metal transfer images show that molten droplets at the initial weld time up to 0.5 s were not spherical, and also the location of droplet impingement on the weld pool was somewhat random during the weld. Therefore, at the initial weld time before 0.5 s, the experimental weld pool was not yet as developed as the simulated one, and the weld metal convection that effectively transfers momentum and heat to the bottom of the weld pool was not as strong.

Sequential simulated weld cross-sectional images from 0.1 to 0.5 s are displayed to show the development of fluid flow at the early weld time in Fig. 9. In simulation, molten spherical droplets were generated at 1.2 mm above the weld surface at the center of the arc and traveled straight down to the base material every time. At 0.1-s simulation time, the molten metal deposited from the welding wire simply lays on the solid base material. The weld does not begin penetrating into the base material until 0.2 s. At around 0.3 s, the fluid flow in the weld pool is fully developed, weld penetration is enhanced, and clockwise and counterclockwise fluid flow circulations are also clearly observed at the edges and the center of the weld pool. The presence of two stable circulations in the weld pool is evidence of a stable weld pool. At 0.5 s, deeper penetration is observed along with larger fluid flow circulations.

From Fig. 9, it is concluded that the inward circulation is very significant to increase penetration at the center of the weld pool. This inward circulation is caused by drop momentum, arc pressure, and Lorentz force. First, the concentrated droplet impact onto the weld pool transfers their momentum along with their enthalpy (which is high) at the center of weld, promoting the inward circulation. The Gaussian arc pressure distribution generated by the arc plasma jet flow depresses the weld pool surface at the center, also enhancing the inward circulation. Additionally, at the high welding current, Lorentz body force adds to the inward circulation. The temperature distribution coloration of the images shows many red cells at the bottom center of the weld pool and a large temperature gradient at the solid/liquid interface, which accelerates melting of the solid phase. Therefore, it is proposed that the weld penetration in the simulation is deeper because the development of inward fluid flow circulation pattern in the simulation occurs earlier rather than in the experiment.

In Fig. 10, the simulated weld penetration vs. weld time is plotted to show the predicted transient weld penetration. As discussed before, the weld penetration is growing quickly due to the efficient drop momentum transfer and heat transfer when the fluid flow is fully developed. In the simulation, the fluid flow is fully developed at 0.2 s, so the slope of the weld penetration curve is steep except for the time between 0.8 and 1.1 s. The absorption of drop momentum depends on the thickness of the molten metal deposit, so the convexity of molten metal at 0.8 s is enough to absorb the drop momentum that stops penetration into the base material. After 1.2 s, the stronger arc pressure due to the transition to one drop per pulse mode depresses the weld pool surface to enhance the efficiency of drop momentum transfer into the weld pool, so the weld penetration increases from 1.2 s until the arc termination time. Interestingly, if the penetration curve is shifted to right about 0.5 s, which is the time for no penetration period due to the unstable metal transfer during the weld shown in Fig. 8, the final predicted weld penetration is 3.35 mm, which closely matches with the actual weld penetration of 3.2 mm.

This also suggests that the time to develop the inward circulation of fluid flow in the weld pool is related to the final weld penetration. Therefore, it is supposed that the random behavior of experimental metal transfer is a significant cause of the discrepancy between the predicted and experimental weld penetrations. Other simulation inputs related to the arc could also affect weld penetration, as will be discussed further below. Presumably, the discrepancy would be reduced if the computer model simulated the random behavior of metal transfer at the initial weld time.

Comparison of Transient Weld Pool Radius and Temperature

The numerical simulation of stationary GMAW-P was also validated by comparing the transient radius of weld deposits. In Fig. 11, the time-varying radius from high-speed video measurements and simulation predictions are plotted vs. weld time. One sample of captured im-

ages shown in Fig. 12 described that the weld pool radius is directly measured from the molten metal image using the electronic image of the ruler. According to both experimental and simulated results, the deposit radius increased rapidly at the beginning of the weld. This is presumed to correspond to rapid spreading of the solidus isotherm on the substrate surface by direct arc heating allowing spreading of the molten metal deposit. The spreading quickly transitions to a more gradual increase. At the later stage of spreading, heat conduction and convection are the main factors to increase the temperature at the liquid-solid junction to allow spreading of the molten metal. Of these two, heat conduction is usually considered to be less effective for heat transfer than thermal convection by fluid motion.

In the experimental deposit radius curve, the initial molten metal radius quickly reached 6.5 mm, which is a little bit larger than a visible arc radius (4 mm) estimated from the video images. The slope of the curve was still steep until the radius reached 6.5 mm, an observation that supports the explanation of the influence of direct arc heat input on the spreading of molten metal deposits. The experimental radius fluctuated at early times but is so less as the deposit grew larger. In the simulated radius curve, the deposit radius quickly increases up to 6.5 mm (about 0.6 s) due to the rapid direct heating from the arc. The time for the simulated weld deposit radius to reach the gradual increase stage and the radius itself are closely matched to experimental results, and the overall trend of the spreading behavior is almost identical between the experiment and the simulation.

Thermocouple measurements taken during welding were also used for simulation validation. In Fig. 13, three curves showing temperature history at a location 0.4 mm away from the final weld edge are plotted to compare the experimental and predicted thermal history. The difference between the two simulation curves is due to a small mesh domain (2.4×2.4 cm) and a large mesh domain (3×3 cm). Both simulation curves are closely matched with the experimental results until 1.5 s, but the small mesh domain results are considerably mismatched after 1.5 s due to an edge effect. This effect causes the temperature for the small mesh domain case to become too large after 1.5 s because heat transfer rate through the simulation boundary by natural convection is much smaller than heat conduction in the base material. Interestingly, the rate of temperature increase before 1.5 s is the same for both simulation cases because the conducted heat does not reach the computational boundary until this time.

Based on the temperature history validation, 3 cm is considered to be a sufficient computational domain size for the accurate computer simulation of the results over the time being considered. A sketch of the large simulation mesh mentioned in the preceding paragraph and used for subsequent simulations is provided in Fig. 14. This mesh consisted of 5 blocks with 132,400 cubical cells. The size of cells in the center block was 0.25 mm, allowing the accurate calculation of surface tension for molten droplets, while that of other blocks was 0.5 mm.

The simulations were run on a dual 3.4-GHz Xeon processor workstation with 2 GB of RAM, and the software was compiled dual process use. The computational time step, limited by the surface tension convergence criteria, was 2.3×10^{-5} s. Simulating 3 s of weld time required 62 h of "wall-clock" time. It was found that mesh size was most critical for accurate simulation of transferring droplets and the center block mesh size mentioned above was chosen for mesh size independent simulation of this aspect of the process.

Based on these three validations of the weld simulation, the stationary GMAW-P weld simulation was considered reasonably accurate for prediction of the final and transient weld profiles. In subsequent simulations, the Gaussian heat distribution parameter, Gaussian current distribution parameter, Gaussian pressure distribution parameter, and total arc pressure were individually varied to understand their effects on fluid and heat flow and weld pool penetration by comparing with validated simulation results.

Simulation Parameter Effects

The Gaussian heat distribution parameter was increased by a factor of 1.5 with same total heat input to study its effect on the weld profile and fluid flow patterns. The larger Gaussian heat distribution parameter corresponds to a broader heat distribution and less heat input intensity at the center of the arc, so it is expected that more time would be required to melt the base material underneath of the arc. According to the transient radius plots in Fig. 15, the weld deposit for the large heat input radius case did not spread as quickly as the validated simulation at initial times because the solid base material adjacent to the molten metal deposit was cooler. At later weld times, the weld pool radius was more well matched with the validated simulation deposit radius.

In Fig. 16, the effect of variation of the heat distribution parameter on the weld penetration transient weld penetration is shown. When the parameter was increased, the final weld penetration was decreased as expected because less energy was deposited at the center of weld pool and transferred to the bottom.

At the initial weld time shown in the cross-sectional view in Fig. 17A, no weld penetration was generated until 0. 2 s due to lower energy deposition from the arc. The weld began penetrating at 0.3 s due to heat conduction from the molten metal deposit and heat convection induced by several forces involved in the weld pool. After 0.3 s, the weld penetration is growing as fast as one for the validated simulation until 0.8 s weld time. The same penetration behavior (no penetration increase) was observed between 0.8 and 1.2 s compared to the validated simulation weld because the sufficient molten metal deposited absorbed drop momentum to prevent the penetration.

Again, the weld penetration is increasing after 1.2 s due to the increase of arc pressure depressed the weld pool surface, but it transitioned to a steady state at the end of a weld time due to the lower enthalpy transferring from the weld pool surface to the bottom of the weld. Figure 17B presented the low temperature of molten metal near the surface and at the bottom of weld pool compared to the validated simulation shown in Fig. 7B.

Lorentz force usually becomes the dominant factor at high welding current, so Gaussian current distribution parameter was reduced by the factor of half to study its effectiveness on the weld pool. The decrease of Gaussian current distribution parameter produces the constricted current flow through the weld pool, so the stronger Lorentz force is generated near the center of the weld pool. Due to the strong body force near the weld pool center, the strong inward circulation is expected to increase the weld penetration.

As shown in Fig. 18, weld penetration increased from 4.6 to 6.35 mm (thickness of plate), and the deep finger-like penetration shape is achieved.

Another interesting characteristic revealed by the flow vectors in this figure is the small counter fluid flow in the edge of the weld pool. Usually, Marangoni force produced by a negative surface tension gradient case and drag force generated by arc plasma jet force the fluid on the weld pool surface to flow outward, a direction that is against that induced by the Lorentz force. In this case, the Lorentz force was so strongly distributed near the weld pool center that it dominated the fluid flow pattern, producing a strong inward circulation of fluid flow. The transient weld penetration plotted in Fig. 16 shows that the slope of curve is steeper than other cases, and the weld penetrated through the base material at 1.55 s before the termination of the arc shown in Fig. 18.

One interesting point in this plot between 0.8 and 1.2 s is that the inward circulation mainly enhanced by the Lorentz force overcomes the barrier generated by the molten metal deposit as a momentum absorber so the weld penetration keeps increasing but it slows down. After 1.2 s, the slope is even steeper due to the combination of the increased arc pressure and high Lorentz force.

Figure 15 shows the transient radius of molten metal deposit. As discussed before, the outward circulation is mainly spreading the molten metal deposit, so the molten metal deposit is spreading as fast as the validated simulation until 0.5 s, but it slows down due to the small outward circulation at the edge of the weld pool shown in Fig. 18.

To demonstrate the effect of arc pressure, the total force and Gaussian pressure distribution parameter were individually varied while other simulation variables were held fixed. First, one fifth of arc force is applied to study because the arc pressure used in the simulation is strong enough to obtain a deep penetration. As discussed in the previous section, arc pressure and drag force are coupled together, so their magnitudes are proportional to each other. Therefore, the decrease of total force induces the weaker drag force. In Fig. 15, the trend of transient weld pool radius for the reduced arc pressure is showing no influence on the molten metal spreading. The weld penetration was plotted in Fig. 16. Before 1.3 s, the trend of weld penetration is following the validated simulation case, but at the later time the weld penetration is suddenly becoming steady. The final weld penetration is eventually decreased by 0.75 mm.

As discussed before, the inward circulation of fluid flow causes the increase of weld penetration. The magnitude of this circulation and the amount of enthalpy contained in molten metal are the main factors to determine the depth of weld penetration. Therefore, the stronger inward fluid flow circulation and the hotter molten metal accelerate the weld penetration. The amount of enthalpy in the molten metal on the weld pool surface is proportional to the arc direct heat deposit, so this factor is not required to consider the change of weld penetration as long as the same arc heat input distribution applied.

The mechanism to explain the decrease of final weld penetration can be described by the inward circulation of fluid flow. There are three forces involved to determine the magnitude of inward circulation. First, the lateral distribution of arc pressure causes the inward fluid flow so that the hot molten metal heated by the direct heat input to increase weld penetration. Second, metal transfer is a major source of heat and drop impact momentum to increase GMA weld penetration. Finally, Lorentz force at the high welding current induces the inward fluid flow to increase the weld penetration. During the weld, these forces are simultaneously acting on the weld pool to determine the magnitude of the inward fluid flow circulation.

In Fig. 19, there are two cross-sectional views at 0.5 and 1.7 s weld times displayed to explain the weld penetration characteristics during the weld. At the early weld time, there is not enough molten metal deposit to form the sufficient convexity of weld reinforcement acting as a damper to reduce the weld penetration even though the weak arc pressure was applied on the weld pool surface.

During the early weld time, Lorentz force and drop impact momentum are the dominant factors to increase the weld penetration. Molten metal eventually piled up as weld time goes on, so the amount of molten metal deposit on the substrate is sufficient enough to form the thick convexity to absorb the drop impact momentum displayed in Fig. 19. Therefore, the weld penetration is transitioned to a gradual increase as shown in Fig. 16.

Another variable to change the arc pressure distribution is a Gaussian pressure distribution parameter that increased by the factor of 1.5 with a fixed total force. The increase of this parameter decreases the maximum pressure and increases the area to apply. The transient weld pool radius and penetration were plotted in Figs. 15 and 16. The trend of transient weld pool radius is following the validated simulation, but the penetration curve is different from the validated simulation at the later weld time (after 1.2 s). Therefore, the final weld penetration is decreased to 3.6 mm due to the decrease of maximum arc pressure at the weld center.

In summary, the weld radius is not strongly influenced by simulation parameters except the Gaussian current distribution parameter, but the weld penetration is affected by all simulation parameters tested so far. According to previous demonstrations, it is not easy to modify the final weld profile, especially the spreading of molten metal, by given welding parameters demonstrated so far, thus the additional heat source such as a laser beam can be applied into the welding process in order to increase the controllability of the final weld shape during the weld.

Preliminary Demonstration of Additional Heat Source

Previous sections demonstrated how welding parameters could control the final weld shape, but in this section, the effect of the additional heat source that can enhance the controllability of the final weld shape is investigated. To improve the wetting characteristics of molten metal for the desired weld shape, the additional heat source such as laser beam is applied to demonstrate the controllability of the final weld shape using the numerical simulation as a tool.

For the demonstration of the improvement of molten metal wetting, the simulation of two heat sources is performed to show the effectiveness of additional heat source (it can be any heat source) adjacent to the edge of weld pool. The defocused laser beam as the second heat source was modeled to perform, and the results are shown in Fig. 20. According to Fig. 20, the molten metal wet over into the additional heat spot (laser spot), and it demonstrates the change of the final weld shape. Especially, the toe angle where the wetting occurred became smoother due to the additional heat source. Consequently, this preliminary test result using the 3-D numerical simulation as a process development tool can provide the insight for the process development of improving the controllability of the final weld shape for the further investigation.

Conclusions

The VOF technique was used to implement a simulation of stationary pulsed GMA welding that included nonisothermal free-surface fluid flow. Buoyancy, Marangoni, arc pressure, drag, and Lorentz forces were mathematically modeled and implemented in the numerical simulation. Pulsed gas metal arc size and droplet transfer were measured from arc images and used to determine some simulation variables. Direct comparisons of predicted and measured weld cross-section geometry, time-varying deposit radius, and temperature history from thermocouple measurements showed general agreement and validated the GMAW-P stationary welding simulation.

The weld penetrations predicted by simulation were somewhat deeper than the experimental measurements. This discrepancy was mainly attributed to the consistent droplet impact location in the simulations versus random droplet impact location in the experiments.

Simulation tests with individual changes of variables provided insight into the effects of these variables on fluid flow patterns and weld pool shape. When the radius of the distribution of current flow into the weld pool was decreased, the larger current density drastically increased the weld penetration but de-

creased the weld radius because it produced a dominant inward and downward circulation of weld metal.

Reduced total force and increased arc pressure distribution radius both decreased the weld penetration because they produced a weld deposit that was more convex, which absorbed the momentum of impinging droplets. Conversely, weld pools subjected to increased arc pressure and smaller pressure distribution were more concave at their center and thus had deeper penetration. Understanding of the effects of these variables on weld pool fluid flow and weld shapes provided key insights that are useful for future investigations that use the simulation as a tool to assist in weld process development.

Acknowledgments

Partial support of this work by EWI under contract 47412-GTO and ONR under contract N00014-05-1-0375 is acknowledged.

References

1. Nguten, T., and Wahab, M. 1995. A theoretical study of the effect of weld geometry parameters on fatigue crack propagation life. *Engineering Fracture Mechanics* 51: 1–18.

2. Choi, H. W., Farson, D. F., and Cho, M. H. 2006. Using a hybrid laser plus GMAW process for controlling the bead humping defect. *Welding Journal* 85: 174-s to 179-s.

3. Lu, M., and Kou, S. 1988. Power and current distributions in gas tungsten arc welding. *Welding Journal* 67(2): 29-s to 34-s.

4. Lin, M. L., and Eagar, T. W. 1986. Pressures Produced by Gas Tungsten Arcs. *Met. Mat. Trans.* 17B: 601–607.

5. Adonyi, Y., Richardson, R., and Baselack III, A. 1988. Investigation of arc force effects in subsurface GTA welding. *Welding Journal* 71(9): 321-s to 330-s.

6. Tanaka, M., Ushio, M., and Lowke, J. J. 2003. Time dependent numerical analysis of stationary GTA welding process. *Trans. JWRI* 32(2): 259–263.

7. Heiple, C. R., and Roper, J. R. 1982. Mechanism for minor element effect on GTA fusion zone geometry. *Welding Journal* 61(4): 97-s to 102-s.

8. Heiple, C. R., and Burgardt, P. 1985. Effects of SO_2 shielding gas additions on GTA weld shape. *Welding Journal* 64(6): 159-s to 162-s.

9. Joos, G. 1934. *Theoretical Physics*, 3rd Ed. p. 224, Blackie and Son, Glasgow, Scotland.

10. Matsunawa, A., and Ohji, T. 1982. Role of surface tension in fusion welding (Part 1). *Trans. JWRI* 11(2): 145–154.

11. Matsunawa, A., and Ohji, T. 1983. Role of surface tension in fusion welding (Part 2). *Trans. JWRI* 12(1): 123 to 130.

12. Lin, M. L., and Eagar, T. W. 1985. Influence of arc pressure on weld pool geometry. *Welding Journal* 64(6): 163-s to 169-s.

13. Kim, J.-W., and Na, S.-J. 1995. A Study on the effect of contact tube-to-workpiece distance on weld pool shape in gas metal arc welding. *Welding Journal* 74(5): 141-s to 152-s.

14. Cho, S.-H., and Kim, J.-W. 2001. Thermal analysis of horizontal fillet joints by considering bead shape in gas metal arc welding. *Sci. Technol. Weld. Joining.* 6(4): 220–224.

15. Kim, C. H., Zhang, W., and DebRoy, T. 2003. Modeling of temperature field and solidified surface profile during gas-metal arc fillet welding. *J. of Appl Phys.* 94: 2667–2679.

16. Zhang, W., Kim, C. H., and DebRoy, T. 2004. Heat and fluid flow in complex joints during gas metal arc welding — Part I: Numerical model of fillet welding. *J. of Appl Phys.* 95: 5210-5219.

17. Zhang, W., Kim, C. H., and DebRoy, T. 2004. Heat and fluid flow in complex joints during gas metal arc welding — Part II: Application to fillet welding of mild steel. *J. of Appl Phys.* 95: 5220–5229.

18. Kumar, A., and DebRoy, T. 2004. Guaranteed fillet weld geometry from heat transfer model and multivariable optimization. *Int. J. of Heat and Mass Transfer* 47: 5793–5806.

19. Trapaga, G., and Szekely, J. 1991. Mathematical modeling of the isothermal impingement of liquid droplets in spraying processes. *Met. Mat. Trans.* 22B: 901–914.

20. Zheng, L. L., and Zhang, H. 2000. An adaptive level set method for movin-boundary problems: Application to droplet spreading and solidification. *Numer Heat Tr B-Fund.* 41: 437–454.

21. Wang, Y., and Tsai, H. L. 2001. Impingement of filler droplets and weld pool dynamics during gas metal arc welding process. *Int. J. of Heat and Mass Transfer* 44: 2067–2080.

22. Chiang, K. C., and Tsai, H. L. 1992. Shrinkage-induced fluid flow and domain change in two-dimensional alloy solidification. *Int. J. of Heat and Mass Transfer* 35: 1763–1770.

23. Haidar, J., and Lowke, J. J. 1996. Predictions of metal droplet formation in arc welding. *J. Phys. D: Appl Phys.* 29: 2951–2960.

24. Haidar, J. 1998. A theoretical model for gas metal arc welding and gas tungsten arc welding. *I. J. of Appl Phys.* 84: 3518 –3529.

25. Haidar, J. 1998. Predictions of metal droplet formation in gas metal arc welding. II. *J. of Appl Phys.* 84: 3530–3540.

26. Wang, G., Huang, P. G., and Zhang, Y. M. 2003. Numerical analysis of metal transfer in gas metal arc welding. *Met. Mat. Trans.* 34B: 345–353.

27. Wang, F., Hou, W. F., Hu, S. J., Kannatey-Asibu, E., and Schultz, W. W. 2003. Modelling and analysis of metal transfer in gas metal arc welding. *J. Phys. D: Appl Phys.* 36: 1143–1152.

28. Quinn, T. P., Szanto, M., Gilad, I., and Shai, I. 2005. Coupled arc and droplet model of GMAW. *Science and Technology of Welding and Joining* 10: 113–119.

29. Fan, H. G., and Kovacevic, R. 2004. A unified model of transport phenomena in gas metal arc welding including electrode, arc plasma and molten pool. *J. Phys. D: Appl Phys.* 37: 2531–2544.

30. Hirt, C. W., and Nichols, B. D. 1981. Volume of fluid (VOF) method for the dynamics of free boundaries. *J. Comp. Phys.* 39: 201–225.

31. Carman, P. C. 1937. Fluid flow through granular beds. *Trans. Inst. Chem. Engrs. 15: 150–166.*

32. Whitaker, S. 1986. Flow in porous media I: A theoretical derivation of Darch's law. *Transport in Porous Media 1: 3–25.*

33. Voller, V. R., and Prakash, C. 1987. A fixed grid numerical modeling methodology for convection-diffusion mushy region phase-change problems. *Int. J. Heat Mass Transfer* 30(8): 1709–1719.

34. Tsai, N. S., and Eagar, T. W. 1985. Distribution of the heat and current fluxes in gas tungsten arcs. *Met. Mat. Trans.* 16B: 841–845.

35. Sahoo, P., Debroy, T., and McNallan, M. 1988. Surface tension of binary metal-surface active solute systems under conditions relevant to welding metallurgy. *Met. Mat. Trans.* 19B: 483– 491.

36. Phares, D. J., Smedley, G. T., and Flagan, R. C. 2000. The wall shear stress produced by the normal impingement of a jet on a flat surface. *J. Fluid Mech.* 418: 351–375.

37. Kou, S., and Sun, D. K. 1985. Fluid flow and weld penetration in stationary arc welds. Met. *Mat. Trans.* 16A: 203–213.

38. Kumar, A., and DebRoy, T. 2003. Calculation of three-dimensional electromagnetic force field during arc welding. *J. of Appl Phys.* 94: 1267–1277.

39. Anon. 2003. Computer Code Flow-3D. Flow Science Corp, Los Alamos, N.Mex.

40. Jones, L. A., Eagar, T. W., and Lang, J. H. 1985. Investigation of drop detachment control in gas metal arc welding. MIT: 1009–1013.

41. Essers, W. G., and Walter, R. 1981. Heat transfer and penetration mechanisms with GMA and plasma-GMA welding. Welding Journal 60(2): 37-s to 42-s.

42. Borland, J. C. 1960. Generalized theory of super-solidus cracking in welds (and castings). *Br. Weld. J.* 7: 508–512.

43. Joseph, A., Harwig, D., Farson, D., and Richardson, R. 2003. Measurement and calculation of P-GMAW arc power and heat transfer efficiency. *Science and Technology of Welding and Joining* 8(6): 400–406.

44. Rat, V., Antre, P., Aubreton, J., Elchinger, M., Fauchais, P., and Vacher, D. 2002. Transport coefficients including diffusion in a two-temperature argon plasma. *J. Phys. D:Appl. Phys.* 35: 981–991.

A New Heat Source Model for Keyhole Plasma Arc Welding in FEM Analysis of the Temperature Profile

The model takes into consideration keyhole configuration and decay of heat distribution along the workpiece thickness

BY C. S. WU, H. G. WANG, AND Y. M. ZHANG

ABSTRACT. It is a key issue to establish an appropriate model of the heat source in the simulation of keyhole plasma arc welding (PAW). It requires that the model account for the keyhole effect and have the characteristic of volumetric distribution along the direction of the plate thickness. For available heat source models, neither Gaussian nor double ellipsoidal modes of heat source is applicable to the keyhole PAW process. Considering the force of the high-speed plasma jet and the associated strong momentum, a modified three-dimensional conical heat source model is proposed as the basis for the numerical analysis of temperature fields in the keyhole PAW process. Further, a new heat source model for quasi-steady state temperature field in keyhole PAW is developed to consider the "bugle-like" configuration of the keyhole and the decay of heat intensity distribution of the plasma arc along the direction of the workpiece thickness. Based on this heat source model, finite-element analysis of the temperature profile in keyhole PAW was conducted and the weld geometry was determined. The results showed that the predicted location and locus of the melt-line in the PAW weld cross section are in good agreement with experimental measurements.

Introduction

Plasma arc welding (PAW) offers significant advantages over conventional gas tungsten arc welding (GTAW) in terms of penetration depth, joint preparation, and thermal distortion (Refs. 1, 2). The arc used in PAW is constricted by a small nozzle and has a much higher gas velocity (300–2000 m/s) and heat input intensity (10^9–10^{10} w/m^2) than that in GTAW (gas velocity 80–150 m/s, heat input intensity 10^8–10^9 w/m^2) (Refs. 3, 4). As the plasma arc impinges on the area where two workpieces are to be joined, it can melt material and create a molten liquid pool. Because of its high velocity and the associated momentum, the arc can penetrate through the molten pool and form a hole in the weld pool, which is usually referred to as a keyhole (Ref. 5). Moving the welding torch and the associated keyhole will cause the flow of the molten metal surrounding the keyhole to the rear region where it resolidifies to form a weld bead.

The keyhole mode of welding is the primary attribute of high-power density welding processes (PAW, laser welding, and electron beam welding), which makes them penetrate thicker pieces with a single pass. Compared to laser welding and electron beam welding, keyhole PAW is more cost effective and more tolerant of joint preparation, though its energy is less dense and its keyhole is wider (Ref. 4).

Thus, keyhole PAW has found applications on the welding of many important structures (Refs. 6–14). Although keyhole PAW has the potential to replace GTAW in many applications as a primary process for precise joining (Ref. 1), the stable state of the keyhole is an important issue in applying PAW (Ref. 15). In keyhole PAW, the quality of the weld depends on the keyhole stability, which itself depends on a large number of factors, especially the physical characteristics of the material to be welded and the welding process parameters to be used (Ref. 5). Thus, keyhole PAW is susceptible to the variation of welding process parameters, which makes it have a narrower range of applicable process parameters for good weld quality so that keyhole PAW is still limited in its wide application in industry (Ref. 16). The temperature profile around the weld pool has great influence on the formation and stability of keyhole. Through numerical simulation of the temperature field and the weld pool behavior in keyhole PAW, the process parameters can be optimized for obtaining high-quality of weld structure. Therefore, it is of great significance to model and simulate the temperature distribution and weld pool geometry in the keyhole PAW process.

The key issue for numerical analysis of temperature field in keyhole plasma arc welding is how to develop a heat source model that reflects the thermo-physical characteristics of the keyhole PAW process. Because of the complexity of the phenomena associated with the formation of a keyhole, only a limited number of theoretical studies treating the PAW process have been reported, each of varying degrees of approximation, and each focusing on different aspects of the problem (Refs. 11, 17–21). General Gaussian or double-ellipsoidal heat source models used widely in simulation of arc welding processes are not suitable for keyhole PAW. As the first step in a series of study, this paper focuses on developing a suitable heat source model for finite-element analysis of temperature profile in keyhole PAW.

KEYWORDS

Finite Element Analysis
Plasma Arc Welding
Keyhole Welding
Heat Transfer
Thermal Analysis

Models of Heat Source in Keyhole PAW

As mentioned above, the key problem in FEM analysis of keyhole PAW is how to model the welding heat source. Most researchers employed a Gaussian distribution of heat flux (W/m^2) deposited on the sur-

C. S. WU and H. G. WANG are with the Institute for Materials Joining, Shandong University, Jinan, China. Y. M. ZHANG is with the Center for Manufacturing and Department of Electrical and Computer Engineering, University of Kentucky, Lexington, Ky.

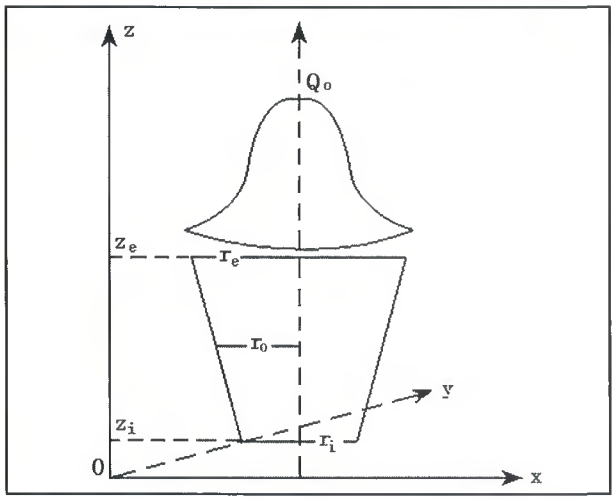

Fig. 1 — Schematic of TDC model.

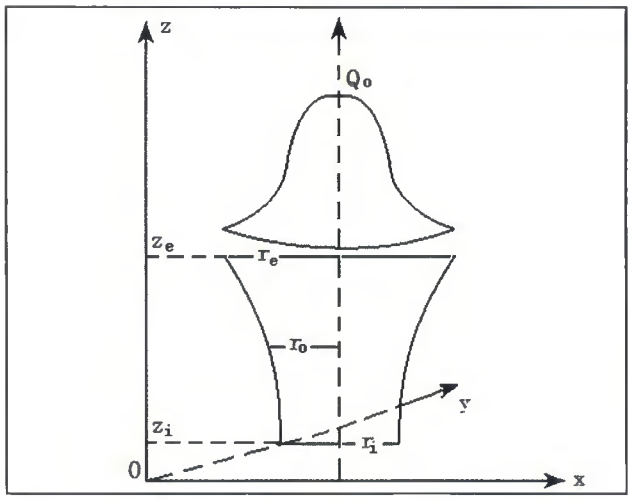

Fig. 2 — Schematic of MTDC model.

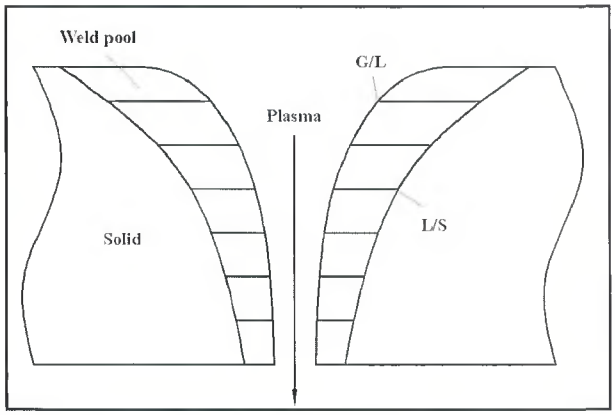

Fig. 3 — Schematic of keyhole and weld pool.

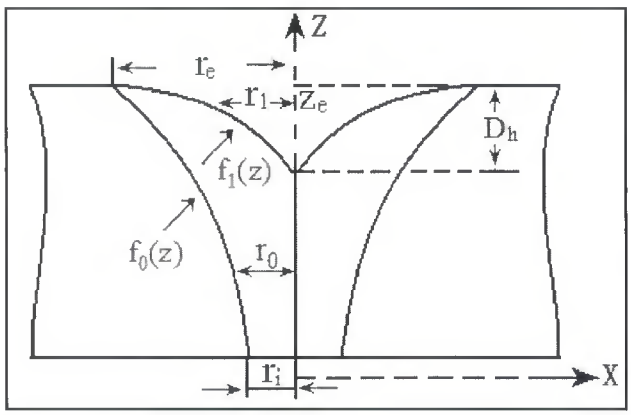

Fig. 4 — Schematic of QPAW model.

face of the workpiece (Refs. 22–24). Although such a surface mode of heat source may be used for the shallow penetration arc welding processes like GTAW, it does not reflect the action of arc pressure on the weld pool surface so that it is not suitable for modeling the welding processes with deeper penetration like gas metal arc welding (GMAW). Goldak proposed a double-ellipsoidal heat source model, which has the capability of analyzing the thermal history of deep penetration welds like GMAW (Ref. 25). However, the double-ellipsoidal distribution of heat intensity (W/m^3) is still not applicable to the high-density welding processes with high ratio of the weld penetration to width, such as keyhole PAW (Ref. 26). Keyhole PAW produces a weld with high ratio of depth to width. The cross section of the weld is of the "bugle-like" configuration. To consider the strong action of the plasma jet and the resulted bugle-like weld configuration in keyhole PAW, new types of welding heat source models must be proposed.

Three-Dimensional Conical Heat Source

Three-dimensional conical heat source (TDC) is a volumetric heat source that considers the heat intensity distribution along the workpiece thickness. As shown in Fig. 1, the heat intensity deposited region is maximum at the top surface of workpiece, and is minimum at the bottom surface of workpiece. Along the thickness of the workpiece, the diameter of the heat density distribution region is linearly decreased. But the heat density at the central axis (z-direction) is kept constant. At any plane perpendicular to z-axis, the heat intensity is distributed in a Gaussian form. Thus, in fact, TDC is the repeated addition of a series of Gaussian heat sources with different distribution parameters and the same central maximum values of heat density along the workpiece thickness. In this way, the heating action of the plasma jet through the workpiece in keyhole PAW is considered.

At any plane perpendicular to the z-axis, the heat intensity distribution may be written as

$$Q_V(r,z) = Q_0 \exp\left(-\frac{3r^2}{r_0^2}\right) \quad (1)$$

where Q_0 is the maximum value of heat intensity, r_0 is the distribution parameter, and r is the radial coordinate. The key problem is how to determine the parameters Q_0 and r_0.

As shown in Fig. 1, the height of the conical heat source is $H = z_e - z_i$, the z-coordinates of the top and bottom surfaces are z_e and z_i, respectively, and the diameters at the top and bottom are r_e and r_i, respectively. The distribution parameter r_0 is linearly decreased from the top to the bottom surfaces of the conic region, and it can be expressed as

$$r_0(z) = r_e - (r_e - r_i)\frac{z_e - z}{z_e - z_i} \quad (2)$$

Through complete derivation (see Appendix), Equation 1 is of the following form

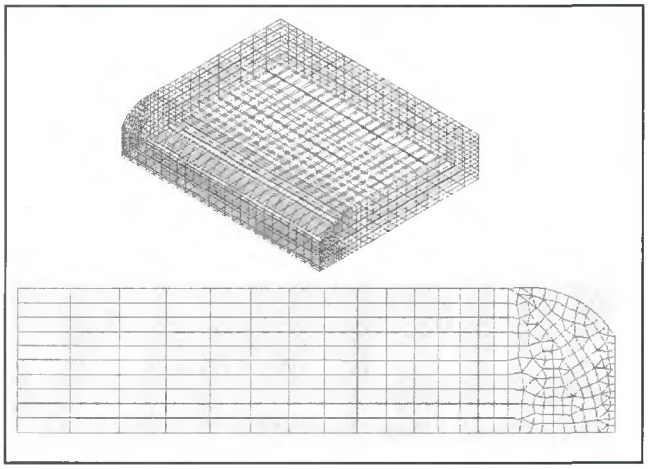

Fig. 5 — The grid system.

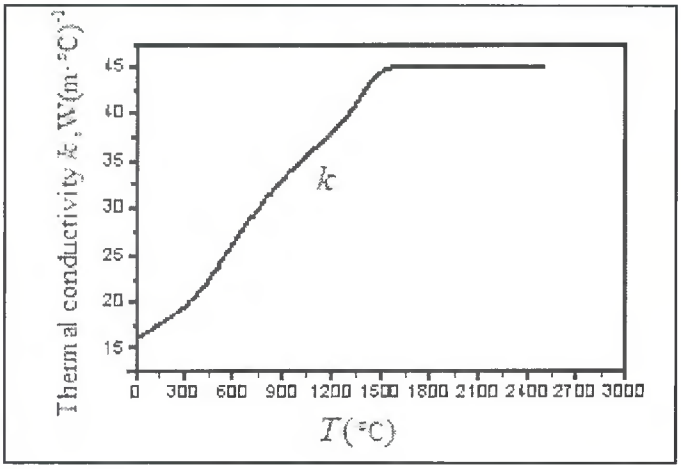

Fig. 6 — The thermal conductivity vs. temperature.

Table 1 — The Parameters Used for Heat Source Modes

Heat Source Modes	r_e (mm)	r_i (mm)	z_e (mm)	z_i (mm)	D_h (mm)
TDC	7.0	2.6	9.5	2.2	
MTDC	7.2	1.05	10.7	1.2	
QPAW	7.2	1.05	10.7	1.2	6.8

Table 2 — Keyhole PAW Welding Process Parameters

Case	Welding Current (A)	Arc Voltage (V)	Welding Speed (mm/min)	Plasma Gas Flow Rate (L/min)	Shielding Gas Flow Rate (L/min)
1	250	31.7	120	4	10
2	240	31.2	120	4	10

Table 3 — Comparison of the Predicted and Experimental Weld Width

Heat Source	Top Weld Width (mm)		Bottom Weld Width (mm)	
	Predicted	Measured	Predicted	Measured
TDC	13.60	14.35	4.25	2.11
MTDC	12.90	14.35	2.30	2.11
QPAW	13.90	14.35	2.30	2.11

$$Q_V(r,z)=\frac{9\eta UIe^3}{\pi\left(e^3-1\right)}\times\frac{1}{\left(z_e-z_i\right)\left(r_e^2+r_e r_i+r_i^2\right)}\exp\left(-\frac{3r^2}{r_0^2}\right) \tag{3}$$

where η is the plasma arc power efficiency, U is the arc voltage, and I is the welding current.

Modified Three-Dimensional Conical Heat Source

Although the three-dimensional conical heat source takes consideration of the heat intensity distribution and decay along the workpiece thickness, its characteristic of linear decline is not appropriate. In keyhole PAW, a bugle-like weld configuration was the result. To reflect this feature, a modified three-dimensional conical (MTDC) heat source is proposed, which is shown in Fig. 2. For the MTDC heat source, the distribution parameter r_0 decreases no longer as linearly as for TDC, but in a curvilinear way.

As shown in Fig. 2, the height of the modified three-dimensional conical (MTDC) heat source is $H = z_e - z_i$, the z-coordinates of the top and bottom surfaces are z_e and z_i, respectively, and the diameters at the top and bottom are r_e and r_i, respectively. Let r_0 represent the distribution parameter at z. r_0 is decreased nonlinearly and can be expressed as

$$r_0(z)=a\ln z+b \tag{4}$$

After complete derivation and manipulation (see Appendix), the heat intensity for MTDC can be written as

$$Q_V(r,z)=\frac{3\eta UIe^3}{\pi\left(e^3-1\right)}\frac{1}{A}\exp\left(-\frac{3r^2}{r_0^2}\right) \tag{5}$$

where

$$A=a^2\left[\begin{matrix}\left(H+z_i\right)\ln^2\left(H+z_i\right)\\-z_i\ln^2 z_i\end{matrix}\right]-2a(a-b)\left[\begin{matrix}\left(H+z_i\right)\ln\left(H+z_i\right)\\-z_i\ln z_i-H\end{matrix}\right]+b^2H \tag{6a}$$

$$a=\frac{r_e-r_i}{\ln z_e-\ln z_i} \tag{6b}$$

$$b=\frac{r_i\ln z_e-r_e\ln z_i}{\ln z_e-\ln z_i} \tag{6c}$$

$$r_0(z)=\frac{\left(r_e-r_i\right)\times\ln(z)}{\ln\left(z_e\right)-\ln\left(z_i\right)}+\frac{r_i\times\ln\left(z_e\right)-r_e\times\ln\left(z_i\right)}{\ln\left(z_e\right)-\ln\left(z_i\right)} \tag{6d}$$

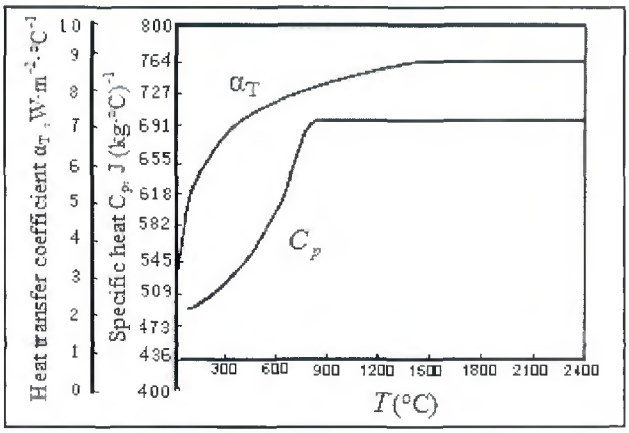

Fig. 7 — The heat transfer coefficiency and specific heat vs. temperature.

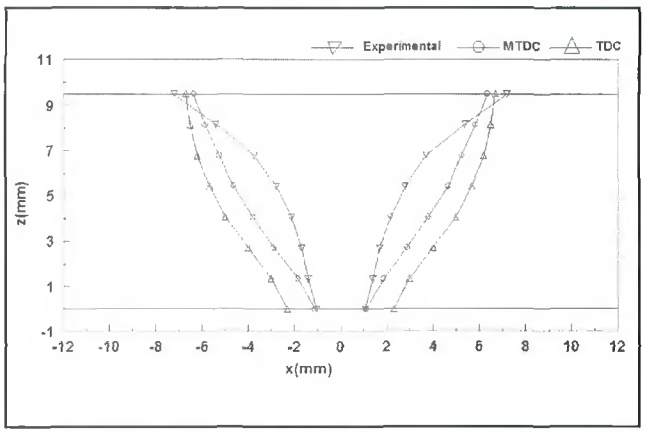

Fig. 8 — Comparison of predicted PAW cross section with experimental results.

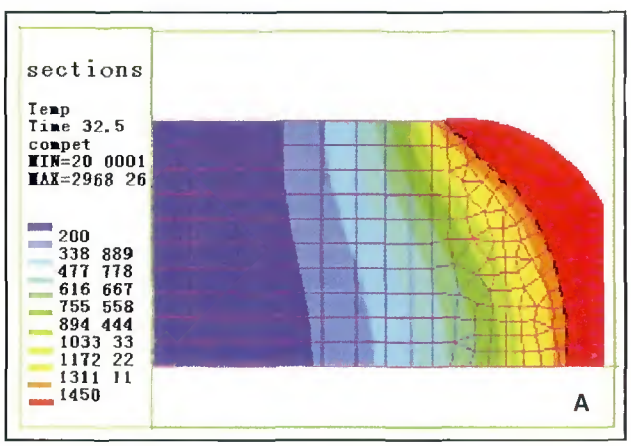

Fig. 9 — The cross section of a plasma arc weld under welding condition Case 1. A — The predicted result based on model QPAW; B — macrograph.

Quasi-Steady State PAW Heat Source

As aforementioned, the arc used in the PAW process is constricted by a small nozzle and has a much higher gas velocity and temperature than that in GTAW. The high plasma gas velocity and the associated momentum force the plasma jet to penetrate the base metal, forming a keyhole in the weld pool of complete penetration. Thus, the plasma jet emerges from the underbead at the bottom of the workpiece — Fig. 3. As the torch moves along the weld, this keyhole progressively cuts through the metal with the molten metal flowing behind to form the weld bead. The size and shape of the keyhole produced by PAW depend mainly on the pressure of the impinging gas. It was found that a typical plasma arc keyhole in 6-mm-thick stainless steel, 3-mm nozzle bore diameter, and 8–10 mm torch standoff is a conical hole with a circumferential diameter of 5 mm at the top and about 1.5–2 mm at the bottom end (Ref. 27). The forces that tend to form and maintain the keyhole include the plasma stream pressure, vapor pressure, and recoil pressure (Ref. 27). The existence of keyhole, on one hand, makes the heat intensity from the plasma arc distribute through the workpiece thickness, but on the other hand, causes some vaporization, which results in some heat losses. Therefore, the net heat input is not deposited on the workpiece totally. To consider this point, part of the heat density at the upper section of the keyhole is excluded. As shown in Fig. 4, the heat intensity is distributed within a domain bounded by the curves $f_0(z)$ and $f_1(z)$ at the upper section of the keyhole, while at the lower section of the keyhole, the heat intensity is distributed as a modified conical heat source. This model of heat source is proposed for the quasi-steady state PAW process, so it is referred to as QPAW for short. It can be expressed as

For the upper part, $(z_e - D_h) \le z \le z_e$

$$Q_V(r.z) = \frac{3\eta IUe^3}{\pi\left(e^3-1\right)A}\exp\left(-\frac{3r^2}{f_0^2(z)}\right), \quad f_1(z) \le r \le f_0(z) \tag{7}$$

where

$$f_0(z) = \frac{(r_e - r_i)\times \ln(z)}{\ln(z_e)-\ln(z_i)} + \frac{r_i \times \ln(z_e) - r_e \times \ln(z_i)}{\ln(z_e)-\ln(z_i)} \tag{8}$$

$$f_1(z) = \frac{r_e}{\sqrt{D_h}}\sqrt{z - z_e + D_h} \tag{9}$$

For the lower part, $z_i \le z \le (z_e - D_h)$, it is of the same expression as Equations 5 and 6.

FEM Analysis

After establishing a suitable heat

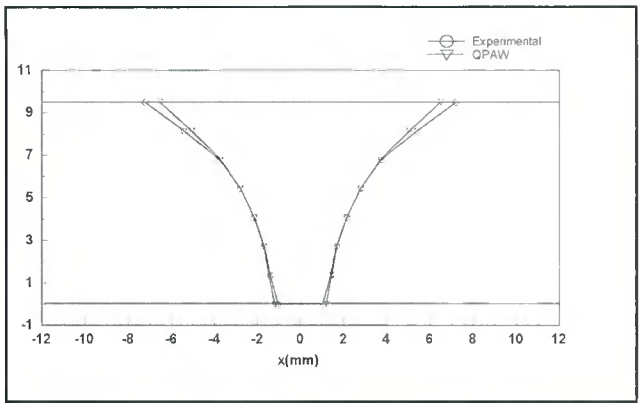

Fig. 10 — Comparison between the predicted and measured weld cross section for Case 1.

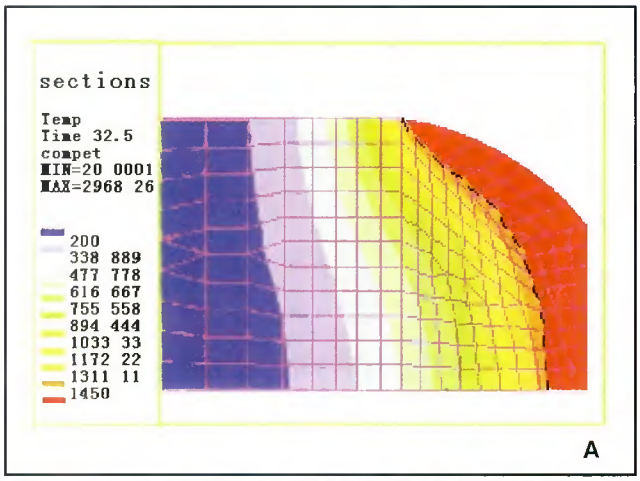

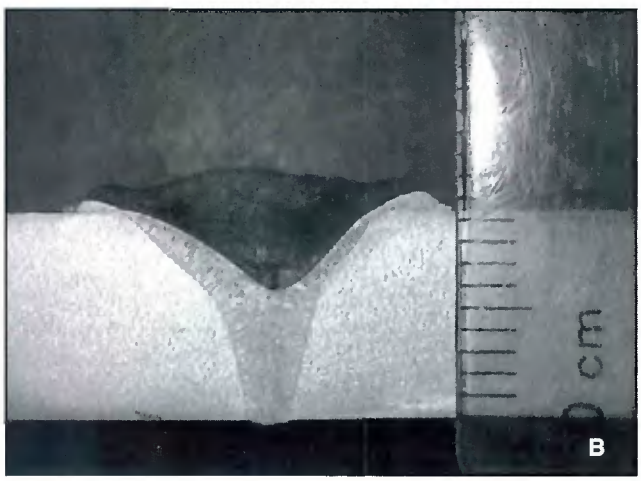

Fig. 11 — The cross section of a plasma arc weld under welding condition Case 2. A — The predicted result based on model QPAW; B — macrograph.

source model for keyhole PAW, the temperature profile and weld pool geometry are able to be determined by the finite element method (FEM). In a moving coordinate system *o-xyz* in which the origin coincided with the intersecting point between the torch centerline and the bottom surface of workpiece, *x*-axis along the welding direction and *z*-axis normal to the workpiece surface, the quasi-steady state temperature field during keyhole PAW is governed by the following equation

$$\rho C_P\left(-v_0\frac{\partial T}{\partial x}\right)=\frac{\partial}{\partial x}\left(k\frac{\partial T}{\partial x}\right)+\frac{\partial}{\partial y}\left(k\frac{\partial T}{\partial y}\right)+\frac{\partial}{\partial z}\left(k\frac{\partial T}{\partial z}\right)+Q_V \quad (10)$$

where ρ is density, C_P is specific heat, v_0 is welding speed, T is temperature, k is thermal conductivity, and Q_V is volumetric heat source. The boundary conditions for Equation 10 are as follows:

On the workpiece surface,

$$-k\frac{\partial T}{\partial z}=\alpha_T\left(T-T_\infty\right) \quad (11)$$

where T_∞ is the ambient temperature, and α_T is the combined heat transfer coefficient.

At the symmetric plane *xoz*,

$$\frac{\partial T}{\partial y}=0 \quad (12)$$

So only half of the workpiece is taken as the calculation domain. The workpiece dimension is 200 mm in length, 80 mm in width, and 9.5 mm in height.

The half domain is divided into 8-node hexahedrons. As aforementioned, part of heat density at the upper section of keyhole is excluded because of evaporation loss and keyhole effect. To reflect this characteristic and match the distribution mode of heat source QPAW, some elements in the upper section of the keyhole are treated as "dead." The discrete grids are shown in Fig. 5.

Results

The workpiece material is stainless steel 304. Its thermal conductivity k, specific heat C_P, and the combined heat transfer coefficient α_T are shown in Figs. 6 and 7. Its density is ρ = 7860 (kg m^{-3}), and ambient temperature is T_∞ = 300 K. The parameters used for describing heat source modes are given in Table 1. Keyhole PAW experiments are conducted under two welding conditions (Table 2). The arc power efficiency η takes a value of 0.66 based on the literature (Ref. 3). After welding, a macrograph of the weld is made to show its cross section.

Firstly, two kinds of volumetric heat source models, i.e., three-dimensional conical (TDC) and modified three-dimensional conical (MTDC), are used to predict the plasma arc weld geometry. Figure 8 shows the comparison of the experimental results with the predicted ones based on different models. Table 3 gives the data of weld width. From the point of view of agreement, the calculation precision of TDC is poorer. It can be seen that TDC is not suitable for determining keyhole plasma arc weld dimensions. Though the precision of MTDC is improved compared to TDC, especially the weld width at both top and bottom surfaces, the calculation precision for the location and locus of the melt-line in the weld cross section is still lower.

Secondly, the developed heat source model for quasi-steady state keyhole PAW, i.e., QPAW, is employed to calculate the weld geometry. Figures 9–12 show the comparison of experimental results with the predicted ones based on QPAW model for welding conditions Case 1 and Case 2, respectively. In Figs. 9A and 11A, the dotted lines are drawn along the isotherm of melting temperature. It can be seen that the predicted weld geometry agrees well with experimental measurements. Since the model QPAW depicts the character of the keyhole PAW process through considering the "bugle-like" configuration of the keyhole and the decay of heat intensity distribution of the plasma arc along the direction of the workpiece thickness, the calculation precision of the weld geometry at the cross section is quite satisfactory.

Conclusion

Because of the keyhole effect, a plasma arc weld has a large penetration-to-width ratio. For numerical analysis of welding temperature profile in keyhole PAW, an

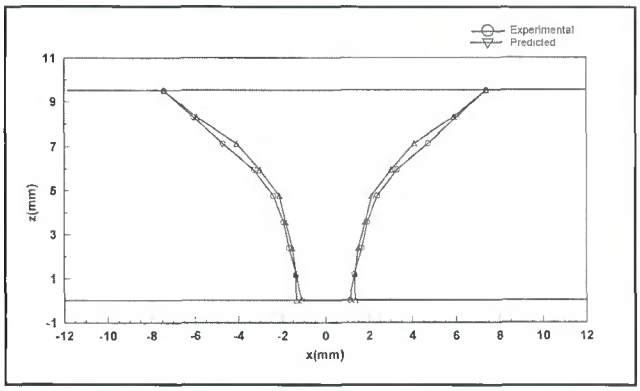

Fig. 12 — Comparison between the predicted and measured weld cross section for Case 2.

appropriate heat source model must be developed to consider the high-speed plasma jet and the associated strong momentum acted to the weld pool and the distribution of heat intensity along the direction of the workpiece thickness. Because neither the double-ellipsoidal mode of the heat source nor the three-dimensional conical mode of the heat source can be appropriate for the finite element analysis of the keyhole PAW process, a modified three-dimensional conical heat source model (MTDC) is put forward to reflect the nonlinear decay of heat intensity distribution along the direction of the workpiece thickness. Although MTDC can be used to calculate the weld width on both the top and the bottom surfaces of the workpiece, for the location and locus of the melt-line in the weld cross section, its calculating precision is lower.

A new heat source model for the quasi-steady state keyhole PAW, i.e., QPAW, is proposed, which depicts the characteristic of the keyhole PAW process quite well, because it considers both the "bugle-like" configuration of the keyhole, and the decay of heat intensity distribution of the plasma arc along the direction of the workpiece thickness. The QPAW heat source model is applied in finite element analysis of the temperature field. The results show that the calculated weld geometry at the cross section is in good agreement with the experimental one.

Acknowledgments

The authors wish to thank the financial support for this research from the National Natural Science Foundation of China (Grant No. 50540420570) and the Key Project of Chinese Ministry of Education (Grant No.104109).

References

1. Graig, E. 1988. The plasma arc welding — A review. *Welding Journal* 67(2): 19–25.

2. Tomsic, M., and Barhost, S. 1984. Keyhole plasma arc welding of aluminum with variable polarity power. *Welding Journal* 63(2): 25–32.

3. Metcalfe, J. C., and Quigley, M. B. C. 1975. Heat transfer in plasma-arc welding. *Welding Journal* 54(3): 99-s to 103-s.

4. Lancaster, J. F. 1984. *The Physics of Welding*, chapter 8, Perganon Press, Oxford.

5. Metcalfe, J. C., and Quigley, M. B. C. 1975. Keyhole stability in plasma arc welding. *Welding Journal* 54(11): 401-s to 404-s.

6. Martikainen, J. K., and Moisio, T. J. 1. 1993. Investigation of the effect of welding parameters on weld quality of plasma arc keyhole welding of structural steels. *Welding Journal* 72(7): 329-s to 340-s.

7. Vilkas, E. P. 1991. Plasma arc welding of exhaust pipe system components. *Welding Journal* 70(4): 49–52.

8. Irving, B. 1997. Why aren't airplanes welded? *Welding Journal* 76(1): 34–41.

9. Irving, B. 1992. Plasma arc welding takes on the advanced solid rocket motor. *Welding Journal* 71(12): 49-52.

10. Nunes, A. C. 1984. Variable polarity plasma arc welding on the space shuttle external tank. *Welding Journal* 63(9): 27–35.

11. Keanini, R. G., and Rubinsky, B. 1990. Plasma arc welding under normal and zero gravity. *Welding Journal* 69(6): 41–50.

12. Zhang, Y. M., and Liu, Y. C. 2003. Modeling and control of quasi-keyhole arc welding process. *Control of Engineering Practice* 11(12): 1401–1411.

13. Liu, Y. C. 2004. Control of dynamic keyhole welding process. PhD thesis. University of Kentucky.

14. Chen, K. X. Li, H. Q., and Li, C. X. 2004. Survey of variable polarity plasma arc welding. *Transactions of the China Welding Institution* 25(1): 124–128.

15. Zhang, Y. M., and Zhang, S. B. 1999. Observation of the keyhole during plasma arc welding. *Welding Journal* 75(2): 53-s to 59-s.

16. Dong, C. L, Wu, L., and Shao, Y. C. 2000. The history and present situation of keyhole plasma arc welding. *Chinese Mechanical Engineering* 11(5): 577–581.

17. Hsu, Y. F., and Rubinsky, B. 1987. Transient melting of a metal plate by a penetrating plasma arc. *ASME J Heat Transfer* 109(5): 463–469.

18. Hsu, Y. F., and Rubinsky, B. 1988. Two-dimensional heat transfer study on the keyhole plasma arc welding process. *Int. J Heat Mass Transfer* 31(7):1409–1421.

19. Nchad, A. K. 1995. Enthalpy technique for solution of Stefan problems: Application to the keyhole plasma arc welding process involving moving heat source. *Int. Comm. Heat Mass Transfer* 22(6): 779–790.

20. Keanini, R. G., and Rubinsky, B. 1993. Three-dimensional simulation of the plasma arc welding process. *Int. J Heat Mass Transfer* 36(13): 3283–3298.

21. Fan, H. G., and Kovacevic, R. 1999. Keyhole formation and collapse in plasma arc welding. *J Phys D: Appl. Phys.* 32: 2902–2909.

22. Kou, S., and Wang, Y. H. 1986. Computer simulation of convection in moving arc weld pools. *Metall. Trans.* 17A: 2271–2277.

23. Fan, H. G., Na, S. J., and Shi, Y. W. 1997. Mathematical model of arc in pulsed current gas tungsten arc welding. *J Phys D: Appl. Phys.* 30: 94–102.

24. Wu, C. S., and Yan, F. 2004. Numerical simulation of transient development and diminution of weld pool in gas tungsten arc welding. *Modeling and Simulation in Materials Science and Engineering* 13: 13–20.

25. Goldak, J., Chakravarti, A., and Bibby, M. 1984. A new finite element model for welding heat sources. *Metall. Trans. B* 15(6): 299–305.

26. Wang, H. X., Wu, C. S., and Zhang, M. X. 2005. Finite element method analysis of temperature field in keyhole plasma arc welding. *Transactions of the China Welding Institution* 26(7): 49–53.

27. Bertoluzzo, G. O. 1996. Plasma variable polarity pulsed arc welding 12.7 mm thick aluminium. *Proc of IIW Asian Pacific Welding Conference*, Auckland, New Zealand. pp. 875–896.

Appendix 1

Derivation for Heat Intensity Distribution Equations

For a volumetric distribution of heat intensity, the following assumptions are made:

1) The heat intensity deposited region is maximum at the top surface of workpiece, and is minimum at the bottom surface of workpiece.

2) Along the thickness of the workpiece, the diameter of the heat density distribution region is decreased in some way. But the heat density at the central axis (*z*-direction) is kept constant.

At any plane perpendicular to *z*-axis, the heat intensity distribution may be written as

$$Q_V(r,z) = Q_0 \exp\left(-\frac{3r^2}{r_0^2}\right) \quad \text{(A1)}$$

where Q_0 is the maximum value of heat intensity, r_0 is the distribution parameter, and r is the radial coordinate. The key

problem is how to determine the parameters Q_0 when the decay rule of r_0 is known.

Because of thermal energy conservation, we have

$$\eta UI = \int_0^H \int_0^{2\pi} \int_0^{r_0} Q_V(r,z) r dr d\theta dh$$

$$= \int_0^H \int_0^{2\pi} \int_0^{r_0} Q_0 \exp\left(-\frac{3r^2}{r_0^2}\right) r dr d\theta dh$$

$$= -\frac{\pi Q_0}{3} \int_0^H r_0 \int_0^{r_0} \exp\left(-\frac{3r^2}{r_0^2}\right) d\left(-\frac{3r^2}{r_0^2}\right) dh$$

$$= \frac{\pi Q_0 \left(1-e^{-3}\right)}{3} \int_0^H r_0^2 dh \tag{A2}$$

where η is the plasma arc power efficiency, U is the arc voltage, and I is the welding current.

Three-Dimensional Conical Heat Source (TDC)

As shown in Fig. 1, r_0 decreases linearly for TDC. The height of the conical heat source is $H = z_e - z_i$, the z-coordinates of the top and bottom surfaces are z_e and z_i, respectively, and the diameters at the top and bottom are r_e and r_i, respectively. The distribution parameter r_0 can be expressed as

$$r_0(z) = r_e - (r_e - r_i)\frac{z_e - z}{z_e - z_i} \tag{A3}$$

or

$$r_0^2 = \left[r_i + (r_e - r_i)\frac{h}{H}\right]^2, \quad h = z - z_i \tag{A4}$$

Since

$$\int_0^H r_0^2 dh = \int_0^H \left[r_i + (r_e - r_i)\frac{h}{H}\right]^2 dh = \frac{H}{3}\times\left(r_e^2 + r_e r_i + r_i^2\right) \tag{A5}$$

Substituting A5 into A2, then

$$\eta UI = \frac{\pi Q_0 H\left(1-e^{-3}\right)}{9}\left(r_e^2 + r_e r_i + r_i^2\right)$$

$$Q_0 = \frac{9\eta UIe^3}{\pi\left(e^3-1\right)} \times \frac{1}{H\left(r_e^2 + r_e r_i + r_i^2\right)} \tag{A6}$$

Finally, substituting A6 into A1, we get

$$Q_V(r,z) = \frac{9\eta UIe^3}{\pi\left(e^3-1\right)} \times \frac{1}{(z_e - z_i)\left(r_e^2 + r_e r_i + r_i^2\right)} \exp\left(-\frac{3r^2}{r_0^2}\right) \tag{A7}$$

Modified Three-Dimensional Conical Heat Source

As shown in Fig. 2, the height of the modified three-dimensional conical (MTDC) heat source is $H = z_e - z_i$, the z-coordinates of the top and bottom surfaces are z_e and z_i, respectively, and the diameters at the top and bottom are r_e and r_i, respectively. Let r_0 represents the distribution parameter at z. r_0 can be expressed as

$$r_0(z) = a \ln z + b \tag{A8}$$

Because

$$r_i = a \ln z_i + b$$

$$r_e = a \ln z_e + b$$

thus

$$a = \frac{r_e - r_i}{\ln z_e - \ln z_i} \tag{A9}$$

$$b = \frac{r_i \ln z_e - r_e \ln z_i}{\ln z_e - \ln z_i} \tag{A10}$$

Substituting A9 and A10 into A8,

$$r_0(z) = \frac{(r_e - r_i)\times \ln(z)}{\ln(z_e) - \ln(z_i)} + \frac{r_i \times \ln(z_e) - r_e \times \ln(z_i)}{\ln(z_e) - \ln(z_i)} \tag{A11}$$

Let $h = z - z_i$. Since

$$\int_0^H r_0^2 dh = \int_0^H (a\ln z + b)^2 dh = \int_0^H \left[a\ln(h+z_i) + b\right]^2 dh$$

$$= a^2 \int_0^H \ln^2(h+z_i) dh + 2ab\int_0^H \ln(h+z_i) dh + b^2 H \tag{A12}$$

Based on the *Mathematics Handbook*,

$$\int \ln u du = u\ln u - u + C$$

$$\int \ln^2 u du = u\ln^2 u - 2\int \ln u du = u\ln^2 u - 2(u\ln u - u) + C$$

$$\int_0^H r_0^2 dh = a^2 \int_0^H \ln^2(h+z_i) dh + 2ab\int_0^H \ln(h+z_i) dh + b^2 H$$

$$= a^2\left[(h+z_i)\ln^2(h+z_i) - 2(h+z_i)\ln(h+z_i) + 2(h+z_i)\right]\Big|_0^H$$

$$+2ab\left[(h+z_i)\ln(h+z_i) - (h+z_i)\right]\Big|_0^H + b^2 H$$

$$= a^2\left[(H+z_i)\ln^2(H+z_i) - z_i\ln^2 z_i\right]$$

$$-2a(a-b)\left[(H+z_i)\ln(H+z_i) - z_i\ln z_i - H\right] + b^2 H$$

Let

$$A = \int_0^H r_0^2 dh = a^2\left[(H+z_i)\ln^2(H+z_i) - z_i\ln^2 z_i\right]$$

$$-2a(a-b)\left[(H+z_i)\ln(H+z_i) - z_i\ln z_i - H\right] + b^2 H \tag{A13}$$

Substituting A13 into A2

$$\eta UI = \frac{\pi Q_0\left(1-e^{-3}\right)}{3}\int_0^H r_0^2 dh = \frac{\pi Q_0\left(1-e^{-3}\right)}{3} A$$

$$Q_0 = \frac{3\eta UIe^3}{A\left(e^3-1\right)} \tag{A14}$$

Substitute A14 into A1, we obtain

$$Q_V(r,z) = \frac{3\eta UIe^3}{A\pi\left(e^3-1\right)}\exp\left(-\frac{3r^2}{r_0^2}\right) \tag{A15}$$

Appendix 2 — Nomenclature

a	variable, defined in Equation A9
A	variable, defined in

Equation A13

b	variable, defined in Equation A10	r	$\sqrt{x^2 + y^2}$	η	arc power efficiency
C_P	specific heat	r_0	radial coordinate in heat source mode	θ	angular variable
D_h	variable, defined in Fig. 4	r_c	variable, defined in Figs. 1, 2, 4	ρ	density
e	base of natural lagarithm	r_i	variable, defined in Figs. 1, 2, 4		
f_0	function, defined in Fig. 4	T	temperature		
f_1	function, defined in Fig. 4	T_∞	ambient temperature		
h	$z - z_i$	U	arc voltage		
H	$z_e - z_i$	v_0	welding speed		
k	thermal conductivity	x, y, z	coordinate		
Q_0	maximum value of heat intensity	z_c	variable, defined in Figs. 1, 2, 4		
Q_v	heat intensity distribu	z_i	variable, defined in Figs. 1, 2, 4		
		α_T	heat loss coefficient		

WELDING JOURNAL

Instructions and Suggestions for Preparation of Articles

Text

- approximately 1500–3500 words in length
- submit hard copy
- submissions via disk or electronic transmission — preferred format is Mac but common PC files are also acceptable
- acceptable disks include floppy, zip, and CD.

Format

- include a title
- include a subtitle or "blurb" highlighting major point or idea
- include all author names, titles, affiliations, geographic locations
- separate paper into sections with headings

Photos/Illustrations/Figures

- glossy prints, slides, or transparencies are acceptable
- black and white and color photos must be scanned at a minimum of 300 dpi
- line art should be scanned at 1000 dpi
- photos must include a description of action/object/person and relevance for use as a caption
- prints must be a minimum size of 4 in. x 6 in., making certain the photo is sharp
- do not embed the figures or photos in the text
- acceptable electronic format for photos and figures are EPS, JPEG, and TIFF. TIFF format is preferred.

Other

- illustrations should accompany article
- drawings, tables, and graphs should be legible for reproduction and labeled with captions
- references/bibliography should be included at the end of the article

Editorial Deadline

- January issue deadline is November 11
- February issue deadline is December 10
- March issue deadline is January 13
- April issue deadline is February 10
- May issue deadline is March 10
- June issue deadline is April 9
- July issue deadline is May 12
- August issue deadline is June 13
- September issue deadline is July 11
- October issue deadline is August 11
- November issue deadline is September 12
- December issue deadline is October 10

Suggested topics for articles

- case studies, specific projects
- new procedures, "how to"
- applied technology

Mail to:

Andrew Cullison
Editor, Welding Journal
550 NW LeJeune Road
Miami, FL 33126
(305) 443-9353, ext. 249; FAX (305) 443-7404
cullison@aws.org

Toward a Unified Model to Prevent Humping Defects in Gas Tungsten Arc Welding

The model can be used to help prevent humping when the effects of arc current, welding speed, shielding gas, electrode geometry, ambient pressure, torch angle, and external magnetic field are considered

BY A. KUMAR AND T. DEBROY

ABSTRACT. During gas tungsten arc (GTA) welding, high welding speed and current can lead to a serious weld defect with a bead-like appearance known as humping. Currently, there is no unified model to predict the formation of humping defects in GTA welding. Here we propose and test a new comprehensive computational model that can predict and prevent the formation of humping defects considering the values of arc current, welding speed, nature of the shielding gas, electrode geometry, ambient pressure, torch angle, and external magnetic field during gas tungsten arc (GTA) welding. The model considers stability of the waves on the weld pool surface due to relative motion between the shielding gas and the liquid metal based on the Kelvin-Helmholtz instability theory. The main factors for the instability were found to be the velocities of the shielding gas and the weld metal, densities of the molten metal and shielding gas, weld pool size, and surface tension of the molten weld metal. The weld pool size and weld metal velocities were calculated by a numerical heat transfer and fluid flow model, and the shielding gas velocity was calculated from an analytical relation. Good agreement between the model predictions of humping and the independent experimental results from various sources show that the model can be used to prevent humping considering the effects of arc current, welding speed, nature of the shielding gas, electrode geometry, ambient pressure, torch angle, and external magnetic field during GTA welding. Recommendations are provided for the use of special electrodes and an external magnetic field and, where practical, controlled pressure and careful selection of shielding gas to prevent humping under conditions when high welding speed and current are needed to sustain productivity goals.

Introduction

Productivity enhancement in the manufacturing of fabricated parts is often achieved by increasing welding speed and power. During arc welding, a continuous increase in the welding speed and current often results in a weld defect with bead-like appearance known as humping (Refs. 1–9). Various experimental investigations have been undertaken to understand and prevent humping. In addition, several theoretical models were proposed based on capillary instability (Refs. 1, 6), force balance, and scaling analysis (Refs. 7–9). The previous work on humping can be classified into three groups. First, efforts have been made to experimentally determine the onset of humping (Refs. 2, 3) during gas tungsten arc welding (GTAW). These results have provided an improved understanding of the effects of various variables on humping. Second, some of the previous modeling work (Refs. 1, 6) used Rayleigh's theory of instability of liquid metal cylinders to understand humping during welding. These efforts ignored important physical processes in welding and, therefore, the results are preliminary. Finally, force balance (Refs. 7–9) and nondimensional scaling analysis (Refs. 8, 9) were used to calculate conditions for humping. The nondimensional parameter-based calculations are accurate only within an order of magnitude. They are not designed to explain the effects of all important welding variables and cannot precisely calculate the onset of humping. No comprehensive unified theoretical model exists today that can predict the formation of humping defects considering the effects of important welding variables such as the arc current, voltage, welding speed, nature of the shielding gas, electrode geometry, torch angle, and ambient pressure.

During GTA welding, a surface wave forms owing to the flow of shielding gas on the weld pool surface driven by a balance between molten metal's inertia, surface tension, and gravity forces (Refs. 10–12). The elevation and the velocity of the wave depend on various parameters such as the surface tension of liquid metal, densities of liquid metal and shielding gas, weld pool size, and the relative velocity between the shielding gas and the liquid metal. Any phenomenological model for understanding humping must take into account the effects of all the welding variables on the stability of the surface waves. An unstable surface wave can carry packets of liquid metals toward the solidifying region of the weld pool and contribute to humping.

Here we develop and extensively test a comprehensive mathematical model to quantitatively understand the welding conditions that result in humping defects. The model is based on Kelvin-Helmholtz hydrodynamic instability (Refs. 10–12) of waves on the surface of the weld pool. The model predicts humping when the elevation of the surface wave increases with time. Since the original Kelvin-Helmholtz model uses semi-infinite thickness of both the layers, a modified version is used here to take into account the finite depths of weld pools and specific thicknesses of the shielding gas layer depending on welding conditions. The velocity of the surface wave was determined by solving the potential flow equations with appropriate boundary conditions. The model indicates that the velocity of the surface wave is affected by

KEYWORDS

Gas Tungsten Arc Welding
Humping Defects
Kelvin-Helmholtz Hydrodynamic Instability
Welding Speed
Welding Current

A. KUMAR and T. DEBROY are with Department of Materials Science and Engineering, The Pennsylvania State University, University Park, Pa.

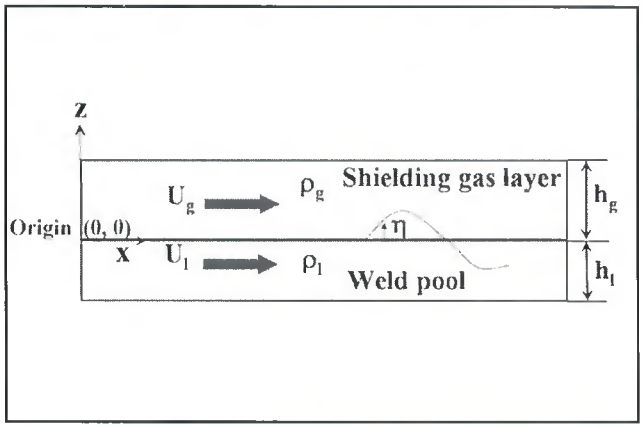

Fig. 1 — The waves generated at the interface of shielding gas layer and liquid metal in the weld pool due to shear across the interface.

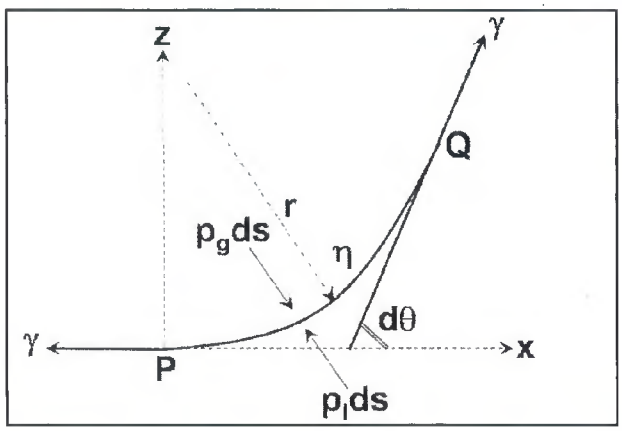

Fig. 2 — Segment of a free surface under the action of surface tension.

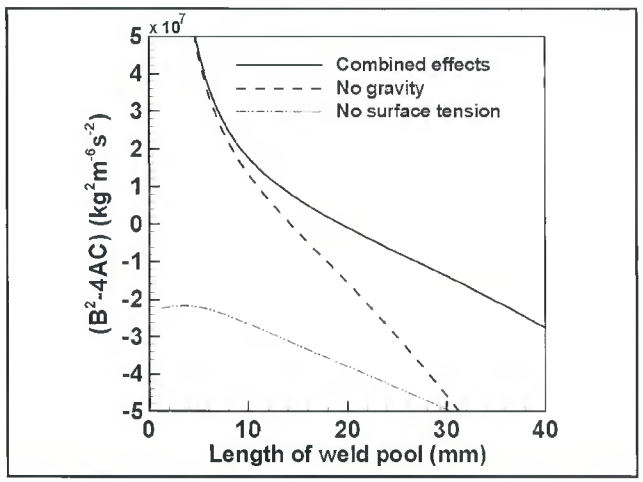

Fig. 3 — Effects of gravity and surface tension forces on the $(B^2–4AC)$ term calculated by using Equations 16B–D and 17. The negative value of $(B^2–4AC)$ term signifies the instability of surface wave or the initiation of humping in the weld pool. Values of different variables used in the calculation are: h_l = 1.5 mm, h_g = 7.5 mm, U_l = 0.7 m/s, U_g = 210.0 m/s, ρ_l = 7200 kg/m^3, ρ_g = 0.018 kg/m^3, and γ = 1.8 N/m. These values are selected because they represent the same order of the values in GTA welding with Ar shielding gas at 300 A, 11 mm/s welding speed, and arc length = 2.4 mm.

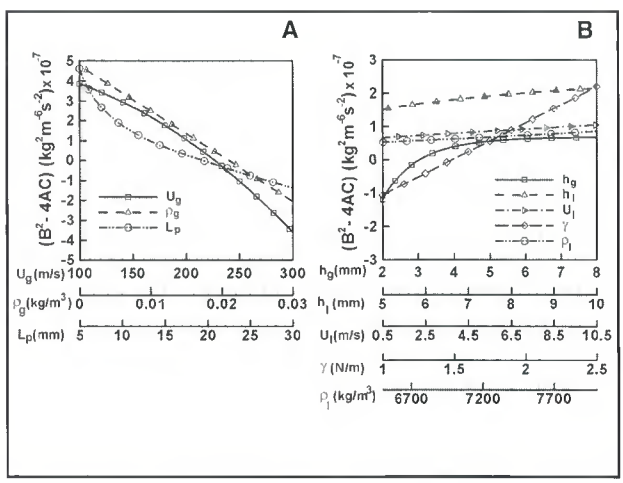

Fig. 4 — A — Sensitivity of U_g, ρ_g, and L_p on $(B^2–4AC)$ term given by Equations 16A–D; B — sensitivity of h_g, h_l, U_l, γ, and ρ_l on $(B^2–4AC)$ term. The negative value of $(B^2–4AC)$ term signifies the instability of the surface wave or the initiation of humping in the weld pool.

the surface tension of the liquid metal, densities of liquid metal and shielding gas, weld pool size, and the velocities of plasma and liquid metal on the weld pool surface. The weld pool size and liquid metal velocity were calculated by solving the equations of conservation of mass, momentum, and energy in three dimensions with appropriate boundary conditions (Refs. 13–21). The shielding gas velocity was calculated from an analytical relation of jet flow over a flat surface (Ref. 22). The computed results indicate how the values of arc current, welding speed, electrode tip angle, electrode type, nature of the shielding gas, ambient pressure, inclination of the torch, and the external magnetic field affect humping formation in GTA steel welds. The computed welding conditions for the formation of humping were compared with the corresponding independent experimental results available in the literature for various GTA welding conditions. Recommendations are made to prevent humping under difficult conditions when high welding speed and current are needed to sustain productivity goals.

Background

Several researchers have proposed theories to predict humping. Based on the experiments on gas metal arc welding (GMAW) of plain carbon steel in spray mode, Bradstreet (Ref. 1) suggested that humping occurs due to capillary instability. He applied Rayleigh's theory of instability of a free liquid cylinder and suggested the following expression:

$$L_c = 2\pi R \qquad (1)$$

where L_c is the critical length of the weld pool and R is the radius of the cylindrical liquid metal that was claimed to represent the weld pool width. He suggested that when the length of the weld pool exceeds this critical length, L_c, humping occurs due to breakage of the cylindrical liquid metal and its premature solidifica-

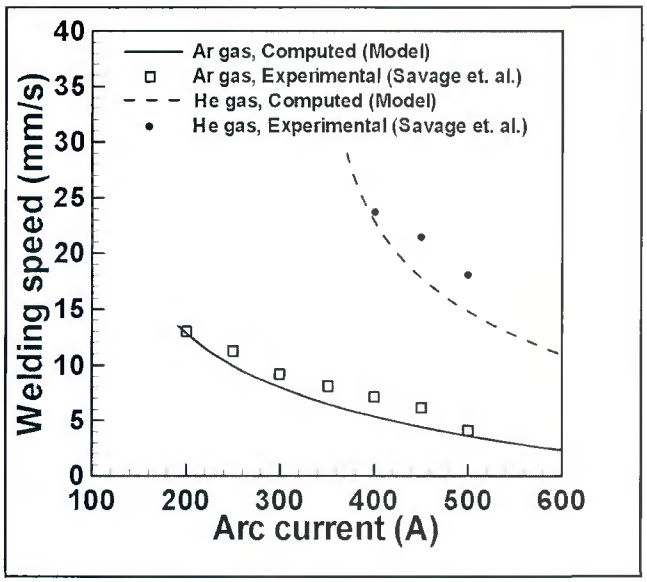

Fig. 5 — The variation of critical welding speed with arc current for argon and helium as shielding gases. The welding conditions used in the calculation are 2.4-mm arc length, 90-deg electrode tip angle, 3.2-mm-thick tungsten electrode, and the 1-atm ambient pressure. The welding speed higher than the critical speed will produce humping.

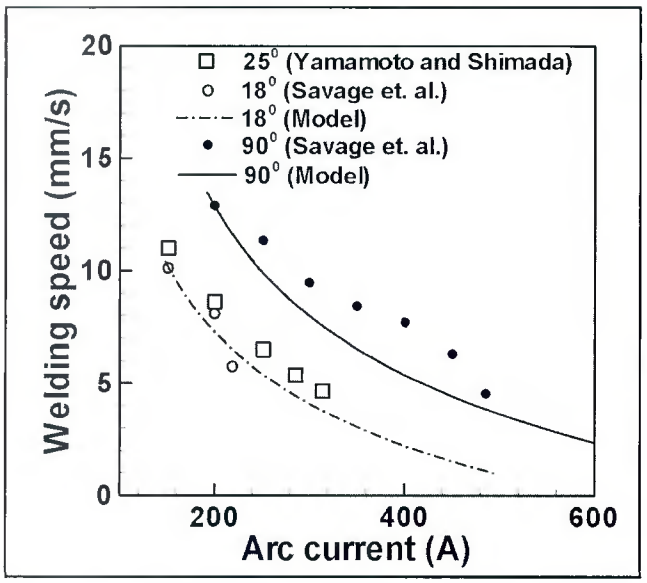

Fig. 6 — The effect of the electrode tip angle on humping. The welding conditions used in the calculations are 2.4-mm arc length, 3.2-mm-diameter tungsten electrode, argon shielding gas, and 1-atm. ambient pressure. The results show that the electrodes with smaller tip angle produce humping at a lower welding speed than those with larger tip angles.

Table 1 — Data Used for the Calculation of Weld Pool Geometry and the Velocity of the Liquid Metal by Three Dimensional Heat Transfer and Fluid Flow Model

Liquidus temperature (K)	1802
Solidus temperature (K)	1779
Density of liquid metal (kg m^{-3})	7.87×10^{3}
Viscosity of liquid (kg $m^{-1}s^{-1}$)	6.3×10^{-3}
Thermal conductivity of solid (J $m^{-1}s^{-1}K^{-1}$)	36.4
Thermal conductivity of liquid (J $m^{-1}s^{-1}K^{-1}$)	36.4
Specific heat of the solid (J $kg^{-1}K^{-1}$)	754
Specific heat of the liquid (J $kg^{-1}K^{-1}$)	805
Latent heat of melting (J kg^{-1})	2.7×10^{5}
Temperature coefficient of surface tension (N $m^{-1}K^{-1}$)	-0.47×10^{-3}

Table 2 — Constants for Arc Characteristic Used In the Calculation of Arc Voltage (Refs. 25, 26)

Arc length (mm)	A	B	C
1.0	7.2	0.007	170
2.0	6.7	0.010	175
8.0	10.0	0.015	160
16.0	14.0	0.007	160

tion. Savage et al. (Ref. 2) experimentally determined the range of critical welding speed for humping in GTA welding for various welding conditions. Yamamoto and Shimada (Ref. 3) studied low-pressure GTA and suggested that the onset of humping was related to a transition in which the weld pool turns into a thin film under the arc and the metal velocity in the film exceeds a critical value depending on the thickness of the liquid film. Beck et al. (Ref. 4) used a two-dimensional finite element model for calculating fluid flow in the molten pool during laser beam welding neglecting thermocapillary effects and observed that at high travel speeds, humping results from a jet created behind the keyhole. Mills and Keene (Ref. 5) proposed that humping was caused by Marangoni convection. In contrast, Gratzke et al. (Ref. 6) concluded that humping cannot be explained from Marangoni convection. They (Ref. 6) modified the model proposed by Bradstreet (Ref. 1) and calculated instability of a liquid cylinder based on Rayleigh's instability theory. The onset of humping was found to be influenced by the change in potential energy (due to capillarity) of a partially bounded liquid cylinder. The width of the weld pool was represented by the diameter of the cylinder and the weld pool length was taken as the length of the liquid cylinder.

$$L_c > 2\pi RB(\phi_0) \qquad (2A)$$

$$B\left(\phi_0\right) = \left(1 - \left(\frac{\pi}{2\left(\pi - \phi_0\right)}\right)^2\right)^{-0.5} \qquad (2B)$$

Equation 2A differs from Equation 1 by a function $B(\Phi_0)$. In Equation 2A, Φ_0 represents the half angle between the axis of the cylinder and the contact location of the cylinder with the workpiece (Ref. 6). Based on the shapes of typical arc and laser weld pools, Gratzke et al. (Ref. 6) suggested values of B as 1.5 and 2 for arc and laser beam welding, respectively. Thus, for arc welding, Equation 2A can be simplified to the following:

$$\frac{L_c}{R} = \frac{\text{Weld pool length}}{\text{Weld pool width}} > 3\pi \qquad (3)$$

Apart from the simplification of the weld pool geometry, the gravitational and shear forces are ignored in Equations 1

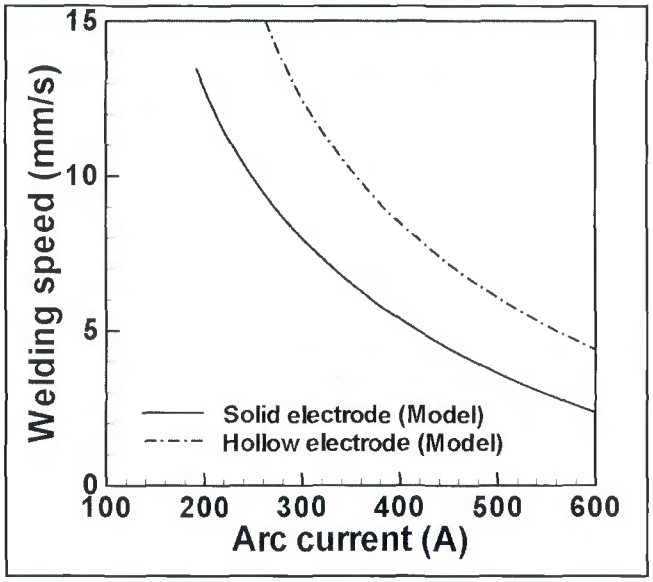

Fig. 7 — The effect of the hollow and solid electrodes on the critical welding speed to initiate humping. The welding conditions used in the calculation are 2.4-mm arc length, 90-deg electrode tip angle, argon shielding gas, and 1-atm. ambient pressure. The results show that solid electrodes produce humping at lower welding speeds than hollow electrodes.

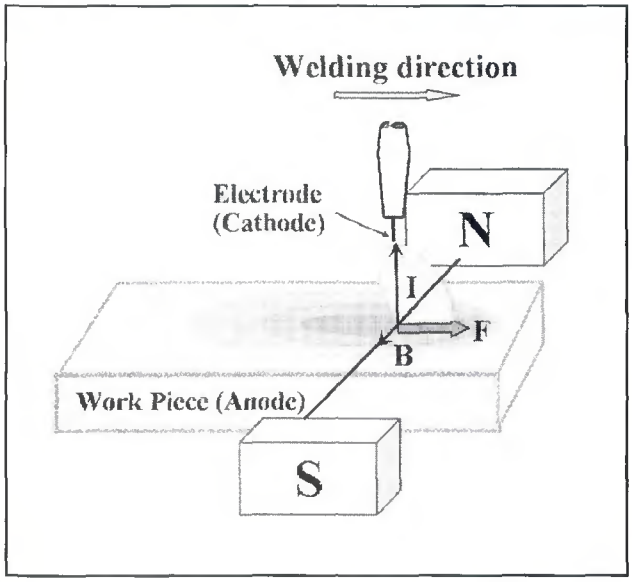

Fig. 8 — The effect of the externally applied transverse magnetic field on arc deflection based on Fleming's left-hand rule. The arc is deflected in the welding direction when the north pole is on the left side of the moving electrode. If the north and south poles are interchanged, the arc will be deflected in the reverse direction.

and 3, and they cannot predict the conditions for the initiation of humping.

Yamauchi and Taka (Ref. 7) compared the arc and the metallostatic pressures at the tail of the weld pool to explain humping. Mendez and Eagar (Ref. 8) and Mendez et al. (Ref. 9) explained the periodic nature of humping by finding the location of the transition line between the arc gouge and the trailing region based on pressure balance. Their model was based on scaling laws, and they predicted humping at high arc currents (Refs. 8, 9).

Mathematical Model

Humping Model Based on Kelvin-Helmholtz Hydrodynamic Instability

The following simplifying assumptions were made.

a) The motion of the surface waves along the direction of welding is considered in the model.

b) The liquid is assumed to be incompressible and inviscous for the calculation of the surface wave velocity for simplicity.

c) The shielding gas flow is assumed to be steady and specified by a constant horizontal velocity.

On the weld pool surface, the wave propagation is represented by the following wave equation:

$$\frac{\partial^2 \eta}{\partial x^2} = \frac{1}{c^2}\frac{\partial^2 \eta}{\partial t^2} \qquad (4)$$

Table 3 — Effect of Various Welding Variables on the Parameters Required to Predict the Humping Defects

Welding variable	Parameters affected
Arc current	Depth of weld pool, velocity of liquid metal, length of the pool, surface tension of the liquid metal, velocity of arc plasma
Arc length	Depth of weld pool, velocity of liquid metal, length of the pool, surface tension of the liquid metal, velocity of arc plasma, height of shielding gas layer
Nature of the shielding gas	Depth of weld pool, velocity of liquid metal, length of the pool, surface tension of the liquid metal, velocity of arc plasma, density of the gas
Nozzle to workpiece distance	Height of shielding gas layer
Electrode tip angle	Depth of weld pool, velocity of liquid metal, length of the pool, surface tension of the liquid metal, velocity of arc plasma
Ambient pressure	Depth of weld pool, velocity of liquid metal, length of the pool, surface tension of the liquid metal, velocity of arc plasma
Electrode inclination angle	Depth of weld pool, velocity of liquid metal, length of the pool, surface tension of the liquid metal, velocity of arc plasma

Table 4 — Values of Effective Arc Radius, r_j, for Current Density Distribution, and Effective Arc Radius for Heat Flux Distribution, r_q, in mm for Different Welding Conditions (Refs. 25, 27, 31–35) Used in the Heat Transfer and Fluid Flow Calculations and Arc Velocity Calculation (Ref. 22). The Variables I and l_a in the Table Represent Arc Current (A) and Arc Length (mm), Respectively

Argon shielding gas, 1 atm. pressure, 90-deg electrode tip angle	$r_j = 1.085 \times I^{0.2892}$ $r_q = 7.543 \times I^{0.2645}\, l_a^{0.3214}$
Argon shielding gas, 1 atm. pressure, 18-deg electrode tip angle	$rj = 1.017 \times I^{0.2892}$ $r_q = 6.786 \times I^{0.2645}\, l_a^{0.3214}$
Argon shielding gas, 32 mm Hg pressure, 25-deg electrode tip angle	$r_j = 10.67 \times I^{0.2892}$ $r_q = 7.466 \times I^{0.2645}\, l_a^{0.3214}$
Helium shielding gas, 1 atm. pressure, 90-deg electrode tip angle	$r_j = 1.391 \times I^{0.2892}$ $r_q = 9.666 \times I^{0.2645}\, l_a^{0.3214}$

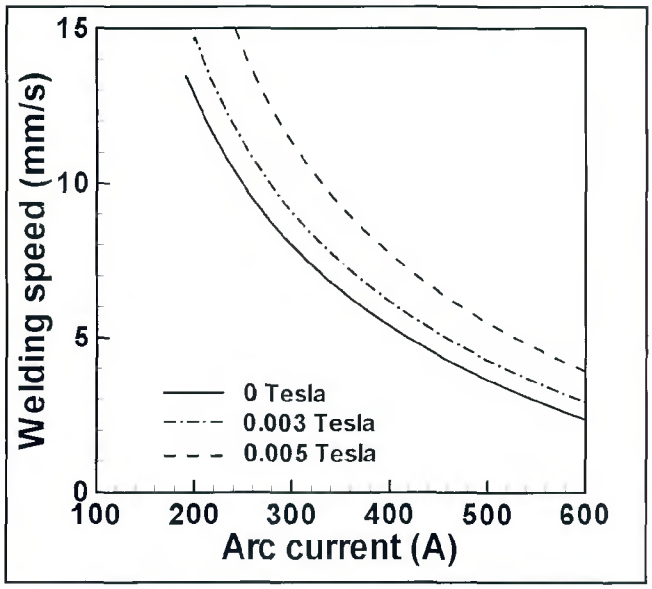

Fig. 9 — The effect of the externally applied transverse magnetic field on the critical welding speed to initiate humping in the weld. The welding conditions used in the calculation are 2.4-mm arc length, 90-deg electrode tip angle, argon shielding gas, and 1-atm. ambient pressure. The results show that the critical welding speed increases with the increase in externally applied transverse magnetic field.

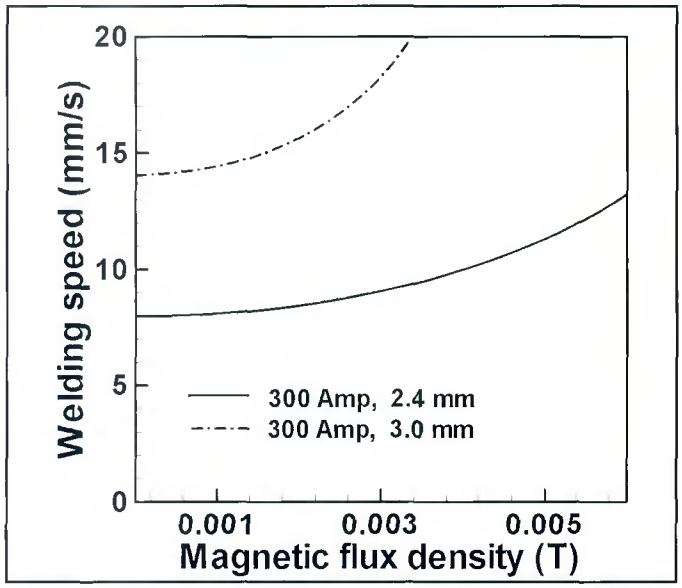

Fig. 10 — The variation of critical welding speed with externally applied transverse magnetic field for different arc lengths. The welding conditions used in the calculation are 300-A arc current, 90-deg electrode tip angle, argon shielding gas, and the 1-atm. ambient pressure. The results show that the critical welding speed increases with the increase in externally applied transverse magnetic field and the arc length.

where η is local elevation that depends on position along the welding direction, x, and time, t, and c is the velocity of the wave opposite to the welding direction x. Equation 4 represents the motion of the wave on the weld pool surface in the x direction since it is assumed that the wave is traveling along the welding direction, and there is no significant motion in the y direction. This assumption is made based on the fact that humping defects appear mainly along the welding direction. The general solution of Equation 4 is given by the following expression (Ref. 10):

$$\eta = ae^{ik(x-ct)} \qquad (5)$$

where a is the amplitude and k is the wave number. The wave speed, c, can be expressed in general form as follows:

$$c = \alpha + i\beta \qquad (6)$$

where α and β are the real and the imaginary parts of the wave speed, respectively. After substituting the expression for c in Equation 5, we get the following:

$$\eta = ae^{ik(x-[\alpha+i\beta]t)} = ae^{ik(x-\alpha t)}e^{k\beta t} \qquad (7)$$

Equation 7 shows that if β is positive, the value of elevation, η, will increase with time and the interface between the liquid metal and shielding gas will become unstable. It should be noted that η cannot be determined from Equation 7 unless the values of α and β that characterize the wave velocity are known. In order to determine the stability of the surface wave, its velocity given by Equation 6 needs to be calculated. The velocity of the wave depends on shape of the weld pool surface in the x-z plane and can be calculated by solving the velocity potentials in the gas and the liquid phases from the following two Laplace equations (Refs. 10–12):

$$\frac{\partial^2 \Phi_1}{\partial x^2} + \frac{\partial^2 \Phi_1}{\partial z^2} = 0 \qquad (8A)$$

Table 5 — Properties of Shielding Gas (Refs. 22, 25, 33, 35) Required for Arc Velocity Calculation Using the Expression Proposed by chang Et Al. (Ref. 22)

At 1 atmospheric pressure (i.e. 760 mm Hg pressure)	Density of argon gas	0.018 kg/m^3
	Viscosity of argon gas	2.32 x 10^{-4} kg. m^{-1} sec^{-1}
	Cathode radius	1.191 x 10^{-3} m
	Density of helim gas	0.0018 kg/m^3
	Viscosity of helium gas	4.32 x 10^{-4} kg^{-1} sec^{-1}
At 32 mm Hg pressure	Density of argon gas	0.0018 kg/m^3
	Viscosity of argon gas	1.90 x 10^{-4} kg. m^{-1} sec^{-1}
	Cathode radius	1.19 x 10^{-3}m

Table 6 — Welding Conditions of Mendez and Eagar (Ref. 8) Used for the Prediction of Humping by the Proposed Model

Arc current (A)	Welding speed (mm/s)	Arc length (mm)	Sulfur content (ppm)	Humping
274	11.6	7.3	6	No
334	14.1	7.5	6	No
500	10.6	9.4	6	No
500	15.0	8.5	6	No
500	10.6	9.2	230	Yes
500	15.0	8.2	230	Yes

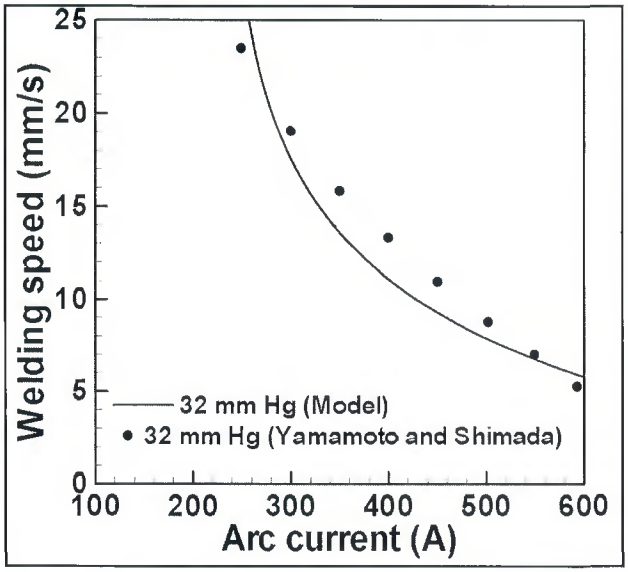

Fig. 11 — The variation of critical welding speed with arc current at low pressure for vertical torch position. The welding conditions used in the calculation are 2.4-mm arc length, 25-deg electrode tip angle, 3.2-mm-diameter tungsten electrode, argon shielding gas, and 32 mm of Hg ambient pressure. Higher values of critical welding speed were achieved at low ambient pressures.

$$\frac{\partial^2 \Phi_g}{\partial x^2} + \frac{\partial^2 \Phi_g}{\partial z^2} = 0 \qquad (8B)$$

where x is the direction opposite to the welding direction, z is the vertical direction, and Φ_l and Φ_g are the velocity potentials in the liquid metal and shielding gas, respectively. These velocity potentials (i.e., Φ_l and Φ_g) are the functions of wave speed, c, and need to be calculated using appropriate boundary conditions. The welding torch position is selected as the origin of Cartesian coordinate system to simplify the solution of governing Laplace equations. It should be noted that we need four sets of boundary conditions in each layer to solve the velocity potentials defined by Equations 8A and B. The first set of boundary conditions can be written using the known velocities of the liquid metal (U_l) and shielding gas (U_g) as follows:

$$\frac{\partial \Phi_l}{\partial x} = U_l \qquad (9A)$$

$$\frac{\partial \Phi_g}{\partial x} = U_g \qquad (9B)$$

The liquid metal velocity, U_l, was calculated from three-dimensional heat transfer and fluid flow calculations while the shielding gas velocity, U_g, was calculated using the analytical expressions as explained in the next section. The velocities of the liquid and gas at the surface depend on the location on the surface. The calculations were performed with maximum velocities on the weld pool surface to ensure consideration of the location most susceptible to humping. The second set of boundary conditions can be written by linking the velocity potentials with the local elevation position function through the following expression (Refs. 10–12):

$$\frac{D\eta}{Dt} = \left(\frac{\partial \Phi_l}{\partial z}\right)_{z=\eta} = \left(\frac{\partial \Phi_g}{\partial z}\right)_{z=\eta} \qquad (10)$$

$$\text{where } \frac{D}{D_t} = \frac{\partial}{\partial t} + U\frac{\partial}{\partial x}$$

Equation 10 represents that the substantial derivative of the surface position function of the wave, η, is equal to the normal velocity of the fluids at the interface since the fluid particles at the interface move with the surface wave. After expanding the

$$\left(\frac{\partial \Phi_l}{\partial z}\right)_{z=\eta} \text{ and } \left(\frac{\partial \Phi_g}{\partial z}\right)_{z=\eta}$$

using Taylor's theorem and neglecting the higher-order terms, the following expressions are obtained for both the liquid and gas layers (Refs. 10–12):

$$\frac{\partial \eta}{\partial t} + U_l \frac{\partial \eta}{\partial x} = \left(\frac{\partial \Phi_l}{\partial z}\right)_{z=0} \qquad (11A)$$

$$\frac{\partial \eta}{\partial t} + U_g \frac{\partial \eta}{\partial x} = \left(\frac{\partial \Phi_g}{\partial z}\right)_{z=0} \qquad (11B)$$

where $z = 0$ is the interface between the shielding gas layer and liquid metal as shown in Fig. 1. The first and second terms on the left-hand side in Equations 11A and B represent the local rate of change of surface wave profile at a given point and convective term due to change in η as a result of flow of the fluids. The third set of boundary conditions is written based on the assumption made earlier that there is no net flow across the shielding gas and liquid metal layer along the vertical direction as follows:

$$\left(\frac{\partial \Phi_l}{\partial z}\right)_{z=-h_l} = 0 \qquad (12A)$$

$$\left(\frac{\partial \Phi_g}{\partial z}\right)_{z=h_g} = 0 \qquad (12B)$$

where h_l is the depth of the weld pool, and h_g is the height of the shielding gas layer as shown in Fig. 1. The fourth and the final set of boundary conditions is written based on pressure and energy balance using the unsteady Bernoulli's theorem to keep the pressure continuous at the interface. These boundary conditions in each layer are (Refs. 10–12) as follows:

$$P_l + \rho_l \left[\frac{\partial \Phi_l}{\partial t} + \frac{1}{2}\left\{\left(\frac{\partial \Phi_l}{\partial x}\right)^2 + \left(\frac{\partial \Phi_l}{\partial z}\right)^2\right\} + g\eta\right] = \text{constant} \qquad (13A)$$

$$P_g + \rho_g \left[\frac{\partial \Phi_g}{\partial t} + \frac{1}{2}\left\{\left(\frac{\partial \Phi_g}{\partial x}\right)^2 + \left(\frac{\partial \Phi_g}{\partial z}\right)^2\right\} + g\eta\right] = \text{constant} \qquad (13B)$$

where ρ_l and ρ_g are the densities of liquid metal and shielding gas, respectively, P_l and P_g are the pressures in lower liquid and upper gaseous layers, respectively, and g is the acceleration due to gravity. The first, second, third, and fourth terms

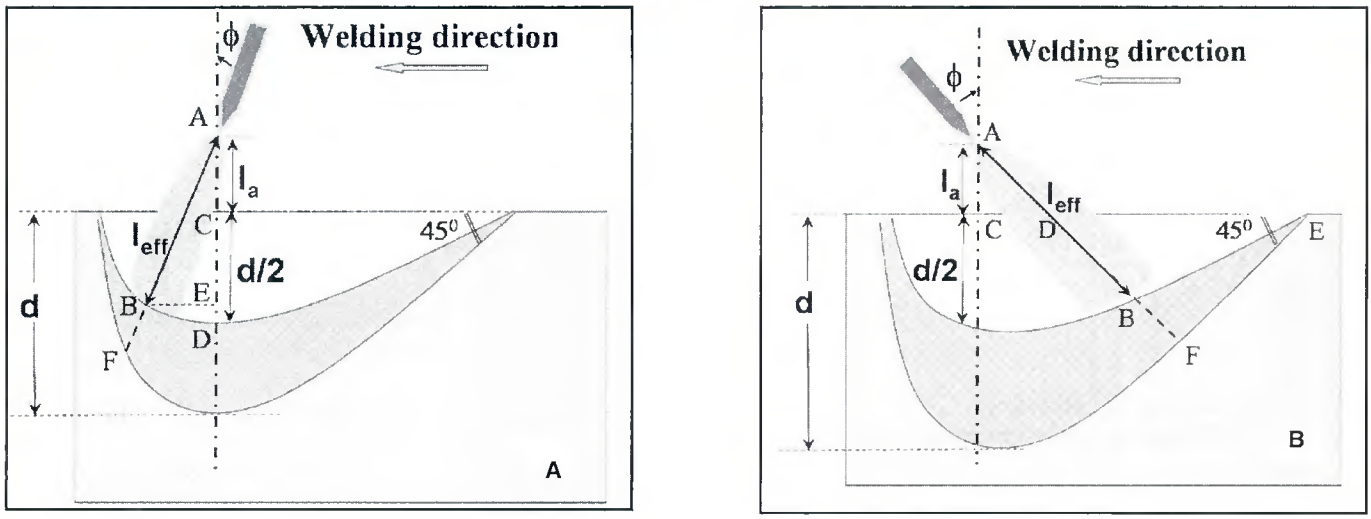

Fig. 12 — The effect of torch inclination on the effective arc length. A — The welding torch in push position; B — the pull position.

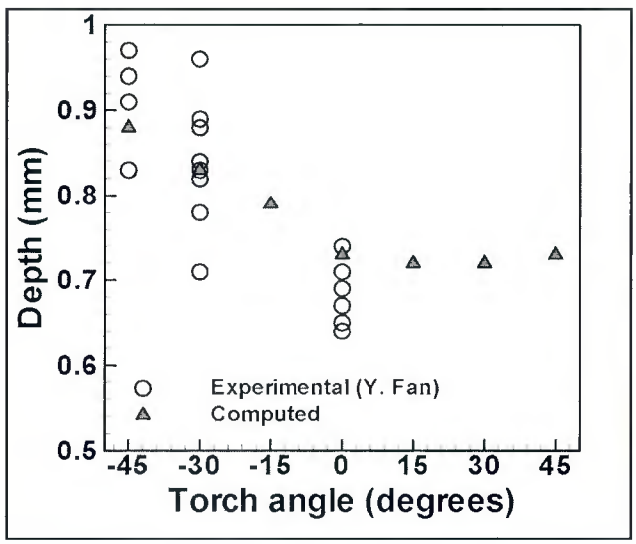

Fig. 13 — The variation of weld pool depth with inclination of torch for 67.0-A arc current, 9.0 arc voltage, and 4.0 mm/s welding speed. The positive torch angle means that the welding torch is in push position while the negative angle means that the torch is used in the pull position.

on the left-hand side of Equations 13A and B represent the pressure, unsteady velocity potential, kinetic energy, and potential energy terms, respectively (Ref. 10). The effect of surface tension was calculated by considering a force balance on the free liquid pool surface as shown in Fig. 2. The pressure difference at the interface due to surface tension can be written as follows:

$$P_g - P_l = \gamma \frac{\partial^2 \eta}{\partial x^2} \qquad (14)$$

where γ is the surface tension of the liquid weld metal. Equation 14 was obtained by balancing forces in a direction perpendicular to an arc segment PQ of the free surface as explained in Appendix A. The final expressions of velocity potentials obtained after solving Equations 8A and B using the boundary conditions given by Equations 9–14 are the values of local elevation, η, as a function of time, t. After subtracting Equation 13A from 13B and substituting the values of velocity potentials, the following relation was obtained as derived in Appendix A:

$$\begin{aligned} &k\rho_l(U_l - c)^2 coth(h_l k) \\ &+ k\rho_g(U_g - c)^2 \\ coth(h_g k) &= \gamma k^2 + g(\rho_l - \rho_g) \end{aligned} \qquad (15)$$

Equation 15 provides the velocity of surface wave traveling opposite to the welding direction (Refs. 10–12). The velocity of the traveling wave is given by

$$c = \alpha + i\beta = \frac{-B + \sqrt{B^2 - 4AC}}{2A} \qquad (16A)$$

$$\text{where } A = -k\left(\begin{matrix}\rho_l coth(h_l k) \\ +\rho_g coth(h_g k)\end{matrix}\right) \qquad (16B)$$

$$B = 2k\left(\begin{matrix}U_l \rho_l coth(h_l k) \\ +U_g \rho_g coth(h_g k)\end{matrix}\right) \qquad (16C)$$

$$C = \gamma k^2 + g(\rho_l - \rho_g) - k\left(\begin{matrix}U_l^2 \rho_l coth(h_l k) \\ +U_g^2 \rho_g coth(h_g k)\end{matrix}\right) \qquad (16D)$$

A three-dimensional heat transfer and fluid flow model described in the next section was used to calculate the length, L_p, the depth, h_l, and the surface velocity, U_l, of the weld pool. The wave number, k, is $2\pi/L$ where L is the length scale that is taken as the length of the weld pool, L_p:

$$k = \frac{2\pi}{L_p} \qquad (17)$$

Equation 16A shows that the velocity of the wave can be real or complex depending on the value of term ($B^2 - 4AC$). If this term is negative and, consequently, β is positive, the instability will grow in the weld pool because value of elevation, η, will increase with time as indicated in Equation 7.

Three-Dimensional Heat Transfer and Fluid Flow Model

The equations of conservation of mass, momentum, and energy are solved

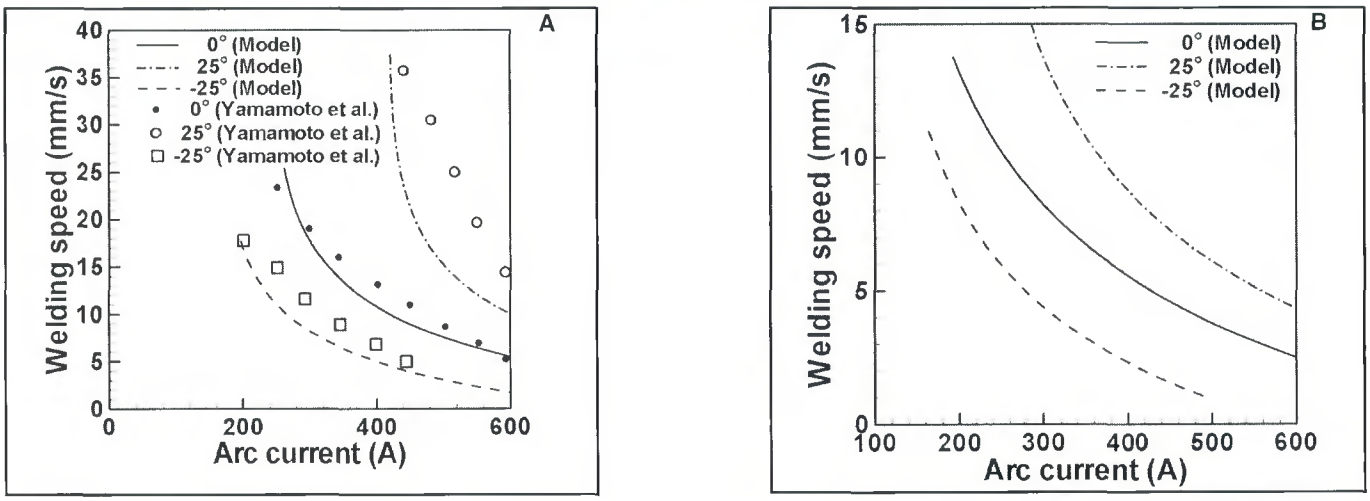

Fig. 14 — The variation of critical welding speed with arc current for the initiation of humping defects in the weld for different torch angles at the following: A — Atmospheric pressure; B — at 32-mm Hg pressure. Higher values of critical welding speed were achieved when the welding torch was in the push configuration, i.e., when the arc strikes ahead of the torch axis.

numerically in three-dimensional Cartesian coordinate system (Refs. 13–21) to obtain the values of weld pool length, liquid metal velocity, and the peak temperature. Two-dimensional calculations of heat transfer and fluid flow can also be performed to calculate the values of these variables. The governing equations and the boundary conditions used to calculate the temperature and velocity profiles and the weld pool geometry are explained in Appendix B. The governing equations are discretized using the control volume approach based on the power law scheme (Ref. 23). At each time step, the discretized equations are solved using the widely used SIMPLE algorithm (Ref. 23). Fine, nonuniform grids with finer grid spacing near the heat source were used to achieve high computational accuracy. A typical grid system contained 101 × 61 × 41 grid points in a 8-cm long, 5-cm wide, and 2-cm deep computational domain. The minimum grid spacing along the x, y, and z directions were about 200, 200, and 125 μm, respectively.

The surface tension of the molten steel (γ) in the weld pool was calculated by using the following expression (Ref. 24):

$$\gamma = 1.943 - 4.3 \times 10^{-4}(T - 1809) - 1.3 \times 10^{-8} RT \cdot \ln[1 + 0.00318 a_s e^{(1.66 \times 106/RT)}] \quad (18)$$

where T is the average of liquidus temperature and peak temperature of the liquid metal in the weld pool in K, R is the universal gas constant, and a_s is the activity of the sulfur in steel. The material properties used in the heat transfer and fluid flow calculations are listed in Table 1. The liquid metal velocity, U_l, is taken as the peak velocity present on the weld pool surface. The arc voltage (V) required for the calculation of input power at any current level for constant arc length was calculated by using the following volt-ampere characteristic expression:

$$V = A + B \times I + C/I \quad (19)$$

where A, B, and C are the constants whose values are available in the literature (Refs. 25, 26) and listed in Table 2.

Average Velocity and Other Arc Parameters

During GTA welding, the Lorentz force creates a pressure difference between the anode (workpiece) and the cathode (electrode). Due to high current density near the electrode compared to the workpiece surface, the static pressure at the cathode was higher than the anode. This pressure difference produces a jet of plasma toward the anode. In GTAW, the arc pressure is caused by the momentum transfer of the impinging plasma jet on the weld pool and is a major factor in producing surface depressions and weld defects (Refs. 8, 9). The dependence of arc pressure (p_{arc}) on the arc velocity (V_{arc}) could be expressed as follows (Refs. 25, 27):

$$p_{arc} = \frac{1}{2}\rho_g V_{arc}^2 \quad (20)$$

The arc velocity depends on the welding current, arc length, electrode shape, and the shielding gas composition, and was calculated using the expressions proposed by Chang et al. (Ref. 22).

The current density distribution required for the calculation of arc velocity was assumed to be Gaussian and could be described by the following function (Refs. 28, 29):

$$J = \frac{3I}{\pi r_j^2} \exp\left(-\frac{3r^2}{r_j^2}\right) \quad (21)$$

where J is the current density, I is current, r is the radial distance from the arc location, and r_j is the effective radius of the arc. Using Equation 21, the maximum and average current density could be written as (Refs. 25, 27) the following:

$$J_{max} = \frac{3I}{\pi r_j^2} \quad (22)$$

$$J_{avg} = \frac{I}{\pi r_j^2} = \frac{1}{3}\left(J\right)_{max} \quad (23)$$

Lin and Eagar (Ref. 27) suggested that current density is proportional to arc velocity based on the following relation:

$$p_{arc} = \frac{1}{2}\rho_g V_{arc}^2 = \frac{\mu_o J^2 r_j^2}{4} \quad (24)$$

where μ_o is the magnetic permeability of free space. Using Equations 22–24, we can write

$$U_g = \left(V_{arc}\right)_{avg} = \frac{1}{3}\left(V_{arc}\right)_{max} \quad (25)$$

where $(V_{arc})_{max}$ is the maximum value of arc velocity (i.e., at r = 0) along the arc axis.

At high arc pressures, the weld pool

surface gets deformed and the distance between the electrode and the workpiece increases (Ref. 30). Therefore, the following expression of effective arc length (l_{eff}) was used to calculate the maximum arc velocity (Ref. 8):

$$l_{eff} = arc\ length + 0.5 \times depth\ of\ weld\ pool = l_a + 0.5 \times h_l \quad (26)$$

Results and Discussion

Sensitivity of Different Variables on Humping

The effects of various welding variables on the parameters that affect humping are listed in Table 3. It can be seen from this table that almost all of the welding variables affect the depth and length of the weld pool, liquid metal velocity in the weld pool, surface tension of the liquid metal, and the velocity of the arc jet. The values of these variables also affect the velocity of the surface wave given by Equation 15, which includes the effects of surface tension, shear force, pressure gradient, and gravity.

Figure 3 shows the effects of ignoring either the gravity or the surface tension effect on the humping formation based on the value of (B^2–4AC). The values of A, B, and C are calculated from Equations 16B–D, and the data indicated in the caption of Fig. 3. If the effect of the gravity in the instability criteria given by is neglected, the (B^2–4AC) term is positive only for smaller weld pool length and the model will predict humping even for the safe welding conditions. The results indicate that the gravitational force has a significant stabilizing effect that cannot be ignored. On the other hand, if the surface tension effect is neglected, the weld pool is unstable under all welding conditions. So consideration of both the surface tension and gravity effects are necessary to accurately predict humping.

Figure 4A, B shows the sensitivity of various variables such as U_g, ρ_g, L_p, U_l, h_g, h_l, ρ_l, and γ, on the value of the (B^2–4AC) term. Higher values of U_g, ρ_g, and L_p decreases the value of (B^2–4AC), making the weld pool more susceptible to humping due to higher drag force as shown in Fig. 4A. Figure 4B shows that the liquid weld metal with high surface tension (i.e., low percentage of sulfur and relatively lower temperature) is more stable than a liquid metal with low surface tension. The increase in γ enhances the resistive power of the liquid metal against the drag force. Furthermore, the prominent effect of increase of γ on humping can be observed from the steep slope of (B^2–4AC) vs. γ plot in Fig. 4B. On the other hand, the increase in the values of h_g, h_l, U_l, and ρ_l have a significantly mild effect on the value of the (B^2–4AC) term as can be seen from the relatively low slopes of plots in Fig. 4B. The relatively mild effect of U_l on the value of the (B^2–4AC) term justifies the use of the peak surface velocity in the calculations.

Effect of Arc Current and Welding Speed

The length of the weld pool and the arc velocity significantly affects humping. The effective arc radius used for the calculation of the depth and length of the weld pool from heat transfer and fluid flow calculations are listed in Table 4. The properties of shielding gas used for calculating the arc velocity are given in Table 5 for different welding conditions. For each combination of arc current and welding speed, values of U_l, U_g, ρ_l, ρ_g, h_l, h_g, L_p, and γ were substituted in Equation 16A to calculate the value of (B^2–4AC). The calculated line in Fig. 5 represents zero value of the (B^2–4AC). The region above this line has a negative value of (B^2–4AC); as a result, humping defects appear for those welding conditions.

With the increase in arc current, both the temperature in the weld pool and the arc velocity increase. The high arc velocity increases the viscous drag force on the weld pool surface and decreases the (B^2–4AC) term. The higher current also increases the temperature in the weld pool, which decreases the surface tension of the liquid metal. Figure 5 shows that humping may occur due to decreased surface tension and increased drag force at high currents even at low welding speeds.

When the current is kept constant, the depth of the weld pool decreases with the increase in the welding speed. The lower weld pool depth decreases the effective arc length and increases the arc velocity. Thus, the higher welding velocity increases the drag force and makes humping more likely as shown in Fig. 5. Calculations were done for the conditions similar to those chosen by Savage et al. (Ref. 2) in their experiments. In particular, argon shielding gas, the electrode-to-workpiece distance of 2.4 mm, electrode thickness of 3.2 mm, and vertex angle of 90 deg were considered. Humping would occur if the welding speed is higher than the critical speed in Fig. 5 for the welding conditions considered as can be observed from both experimental data and the calculations. Table 6 also shows a good agreement in predicting humping for a different set of experiments conducted by Mendez et al. (Ref. 8). Good agreement between the calculated and the experimentally obtained critical speed limits (Refs. 2, 8) shows that the model can satisfactorily predict humping for a wide variety of welding conditions.

Effect of Shielding Gas

Since the nature of the shielding gas affects arc shape (Refs. 25, 27, 31, 32), it also influences the current density distribution. The arc shape influences the pressure difference between the cathode and the anode and, therefore, the arc pressure. According to Lin and Eagar (Ref. 27), the spread of the plasma or the effective current radius is proportional to η^2/ρ, where η is the viscosity and ρ is the density of the gas. Since the density and viscosity of helium was about 1/10th and twice, respectively, those of argon, at high temperatures (Refs. 27, 33), the helium arc is broader than that of argon. Savage et al. (Ref. 2) also reported that the argon arc was brighter and more cylindrical than the helium arc. The density and viscosity of helium used in the calculations are listed in Table 5.

The arc velocity is lower in He than in Ar due to the low density and high viscosity of helium. As a result, the drag force of He on the liquid metal is lower than that of Ar. The critical welding speed for humping was higher by a factor of 3 in helium than in argon for the same values of arc current and voltage as shown in Fig. 5. Comparisons of the results for He and Ar show that in He humping does not occur at low arc currents even at high welding speeds. Use of Ar makes welds more susceptible to humping. The computed critical welding speed for humping shows good agreement with the corresponding experimental values reported in the literature (Ref. 2).

Effect of the Electrode Tip Angle

Several researchers (Refs. 24, 26, 31, 32, 34, 35) have shown that the electrode tip angle significantly affects arc behavior. Tsai and Eagar (Ref. 31) found that the arc radius increased by approximately 15% when the current increased from 100 to 200 amps in Ar-plasma with a 75-deg tip angle and 5.5-mm arc length. Yamauchi and Taka (Ref. 32) have shown that the effect of electrode tip angle on arc pressure was more pronounced at high current levels. Lin and Eagar (Ref. 27) observed that the arc pressure increased when electrodes with sharper tip angles were used. With an increase in arc pressure for sharper tip electrodes (e.g., 18-deg tip), the peak current density and arc velocity also increases. As a result, the drag force on the liquid metal increases, which makes humping more

likely as shown in Fig. 6. The experimental values of critical welding speed for humping reported by Savage et al. (Ref. 2) and Yamamoto and Shimada (Ref. 3) for 18-, 25-, and 90-deg electrode tip angles show a good agreement with the corresponding computed values. Therefore, electrodes with a large tip angle can be used to achieve high welding speed and prevent humping.

Effect of Electrode Shape

Yamauchi and Taka (Ref. 32) showed that the use of hollow electrodes in place of solid electrodes reduced the arc force. They (Ref. 32) found that the arc root formed symmetrically inside the hole for a typical 5-mm-diameter tungsten electrode with a 3-mm central hole. They suggested that the average arc velocity reduced by about 15% compared to a solid electrode based on the measurement of arc force by Yamauchi and Taka (Ref. 32). The decrease in the arc velocity reduced the drag force on the liquid metal and increased the computed critical welding speed for humping by about 50% as shown in Fig. 7. The computed results are consistent with the fact that the hollow electrodes reduce the arc pressure (Ref. 36) and, therefore, they may be used to achieve a high fabrication rate and prevent humping under welding conditions where humping may occur when solid electrodes are used.

Effect of External Magnetic Field

An external magnetic field applied transverse to the welding direction will deflect the arc due to electromagnetic force. Depending on the direction of the field, a transverse magnetic field will deflect the arc either in the welding direction or opposite to it (Refs. 25, 37, 38) as shown in Fig. 8. The deflection of the arc increases the effective arc length and arc radius. The increase in arc length decreases the arc velocity and drag force on the weld pool surface.

The extent of the arc deflection (δ) depends linearly on the magnitude of the externally applied magnetic field and the effective arc length (l_{eff}) as represented by the following equation (Refs. 24, 37, 38):

$$\delta = K_1 B_x l_{eff} \qquad (27)$$

where K_1 is a constant and B_x is the externally applied magnetic field in Tesla. The value of constant, K_1, was obtained to be 100.0 Tesla^{-1} by fitting the above equation with the experimental results reported in the literature (Ref. 37) for Ar shielding gas. However, the value of the constant, K_1, may vary with welding conditions like welding current, shielding gas composition, and the ambient pressure. The modified effective arc length (l_{eff}) could be calculated by using the value of arc deflection (δ) as follows:

$$l_{eff} = \sqrt{\delta^2 + \left(\begin{matrix} arc\ length + 0.5 \\ \times depth\ of\ weld\ pool \end{matrix}\right)^2} \qquad (28)$$

The higher effective arc length decreased the magnitude of the drag force created by the flow of the plasma on the liquid metal in the weld pool. The reduction in drag force with increase in the magnitude of the external magnetic field reduced the chances of humping in the weld and increased the critical welding speed by 10–15% for magnetic field of 0.003 Tesla as shown in Fig. 9. Furthermore, the critical welding speed increases by more than 75% when the arc length increases from 2.4 to 3.0 mm as shown in Fig. 10. The computed results show that the longer arc length and an appropriate transverse external magnetic field during welding would provide a higher operating welding speed without any humping.

Effect of Ambient Pressure

Higher ambient pressure increases the current density in the arc column (Refs. 3, 25, 39, 40). Matsunawa and Nishiguchi (Ref. 39) observed that the arc column becomes narrower and brighter at high pressures and more diffused and rounded at low pressures. Yamamoto and Shimada (Refs. 3, 40) observed that the arc pressure at 32-mm Hg reached about one-tenth of that at atmospheric pressure. Based on these observations, the effective arc radius for current and heat distribution at 32-mm Hg pressure were assumed to be 10% more than their values at the atmospheric pressure. The effective arc radius is required for both heat transfer and fluid flow calculations as well as the arc velocity estimation. The expressions used in the calculations of arc radius are presented in Table 4, and the properties of shielding gas are given in Table 5. For each combination of arc current and welding speed, values of liquid metal velocity in the weld pool, U_l, shielding gas velocity, U_g, density of liquid metal, ρ_l, density of shielding gas, ρ_g, depth of weld pool, h_l, shielding gas layer height, h_g, length of weld pool, L_p, and surface tension of liquid metal, γ, were substituted in Equations 16B–D to calculate the value of (B^2–4AC). The calculated line in Fig. 11 represents zero value of the (B^2–4AC). The region below this line has a positive value of (B^2–4AC) and is free of humping defects. At 32 mm of Hg ambient pressure, the shielding gas density is low, which leads to low drag force and welds free of humping as shown in Fig. 11. A comparison of Figs. 4 and 11 shows that by reducing the ambient pressure, critical welding speed can be increased by more than 200%. The computed critical welding speed for humping showed good agreement with the corresponding experimental values reported by Yamamoto and Shimada (Ref. 3) indicating accuracy of the model.

Effect of Torch Angle

To capture the effect of the torch angle (inclination) in the model, the effective arc length was modified by assuming an asymmetric weld pool surface shown in Fig. 12A, B. Since the front of the weld pool is depressed significantly more than the trailing region (Ref. 41), the trailing region is assumed to make a 45-deg angle with the horizontal plane along the welding direction as shown in Fig. 12. Based on the above assumption, the effective arc length was calculated using the geometry of the system shown in Fig. 12A for different torch angles. For inclined torch practice, the torch can have two orientations, pull and push, as shown in Fig. 12. A drag or pull technique provides more penetration and a narrower bead compared to a push technique where the arc is directed ahead of the weld bead. For the push configuration, $\phi > 0$, and the effective arc length was calculated using the following expression:

$$l_{eff} = \left(\frac{l_a + 0.5 \times depth\ of\ weld\ pool}{cos(\phi)}\right) \quad for\ \phi \geq 0 \qquad (29)$$

The presence of cosine of the inclination angle in the denominator increases the arc length and the arc radius on the weld pool surface. With increase in arc radius, the peak heat intensity decreases, which leads to a wider and shallower pool. The effective arc length for the pull technique when the arc was directed behind the weld bead, i.e., for $\phi < 0$, was calculated based on the geometry. The effective arc length for the pull technique (i.e., negative ϕ) shown in Fig. 12B was calculated from the following expression:

$$l_{eff} = \frac{l_a}{cos(\phi)} + 0.5 \left(\frac{sin(\pi/4) \times depth\ of\ weld\ pool - l_a\ tan(\phi)}{sin(\phi + \pi/4)}\right) \quad for\ \phi < 0 \qquad (30)$$

Figure 13 shows the variation of weld pool depth with torch inclination angle,

ϕ. A reasonable agreement with the experimental results for different torch angles (Ref. 42) suggested that the above expressions of effective arc length could be used in the model. The depth and length of the weld pool was larger during the pull technique compared to the push technique for similar welding conditions. The calculations were done using a three-dimensional heat transfer and fluid flow model with modification for the electromagnetic force calculation (Refs. 28, 42) at different torch angles. This behavior matched very well with the effect of inclination of torch observed experimentally (Ref. 41). Figure 14 shows that the critical welding speed for humping defects increases with inclination of arc ahead of weld bead, i.e., during the push technique. For a 25-deg inclination, the computed critical welding speed increased by about 60%. This behavior was due to the decrease in both arc velocity and arc pressure on the weld pool surface with increase in the effective arc length. The inclination of torch in the negative direction (i.e., in pull or drag technique) reduced the critical welding speed and generated humping even at a lower speed as shown in Fig. 14A. Recently, Nguyen et al. (Ref. 43) observed that the critical welding speed during gas metal arc welding in spray mode increases when the gun is directed ahead of the weld bead. Lancaster (Ref. 25) also recommended the use of the welding torch in the push position to avoid humping. The computed results also showed a similar behavior.

Yamamoto and Shimada (Ref. 3) also showed the effect of the inclination of the torch on the critical welding speed at low ambient pressure. They found that at low ambient pressure, the inclination of the torch in the push direction increased the critical welding speed and vice versa. The computed critical welding speed, shown in Fig. 14B, for different torch inclination angles and 32-mm Hg ambient pressure, showed good agreement with the corresponding experimental values reported by Yamamoto and Shimada (Ref. 3) indicating the accuracy of the calculations.

Conclusions

A phenomenological model based on the stability of waves on the weld pool surface due to relative motion between the plasma and the liquid weld metal was developed to examine the conditions for the formation of humping defects. Good agreement was obtained between the model predictions for humping and independent experimental results from various sources for a wide variety of welding conditions. This model can estimate the critical welding conditions for humping considering the values of arc current, welding speed, nature of the shielding gas, electrode geometry, ambient pressure, torch angle, and external magnetic field during gas tungsten arc (GTA) welding. The following conclusions can be drawn from the results.

1) Increase in welding speed above certain critical speed leads to initiation of humping defects.

2) The value of the critical speed varies with the welding conditions. The critical welding speed decreases with increase in arc current.

3) The nature of the shielding gas affects humping. Chances of humping are lower in He than in Ar.

4) Blunt electrodes with large tip angles help in preventing humping.

5) Application of external magnetic field in transverse direction that deflects arc in the welding direction helps in avoiding humping.

6) Low ambient pressure reduces the occurrence of humping.

7) The inclination of the torch away from the welding direction, i.e., in push position, suppresses humping while the torch in pull position favors humping.

These results show that the adjustment of welding variables can prevent humping. Even when high welding speed and current are needed to sustain productivity goals, several steps can be taken to prevent humping. These include selection of hollow electrodes, imposition of appropriate external magnetic field, inclination of the torch, careful selection of shielding gas and, where practical, reduced pressure.

Acknowledgments

This research was supported by a grant from the U.S. Department of Energy, Basic Energy Sciences, Division of Materials Sciences, under grant number DE-FGO2-01ER45900. Amit Kumar gratefully acknowledges award of a Fellowship from the American Welding Society.

Appendix A: Derivation of Kelvin-Helmholtz Instability Model

The pressure difference along the interface was calculated by considering the force balance in a direction perpendicular to arc segment PQ of length ds shown in Fig. 2, as follows (Refs. 10–12):

$$-P_g ds + P_1 ds + \gamma d\theta = 0$$

where γ is the surface tension of the liquid metal in the weld pool and $d\theta$ is the included angle between the tangential forces acting on arc segment PQ. Furthermore, the pressure difference is related to the radius of curvature, r, by the following relation (Refs. 10–12):

$$P_g - P_1 = \gamma \frac{d\theta}{ds} = \frac{\gamma}{r} \qquad \text{(A1)}$$

The curvature 1/r of the surface wave profile, η, is given by (Refs. 10–12)

$$\frac{1}{r} = \frac{\partial^2 \eta / \partial x^2}{\left[1 + \left(\partial \eta / \partial x\right)^2\right]^{3/2}} \approx \frac{\partial^2 \eta}{\partial x^2} \qquad \text{(A2)}$$

Equation A2, valid for small slopes, can be substituted in Equation A1 to obtain the following equation:

$$P_g - P_1 = \gamma \frac{\partial^2 \eta}{\partial x^2} \qquad \text{(A3)}$$

After subtracting Equation 13A from Equation 13B and neglecting the nonlinear velocity terms, for small amplitude waves, we get

$$P_g - P_1 + \rho_g \left[\frac{\partial \Phi_g}{\partial t} + g\eta\right] - \rho_1 \left[\frac{\partial \Phi_1}{\partial t} + g\eta\right] = 0$$

After substituting the value of pressure difference at the interface (i.e., Equation A3) in the above expression, we get

$$\gamma \frac{\partial^2 \eta}{\partial x^2} + \rho_g \left[\frac{\partial \Phi_g}{\partial t} + g\eta\right] - \rho_1 \left[\frac{\partial \Phi_1}{\partial t} + g\eta\right] = 0 \qquad \text{(A4)}$$

For the lower liquid metal layer and the upper gaseous layers, the velocity potentials, Φ_1 and Φ_g, which satisfy the Equations 8A, 8B, 9A, 9B, 12A, and 12B can be written as

$$\Phi_1 = U_1 x + B_1 e^{ik(x-ct)} \cosh\left[k\left(z + h_1\right)\right] \qquad \text{(A5a)}$$

$$\Phi_g = U_g x + B_2 e^{ik(x-ct)} \cosh\left[k\left(z - h_g\right)\right] \qquad \text{(A5b)}$$

where B_1 and B_2 are constants whose value will be calculated based on the remaining boundary conditions given by Equations 10A, 10B, and A4. After substituting the values of velocity potentials,

Φ_1, Φ_g, and η from Equations A5a, A5b, and 5 in Equations 10A and 10B and rearranging the terms, we get (Refs. 10, 12)

$$B_1 = -\frac{iak\left(c-U_1\right)\cos\alpha\left(h_i k\right)}{k} \quad \text{(A6a)}$$

$$B_2 = \frac{ika\left(c-U_g\right)\cos\alpha\left(h_g k\right)}{k} \quad \text{(A6b)}$$

After substituting the values of Φ_1, Φ_g, and η in Equation A4, we get

$$\begin{aligned} &e^{ik(x-ct)}\gamma ak^2-\rho_1(iB_1ce^{ik(x-ct)}k\cosh(k(h_1+z)) \\ &\quad -iB_1e^{ik(x-ct)}kU_1\cosh(k(h_1+z))-e^{ik(x-ct)}ga) \\ &\quad +\rho_g(iB_2ce^{ik(x-ct)}k\cosh(k(z-h_g)) \\ &\quad -iB_2e^{ik(x-ct)}kU_g\cosh(k(z-h_g)) \\ &\quad -e^{ik(x-ct)}ga) = 0 \end{aligned} \quad \text{(A7)}$$

Dividing Equation A7 by the term $e^{ik(x-ct)}$ and putting $z = 0$ at the interface, we get

$$\begin{aligned} &\gamma ak^2-\rho_1(iB_1ck\cosh(kh_1) \\ &\quad -iB_1kU_1\cosh(kh_1)-ga) \\ &\quad +\rho_g(iB_2ck\cosh(kh_g) \\ &\quad -iB_2kU_g\cosh(kh_g)-ga) = 0 \end{aligned} \quad \text{(A8)}$$

Substituting the values of B_1 and B_2 in Equation A8 and rearranging the terms:

(A9)

After canceling the amplitude 'a' from all the terms in Equation A9, we get the following dispersion relation for wave speed.

$$\begin{aligned} &k\rho_1(U_1-c)^2\coth(h_1k) \\ &\quad +k\rho_g(U_g-c)^2\coth(h_gk) \\ &\quad = \gamma k^2+g(\rho_1-\rho_g) \end{aligned} \quad \text{(A10)}$$

Equation A10 describes the dependency of various variables on surface wave velocity.

Appendix B: Heat Transfer and Fluid Flow Model

The flow of liquid metal in the weld pool in a three-dimensional Cartesian coordinate system is represented by the following momentum conservation equation (Refs. 13–21):

$$\begin{aligned} &\rho\frac{\partial u_j}{\partial t}+\rho\frac{\partial\left(u_iu_j\right)}{\partial x_i} \\ &=\frac{\partial}{\partial x_i}\left(\mu\frac{\partial u_j}{\partial x_i}\right)+S_j \end{aligned} \quad \text{(B1)}$$

where ρ is density of the metal, x_i is the distance along the i = 1, 2, and 3 directions, u_j is the velocity component along the j direction, μ is the viscosity of the liquid metal, and S_j is the source term for the j^{th} momentum equation and is given as (Refs. 13–21):

$$\begin{aligned} S_j &= -\frac{\partial p}{\partial x_j}+\frac{\partial}{\partial x_i}\left(\mu\frac{\partial u_i}{\partial x_j}\right)-C\left(\frac{\left(1-f_L\right)^2}{f_L^3+B}\right)u_j \\ &\quad +\rho g\beta\left(T-T_{ref}\right)-\rho U\frac{\partial u_j}{\partial x_1}+Sb_j \end{aligned} \quad \text{(B2)}$$

where p is the pressure, f_L is the liquid fraction, B is a constant introduced to avoid division by zero, C ($=1.6\times10^4$) is a constant that takes into account mushy zone morphology, g is acceleration due to gravity, β is thermal expansion coefficient, T_{ref} is the reference ambient temperature, U is the welding speed along direction 1, and Sb_j represents the electromagnetic source term (Refs. 13, 14, 28). The third term on the right-hand side (RHS) represents the frictional dissipation in the mushy zone according to the Carman-Kozeny equation for flow through a porous media (Refs. 44, 45). The pressure field was obtained by solving the following continuity equation simultaneously with the momentum equation:

$$\frac{\partial\left(\rho u_i\right)}{\partial x_i}=0 \quad \text{(B3)}$$

The total enthalpy H is represented by a sum of sensible heat h and latent heat content ΔH, i.e., $H = h + \Delta H$ where $h = \int C_p dT$, $\Delta H = f_L L$, and C_p is the specific heat of the liquid metal. The liquid fraction f_L is assumed to vary linearly with temperature in the mushy zone (Refs. 13–21):

where T is the temperature, T_L is liquidus temperature, and T_S is the solidus temperature. The thermal energy transport in the weld workpiece can be expressed by the following modified energy equation (Refs. 13–21):

$$f_L=\begin{cases}1 & T>T_L\\ \dfrac{T-T_S}{T_L-T_S} & T_S\le T\le T_L\\ 0 & T<T_S\end{cases} \quad \text{(B4)}$$

$$\begin{aligned} &\rho\frac{\partial h}{\partial t}+\rho\frac{\partial\left(u_ih\right)}{\partial x_i}=\frac{\partial}{\partial x_i}\left(\frac{k}{C_p}\frac{\partial h}{\partial x_i}\right) \\ &-\rho\frac{\partial\left(\Delta H\right)}{\partial t}-\rho\frac{\partial\left(u_i\Delta H\right)}{\partial x_i}-\rho\frac{\partial\left(U\Delta H\right)}{\partial x_i} \\ &-\rho\frac{\partial\left(Uh\right)}{\partial x_i} \end{aligned} \quad \text{(B5)}$$

Since the weld is symmetrical about the weld centerline only half of the workpiece is considered. The weld top surface is assumed to be flat. The velocity boundary condition is given as (Refs. 13-21)

$$\begin{aligned} \mu\frac{\partial u}{\partial z} &= f_L\frac{d\gamma}{dT}\frac{\partial T}{\partial x} \\ \mu\frac{\partial v}{\partial z} &= f_L\frac{d\gamma}{dT}\frac{\partial T}{\partial y} \\ w &= 0 \end{aligned} \quad \text{(B6)}$$

where $d\gamma/dT$ is temperature coefficient of surface tension and u, v, and w are the velocity components along the x, y, and z directions, respectively. As shown in this equation, the u and v velocities are determined from the Marangoni effect. The w velocity is equal to zero since there is no flow of liquid metal perpendicular to the pool top surface. The heat flux at the top surface is given as (Ref. 42)

$$\begin{aligned} k\frac{\partial T}{\partial z} &= \frac{dQ\eta}{\pi r_b^2}\exp\left(-d\left\{\frac{x^2}{r_b^2\cos^2\phi}+\frac{y^2}{r_b^2}\right\}\right) \\ &\quad -\sigma\varepsilon\left(T^4-T_a^4\right)-h_c\left(T-T_a\right) \end{aligned} \quad \text{(B7)}$$

where k is thermal conductivity, d is the energy distribution factor, Q is total arc power, η is the arc efficiency, r_b is the effective arc radius, ϕ is torch inclination angle, σ is Stefan-Boltzmann constant, ε is the emissivity, T_a is ambient temperature, and h_c is the convective heat transfer coefficient. The first term on the right-hand side is the heat input from the heat source, defined by an ellipsoidal Gaussian heat distribution (Ref. 42). For zero torch inclination angle, the ellipsoidal Gaussian heat distribution becomes the same as the symmetric circular Gaussian heat distribution. The second and third terms represent the heat loss by radiation and convection, respectively. The boundary conditions are defined as zero flux across the symmetric surface as

$$\frac{\partial u}{\partial y}=0,\ v=0,\ \frac{\partial w}{\partial y}=0 \quad \text{(B8)}$$

$$\frac{\partial h}{\partial y} = 0 \qquad \text{(B9)}$$

At all other surfaces, temperatures are set at ambient temperature and the velocities are set to be zero. The electromagnetic source term in Equation B2 was calculated using the modified electromagnetic force model (Refs. 28, 42), which can calculate the electromagnetic force for any current density distribution.

References

1. Bradstreet, B. J. 1968. Effect of surface tension and metal flow on weld bead formation. *Welding Journal* 47(7): 314-s to 322-s.

2. Savage, W. F., Nippes, E. F., and Agusa, K. 1979. Effect of arc force on defect formation in GTA welding. *Welding Journal* 58(7): 212-s to 224-s.

3. Yamamoto, T., and Shimada, W. 1975. A study on bead formation in high speed TIG arc welding. *International Symposium in Welding*, Osaka, Japan.

4. Beck, M., Berger, P., Dausinger, F., and Hugel, H. 1991. Aspects of keyhole/melt interaction in high speed laser welding. *Proceedings of 8th International Symposium on Gas Flow and Chemical Lasers*, Madrid, Spain.

5. Mills, K. C., and Keene, B. J. 1990. Factors affecting variable weld penetration. *International Materials Reviews* 35(4): 185–216.

6. Gratzke, U., Kapadia, P. D., Dowden, J., Kroos, J., and Simon, G. 1992. Theoretical approach to the humping phenomenon in welding processes. *Journal of Physics D: Applied Physics* 25: 1640–1647.

7. Yamauchi, N., and Taka, T. 1978. Bead formation in TIG welding. *International Institute of Welding*, document no.: 212-437-78.

8. Mendez, P. F., and Eagar, T. W. 2003. Penetration and defect formation in high-current arc welding. *Welding Journal* 82(10): 296-s to 306-s.

9. Mendez, P. F., Niece, K. L., and Eagar, T. W. 2000. Humping formation in high current GTA welding. *Proceedings of the International Conference on Joining of Advanced and Specialty Materials II, Materials Solutions '99*, Cincinnati, Ohio, pp 151–158.

10. Kundu, P. K., and Cohen, I. M. 2004. *Fluid Mechanics*. San Diego, Calif.: Elsevier Academic Press. pp 2004–235.

11. Thomson, L. M. 1968. *Theoretical Hydrodynamics*. New York, N.Y.: Macmillan. pp 426–464.

12. Drazin, P. G., and Reid, W. H. 2004. *Hydrodynamic Stability*. Cambridge, UK: University Press. pp 8–31.

13. Mundra, K., DebRoy, T., and Kelkar, K. M. 1996. Numerical prediction of fluid flow and heat transfer in welding with a moving heat source. *Numerical Heat Transfer A* 29: 115–129.

14. Zhang, W., Roy, G. G., Elmer, J. W., and DebRoy, T. 2003. Modeling of heat transfer and fluid flow during gas tungsten arc spot welding of low carbon steel. *Journal of Applied Physics* 93(5): 3022–3033.

15. De, A., and DebRoy, T. 2004. A smart model to estimate effective thermal conductivity and viscosity in weld pool. *Journal of Applied Physics* 95(9): 5230–5239.

16. De, A., and DebRoy, T. 2004. Probing unknown welding parameters from convective heat transfer calculation and multivariable optimization. *Journal of Physics D: Applied Physics* 37: 140–150.

17. De, A., and DebRoy, T. 2005. Reliable calculations of heat and fluid flow during conduction mode laser welding through optimization of uncertain parameters. *Welding Journal* 84(7): 101–112.

18. Mishra, S., and DebRoy, T. 2005. A computational procedure for finding multiple solutions of convective heat transfer equation. *Journal of Physics D* 38: 2977–2985.

19. Mishra, S., and DebRoy, T. 2005. A heat transfer and fluid flow based model to obtain a specific weld geometry through multiple paths. *Journal of Applied Physics* 98(4): Article No. 044902.

20. He, X., Fuerschbach, P., and DebRoy, T. 2003. Heat transfer and fluid flow during laser spot welding of 304 stainless steel. *Journal of Physics D: Applied Physics* 36: 1388–1398.

21. Mundra, K., Blackburn, J. M., and DebRoy, T. 1997. Absorption and transport of hydrogen during GMA welding of mild steels. *Science and Technology of Welding and Joining* 2: 174–184.

22. Chang, C. W., Eagar, T. W., and Szekely, J. 1980. The modeling of gas velocity fields in welding arc. *Arc Physics and Weld Pool Behavior*, The Welding Institute, Cambridge, England, pp 381–388.

23. Patankar, S. V. 1982. *Numerical Heat Transfer and Fluid Flow*. New York, N.Y.: McGraw-Hill. pp 41–71.

24. Sahoo, P., DebRoy, T., and McNallan, M. J. 1988. Surface tension of binary metal-surface active solute systems under conditions relevant to welding metallurgy. *Metallurgical Transaction B* 19B: 483–491.

25. Lancaster, J. F. 1986. *The Physics of the Welding*. Oxford, UK: Pergamon. pp 120–225.

26. Goldman, K. 1966. Electric arcs in argon. *Physics of the Welding Arc*. London, UK: Institute of Welding.

27. Lin, M. L., and Eagar, T. W. 1985. Influence of arc pressure on weld pool geometry. *Welding Journal* 64(6): 163-s to 169-s.

28. Kumar, A., and DebRoy, T. 2003. Calculation of three-dimensional electromagnetic force field during arc welding. *Journal of Applied Physics* 94 (2): 1267–1277.

29. Kou, S., and Sun, D. K. 1985. Fluid flow and weld penetration in stationary arc welds. *Metallurgical Transactions A* 16A: 203–213.

30. Rokhlin, S. I., and Guu, A. C. 1993. A study of arc force, pool depression and weld penetration during gas tungsten arc welding. *Welding Journal* 72(8): 381–390.

31. Tsai, N. S., and Eagar, T. W. 1985. Distribution of arc and current fluxes in gas tungsten arcs. *Metallurgical Transactions B* 16(12): 841–846.

32. Yamauchi, N., and Taka, T. 1979. TIG arc welding with a hollow tungsten electrode. *International Institute of Welding*, document no.: 212-452-79.

33. Mondain-Monval. 1973. The physical properties of fluids at elevated temperatures. *IIW document* 212-264-73.

34. Goodarzi, M., Choo, R., and Toguri, J. M. 1997. The effect of the cathode tip angle on the GTAW arc and weld pool: I. Mathematical model of the arc. *Journal of Physics D: Applied Physics* 30: 2744–2756.

35. Choo, R. T. C., Szekely, J., and Westhoff, R. C. 1990. Modelling of high current arcs in welding with emphasis on free surface phenomena in weld pool. *Welding Journal* 69(9): 346-s to 361-s.

36. Chernyshov, G. G., and Kovtun, V. L. 1985. Effect of heat flow and arc pressure on maximum welding speed. *Welding Production* 32(2): 23–25.

37. Kang, Y. H., and Na, S. J. 2002. A study on the modeling of magnetic arc deflection and dynamic analysis of arc sensor. *Welding Journal* 81(1): 8–13.

38. Kovalev, I. M. 1965. Deflection of a welding arc in a transverse magnetic field. *Welding Production* 12(10): 9–14.

39. Matsunawa, A., and Nishiguchi, K. 1979. Arc characteristics in high pressure argon atmospheres. *Arc Physics and Weld Pool Behavior*. The Welding Institute, Cambridge, UK.

40. Yamamoto, T., and Shimada, W. 1968. Cathode zone and its effect on the penetration of the TIG arc at low pressure atmosphere. *International Institute of Welding*, document no.: 212-157-68.

41. *Welding Handbook*. 2004. Miami, Fla.: American Welding Society.

42. Fan, Y. 2003. The effect of torch angle on fluid flow and heat transfer during GTA welding. M.S. thesis, The Pennsylvania State University, Pa.

43. Nguyen, T. C., Weckman, D. C., Johnson, D. A., and Kerr, H. W. 2005. The humping phenomenon during high speed gas metal arc welding. *Science and Technology of Welding and Joining* 10(4): 447–459.

44. Voller, V. R., and Prakash, C. 1987. A fixed grid numerical modeling methodology for convection diffusion mushy region phase change problems. *International Journal of Heat and Mass Transfer* 30(8): 1709–1719.

45. Brent, A. D., Voller, V. R., and Reid, K. J. 1988. Enthalpy-porosity technique for modeling convection-diffusion phase change – Application to the modeling of a pure metal. *Numerical Heat Transfer* 13: 297–318.

Exploring the Mechanical Properties of Spot Welded Dissimilar Joints for Stainless and Galvanized Steels

Numerous tests were performed to determine the spot welding parameters for the dissimilar metal joints and to characterize their mechanical properties

BY M. ALENIUS, P. POHJANNE, M. SOMERVUORI, AND H. HÄNNINEN

ABSTRACT. Spot weldability of dissimilar metal joints between stainless steels and nonstainless steels was investigated. The aim was to determine the spot welding parameters for the dissimilar metal joints and to characterize the mechanical properties of the joints. Metallographical investigations, microhardness measurements, peel tests, lap shear tests, cross-tension tests, corrosion fatigue tests, and stress corrosion cracking tests were performed.

It was found that in the dissimilar metal joints between stainless steel and nonstainless steel, the failure load of the cross-tension specimens was around 72–78% of that of the lap shear specimens. The weld nugget of the dissimilar metal joints was fully martensitic, but it was ductile enough so that the failure type was plug failure in both lap shear and cross-tension tests.

In the case of the corrosion fatigue testing of the spot welded joints, different strength levels of the base materials did not have an effect on the corrosion fatigue strength, but the sheet thickness had a significant effect. The fatigue strength of a spot welded specimen increased with the increasing sheet thickness. Electro-coating of the test specimens did not have an effect on the corrosion fatigue properties of the spot welded joints.

Stress corrosion cracking tests showed that the stainless steel EN 1.4318 and zinc-coated nonstainless steel ZStE260BH dissimilar metal joints are susceptible to hydrogen embrittlement in 3.5% sodium chloride solution at room temperature. Comparable cracking was also observed in the stainless-stainless steel joints, when they were galvanically coupled to zinc. The reason for hydrogen embrittlement of the dissimilar metal welds is that the weld nugget is fully martensitic and the corrosion potential is low due to the zinc plating.

M. ALENIUS, M. SOMERVUORI, and H. HÄNNINEN are with Laboratory of Engineering Materials, Helsinki University of Technology, Finland. P. POHJANNE is with VTT Industrial Systems, Finland.

Introduction

Dissimilar metal welds are common in welded construction, and their performance is often crucial to the function of the whole structure. Dissimilar metal welding involves the joining of two or more different metals or alloys. There are several types of dissimilar metal welds, and the most common type is the joining of stainless steel to nonstainless steel. In the case of arc welding, filler metal is typically used, but in the case of resistance spot welding, the use of filler metal is very rare.

Resistance spot welding has a very important role as a joining process in the automotive industry, and a typical vehicle contains more than 3000 spot welds. The quality and strength of the spot welds are very important to the durability and safety design of the vehicles. The development of the new materials results constantly in the resistance spot welding tasks with new materials or combinations of them. The lack of experience with the new materials or combinations of them often results in the use of the welding parameters, which are not optimal. A few common guideline values and weldability diagrams for spot welding of steels exist and most of the guidelines are for nonstainless steels.

KEYWORDS

Spot Welding
Dissimilar Metal Joints
Stainless Steel
Nonstainless Steel
Spot Welded Joints

In general, an unlimited number of weld metal compositions can be obtained in the dissimilar metal welding, depending on the combination of the base and filler metals and the welding process. In the case of spot welding, the microstructure of the weld nugget can be predicted by using constitution diagrams, e.g., the Schaeffler diagram. The use of the Schaeffler diagram may be inaccurate because of the high cooling rate of the resistance spot weld. Other well-known constitution diagrams are DeLong, WRC-1988, and WRC-1992 diagrams. They can be used for the prediction of the ferrite content of the austenitic welds, but the diagrams are not so well suitable for the prediction of the martensite contents of the dissimilar metal welds when no filler metal is used.

In Fig. 1, an example is shown how to use the Schaeffler diagram in the case of spot welded dissimilar metal joints. If the dilution is, e.g., 50%, the microstructure of the weld nugget is lying in the middle of the line, which is drawn between stainless steel EN 1.4318 (AISI 301LN) and nonstainless steel ZStE260BH — Fig. 1. Thus, the microstructure of the weld nugget will be fully martensitic. The dilution in resistance spot welding of dissimilar metals can vary between 30 and 70%, and the microstructure of the weld nugget is still fully martensitic.

Hard martensitic weld metal may be a problem during welding and service. Hard martensitic weld metal can be susceptible to hydrogen embrittlement in service conditions, if the corrosion potential is in the region where hydrogen evolution is possible.

Arc welding is the most common technique in dissimilar metal welding, and resistance welding is a rare technique for joining stainless steels to nonstainless steels, respectively. There are a

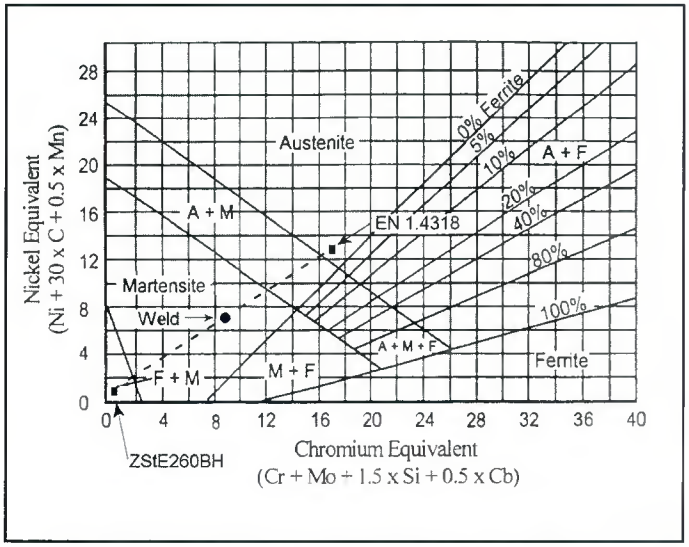

Fig. 1 — The microstructure of the weld nugget of a dissimilar metal joint EN 1.4318 – ZStE260 BH, predicted by means of the Schaeffler diagram when dilution is 50%.

Fig. 2 — The corrosion cell used in the corrosion fatigue test.

Table 1 — The Chemical Compositions of Test Materials, Wt-%

Steel	C	Cr	Cu	Mn	Mo	N	Ni	P	S	Si
DX54DZ 1.50	0.0023	—	—	0.16	—	—	0.02	0.01	0.004	0.004
ZStE260BH 1.50	0.0018	—	—	0.6	—	—	—	0.06	0.008	0.07
FeP06GZ 0.70	0.0023	—	—	0.16	—	—	0.02	0.01	0.004	0.004
EN 1.4318 2B 1.00	0.019	17.6	0.22	1.61	0.14	0.094	6.6	0.028	0.002	0.48
EN 1.4318 2H 1.00	0.019	17.6	0.22	1.61	0.14	0.094	6.6	0.028	0.002	0.48
EN 1.4318 2B 1.92	0.024	17.5	0.28	1.23	0.17	0.106	6.4	0.027	0.001	0.52
EN 1.4318 2H 1.92	0.024	17.5	0.28	1.23	0.17	0.106	6.4	0.027	0.001	0.52
EN 1.4301 2B 1.00	0.041	18.2	0.37	1.71	0.32	0.054	8.1	0.031	0.002	0.33
EN 1.4301 2H 1.00	0.052	18.1	0.43	1.77	0.34	0.059	8.1	0.029	0.001	0.33
EN 1.4301 2B 1.95	0.046	18.1	0.23	1.73	0.24	0.050	8.1	0.031	0.002	0.38
EN 1.4301 2H 1.95	0.048	18.0	0.35	1.78	0.35	0.046	8.1	0.031	0.003	0.37

Table 2 — The Mechanical Properties of Test Materials

Steel	Thickness (mm)	$R_{p0.2}$ (MPa)	R_m (MPa)	A_{80} (%)
DX54DZ	1.50	165	294	47
ZStE260BH	1.50	302	415	30
FeP06GZ	0.70	165	294	47
EN 1.4318 2B	1.00	310	885	46
EN 1.4318 2H	1.00	495	945	36
EN 1.4318 2B	1.92	360	920	42
EN 1.4318 2H	1.92	500	1010	32
EN 1.4301 2B	1.00	330	730	64
EN 1.4301 2H	1.00	510	765	51
EN 1.4301 2B	1.95	315	705	63
EN 1.4301 2H	1.95	435	725	58

lot of scientific papers dealing with arc-welded dissimilar metal joints, but only a few studies have been published concerning spot-welded dissimilar metal joints (Refs. 1–3). The majority of the spot welding studies deal, however, with the spot welding of nonstainless steels.

Experimental Procedures

Materials

The test materials for this resistance spot welding study were DX54DZ, FeP06GZ, and ZStE260BH nonstainless steels and EN 1.4301 (AISI 304) and EN 1.4318 (AISI 301LN) austenitic stainless steels, which were studied both in 2B and 2H conditions. All nonstainless steels were galvanized. The test materials are listed in Table 1 and their measured tensile properties are presented in Table 2.

Because of the different chemical compositions of the nonstainless steels and stainless steels, their thermal conductivity values are also different. In the case of austenitic stainless steels, thermal conductivity is about 16 W/mK (Ref. 4) and for low-carbon nonstainless steels about 52 W/mK (Ref. 5), respectively. Electrical resistivity is also an important parameter when nonstainless steels are spot welded to stainless steels. Electrical resistivity of stainless steels EN 1.4301 and EN 1.4318 is about 72 μΩ cm (Ref. 4), and the electrical resistivity of low-carbon nonstainless steels is about 12 μΩ cm (Ref. 5). Differences in the thermal conductivity and in the electrical resistivity lead to an asymmetrical weld nugget in the dissimilar metal joints (Ref. 3).

Resistance Spot Welding Equipment

Resistance spot welding equipment CEA MF90 MFDC (medium frequency direct current, 1000 Hz) was used in the spot welding studies. Two types of spot welding electrodes were used — truncated cone and radius electrodes. The electrode material was CuNi2Be. The tip of the truncated electrode was 6 mm diameter for 1.5/0.7-mm nonstainless steel and 1.0-mm stainless steel and 8 mm diameter for 1.5-mm nonstainless steel and 1.9-mm stainless steel. R75 radius electrode was used for the triple sheet dissimilar metal joints FeP06GZ + EN 1.4318 2H + FeP06GZ and FeP06GZ + EN 1.4301 2H + FeP06GZ.

Welding Parameter Determination

It is well known that expulsion reduces the strength of a spot weld due to the smaller size of the nugget formed and the porosity of the nugget. The welding parameters and weldability diagrams were determined in this study after several welding trials. Electrode force was selected depending on the thickness of the base materials, and the force was

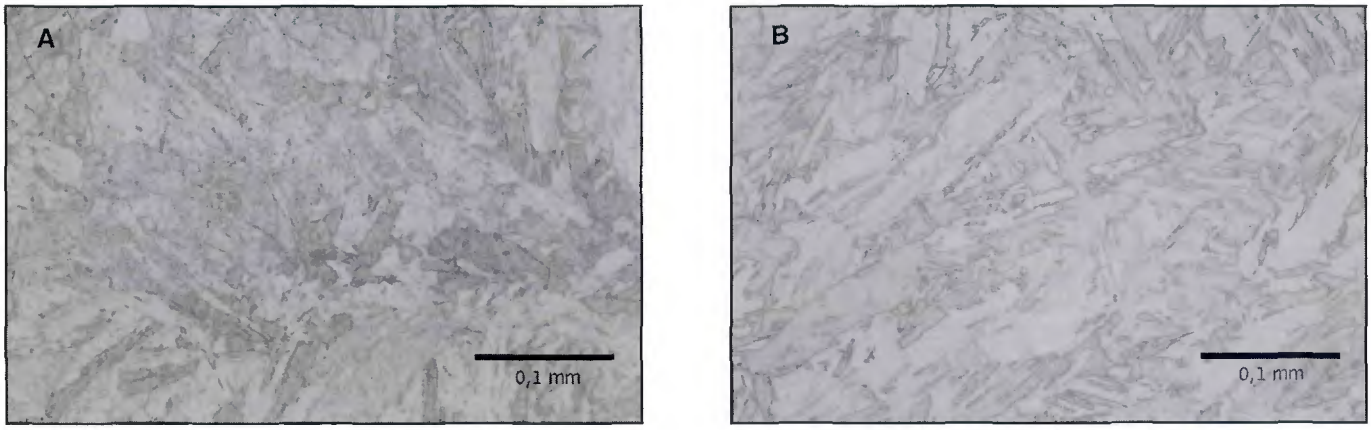

Fig. 3 — Typical martensitic microstructure of weld nugget of dissimilar metal joints. A — Stainless steel EN 1.4318 2H and nonstainless steel DX54DZ; and B — nonstainless steel DX54DZ – stainless steel EN 1.4318 2B – nonstainless steel DX54DZ.

kept constant during the tests. Welding current and welding time were changed during the weldability studies. Welding current was increased step by step, and welding time was kept constant. Then the welding current was kept constant, and the welding time was increased step by step. The diameter of the weld nugget was measured after the peel tests and the lap shear tests. The final spot welding parameters used in the further studies were selected so that expulsion would not occur, and the required $5\sqrt{t}$ nugget diameter was obtained where t = the thickness of the welded steel sheet. In the case of sheets of different thickness, t = the thickness of the thinner sheet. The spot welding parameters are presented in Table 3.

Table 3 — The Spot Welding Parameters of Joints Used for Mechanical Testing

Spot-Welded Joint	Welding Current (kA)	Welding Time (ms)	Electrode Force (kN)
EN 1.4301 2B 1.00 + FeP06GZ 0.7	7.6	160	3.8
EN 1.4301 2H 1.00 + FeP06GZ 0.7	7.4	160	3.8
EN 1.4318 2B 1.00 + DX54DZ 1.5	8.6	160	3.8
EN 1.4318 2H 1.00 + DX54DZ 1.5	8.5	160	3.8
EN 1.4301 2B 1.00 + DX54DZ 1.5	8.6	160	3.8
EN 1.4301 2H 1.00 + DX54DZ 1.5	8.5	160	3.8
EN 1.4318 2B 1.92 + ZStE260BH 1.5	9.6	240	5.0
EN 1.4318 2H 1.92 + ZStE260BH 1.5	9.1	240	5.0
EN 1.4301 2B 1.92 + ZStE260BH 1.5	9.8	240	5.0
EN 1.4301 2H 1.92 + ZStE260BH 1.5	9.3	240	5.0
FeP06GZ 0.7 + EN 1.4318 2H 1.00 + FeP06GZ 0.7	6.2	160	2.3
FeP06GZ 0.7 + EN 1.4301 2H 1.00 + FeP06GZ 0.7	6.1	160	2.3
DX54DZ 1.5 + EN 1.4318 2B 1.00 + DX54DZ 1.5	9.5	240	3.8
DX54DZ 1.5 + EN 1.4318 2H 1.00 + DX54DZ 1.5	9.5	240	3.8
DX54DZ 1.5 + DX54DZ 1.5	14.0	240	5.0
ZStE260BH 1.5 + ZStE260BH 1.5	14.0	240	5.0

Metallography

Cross sections for the microstructural investigations were taken from the spot welded joints. The microstructural studies of the weld nuggets and the heat-affected zones (HAZ) were carried out using an optical microscope. Martensite contents of the weld nuggets of the dissimilar metal joints were measured using Feritscope MP30.

Microhardness Measurements

The microhardness measurements vertical to the dissimilar metal joints were carried out for the metallographical samples. Vickers hardness measurements were carried out with 0.2-kg load (HV0.2).

Lap Shear Tests

The lap shear test samples of two 30 × 100-mm coupons were first spot welded. The lap shear tests were performed with a servohydraulic testing equipment MTS 810 in accordance with standard SFS-EN 14273. Maximum shear force and plug or weld diameter were measured.

Lap shear tests were also performed after EN 1.4318 – ZStE260BH specimens were exposed to 3.5% NaCl solution at room temperature. Hydrogen-induced cracking susceptibility was characterized by the lap shear testing.

Cross-Tension Tests

The cross-tension test samples of two 50 × 150-mm coupons were first spot welded. The cross-tension tests were performed with a servohydraulic testing equipment MTS 810 in accordance with standard SFS-EN 14272. The test fixture for the cross-tension samples was also fabricated according to SFS-EN 14272. Maximum cross-tension force and plug diameter were measured. The test was terminated when the two coupons of the test sample were separated completely.

Corrosion Fatigue Tests

Corrosion fatigue properties of spot welded dissimilar metal joints were investigated in 3.5% (0.6 mol Cl^-/l) NaCl solution. The corrosion cell (Fig. 2) was used in the corrosion fatigue tests. The cell was located around the test specimen so that the whole experimental part of the specimen containing the spot weld was exposed to the corrosion solution. To ensure that the concentration of the solution did not change significantly during the experiment, the solution was circulated with a pump. The electrolyte was flowing into the lower part of the cell and out through the upper tube. The corrosion fatigue test results of dissimilar metal joints were compared to the

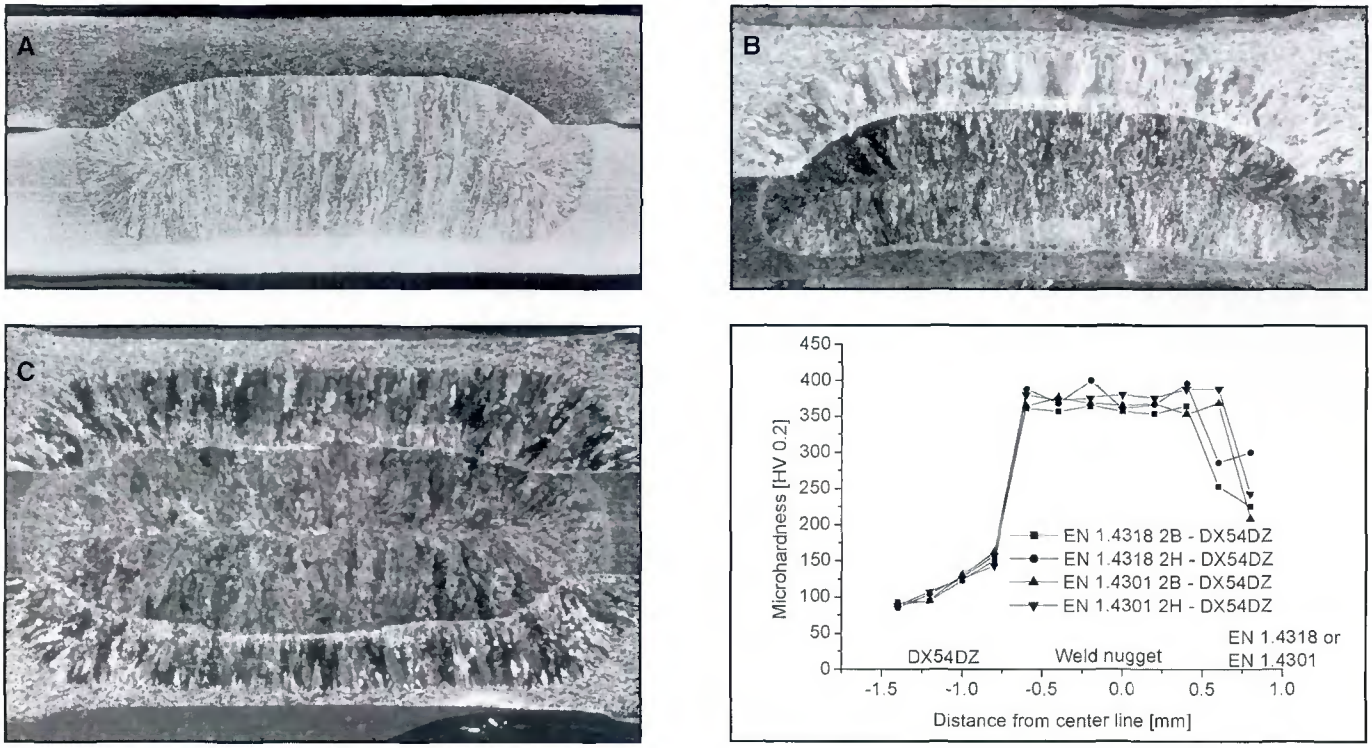

Fig. 4 — A — Asymmetric penetration in the dissimilar metal joint of EN 1.4318 2B and ZStE260BH steels; B — dissimilar metal joint of EN 1.4318 2H and DX54DZ steels; C — structure of triple sheet dissimilar metal joint of DX54DZ - EN 1.4318 2H - DX54DZ steels.

Fig. 5 — Vertical microhardness profiles of dissimilar metal joints of 1.0-mm stainless steels and 1.5-mm nonstainless steel DX54DZ.

Table 4 — Results of Martensite Content Measurements

Spot-Welded Joint	Ferrite Number, FN
EN 1.4318 2B 1.00 + DX54DZ 1.5	45.2 – 48.0
EN 1.4318 2H 1.00 + DX54DZ 1.5	46.0 – 48.5
EN 1.4301 2B 1.00 + DX54DZ 1.5	45.5 – 47.0
EN 1.4301 2H 1.00 + DX54DZ 1.5	47.0 – 48.5
EN 1.4318 2B 1.92 + ZStE260BH 1.5	47.0 – 49.5
EN 1.4318 2H 1.92 + ZStE260BH 1.5	47.0 – 49.0
EN 1.4301 2B 1.92 + ZStE260BH 1.5	43.0 – 45.0
EN 1.4301 2H 1.92 + ZStE260BH 1.5	45.0 – 48.5

corrosion fatigue test results of nonstainless steel and stainless steel joints. Electro-coated specimens were also corrosion fatigue tested. Electro-coating has been developed for the automotive industry, and it is an electrically applied paint coating process that improves the corrosion resistance.

The shear loaded corrosion fatigue test specimen consisted of two halves welded by one spot weld in the center of the overlapping area (20 mm). The width of the test specimen was 30 mm. The corrosion fatigue tests were performed using a servo-hydraulic testing equipment MTS 810. The frequency of 15 Hz was used. Sinusoidal waveform was applied, and the R-value was 0.1. The failure criterion was 0.5 mm displacement at the maximum load (Ref. 6).

Nordberg (Ref. 7) has used a "line load" method when fatigue data of spot welded joints of dissimilar sheet thickness has been analyzed. In most of the fatigue studies, the fatigue strength is given in terms of the net-section stress. This is also the case for butt joints of continuous joining methods, but there seems to be no general rule for the spot welded joints. Some studies give total load and define the number of spot welds; others report the strength as the net-section stress of the specimen. Some studies report strength as the corresponding shear stress on the spot weld. To be able to compare the mechanical properties of different joining methods, the strength of the joints is given both as the load range and as the "line load." By using "line load," it is possible to compare continuous joining methods such as laser welding with discontinuous methods like spot welding. Line load is the load divided by the width of the joint, and the width of the joint, e, is calculated as follows:

$$e = (14 * t_2 + 3)\sqrt[3]{\frac{t_1}{t_2}} \quad (1)$$

where $t_1 > t_2$.

The width of the joint, e, is the optimum distance between the two spot welds. Dividing the line load with the thickness of the sheet gives the net-section stress.

Stress Corrosion Cracking

Stress corrosion cracking resistance of the spot welded dissimilar metal joints was investigated both in 3.5% (0.6 mol Cl^-/l) and in 23% (3.9 mol Cl^-/l) NaCl solutions with slow strain rate tests (SSRT). Reference tests were made in air at room temperature. The corrosion cell and the specimen type were the same as in the corrosion fatigue tests. The tests were performed at room temperature with crosshead speed of 6×10^{-6} mm/s. In addition to time to failure and maximum load, corrosion potentials were also recorded in all tests. For comparison purposes, SSRT tests were also performed with stainless-stainless joints. These tests were performed both in freely corroding conditions and under cathodic protection, i.e., coupled to a zinc anode.

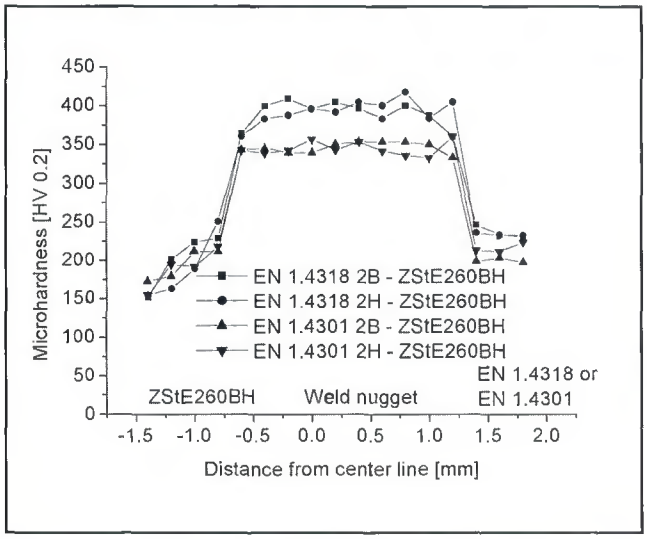

Fig. 6 — Vertical microhardness profiles of dissimilar metal joints of 1.9-mm stainless steels and 1.5-mm nonstainless steel ZStE260BH.

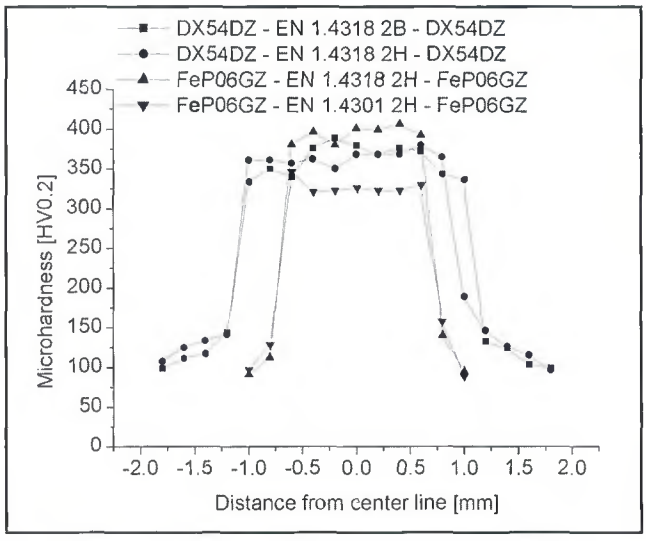

Fig. 7 — Vertical microhardness profiles of triple sheet dissimilar metal joints.

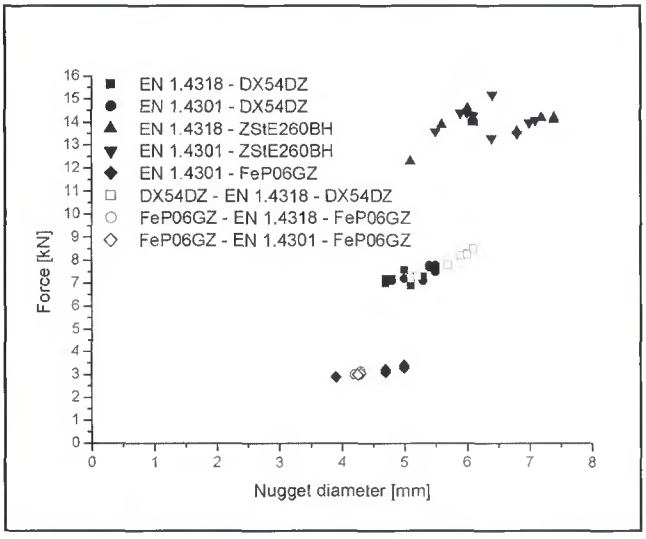

Fig. 8 — Lap shear test results of dissimilar metal joints show the effect of the different strengths and sheet thicknesses of the nonstainless steels.

Results and Discussion

Metallography

The typical microstructures of the dissimilar metal spot welds are shown in Fig. 3. In the dissimilar metal joints, the microstructure of the weld nugget consisted of martensite. The results of the martensite content measurements of the weld nuggets are presented in Table 4. Feritscope reading between 45 and 50 FN indicates that the martensite content of the weld nugget is in the range of 95–100%.

Surface indentation was very slight, a few percent, in the dissimilar metal joints. Separation of the sheets was also small. In the case of the double sheet dissimilar metal joints, penetration was asymmetric. In the double sheet dissimilar metal joints, penetration was between 50 and 60% on the side of nonstainless steel and 70–80% on the side of stainless steel — Fig. 4. In the triple sheet dissimilar metal joints, penetration was around 50% on the side of nonstainless steels. In general, the surface indentation should be less than 10% of the thickness of the sheet, the penetration should be 20–80% of the thickness of the sheet, and the separation should not be more than 10% of the sheet thickness.

Microhardness Measurements

Results of the microhardness measurements are presented in Figs. 5–7. In the dissimilar metal joints, the microhardness values of the weld nuggets were high due to the martensitic microstructure of the weld nugget. The highest hardness values of the dissimilar metal weld nuggets were slightly over 400 HV0.2. There was a clear difference in the microhardness levels of the weld nuggets between EN 1.4318 – ZStE260BH and EN 1.4301 – ZStE260BH dissimilar metal joints — Fig. 6. Nitrogen content has a large effect on the hardness of the martensite, and thus the difference is attributed to the smaller nitrogen content of EN 1.4301 stainless steels.

In the dissimilar metal joint of 1.0-mm stainless steel and 1.5-mm nonstainless steel, the dilution differs from that of a 1.9-mm stainless steel and 1.5-mm nonstainless steel joint. The dilution rate of stainless steel in the weld nugget is less in the case of the 1.0-mm stainless steel and 1.5-mm nonstainless steel joint. That is why there are no significant differences in the hardness level of the weld nuggets between different 1.0-mm stainless steel and 1.5-mm nonstainless steel joints.

Table 5 — Lap Shear Test Results After Exposure to 3.5% NaCl Solution for EN 1.4318 2H – ZStE260BH Steel Joints

Exposure Time (h)	Max. Force (kN)	Failure Type	Displacement Rate (mm/s)
—	13.9	plug	0.02
—	14.0	plug	0.02
24	13.7	plug	0.02
24	13.8	plug	0.02
120	13.9	plug	0.02
120	13.8	plug	0.02
720	13.9	plug	0.02
720	13.9	plug	0.02
1440	13.7	plug	0.02
1440	13.0	plug	0.0002
1440	13.4	plug	0.0001
2160	13.2	plug	0.02
2160	13.2	plug	0.0002
2160	13.0	plug	0.0001

Lap Shear Test Results

The results of the lap shear tests are shown in Fig. 8. The results of the lap shear tests after exposure to 3.5% NaCl

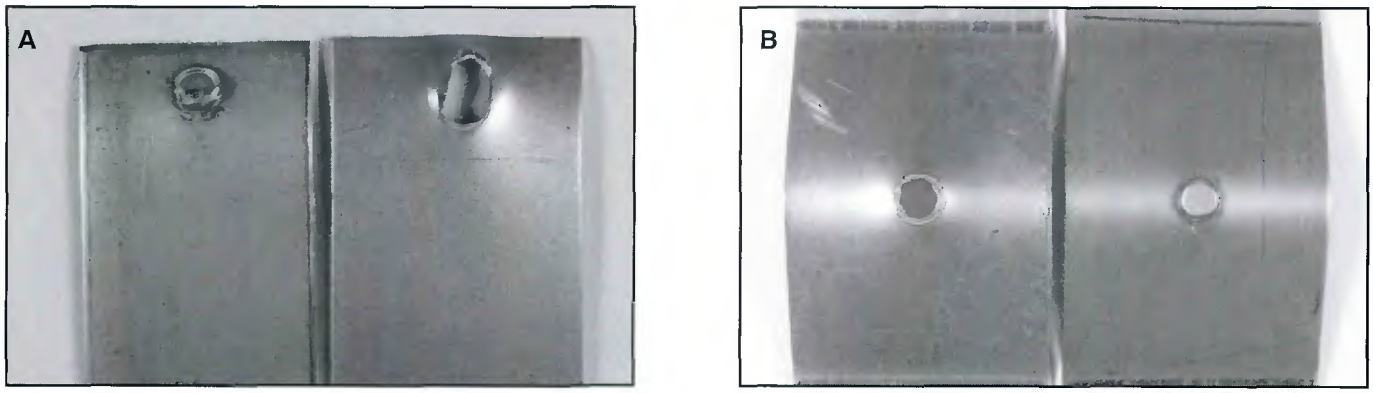

Fig. 9 — Typical plug failures. A — lap shear test; B — cross-tension test.

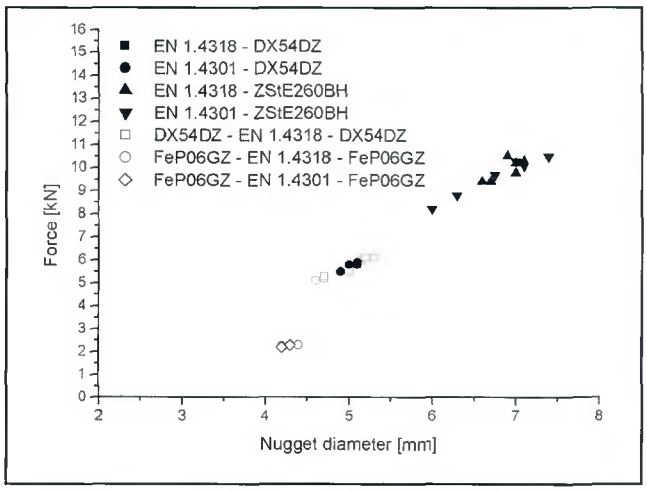

Fig. 10 — Cross-tension test results of dissimilar metal joints.

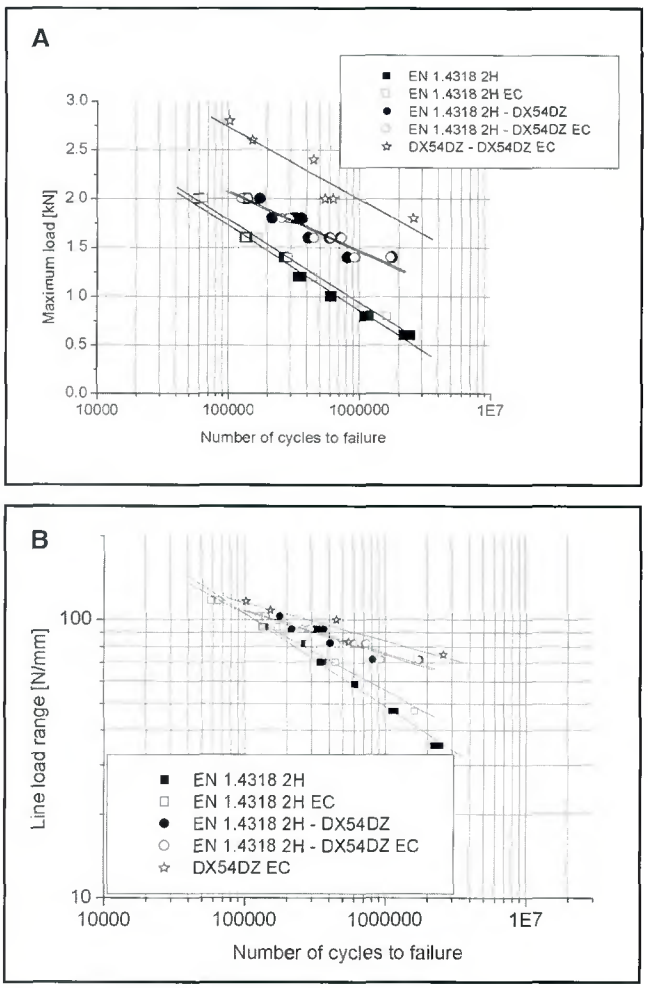

Fig. 11 — A — Corrosion fatigue test results of spot welded joints in 3.5% NaCl solution at 50°C; B — corrosion fatigue test results of spot welded joints in 3.5% NaCl solution at 50°C. Line load range analysis of the data.

solution are presented in Table 5. Hydrogen-induced cracking was not found after exposure to 3.5% NaCl solution. The strength level of exposed specimens was as high as the strength level of the specimens without exposure to 3.5% NaCl solution with the same nugget diameter. The failure type of all lap shear test specimens of the dissimilar metal joints was plug failure — Fig. 9A. Lap shear strength of the dissimilar metal joints depended on the strength and thickness of the nonstainless steels. Strength level of the nonstainless steels FeP06GZ and DX54DZ was the same, but the thickness of FeP06GZ steel was 0.7 mm and the thickness of DX54DZ steel was 1.5 mm. Thickness of the nonstainless steels DX54DZ and ZStE260BH was the same but the strength level was different. That is why there are three distinct strength levels between the different dissimilar metal joints when the nugget diameter is about 5 mm — Fig. 8.

Cross-Tension Test Results

The results of the cross-tension tests are shown in Fig. 10. The failure type of dissimilar metal joint cross-tension test specimens was plug failure — Fig. 9B. The cross-tension load correlates well with the nugget diameter of dissimilar metal joints.

In the dissimilar metal joints, the microstructure of the weld nugget was fully martensitic as predicted by means of the constitution diagram. Although the weld nugget of the dissimilar metal joints was fully martensitic, it was tough enough so that the failure type was plug failure in both lap shear and cross-tension tests.

Corrosion Fatigue Tests

The corrosion fatigue test results of the spot welded joints are presented in Fig. 11A (maximum load) and 11B (line load range). In the case of the spot welded joints, different strength levels of the base materials did not seem to affect the corrosion fatigue strength, but the sheet thickness had a significant effect. The fatigue strength of a spot welded joint increased with the increasing sheet

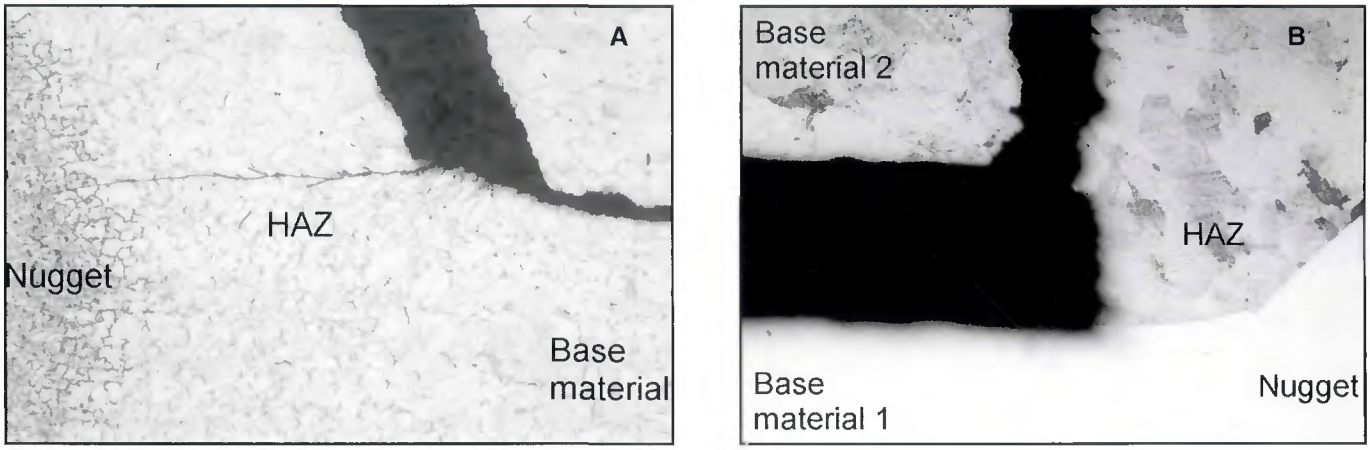

Fig. 12 — Crack initiation and growth. A — EN 1.4318 2H-EN 1.4318 2H steel joint; B — EN 1.4318 2H-DX54DZ dissimilar metal joint in the nonstainless steel side.

thickness. Especially at low loads, dissimilar metal and nonstainless steel joints exhibited higher fatigue strength than 1.0-mm-thick stainless steel joints. The fatigue strength of the dissimilar metal joints was found to be between the fatigue strength of the nonstainless steel and the stainless steel. The diameter of the weld nugget of the stainless-stainless steel joints and dissimilar metal joints was the same, 5 mm. The diameter of the weld nugget of the nonstainless steel joints was around 6.2 mm. This can also affect the better corrosion fatigue strength of nonstainless steel joints as compared to the other studied joints. Electro-coating did not have an effect on the corrosion fatigue properties of the studied spot welded joints significantly. The fatigue strength of the electro-coated EN 1.4318 2H joints seemed to be slightly higher than the fatigue strength of the EN 1.4318 joints without electro-coating. In dissimilar metal joints, a difference was not observed between electro-coated specimens and specimens without electro-coating. In dissimilar metal joints, fatigue cracks initiated at the tip of the corona bond of both nonstainless steel and stainless steel. Similar phenomenon was observed by Somervuori et al. (Ref. 6), who investigated the corrosion fatigue properties of spot welded joints of 1.9-mm-thick austenitic stainless steels. After initiation, the crack propagation occurred through the thickness of the sheets in the heat-affected zone — Fig. 12.

Table 6 — Summary of the SSRT Tests Performed at Room Temperature

Environment	Max Load (kN)	Reduction in Load-Carrying Capacity (%)	Average E_{corr} ($mV_{Ag/AgCl}$)	Comments
EN 1.4318 2B 1.92-EN 1.4318 2B 1.92				
Air	17.20	—	—	Ductile fracture
3.5% NaCl, air purging	15.70	9	–49	Ductile fracture
3.5% NaCl, O_2 purging + coupled to Zn anode	9.87	42	–980	HE
EN 1.4318 2B 1.92-ZStE260BH 1.5				
Air	12.79	—	—	Ductile fracture
3.5% NaCl, O_2 purging	9.10	29	–776	HE
23% NaCl, O_2 purging	8.25	35	–1046	HE

Stress Corrosion Cracking

The results of the stress corrosion tests with spot welded joints are presented in Fig. 13 and Table 6. The SSRT tests showed that the dissimilar metal joints are susceptible to hydrogen embrittlement both in 3.5% NaCl and in 23% NaCl solutions at room temperature. Spot welded EN 1.4318-EN 1.4318 stainless steel joints were also susceptible to hydrogen embrittlement in 3.5% NaCl when galvanically coupled to the zinc anode — Fig. 13.

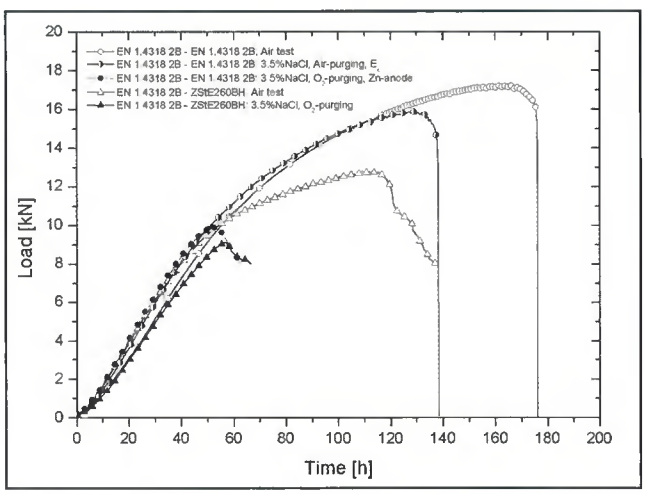

Fig. 13 — Results of the slow strain rate tests with spot welded EN 1.4318-EN 1.4318 and EN 1.4318-ZStE260BH steel joints in 3.5% NaCl solution at room temperature.

Corrosion potential measurements performed during the tests showed that the corrosion potentials of the dissimilar metal joints and EN 1.4318 steel, when it is coupled to zinc, are so low that hydrogen evolution takes place. In dissimilar metal joints, failure occurred through the weld nugget (Fig. 14A), whereas in the galvanically coupled stainless-stainless joint, failure initiated from the crevice of the lap joint. After initiation, the crack propagation occurred through the thickness of the sheet in the proximity of the weld interface —

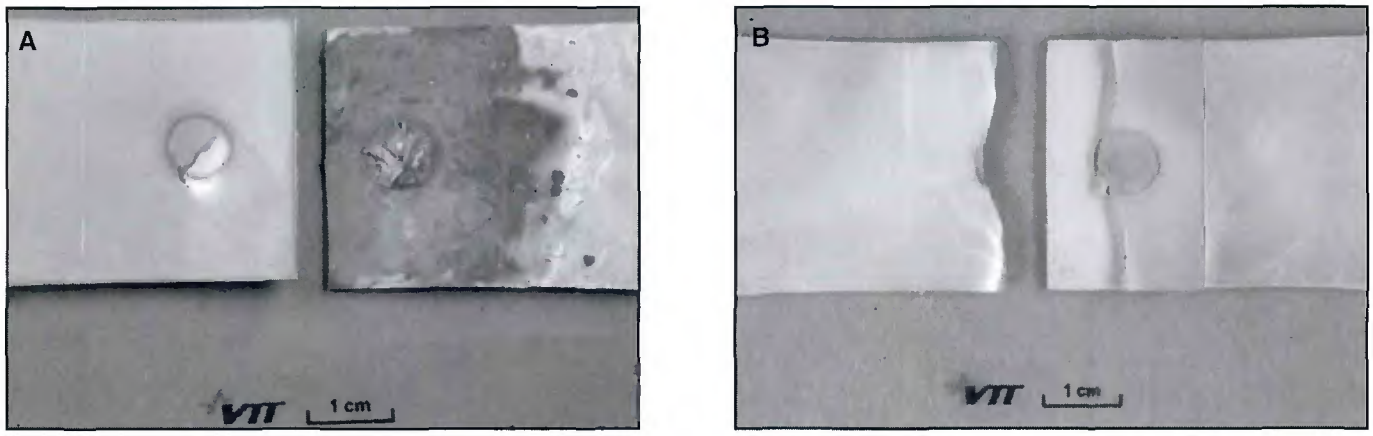

Fig. 14 — Macrographs of dissimilar metal joint EN 1.4318-ZStE260BH after SSRT test in 3.5% NaCl solution at room temperature (A) and EN 1.4318-EN 1.4318 steel sample with Zn-anode after SSRT test in 3.5% NaCl solution at room temperature (B).

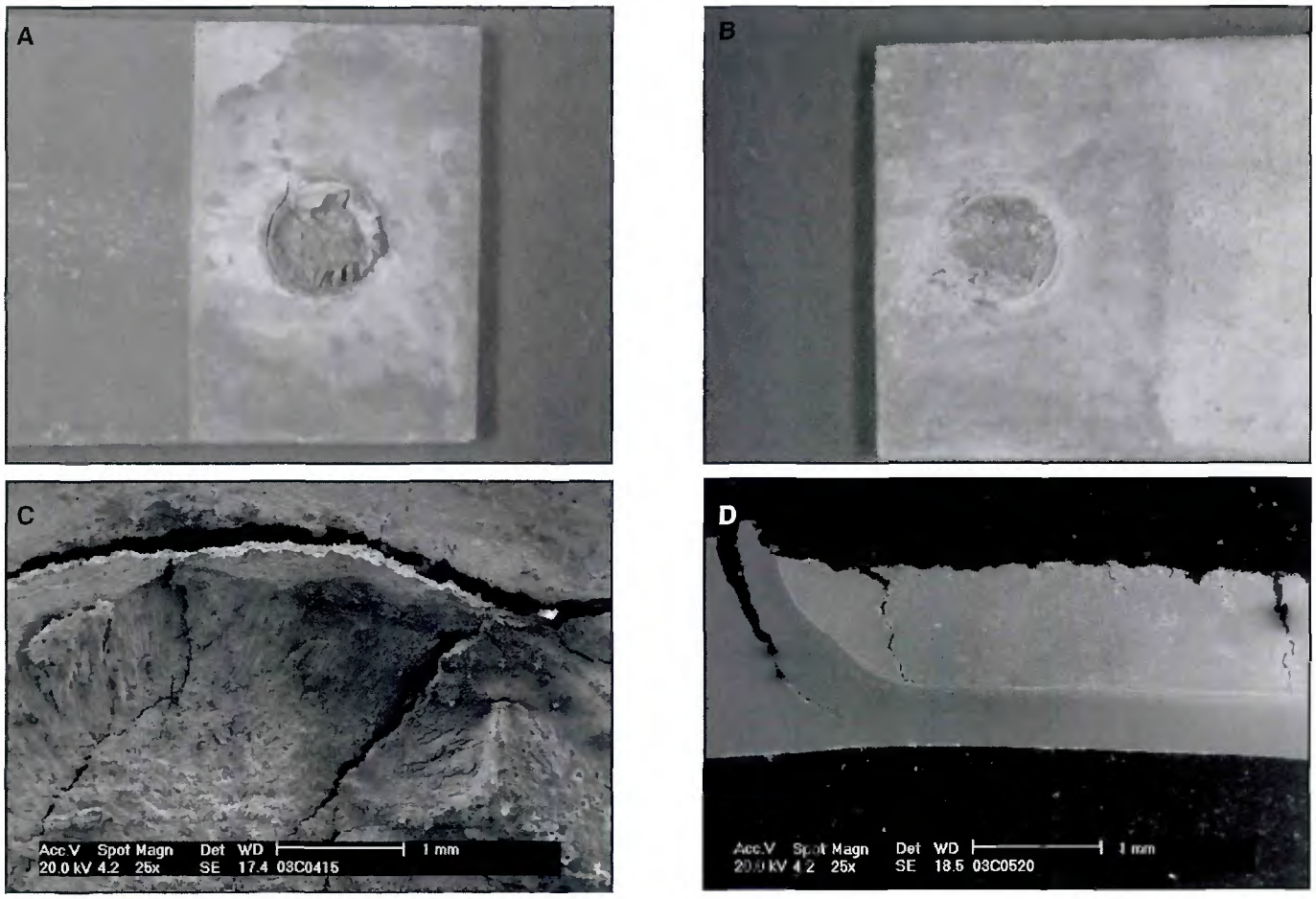

Fig. 15 — Shear loaded EN 1.4318 2B-ZStE260BH dissimilar metal joint sample after SSRT test in 23% NaCl at room temperature (O_2 purging). A — Fracture in the EN 1.4318 2B side; B — fracture in the ZStE260BH side; C — fracture surface of the EN 1.4318 2B side; D — cross section of the fracture surface of the EN 1.4318 2B side.

Fig. 14B. Fracture surface and cross section of EN 1.4318 2B-ZStE260BH dissimilar metal joint sample after SSRT test in 23% NaCl at room temperature is shown in Fig. 15.

Based on the metallography and the Feritscope measurements, dissimilar metal joints are susceptible to hydrogen embrittlement because the weld nugget is fully martensitic. The observed hydrogen embrittlement of stainless-stainless joints is attributed to strain-induced martensite forming during the SSRT test and hydrogen evolution reaction due to zinc anode. Without galvanic coupling, neither hydrogen embrittlement nor stress corrosion cracking of spot welded EN 1.4318-EN 1.4318 steel joints were observed — Fig. 13. In this case a ductile failure, similar to air test, was observed.

Conclusions

The mechanical properties of the dissimilar metal joints were studied. It was found that for the dissimilar metal joints, the failure load of the cross-tension specimens was about 72–78% of that of the lap shear specimens and the failure type was plug failure in both tests. The lap shear strength of the dissimilar metal

joints depended on the strength and thickness of the nonstainless steel.

In the case of the spot welded joints, the different strength levels of the base materials did not have an effect on the corrosion fatigue strength, but the sheet thickness had a significant effect. The fatigue strength of a spot welded structure increases with the increasing sheet thickness. The fatigue strength of the dissimilar metal joints was found to be between the fatigue strength of the nonstainless steel and the stainless steel. Electro-coating of the test specimens did not have a significant effect on the corrosion fatigue properties of spot welded joints.

It was found that dissimilar metal joints are susceptible to hydrogen embrittlement in chloride solutions at room temperature. The same was also observed with stainless-stainless joints when they were galvanically coupled to zinc. Without galvanic coupling stainless-stainless steel joints were found to be resistant to both hydrogen embrittlement and stress corrosion cracking in this type of test.

Acknowledgments

This study was accomplished as part of the project "Weight reduction for safer, affordable passenger cars by using extra formable high-strength austenitic steel," G5RD-CT-2001-00454. Project is funded by the Fifth European Community Framework Program and European industry.

References

1. Bernabai, U., Brotzu, A., Felli, F., and Polidori, A. 1997. Analysis of the problems in spot welding AISI 301 high-strength austenitic stainless steels and galvanized steel plates. *Welding International* 11(10): 788-s to 794-s.

2. Akdut, N., Corostola, J. R., Koruk, A. I., Cretteur, L., and Maronna, I. 2001. Joining technologies to realize dissimilar joints for automotive applications. Automotive and Transportation Technology Congress and Exposition, Barcelona, Spain.

3. Tsai, C. L., Jammal, O. A., Papritan, J. C., and Dickinson, D. W. 1992. Modeling of resistance spot weld nugget growth. *Welding Journal* 71(2): 47-s to 54-s.

4. Anon. 1999. Avesta Polarit Stainless Steel. Products guide. Nelita Oy.

5. Anon. 1989. Technical Data Blue Sheet. Allegheny Ludlum Corporation.

6. Somervuori, M., Alenius, M., Karppi, R., and Hänninen, H. 2004. Corrosion fatigue of spot-welded austenitic stainless steels in 3.5 % NaCl solution. *Materials and Corrosion* 55(12): 921-s to 929-s.

7. Nordberg, H. 2006. Fatigue Properties of Stainless Steel Lap Joints. *SAE Transactions: Journal of Materials & Manufacturing* 114: 675-s to 690-s.

WELDING Journal

Guidelines for submitting electronic files

1. **Platform:**
   Macintosh or PC accepted
2. **Files accepted:**
   QuarkXpress, Adobe Photoshop, Adobe Illustrator, TIFF, EPS and PDF files only.
3. **Color:**
   Send all files in as CMYK (for color) or Grayscale (for b/w).
4. **Images:**
   Minimum resolution required for magazine printing is 300 dpi for full color artwork or grayscale at least 1000 dpi for bitmap (B&W/line art). Images and logos from Web sites are NOT usable for printing. They are low resolution images (72 dpi). Images taken with a digital camera are not acceptable unless they meet the minimum 300 dpi requirement.
5. **Proof:**
   A proof of the images should **always** be provided.
6. **Electronic File Transfer:**
   Files larger than 68k are not acceptable as an email attachment; please CD or Zip, may also send files to the printer's FTP site (a user name and password will be provided when requested)

Check list for submitting electronic files:

Colors: ❒ 4/C ❒ Grayscale ❒ B&W/line art

File Type: ❒ TIFF ❒ EPS

File sent via: ❒ Floppy disk ❒ Zip disk ❒ CD ❒ Email (68k limit)

❒ **Proof supplied**/faxed

❒ CMYK images at 300 dpi or higher, B&W/line art at 1000 dpi or higher.

❒ All color in all images set to CMYK process (not RGB)

When submitting ads, please send them to the attention of

Frank Wilson
Advertising Production Manager
American Welding Society
550 NW LeJeune Rd.
Miami, Fla. 33126

Use these convenient, postage-paid inquiry cards to request free information about the products or services advertised in this issue of *Welding Journal*.

For information about specific advertisements: Circle the key number on the card that matches the number on the bottom of the ad.

FREE INFORMATION • FREE INFORMATION

For faster processing, please FAX this card to (630) 739-9700.
Type or print the information and copy before faxing.
This fax number is for the service bureau only, not AWS.

Please send literature on items circled at right:

December 2006 — Card void after June 1, 2007

Name _____ Title _____

Company _____

Address _____

City _____ State _____ Zip _____

Phone: _____ Fax: _____

E-mail _____

Please circle an entry for each category:

I. TYPE OF BUSINESS
1. Construction
2. Primary Metal Products
3. Fabricated Metal Products
4. Transportation
5. Petrochemical
6. Misc. Repair Services
7. Educational Services
8. Utilities
9. Other

II. JOB FUNCTION/TITLE
1. Corp. Management
2. Plant Mgmt.
3. Engineer
4. Welding or Cutting Oper.
5. Quality Control
6. Sales
7. Purchasing
8. Education
9. Other

III. PURCHASING AUTHORITY
1. Recommend
2. Specify
3. Approve

IV. NUMBER OF EMPLOYEES
1. Under
2. 50 to 99
3. 100 to 499
4. 500 to 999
5. 1000 to 2499
6. 2500 to more

V. ANNUAL DOLLAR VOLUME
1. Under $1 Million
2. $1 Million to 5 Million
3. Over $5 Million

VI. THIS INQUIRY IS FOR
1. Immediate Purchase
2. Future Project
3. General Information

1	35	69	103	137	171	205	239	273
2	36	70	104	138	172	206	240	274
3	37	71	105	139	173	207	241	275
4	38	72	106	140	174	208	242	276
5	39	73	107	141	175	209	243	277
6	40	74	108	142	176	210	244	278
7	41	75	109	143	177	211	245	279
8	42	76	110	144	178	212	246	280
9	43	77	111	145	179	213	247	281
10	44	78	112	146	180	214	248	282
11	45	79	113	147	181	215	249	283
12	46	80	114	148	182	216	250	284
13	47	81	115	149	183	217	251	285
14	48	82	116	150	184	218	252	286
15	49	83	117	151	185	219	253	287
16	50	84	118	152	186	220	254	288
17	51	85	119	153	187	221	255	289
18	52	86	120	154	188	222	256	290
19	53	87	121	155	189	223	257	291
20	54	88	122	156	190	224	258	292
21	55	89	123	157	191	225	259	293
22	56	90	124	158	192	226	260	294
23	57	91	125	159	193	227	261	295
24	58	92	126	160	194	228	262	296
25	59	93	127	161	195	229	263	297
26	60	94	128	162	196	230	264	298
27	61	95	129	163	197	231	265	299
28	62	96	130	164	198	232	266	300
29	63	97	131	165	199	233	267	301
30	64	98	132	166	200	234	268	302
31	65	99	133	167	201	235	269	303
32	66	100	134	168	202	236	270	304
33	67	101	135	169	203	237	271	
34	68	102	136	170	204	238	272	

Please mail:
- ❑ 305- List of AWS publications
- ❑ 306- Information on AWS Membership

NO POSTAGE NECESSARY IF MAILED IN THE UNITED STATES

BUSINESS REPLY MAIL
FIRST CLASS PERMIT NO. 11992 MIAMI, FL
POSTAGE WILL BE PAID BY ADDRESSEE

WELDING *Journal*

C/O CREATIVE DATA
519 E BRIARCLIFF RD
BOLINGBROOK IL 60440-9882

NO POSTAGE NECESSARY IF MAILED IN THE UNITED STATES

BUSINESS REPLY MAIL
FIRST CLASS PERMIT NO. 11992 MIAMI, FL
POSTAGE WILL BE PAID BY ADDRESSEE

WELDING *journal*
C/O CREATIVE DATA
519 E BRIARCLIFF RD
BOLINGBROOK IL 60440-9882

Use these convenient, postage-paid inquiry cards to request free information about the products or services advertised in this issue of *Welding Journal*.

For information about specific advertisements: Circle the key number on the card that matches the number on the bottom of the ad.

FREE INFORMATION • FREE INFORMATION

Please send literature on items circled at right:

December 2006 Card void after June 1, 2007

Name _____ Title _____

Company _____

Address _____

City _____ State _____ Zip _____

Phone: _____ Fax: _____

E-mail _____

Please circle an entry for each category:

I. TYPE OF BUSINESS
1. Construction
2. Primary Metal Products
3. Fabricated Metal Products
4. Transportation
5. Petrochemical
6. Misc. Repair Services
7. Educational Services
8. Utilities
9. Other

II. JOB FUNCTION/TITLE
1. Corp. Management
2. Plant Mgmt.
3. Engineer
4. Welding or Cutting Oper.
5. Quality Control
6. Sales
7. Purchasing
8. Education
9. Other

III. PURCHASING AUTHORITY
1. Recommend
2. Specify
3. Approve

IV. NUMBER OF EMPLOYEES
1. Under
2. 50 to 99
3. 100 to 499
4. 500 to 999
5. 1000 to 2499
6. 2500 to more

V. ANNUAL DOLLAR VOLUME
1. Under $1 Million
2. $1 Million to 5 Million
3. Over $5 Million

VI. THIS INQUIRY IS FOR
1. Immediate Purchase
2. Future Project
3. General Information

1	35	69	103	137	171	205	239	273
2	36	70	104	138	172	206	240	274
3	37	71	105	139	173	207	241	275
4	38	72	106	140	174	208	242	276
5	39	73	107	141	175	209	243	277
6	40	74	108	142	176	210	244	278
7	41	75	109	143	177	211	245	279
8	42	76	110	144	178	212	246	280
9	43	77	111	145	179	213	247	281
10	44	78	112	146	180	214	248	282
11	45	79	113	147	181	215	249	283
12	46	80	114	148	182	216	250	284
13	47	81	115	149	183	217	251	285
14	48	82	116	150	184	218	252	286
15	49	83	117	151	185	219	253	287
16	50	84	118	152	186	220	254	288
17	51	85	119	153	187	221	255	289
18	52	86	120	154	188	222	256	290
19	53	87	121	155	189	223	257	291
20	54	88	122	156	190	224	258	292
21	55	89	123	157	191	225	259	293
22	56	90	124	158	192	226	260	294
23	57	91	125	159	193	227	261	295
24	58	92	126	160	194	228	262	296
25	59	93	127	161	195	229	263	297
26	60	94	128	162	196	230	264	298
27	61	95	129	163	197	231	265	299
28	62	96	130	164	198	232	266	300
29	63	97	131	165	199	233	267	301
30	64	98	132	166	200	234	268	302
31	65	99	133	167	201	235	269	303
32	66	100	134	168	202	236	270	304
33	67	101	135	169	203	237	271	
34	68	102	136	170	204	238	272	

Please mail:
❑ 305- List of AWS publications
❑ 306- Information on AWS Membership

NOTE:
To speed the processing of your inquiry, please provide ALL the information requested on the card. This will make it easier for the companies to follow up on your request as soon as possible.

Industrial Durability

OMEGA™ - Designed for Industrial durability...

OMEGA™ MIG-GUNS from ABICOR Binzel USA

- 350 and 450 amperes
- Full 360° positionable and interchangeable swannecks
- Modular torch design offers unmatched stacking options, and is easily recanfigured in the field
- Tight tolerance interface, direct crimped torch body, and neck locking screw enables optimal current transfer
- Swanneck O-ring provides improved gas seal
- Coarse threaded tip holders reduce chance af cross-threading
- One - piece rigid swannecks with covered armor jackets
- Industrial swanneck covering reduces torch damage
- and provides aperator comfort
- New direct crimped style power cable provides impraved gas delivery and cooling

30th Anniversary

1976 - 2006
30 Years in the USA

ABICOR BINZEL®

Alexander Binzel Carporation
650 Research Drive, Suite 110
Frederick, Maryland 21703
Phone: 800.542.4867
Fax: 301.846.4497

www.abicorusa.com